Wavelet estimation for towed streamer data

Zhiqiang Guo* , T. Hing Tan†, and Arthur B. Weglein*
*University of Houston, †Shell

Abstract

Weglein and Secrest (1990) present a method for computing the scattered wavefield between the measurement surface and free surface, and the reference wavefield below the measurement surface, given both the pressure and its normal derivative along the cable. Osen et al. (1998) and Tan (1992) show that the wavelet due to an isotropic source can be determined from pressure on the measurement surface and an extra hydrophone between the measurement surface and the free surface. Tan (1999) observes that in practice it is possible to well-estimate the wavefield above single towed streamer for points not directly under the source. Using the Tan (1999) wavefield prediction the wavelet can in principle be estimated from only a single cable (Weglein et al. 2000). However, the integral required for wavelet estimation requires data along the cable including the region excluded by the Tan's prediction. An approach to addressing that problem is presented here that adopts a generalized inverse viewpoint to find a well estimated approximation to the wavelet. First tests are encouraging and reported here; others are planned.

In this paper we will review the theory and show a new approach to wavelet estimation below the cable from only a single cable. Further work will focus on application to deghosting and multiple attenuation.

1 Introduction

In wave-theoretic multiple attenuation methods (eg. Carvalho, 1992, Weglein et al. 1997, Verschuur 1992), knowledge of the source wavelet is one of the requirements. The energy-minimization criterion is often applied in practice to estimate the wavelet. Current methods based on the energy minimization criterion have proven to be useful under many circumstances. However, under complex conditions, e.g., weak internal multiples proximal to weak subsalt primaries, experience suggests that the energy minimization criterion is too blunt an instrument for that degree of subtlety. This is the motivation for deriving new methods to provide the source wavelet. The industry trend towards complex and costly plays raises the bar of required effectiveness for wave theoretic multiple removal and imaging-inversion techniques, and the prerequisites, such as the wavelet that needs to be provided.

The goal of the research described here is to test and progress the development of new wavelet estimation methods that can be estimated from only the pressure on the cable. In the following we will first discuss extinction theorem; then we show how to predict the normal derivatives of the wavefield above the measurement surface.

2 Extinction Theorem

The acoustic wave equation can be written in the following form in the frequency domain, where $\mathbf{r}'$ is any point in a half space below the free surface, $\mathbf{r}_0$ is the source location, $A(\omega)$ is the source signature, ω is the angular frequency, c is the actual velocity, and P is the pressure field.

$$\nabla^2 P\left(\mathbf{r}', \mathbf{r}_0, \omega\right) + \frac{\omega^2}{c^2\left(\mathbf{r}'\right)} P\left(\mathbf{r}', \mathbf{r}_0, \omega\right) = A\left(\omega\right) \delta\left(\mathbf{r}' - \mathbf{r}_0\right) \tag{1}$$

Using scattering theory, the actual earth can be parameterized as a homogeneous velocity reference medium with embedded reflectors. Hence we replace c with c_0

$$\frac{1}{c^2\left(\mathbf{r}'\right)} = \frac{1}{c_0}\left[1 - \alpha\left(\mathbf{r}'\right)\right] \tag{2}$$

where c_0 is the reference medium velocity, and $\alpha\left(\mathbf{r}'\right)$ is called the scattered index, which is used to characterize the difference between the actual and reference media. Considering the Green's function in a homogenous medium with Dirichlet boundary conditions at both the free surface and the measurement surface due to point source at $\mathbf{r}$, such that

$$\nabla^2 G_0^{DD}\left(\mathbf{r}, \mathbf{r}^{'}, \omega\right) + \frac{\omega^2}{c_0^2} G_0^{DD}\left(\mathbf{r}, \mathbf{r}^{'}, \omega\right) = \delta\left(\mathbf{r} - \mathbf{r}'\right) \tag{3}$$

where $G_0^{DD}\left(\mathbf{r}, \mathbf{r}', \omega\right)$ is a 2-D Green's function, which can be obtained by the method of images based on Poisson sum formula (Morse and Feshbach, 1953, chapter 7 vol. 1). $G_0^{DD}\left(\mathbf{r}, \mathbf{r}', \omega\right)$ converges rapidly in a numerical implementation of the following expression.

$$G_0^{DD}(\mathbf{r}, \mathbf{r}', \omega) = \frac{4\pi i}{H} \sum_{n=1}^{\infty} \sin\left(\frac{\pi z}{H} n\right) \sin\left(\frac{\pi z'}{H} n\right) \frac{1}{\beta} e^{i\beta|x - x'|}$$

where $\mathbf{r}'$ represents a source location, $\mathbf{r}$ represents a receiver location, H is the depth of M.S., and β , which controls whether or not the Green's function is decaying exponentially

or travel horizontally, is defined as following

$$\beta = \sqrt{(\frac{\omega}{c_0})^2 - (\frac{n\pi}{H})^2}$$

Applying Green's theorem to equations (1) and (3)

$$\iint\limits_S d\mathbf{s}' \left[P\left(\mathbf{r}', \mathbf{r}_0, \omega\right) \frac{\partial G_0^{DD}\left(\mathbf{r}, \mathbf{r}', \omega\right)}{\partial \mathbf{n}'} - G_0^{DD}\left(\mathbf{r}, \mathbf{r}', \omega\right) \frac{\partial P\left(\mathbf{r}', \mathbf{r}_0, \omega\right)}{\partial \mathbf{n}'} \right]$$

$$= \iiint\limits_v d\mathbf{r}' \left[P\left(\mathbf{r}', \mathbf{r}_0, \omega\right) \nabla^2 G_0^{DD}\left(\mathbf{r}, \mathbf{r}', \omega\right) - G_0^{DD}\left(\mathbf{r}, \mathbf{r}', \omega\right) \nabla^2 P\left(\mathbf{r}', \mathbf{r}_0, \omega\right) \right] \tag{4}$$

Multiplying equation (3) by $P\left(\mathbf{r}', \mathbf{r}_0, \omega\right)$, and equation (1) by $G_0^{DD}\left(\mathbf{r}, \mathbf{r}', \omega\right)$, and then substituting them into the right hand side of equation (4), we have

$$\begin{aligned}
&\iint\limits_S d\mathbf{s}' \left[P\left(\mathbf{r}', \mathbf{r}_0, \omega\right) \frac{\partial G_0^{DD}\left(\mathbf{r}, \mathbf{r}', \omega\right)}{\partial \mathbf{n}'} - G_0^{DD}\left(\mathbf{r}, \mathbf{r}', \omega\right) \frac{\partial P\left(\mathbf{r}', \mathbf{r}_0, \omega\right)}{\partial \mathbf{n}'} \right] \\
= \quad &\iiint\limits_v d\mathbf{r}' P\left(\mathbf{r}', \mathbf{r}_0, \omega\right) \delta\left(\mathbf{r} - \mathbf{r}'\right) \\
&+ \iiint\limits_v d\mathbf{r}' \left[-\frac{\omega^2}{c_0^2} G_0^{DD}\left(\mathbf{r}, \mathbf{r}', \omega\right) \alpha\left(\mathbf{r}'\right) P\left(\mathbf{r}', \mathbf{r}_0, \omega\right) \right] \\
&\iiint\limits_v d\mathbf{r}' \left[-A\left(\omega\right) G_0^{DD}\left(\mathbf{r}, \mathbf{r}', \omega\right) \delta\left(\mathbf{r}' - \mathbf{r}_0\right) \right]
\end{aligned} \tag{5}$$

If we choose the integral volume V to be between the free surface (F.S.) and the measurement surface (M.S.), then the second term on the right hand side of equation (5) will be zero since the scatterer $\alpha\left(\mathbf{r}'\right)$ (i.e. Earth) is outside of the volume V. We then choose $\mathbf{r}$ above M.S., and applying the Delta function property,

$$\iiint\limits_v d\mathbf{r}' \left[\delta\left(\mathbf{r} - \mathbf{r}'\right) f\left(\mathbf{r}'\right) \right] = f\left(\mathbf{r}\right)$$

we have

$$\begin{aligned}
&\iint\limits_S d\mathbf{s}' \left[P\left(\mathbf{r}', \mathbf{r}_0, \omega\right) \frac{\partial G_0^{DD}\left(\mathbf{r}, \mathbf{r}', \omega\right)}{\partial \mathbf{n}'} - G_0^{DD}\left(\mathbf{r}, \mathbf{r}', \omega\right) \frac{\partial P\left(\mathbf{r}', \mathbf{r}_0, \omega\right)}{\partial \mathbf{n}'} \right] \\
= \quad &P\left(\mathbf{r}, \mathbf{r}_0, \omega\right) - A(\omega) G_0^{DD}(\mathbf{r}, \mathbf{r}_0, \omega)
\end{aligned}$$

Finally, since we have chosen the Green's function $G_0^{DD}(\mathbf{r},\mathbf{r}',\omega)$ to satisfy Dirichlet boundary conditions on both F.S. and M.S., then

$$P(\mathbf{r},\mathbf{r}_0,\omega) - A(\omega)G_0^{DD}(\mathbf{r},\mathbf{r}_0,\omega) = \iint_S d\mathbf{s}' \left[P(\mathbf{r}',\mathbf{r}_0,\omega) \frac{\partial G_0^{DD}(\mathbf{r},\mathbf{r}',\omega)}{\partial \mathbf{n}'} \right] \tag{6}$$

where $\mathbf{r}$ is between F.S. and M.S. (figure 1).

3 Normal derivatives

As showed above in equation (6), $G_0^{DD}(\mathbf{r},\mathbf{r}',\omega)$ is critical in order to get the wavefield above M.S. It is a function of the frequency and the depth of the measurement surface. Tan (1999) discovered that $G_0^{DD}(\mathbf{r},\mathbf{r}',\omega)$ is vanishingly small for typical marine streamer depths of approximately 6m and seismic frequency less than 125Hz (Figure 2). Therefore, the second term on the left hand side of equation (6) can be ignored in comparison with the other terms. Also we choose the Green's function to satisfy Dirichlet boundary conditions on both F.S. and M.S., and we assume that the pressure at F.S. will be vanishing. This results in the key observation:

$$P(\mathbf{r},\mathbf{r}_0,\omega) \approx \iint_{MS} d\mathbf{s}' \left[P(\mathbf{r}',\mathbf{r}_0,\omega) \frac{\partial G_0^{DD}(\mathbf{r},\mathbf{r}',\omega)}{\partial \mathbf{n}'} \right] \tag{7}$$

This equation will be used to predict the wavefield above M.S. through an integral over the measurement surface once we obtain the Green's function, then we can compute the normal derivatives over the cable by a finite difference approximation, or by taking normal derivatives directly from equation (7).

4 Wavelet estimation

Since we require the normal derivatives under the source for wavelet estimation, we modify the idea of calculating the normal derivatives above the cable without dropping the wavelet term $A(\omega)G_0^{DD}(\mathbf{r},\mathbf{r}',\omega)$. Hence

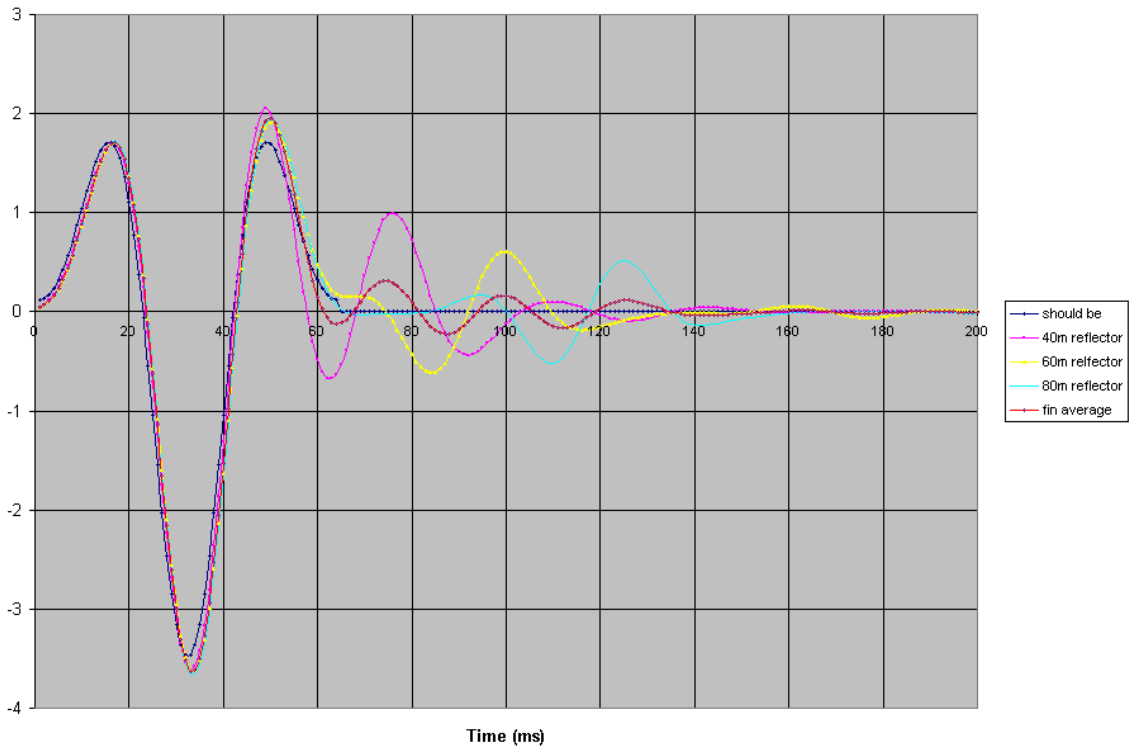

Figure 1: Wavelet estimation from water depth 40m, 60m and 80m reflector respectively. The wavelet estimated from water depth 80m reflector has least artifact; the final averaged (red) of three estimated wavelets is close to the correct one (black).

$$\frac{\partial}{\partial z}P\left(\mathbf{r},\mathbf{r}_0,\omega\right)=A(\omega)\frac{\partial}{\partial z}G_0^{DD}(\mathbf{r},\mathbf{r}_0,\omega)+\frac{\partial}{\partial z}\iint\limits_{.MS.}d\mathbf{r}'\left[P\left(\mathbf{r}',\mathbf{r}_0,\omega\right)\frac{\partial G_0^{DD}\left(\mathbf{r},\mathbf{r}',\omega\right)}{\partial\mathbf{n}'}\right] \tag{8}$$

If we choose $z\rightarrow\tilde{z}$, which represents the depth of M.S., we approximate

$$\frac{\partial}{\partial z}P\left(\mathbf{r},\mathbf{r}_0,\omega\right)\approx\frac{\partial}{\partial\tilde{z}}P\left(\mathbf{r},\mathbf{r}_0,\omega\right) \tag{9}$$

which will be used to estimate the normal derivatives required in wavelet estimation formula (Weglein and Secrest, 1990).

Rewriting the wavelet estimation based on the Green's function $G_0^D\left(\mathbf{r}_b,\mathbf{r}',\omega\right)$, which only satisfies the Dirichlet condition on free surface,

$$-A(\omega)G_0^D(\mathbf{r}_b,\mathbf{r}_0,\omega) = \iint\limits_{MS} d\mathbf{s}\left[P\left(\mathbf{r},\mathbf{r}_0,\omega\right)\frac{\partial G_0^D\left(\mathbf{r}_b,\mathbf{r},\omega\right)}{\partial \mathbf{n}} - G_0^D\left(\mathbf{r}_b,\mathbf{r},\omega\right)\frac{\partial P\left(\mathbf{r},\mathbf{r}_0,\omega\right)}{\partial \mathbf{n}}\right] \quad (10)$$

where $\mathbf{r}_b$ represents the location below M.S.(Figure 1)
Substitute (8) and (9) into above equation, and we can arrive at

$$A(\omega) \approx \frac{\int d\tilde{x}\left[\underbrace{P\left(\mathbf{r},\mathbf{r}_0,\omega\right)\frac{\partial G_0^D\left(\mathbf{r}_b,\mathbf{r},\omega\right)}{\partial \tilde{z}}}_{A} - \underbrace{G_0^D\left(\mathbf{r}_b,\mathbf{r},\omega\right)\frac{\partial T\left(\tilde{x},z,\mathbf{r}_0,\omega\right)}{\partial z}}_{B}\right]}{-G_0^D\left(\mathbf{r}_b,\mathbf{r}_0,\omega\right) + \underbrace{\int d\tilde{x} G_0^D\left(\mathbf{r}_b,\mathbf{r},\omega\right)\mathbf{R}(\tilde{x},z,\mathbf{r}_0,\omega)}_{C}} \quad (11)$$

Where

$$R(\tilde{x},z,\mathbf{r}_0,\omega) = \frac{\partial}{\partial z}G_0^{DD}(\tilde{x},z,\mathbf{r}_0,\omega)$$

$$\frac{\partial}{\partial z}T\left(\tilde{x},z,\mathbf{r}_0,\omega\right) = \int dx'\left[P\left(x',z',\mathbf{r}_0,\omega\right)\frac{\partial^2 G_0^{DD}\left(\tilde{x},z,x',z',\omega\right)}{\partial z \partial z'}\right]$$

In order to avoid the unstable due to denominator close to zero, we always choose z above M.S. in equation (11).

The triangle relationship states that measured values of $P(\mathbf{r},\mathbf{r}_s,\omega)$ and $\frac{\partial}{\partial n}P(\mathbf{r},\mathbf{r}_s,\omega)$ along a cable and $A(\omega)$ satisfy the exact equation (10). One might think Equ (8), when $\mathbf{r}$ is evaluated on the cable, procides a second independent relationship that would allow $A(\omega)$ to be directly determined from $P(\mathbf{r},\mathbf{r}_s,\omega)$ along the cable. However, Weglein and Amundsen (2003) demonstrate that these are the same relationship. If you temporarily ignore this fact, and substitute equation (8) into equation (10) to 'eliminate' $\frac{\partial}{\partial n}P(\mathbf{r},\mathbf{r}_s,\omega)$, then when $\mathbf{r}$ approaches cable, the expression in the denominator of equation (11) will be zero. The inverse is 'unstable'. To avoid this instability in the inversion, what is being suggested here is that values above the cable for $\frac{\partial}{\partial n}P(\mathbf{r},\mathbf{r}_s,\omega)$ and $\frac{\partial}{\partial n}G_0^{DD}(\mathbf{r},\mathbf{r}_s,\omega)$ are substituted for those at the cable in the integral to avoid the singularity. This has the effect of avoiding a singular division by solving a nearby perturbed problem with the anticipation that this will lead to a stable approximate solution.

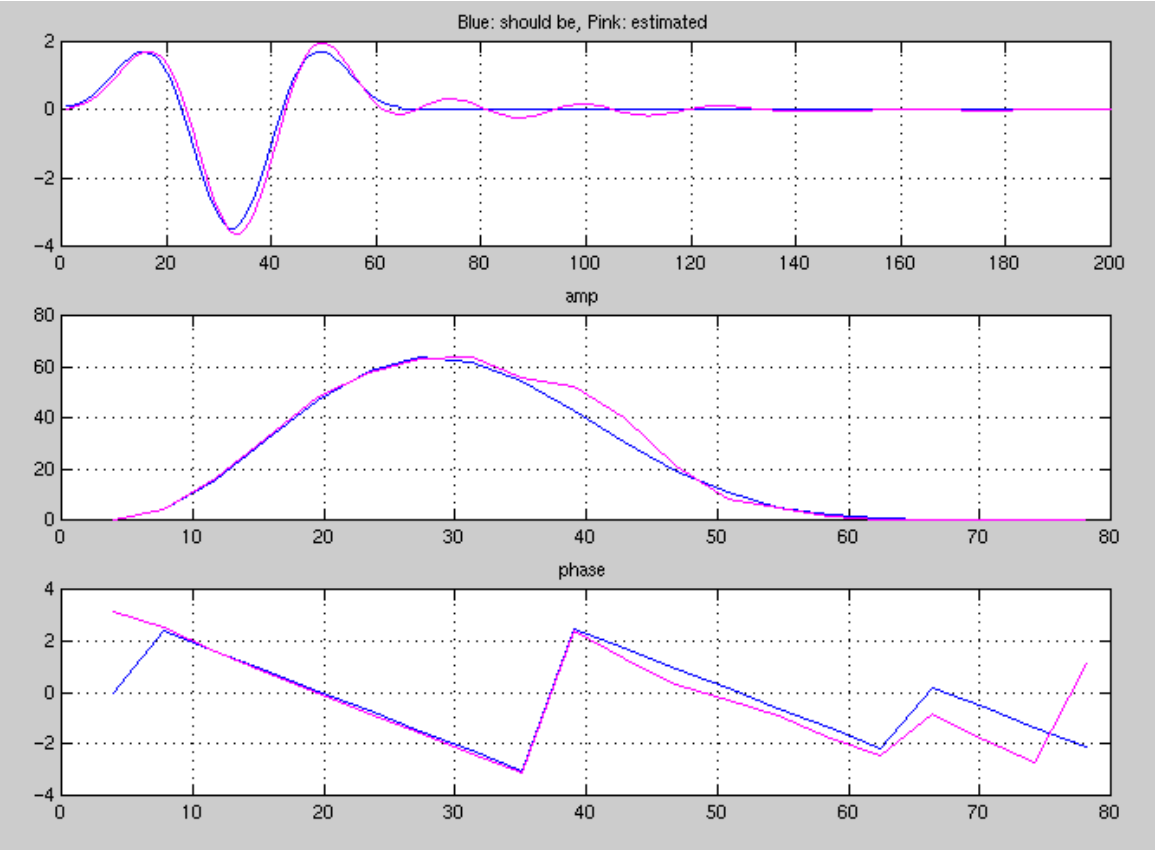

Figure 2: On top is the correct wavelet (blue) and final averaged wavelet (pink); in the middle are the amplitude spectra; and the bottom plot shows the phase spectra.

5 Synthetic example

We make three synthetic datasets with water depth 40m, 60m and 80m respectively. The source is 2m below the free surface, receivers are 6m below the free surface, the receiver interval is 2m (Figure 1). Then equation (10) was used to estimate the wavelet (figure 2). The wavelet estimated from water depth 80m reflector has least artifact; the final averaged of three estimated wavelets is close to the correct one.

Figure 3 shows the amplitudes and phases of correct wavelet and estimated one. We see there are some errors in amplitudes around 40 Hz, and phase change at 8 Hz and 75 Hz.

6 Conclusions

A method for estimating the wavelet directly from the data on a towed streamer was recently proposed by Weglein et al. (2002). That method proposed using the H. Tan (1999) wavefield prediction method to approximate the needed normal derivative along the cable. However, the wavelet method requires an integral over all receivers for a given shot, and the H. Tan prediction is not accurate under the source. In this paper, we propose addressing this problem by not dropping the term which is small only away from the source to achieve an algorithm that is valid for all offsets needed in the integral.

An intrinsic instability in this approach is addressed by seeking an approximate solution that replaces the unstable inversion by a "nearby" (i.e., perturbed) operation. Tests on synthetic data are encouraging; further tests are planned for noise stability and other issues.

Acknowledgements

The authors would like to thank the M-OSRP sponsors and the members of the wavelet estimation working team for their support and helpful discussions.

References

1. Weglein, A.B. and Admundsen, L., 2003, G_0^{DD} and G_0^D integral equations relationships; The triangle relation is intact: Mission-Oriented Seismic Research Program Annual Report, **02**, 40-60.

2. Osen, A., Secrest, B.G., Admundsen, L., and Reitan, A., 1998, Wavelet estimation from marine pressure measurements: Geophysics, **63**, 2108-2119.

3. Tan, T. H., 1999, Wavelet spectrum estimation, Geophysics, **64**, 6, 1836-1846.

4. Verschuur, D. J., Berkhout, A. J. And Wapenaar, C. P. A., 1992, Adaptive surface-related multiple elimination: Geophysics, **57, 1166-1177.**

5. **Weglein, A., Tan, T. H., Matson, etc. 2000, Prediction of the wavefield anywhere above an ordinary towed streamer: Applications to source wavelet estimation, demultiple, and imaging, 70th Ann. Internat. Mtg: Soc. of Expl. Geophys., 2413-2415.**

6. Weglein, A.B., and Secrest, B.G., 1990, Wavelet estimation for a multidimensional acoustic or elastic earth. Geophysics, 55, 902-913.

7. Weglein, A.B., S.A. Shaw, K.H. Matson, J.L. Sheiman, R.H. Stolt, T.H. Tan, A. Osen, G.P. Correa, K.A. Innanen, Z. Guo and J. Zhang, (2002), New approaches to deghosting towed-streamer and ocean-bottom pressure measurements, 72nd SEG Annual Meeting, Salt Lake City, Utah.

Initial tests on deghosting

Jingfeng Zhang and Arthur B. Weglein
University of Houston

Abstract

We present some initial tests on the deghosting algorithm given by Weglein et al. (2002). Given the pressure field on a towed streamer and the wavelet, the algorithm works very well. If the wavelet is not available, we present a way to approximate the wavelet using pressure measurements on a single towed streamer. Numerical tests show that, when using the approximated wavelet, the deghosting algorithm also works well. To the current state of testing, we are encouraged to continue further testing and analysis of the deghosting algorithm for towed streamer data. For ocean bottom pressure measurements and an estimate of the wavelet, we are reporting that early tests indiciate this method will be a stable method for deghosting without a geophone measurement, and is insensitive to the depth of the pressure measurement.

1 Introduction

Deghosting (up/down-going wave field separation) plays an important role in seismic data processing. In particular, it is a prerequisite for wave-theoretic free surface multiple removal algorithms (e.g., Weglein et al. 1997). In turn, the removal of free surface multiples, is a prerequisite for inverse scattering internal multiple attenuation, as well as most imaging algorithms and AVO analysis.

In this paper, we analyze the algorithm presented by Weglein et al. (2002) for the towed streamer case. The basic idea is to first use the data on the measurement surface (ms) to predict the wave field and its derivative on a pseudo-measurement surface ($\tilde{ms}$), then plug the predicted value into an integral which "generates" the deghosted data (or, up-going wave field) on a new surface. The $\tilde{ms}$ must be above the actual ms and then the deghosted data is then output at any point above $\tilde{ms}$.

For the case when the source is positioned between the measurement surface and the free surface, we have also tried to apply this deghosting algorithm without knowledge of the source wavelet.

Calculations, have shown that, without knowledge of the source wavelet, the wave field is well predicted, even directly under the source as long as $\tilde{ms}$ is close to the actual ms; the

predicted derivative of the wave field is good only for the positions with large offset. For positions directly under the source, the result for the derivative of the field is poor. In order to predict a good derivative of the wave field under the source, we provide a way to approximate the wavelet that relies on the assumption that a term containing the integral of the scattered field is relatively small compared to a similiar term containing the integral of the direct wave field $A(\omega)G_0^D(\mathbf{r}^{''},\mathbf{r}_s,\omega)$.

In the following, we briefly list the necessary formulae in the theory section and then present the results of numerical tests.

2 Theory

The deghosting formula is (Weglein et al., 2002):

$$P^{\text{deghosted}}(\mathbf{r},\mathbf{r}_s,\omega)=\int\limits_{ms}\left(P(\mathbf{r}^{'},\mathbf{r}_s,\omega)\frac{\partial G_0^+(\mathbf{r},\mathbf{r}^{'},\omega)}{\partial\mathbf{n}^{'}}-G_0^+(\mathbf{r},\mathbf{r}^{'},\omega)\frac{\partial P(\mathbf{r}^{'},\mathbf{r}_s,\omega)}{\partial\mathbf{n}^{'}}\right)d\mathbf{s}^{'} \qquad (1)$$

where G_0^+ is the causal Green's function in the reference medium. If we have the field and its derivative on the measurement surface, then the integral in equation (1) provides the deghosted field. However, in a conventional towed-streamer marine survey, we usually only measure the field, and not its normal derivative. In this research, we are investigating the effectiveness of equation (1) using data on the ms to predict the field and its derivative on a new pseudo measurement surface ($\tilde{ms}$). If successful, we can perform deghosting using equation (1) on $\tilde{ms}$.

The wavefield and its normal derivative predicted above the cable are (T.H. Tan, 1992 and 1999, A. Osen, 1998 and Weglein et al., 2002):

$$P(\mathbf{r}^{''},\mathbf{r}_s,\omega)=A(\omega)G_0^{DD}(\mathbf{r}^{''},\mathbf{r}_s,\omega)+\int\limits_{ms}P(\mathbf{r}^{'},\mathbf{r}_s,\omega)\frac{\partial G_0^{DD}(\mathbf{r}^{'},\mathbf{r}^{''},\omega)}{\partial\mathbf{n}^{'}}d\mathbf{s}^{'} \qquad (2)$$

$$\frac{\partial P(\mathbf{r}^{''},\mathbf{r}_s,\omega)}{\partial\mathbf{n}^{''}}=A(\omega)\frac{\partial G_0^{DD}(\mathbf{r}^{''},\mathbf{r}_s,\omega)}{\partial\mathbf{n}^{''}}+\int\limits_{ms}P(\mathbf{r}^{'},\mathbf{r}_s,\omega)\frac{\partial^2 G_0^{DD}(\mathbf{r}^{'},\mathbf{r}^{''},\omega)}{\partial\mathbf{n}^{'}\partial\mathbf{n}^{''}}d\mathbf{s}^{'}, \qquad (3)$$

respectively. In equations (2) and (3), the prediction needs the field on the ms and the source wavelet, $A(\omega)$. G_0^{DD} is the Green's function that vanishes both at the free surface and the ms. In principle, the above formulae are exact. We will see in the numerical test that using these formulae, we get very good deghosting results.

In many cases the source wavelet, $A(\omega)$, is not available. However, for cable depths ~ 6.0m, and wave velocity ~ 1500m/s, and frequencies $f < 125$Hz, G_0^{DD} and its derivative vanish very quickly with increasing offset (T.H. Tan, 1999 and Weglein et al., 2002). So, at large offsets, we can safely ignore the first terms in equations (2) and (3). That is,

$$P(\mathbf{r}^{''}, \mathbf{r}_s, \omega) \approx \int\limits_{ms} P(\mathbf{r}^{'}, \mathbf{r}_s, \omega) \frac{\partial G_0^{DD}(\mathbf{r}^{'}, \mathbf{r}^{''}, \omega)}{\partial \mathbf{n}^{'}} d\mathbf{s}^{'} \tag{4}$$

$$\frac{\partial P(\mathbf{r}^{''}, \mathbf{r}_s, \omega)}{\partial \mathbf{n}^{''}} \approx \int\limits_{ms} P(\mathbf{r}^{'}, \mathbf{r}_s, \omega) \frac{\partial^2 G_0^{DD}(\mathbf{r}^{'}, \mathbf{r}^{''}, \omega)}{\partial \mathbf{n}^{'} \partial \mathbf{n}^{''}} d\mathbf{s}^{'} \tag{5}$$

where $\mathbf{r}^{''}$ is on $\tilde{ms}$ and $\mathbf{r}^{'}$ on actual ms, $\mathbf{r}$ is the deghosted output data point, $\mathbf{r}$ is above $\mathbf{r}^{''}$, and $\mathbf{r}^{''}$ is above $\mathbf{r}^{'}$.

We have found, through analytic and numerical tests, that when $\tilde{ms}$ is close to ms, equation (4) works very well everywhere on the $\tilde{ms}$, including at positions directly under the source. However, equation (5) for the derivative of the field works well only at large offsets. For positions under the source, the first term on the right-hand side of equation (3) dominates and so it can not be ignored. In order to work around this issue, we approximate the source wavelet from the data on the measurement surface so that we can include this dominant term.

Notice that the field in the integral in the above formulae consist of two parts: the direct wave $P_0 = A(\omega) G_0^D$ and the scattered field P_s.

$$\begin{aligned}
&\int\limits_{ms} P(\mathbf{r}^{'}, \mathbf{r}_s, \omega) \frac{\partial G_0^{DD}(\mathbf{r}^{'}, \mathbf{r}^{''}, \omega)}{\partial \mathbf{n}^{'}} d\mathbf{s}^{'} \\
= &\int\limits_{ms} \left[A(\omega) G_0^D(\mathbf{r}^{'}, \mathbf{r}_s, \omega) + P_s(\mathbf{r}^{'}, \mathbf{r}_s, \omega) \right] \frac{\partial G_0^{DD}(\mathbf{r}^{'}, \mathbf{r}^{''}, \omega)}{\partial \mathbf{n}^{'}} d\mathbf{s}^{'} \\
= &\ A(\omega) \int\limits_{ms} G_0^D(\mathbf{r}^{'}, \mathbf{r}_s, \omega) \frac{\partial G_0^{DD}(\mathbf{r}^{'}, \mathbf{r}^{''}, \omega)}{\partial \mathbf{n}^{'}} d\mathbf{s}^{'} \\
+ &\int\limits_{ms} P_s(\mathbf{r}^{'}, \mathbf{r}_s, \omega) \frac{\partial G_0^{DD}(\mathbf{r}^{'}, \mathbf{r}^{''}, \omega)}{\partial \mathbf{n}^{'}} d\mathbf{s}^{'}
\end{aligned} \tag{6}$$

and

$$\int\limits_{ms} P(\mathbf{r}^{'}, \mathbf{r}_s, \omega) \frac{\partial^2 G_0^{DD}(\mathbf{r}^{'}, \mathbf{r}^{''}, \omega)}{\partial \mathbf{n}^{'} \partial \mathbf{n}^{''}} d\mathbf{s}^{'}$$

$$= A(\omega) \int_{ms} G_0^{DD}(\mathbf{r}', \mathbf{r}_s, \omega) \frac{\partial^2 G_0^{DD}(\mathbf{r}', \mathbf{r}'', \omega)}{\partial \mathbf{n}' \partial \mathbf{n}''} d\mathbf{s}' + \int_{ms} P_s(\mathbf{r}', \mathbf{r}_s, \omega) \frac{\partial^2 G_0^{DD}(\mathbf{r}', \mathbf{r}'', \omega)}{\partial \mathbf{n}' \partial \mathbf{n}''} d\mathbf{s}' \qquad (7)$$

In the next section, we show that for positions directly under the source on the $\tilde{ms}$, the effect of P_0 is much larger than that of P_s. In that case, we may assume the effect of P_s is zero. Then, since the left-hand side of equation (6) and (7) are known, we can get two estimates of the wavelet, $A(\omega)$: one from equation (6) and the other from equation (7).

For the case when the source is below the ms, equations (4) and (5) are exact and so knowledge of the wavelet $A(\omega)$ is not required. It may be easier to understand through the derivation of equations (2) and (3).

3 Numerical test

We generate a synthetic data set described in Fig. 1. There are four sources in the model. S1 corresponds to the actual air gun with wavelet $A1(\omega)$. S2, S3 and S4 are passive sources, with wavelet $A2(\omega)$, $A3(\omega)$ and $A4(\omega)$ respectively, synthesized in order to give an up-going field on the ms The free surface is modeled as a perfect reflector. The distance between the ms and the free surface is $b = 6.0$ m. All calculations are performed in the frequency domain and we present results for the single frequency k=0.3 m^{-1} (or $f \sim 74Hz$, for water speed=1500m/s). In all cases, the distance between $\tilde{ms}$ and ms is 0.1m and the deghosted data ouput points are 0.1m above $\tilde{ms}$. In our calculations, we have chosen $A(\omega)$ to be real and equal to 1.0. Therefore, we compare only the real part of the P, $\frac{\partial P}{\partial \mathbf{n}}$ and $P^{\mathrm{deg}\,hosted}$.

The total wave field on M.S and exact up-going field are shown in Fig. 2. Figure 3 is the result of the deghosting algorithm using the wavelet $A1(\omega)$ compared to the exact up-going field. The results are very good.

However, if we don't have the wavelet, we use equations (4) and (5) to approximate the field and its derivative, and then use equation (1) to do deghosting. These results are showed in Fig. 10. Why do we get such poor results? Figures 4 and 5 show the predicted wave field and derivative of the wave field, respectively, when we don't know the wavelet. From these graphs, we see that the problem is the derivative of the wave field near the source. For positions near the source, $A(\omega)\frac{\partial G_0^{DD}(\mathbf{r}'', \mathbf{r}_s, \omega)}{\partial \mathbf{n}''}$ in equation (3) makes a large contribution and so we can't ignore it in our prediction.

In order to get a better derivative of the wave field near the source, we first try to get an approximate wavelet so that we can include $A(\omega)\frac{\partial G_0^{DD}(\mathbf{r}'', \mathbf{r}_s, \omega)}{\partial \mathbf{n}''}$. As has been described, we

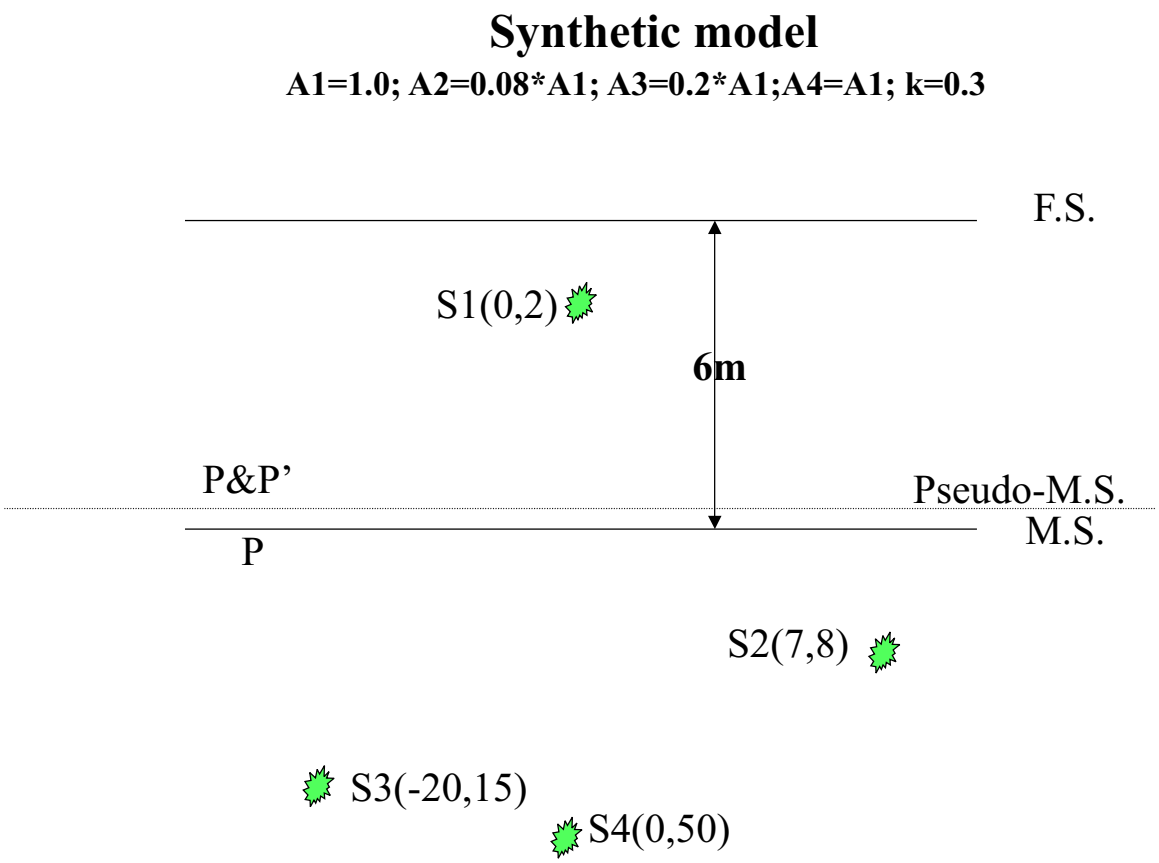

Figure 1: Synthetic model. S1 corresponds to the active source. S2, S3 and S4 are three sources that generate the up-going field. Their (x, z) coordinates are given. All of the calculations are restricted to one frequency k=0.3.

can get an approximation of the wavelet in Fig. 6 and Fig. 7 which show the first term and the sum of the first term and the second term, respectively, in equations (6) and (7). We find that for positions directly under the source, the first term dominates, especially in equation (6). Hence, we can get an approximate value for the wavelet $A = 0.9982$ in Fig. 6 and $A = 1.135$ in Fig. 7., while the exact value is 1.0. Then we add the corresponding first term in equations (2) and (3), respectively, to the predicted value from equations (4) and (5). The new results for the predicted field and its derivative are presented in Fig. 8 and Fig. 9. Using these new results, we do deghosting as before. The results, shown in Fig. 10, are encouraging.

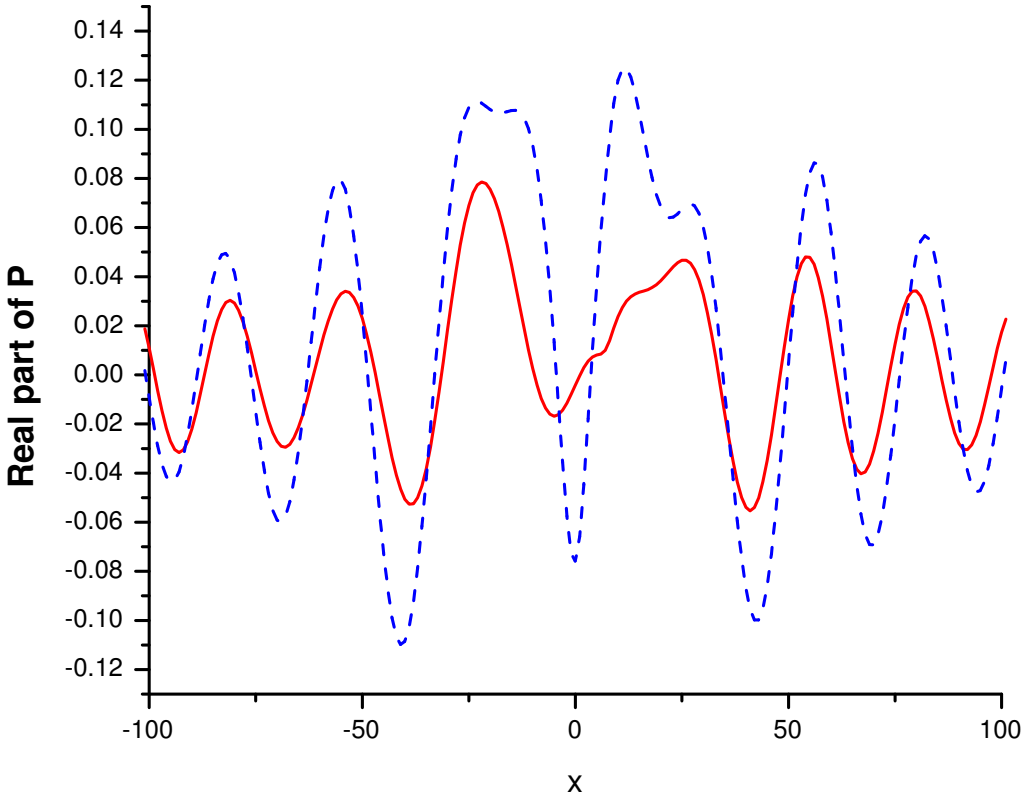

Figure 2: Red solid: Exact total field on ms. Blue dash: Exact up-going field on the surface 0.2m above the ms. x is the source-receiver offset along the ms.

4 Conclusion and discussion

In this paper we have presented some initial tests of the deghosting algorithm given by Weglein et al. (2002). Using the source wavelet, this method works well. For the ocean bottom case, if we have the pressure measurements and the source wavelet, we can use the triangle relationship among pressure, derivative of pressure and the source wavelet to predict the derivative of pressure (Amundsen et al. 1995). We anticipate that this algorithm will be robust (insensitive to depth) and give useful results.

It's important to note that we would like to keep the instrument response factor in the field data and in estimation of the wavelet that derived from other measurements. So, the source wavelet, pressure and the resulted derivative of pressure will have the same factor and the deghosted data will have the same instrument response.

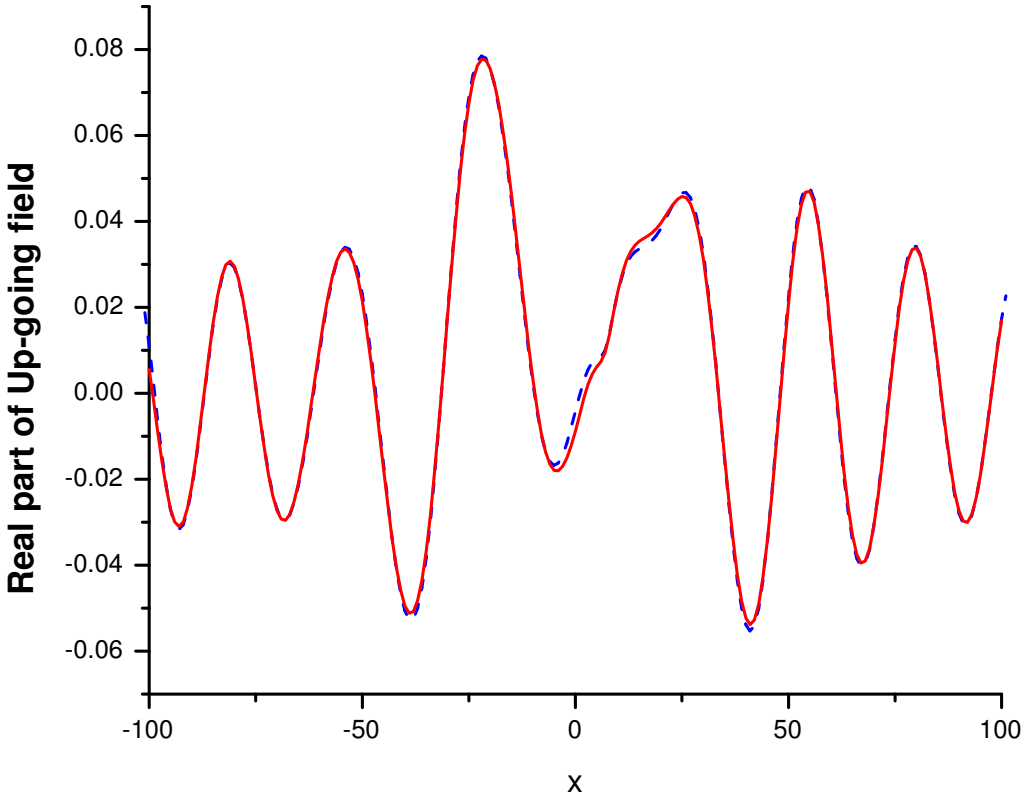

Figure 3: Red solid: Exact up-going field on the surface 0.2m above the ms. Blue dash: Deghosting algorithm results using exact source wavelet. x is the source-receiver offset along the ms.

For towed streamer data if we don't know the wavelet, we provide an approximation method to get the wavelet using only measurements of pressure along the measurement surface. Further tests will be needed before we deal with field data.

Acknowledgements

We thank Simon Shaw, T.H.Tan, Gustavo Correa and Haiyan Zhang for helpful discussions.

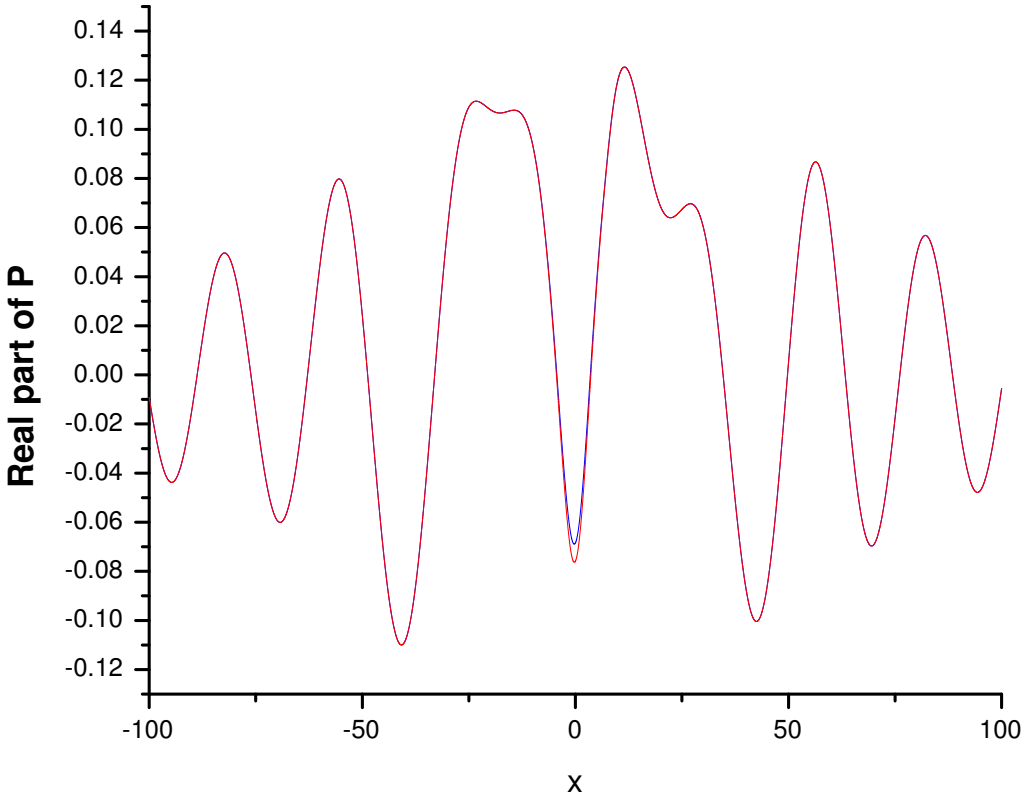

Figure 4: Red solid: Exact field on $\tilde{m}s$. Blue dash: Predicted field on $\tilde{m}s$ without using wavelet.

References

1. Amundsen, L., B.G. Secrest and B. Arntsen, 1995, Extraction of the normal component of the particle velocity from marine pressure data: Geophysics, **60**, 212-222.

2. Osen, A., B.G. Secrest, L.Admundsen and A. Reitan, 1998, Wavelet estimation from marine pressure measurements: Geophysics, **63**, 2108-2119.

3. Tan, T.H., 1992, Source signature estimation: Presented at the Internat. Conf. And Expo. Of Expl. And Development Geophys., Moscow, Russia

4. Tan, T.H., 1999, Wavelet spectrum estimation: Geophysics, **64**, 6, 1836-1846

5. Weglein, A.B., S.A. Shaw, K.H. Matson, J.L. Sheiman, R.H. Stolt, T.H. Tan, A.

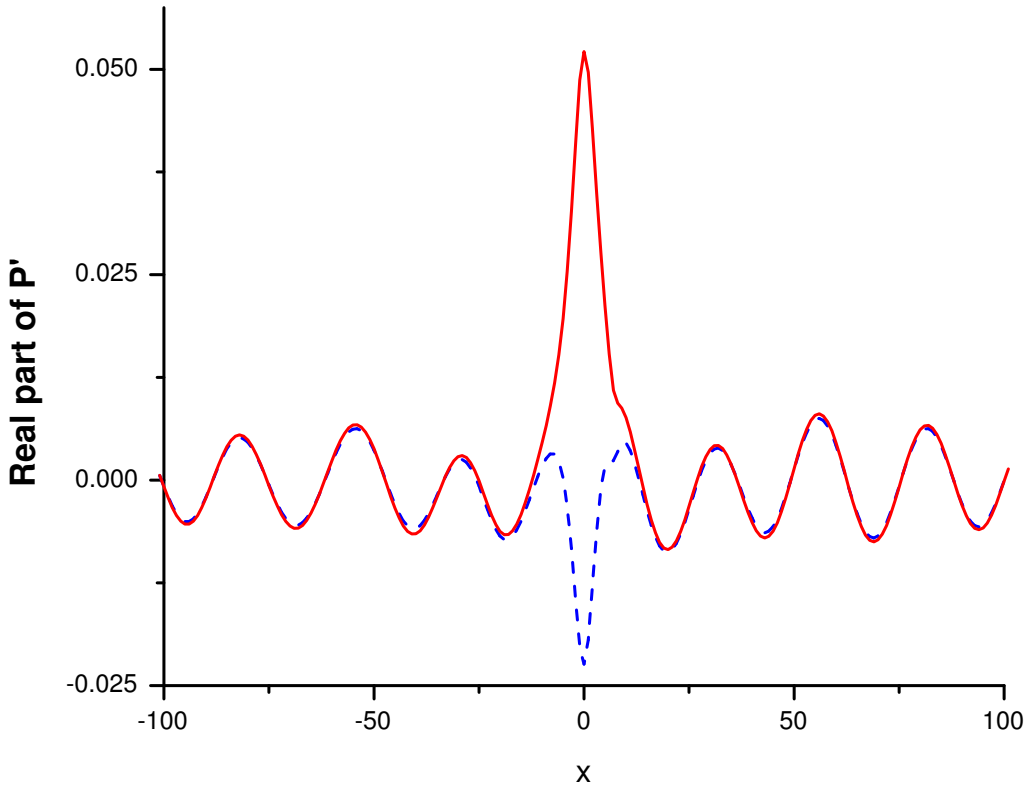

Figure 5: Red solid: Exact derivative of field on $\tilde{m}s$. Blue dash: Predicted derivative of field on $\tilde{m}s$.

Osen, G.P. Correa, K.A. Innanen, Z. Guo and J. Zhang, (2002), New approaches to deghosting towed-streamer and ocean-bottom pressure measurements, 72nd SEG Annual Meeting, Salt Lake City, Utah.

General References

1. Amundsen, L., 1993, Wavenumber-based filtering of marine point source data: Geophysics, **58**, 1335-1348.

2. Ball, V.L. and Corrigan, D., 1996, Dual sensor summation of noisy ocean-bottom data, 66th Ann. Internat. Mtg: Soc. of Expl. Geophys., 28-31.

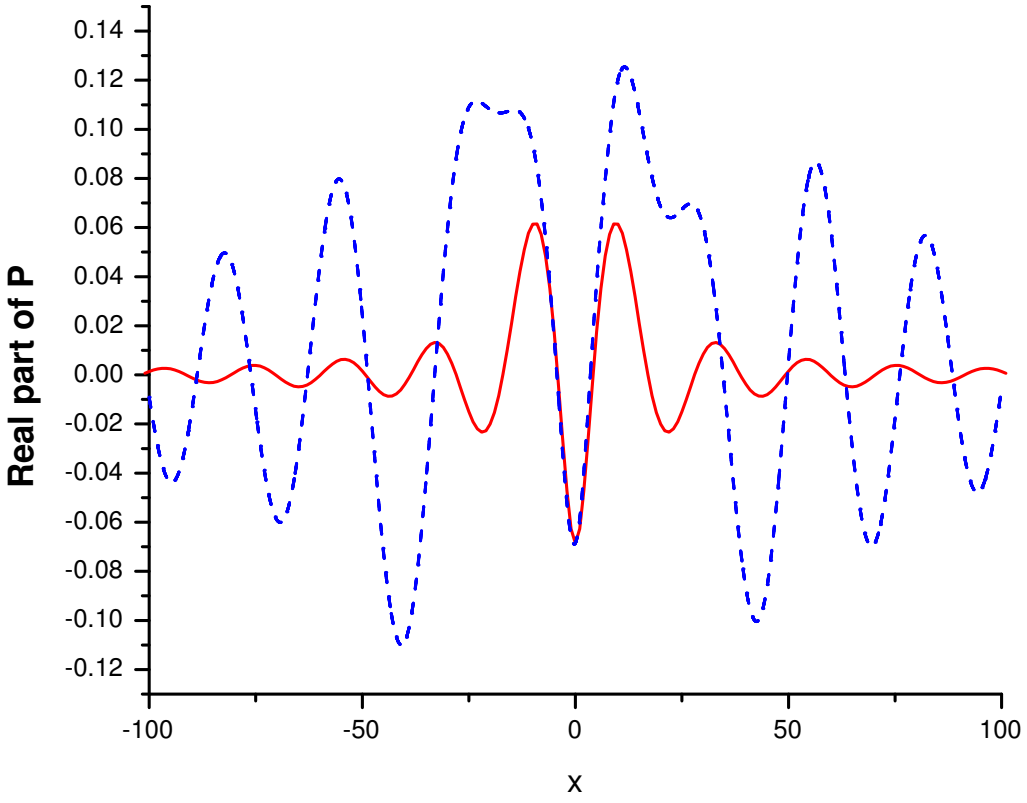

Figure 6: Red solid: The integral value due to the direct wave in Equation (6). Blue dash: The total integral value in Equation (6).

3. Barr, F.F. and Sanders, J.I., 1989, Attenuation of water column reverberations using pressure and velocity detectors in a water-bottom cable, 59th Ann. Internat. Mtg: Soc. of Expl. Geophys., 653-656.

4. Delima, G.R., Weglein, A.B., Porsani, M.J., and Ulrych, T.J., 1990, Robustness of a new source-signature estimation method under realistic data conditions: A deterministic-statistical approach: 60^{th} Ann. Internat. Mtg. SOc. Expl. Geophys. Expanded Abstracts, 1658-1660.

5. Dragoset, B., and Barr, F.J., 1994, Ocean-bottom cable dual-sensor scaling: 64^{th} Ann. Internat. Mtg. SOc. Expl. Geophys. Expanded Abstracts, 857-860.

6. Fokkema, J., and van den Berg, P.M., 1993, Seismic applications of acoustic reciprocity:

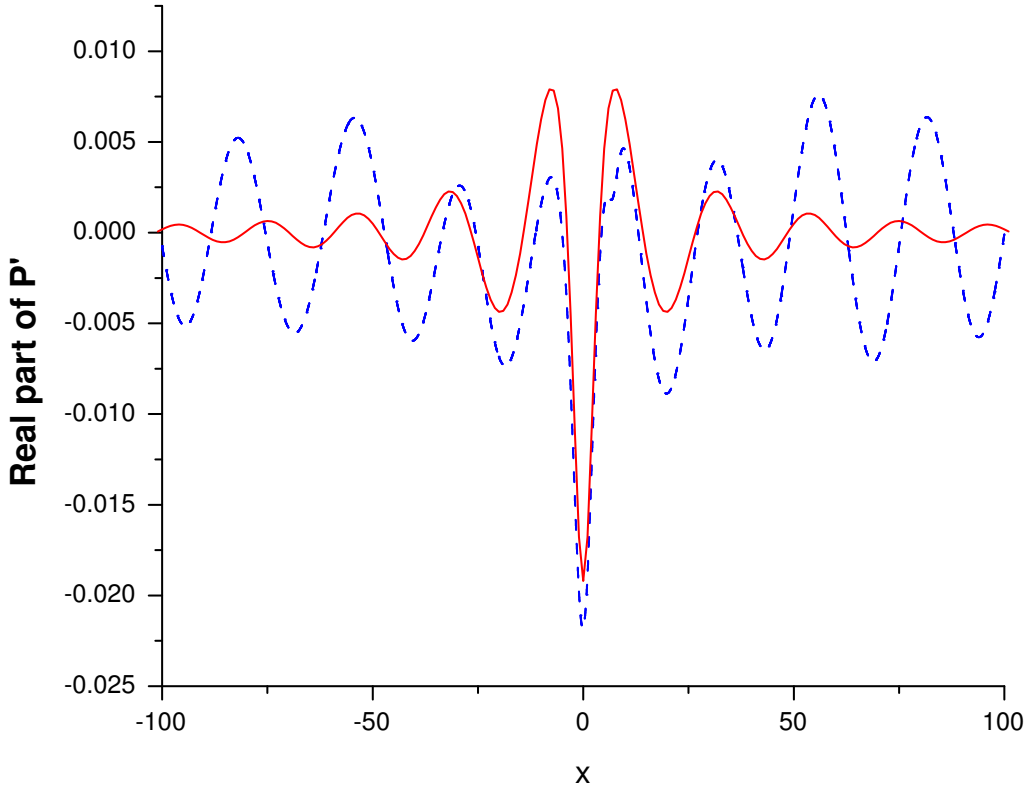

Figure 7: Red solid: The integral value due to the direct wave in Equation (7). Blue dash: The total integral value in Equation (7).

Elsevier Science Publ..

7. Schneinder, W.A., Larner, K.L., Burg, J.P., and Backus, M.M., 1964, A new data processing technique for the elimination of ghost arrivals on reflection seismograms: Geophysics, **29**, 5, p. 783-805

8. Weglein, A.B., Tan, T.H., Shaw, S.A., Matson, K.H., Foster, D.J., 2000, Prediction of the wavefield anywhere above an ordinary towed streamer, 70^{th}Annual Meeting of the Society of Exploration Geophysicists, Calgary, Canada.

9. Ziolkowski, A., 1980, Source array scaling for wavelet deconvolution: Geophysical Prospecting, **28**, 902-918

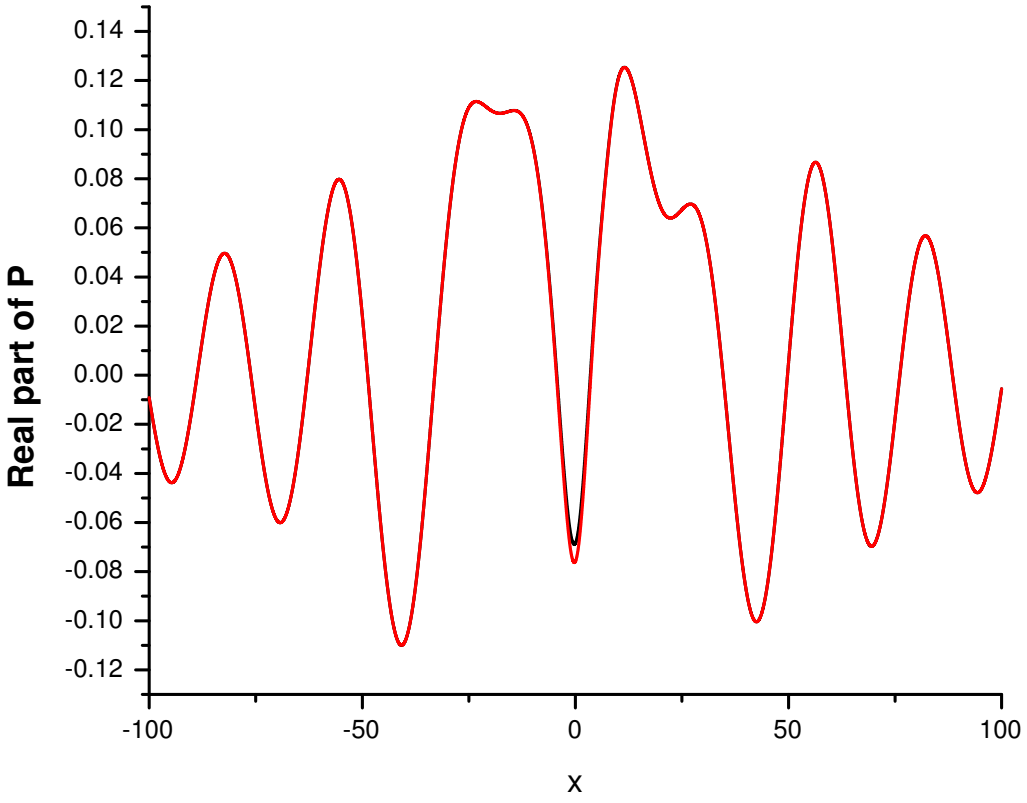

Figure 8: Red solid: Exact field on $\tilde{m}s$. Blue dash: Predicted field on $\tilde{m}s$ using estimated wavelet 0.9982 (covered by red). Black solid: Predicted field on $\tilde{m}s$ without using wavelet.

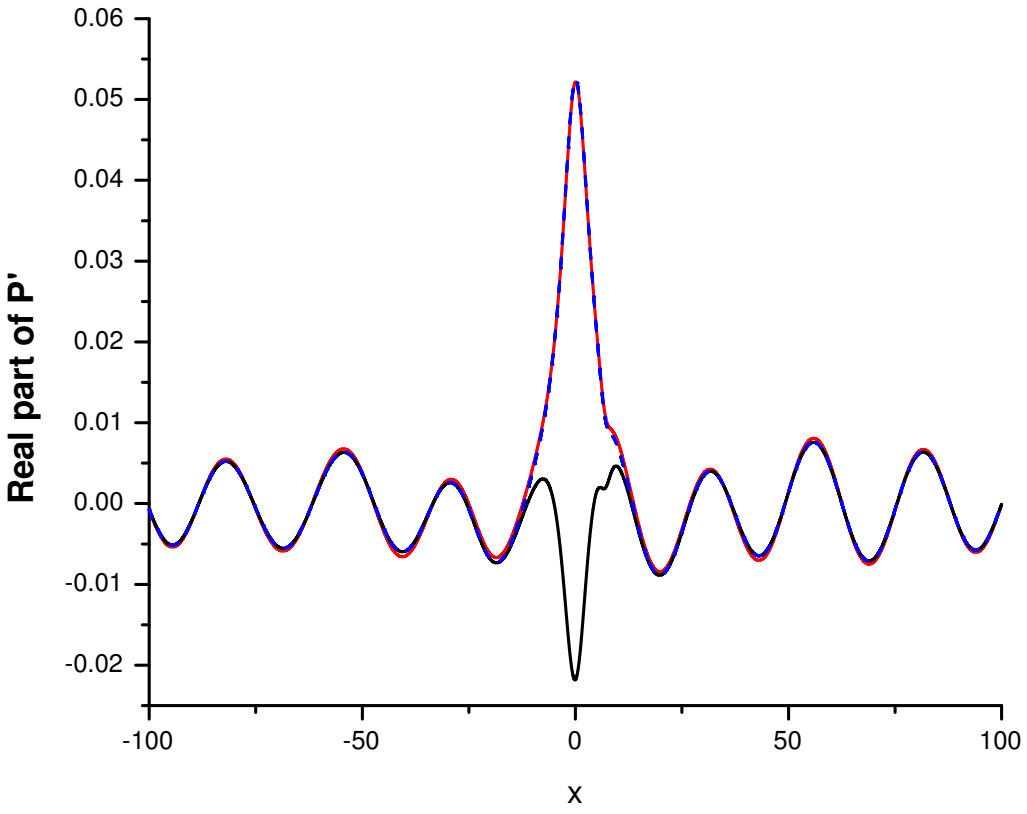

Figure 9: Red solid: Exact derivative of field on $\tilde{m}s$. Blue dash: Predicted derivative of field on $\tilde{m}s$ using estimated wavelet 0.9982 (covered by red). Black solid: Predicted derivative of field on $\tilde{m}s$ without using wavelet.

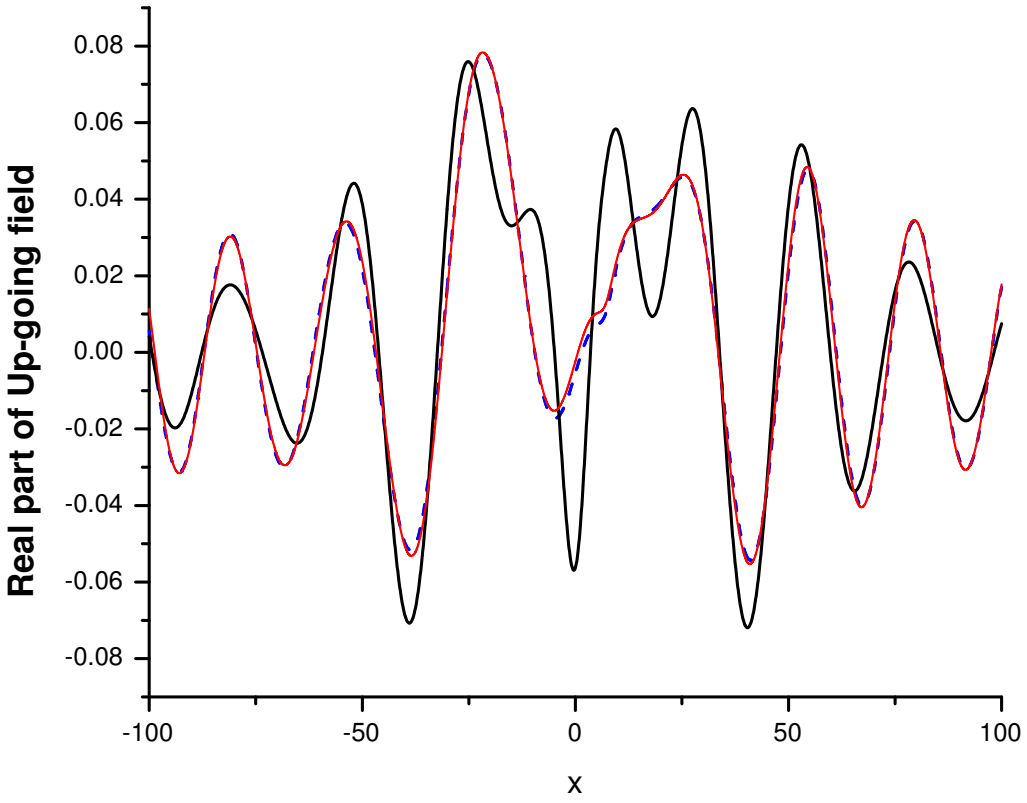

Figure 10: Red solid: Exact up-going field on surface 0.2m above the ms. Blue dash: Deghosting algorithm results using estimated wavelet (0.9982). Black solid: Deghosting algorithm results without using wavelet.

Initial analysis of the effect of receiver arrays on wavelet estimation based on the Extinction Theorem

Lianzhong Feng, Jingfeng Zhang and Arthur B. Weglein
University of Houston

Abstract

We present initial numerical tests on the effect of receiver arrays on the wavelet estimation method presented by Weglein and Secrest (1990). The numerical tests demonstrate that for single sensor receivers, the estimation method is successful. However for group receivers, the results are unsatisfactory, especially when the intended use is for the inverse scattering subseries that are non-linear in the wavelet.

1 Introduction

In 1990, Weglein and Secrest presented the following wavelet estimation formula:

$$A(\omega) = \frac{1}{G_0^D(\vec{r},\vec{r}_s,\omega)} \cdot \oint_S \left[p\left(\vec{r}',\vec{r}_s,\omega\right) \frac{\partial G_0^D\left(\vec{r}',\vec{r},\omega\right)}{\partial \vec{n}'} - G_0^D\left(\vec{r}',\vec{r},\omega\right) \frac{\partial p\left(\vec{r}',\vec{r}_s,\omega\right)}{\partial \vec{n}'} \right] d\vec{s}' \quad (1)$$

where G_0^D is the Green's function which vanishes at the free surface. $\vec{r}$ is any point under the measurement surface and $\vec{r}_s$ is the position of the active source, which is above the measurement surface. $\vec{n}'$ is the unit vector on the measurement surface pointing towards the free surface.

In principle, equation (1) is exact. Tests on synthetic data demonstrated its robustness in the presence of finite aperture and sampling. But when equation (1) was applied to field data with under-over cables and arrays, the results were unsatisfactory. A possible explanation points to the effect of the receiver group. When the wave's propagation direction is near-horizontal, the combination of receivers suffers from the phase difference among the individual receivers in a group (Figure 1). That is, the field and derivative of the field in the above formula are both distorted resulting in a poor approximation of the wavelet.

In this report we provide numerical tests designed to establish whether this conjecture is correct. These tests indicate excellent result for single sensor receivers but even for a short array, harmful effects are observed.

We present the results of numerical tests in the following section which is followed by conclusions drawn from this exercise.

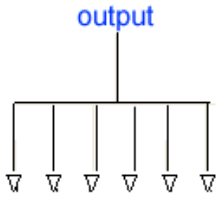

Figure 1: The receiver array.

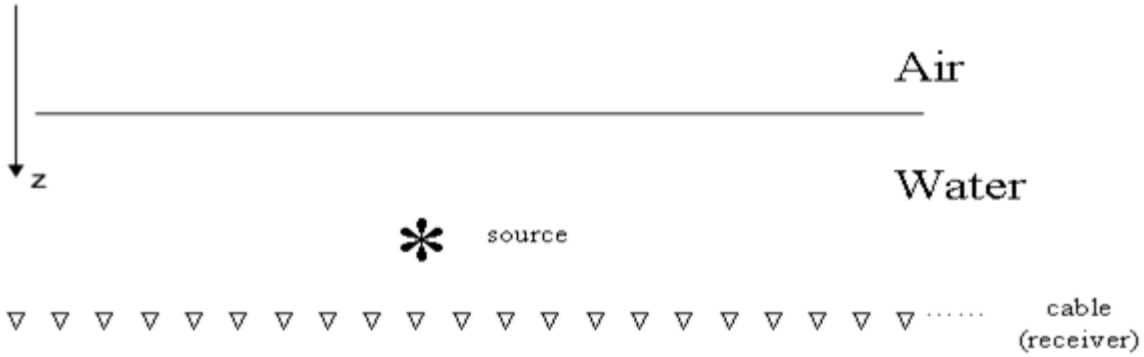

Figure 2: Synthetic model.

2 Numerical test

The synthetic model is showed in Figure.2 where the depth of the measurement surface is 10.0m. There is a perfect reflection on the free surface and this study assumes an infinite water column. The position of the active source is (0,6). We assume that we have the exact field and its derivative everywhere on the measurement surface. We evaluated equation at (0,100).

For single sensor receivers with interval 1.0m (geometry 1 in Figure 3), the resulted wavelet

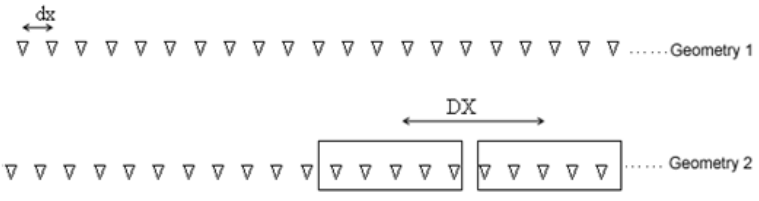

Figure 3: Receiver pattern.

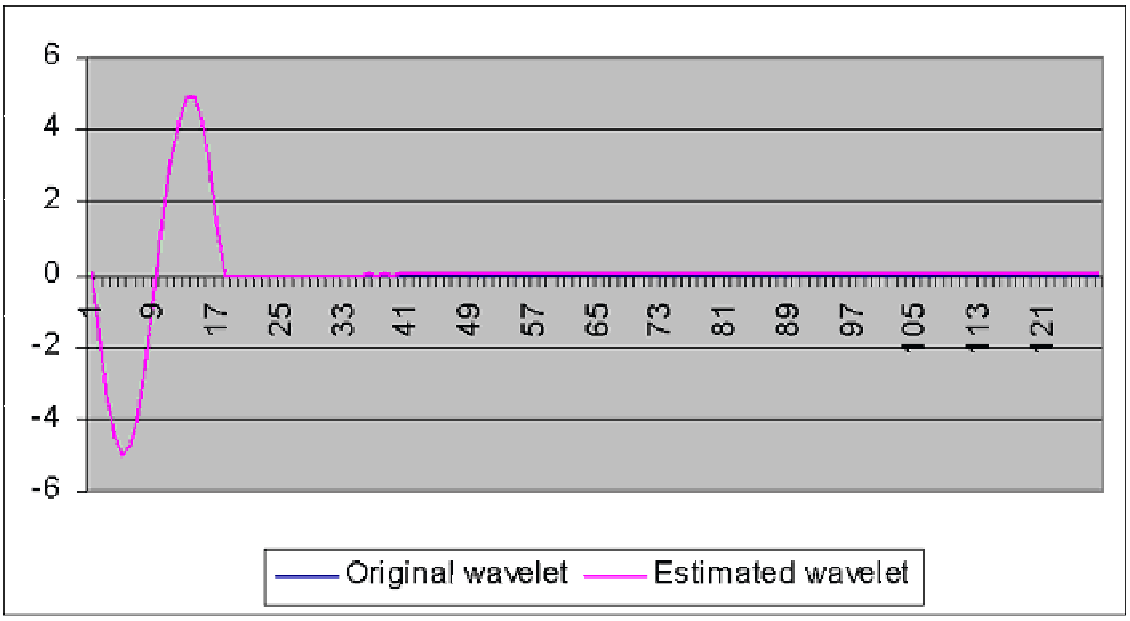

Figure 4: Comparing the original wavelet with the calculated wavelet for geometry 1 (dx=1.0m).

from the equation (1) is compared with the exact wavelet in Figure 4. There is no visible difference between these two signals.

For group receivers (geometry 2 in Figure 3), we consider the case that interval between single receivers is 1.0m and there are 9 receivers in one group. Therefore the group interval will be 9.0m. The results are shown in Figure 5. Clearly, the results are unsatisfactory. In Fig.6, the exact wavelet is compared with the calculated wavelet divided by the number of receivers in an array. The result is also unsatisfactory.

3 Conclusion

We have presented initial numerical tests showing that, even for a small array (9 receivers, 8 meters), using a receiver group can have a deleterious effect on the wavelet estimation methods that are reconstructing the reference wave and canceling the scattered wavefield. The industry trend toward ever-smaller receiver arrays and single sensors is an opportunity to exploit those multidimensional wave theoretic wavelet estimation methods precluded by earlier acquisition formats. For single sensor receivers, the results are acceptable as expected.

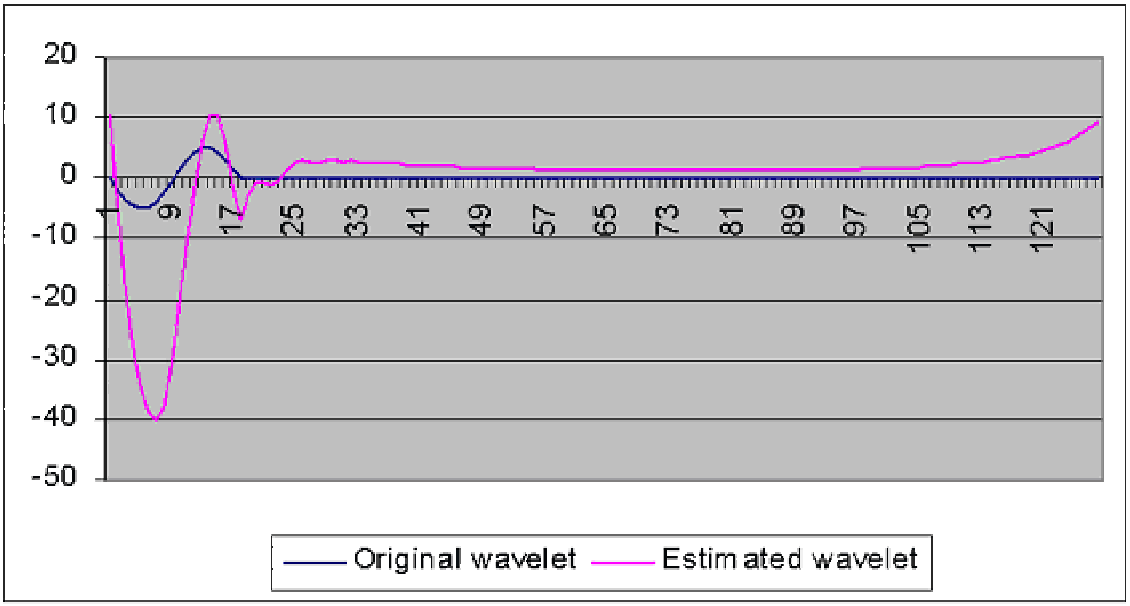

Figure 5: Comparing the original wavelet with the calculated wavelet for geometry 2 (dx=1.0m, nine receivers, DX=9.0m).

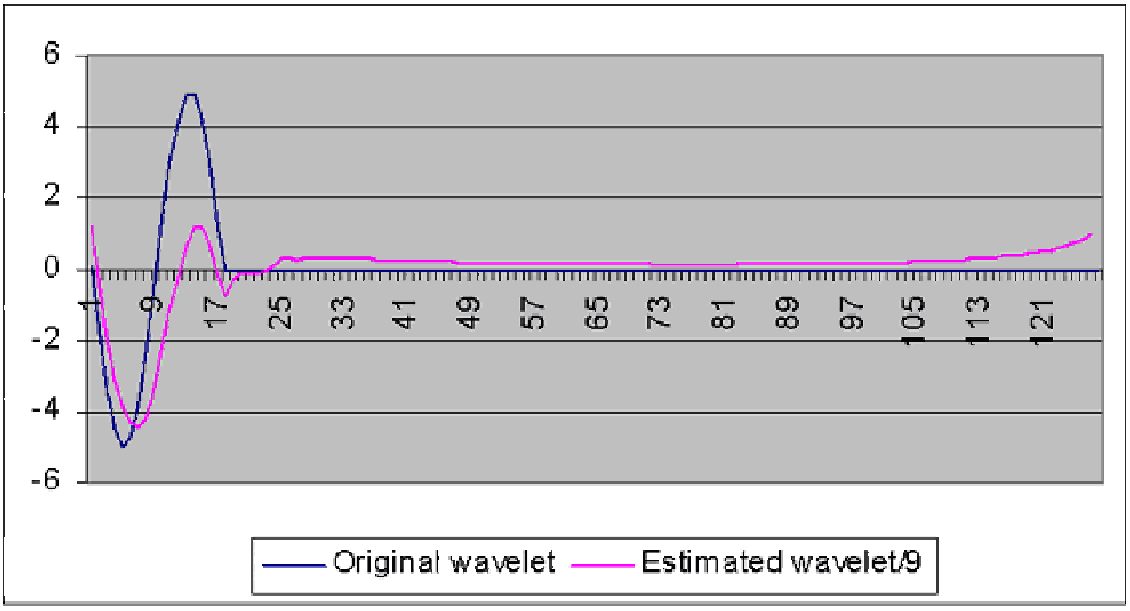

Figure 6: Comparing the original wavelet with the calculated wavelet for geometry 2 (the calculated wavelet has been divided by the number of receivers in one group) (dx=1.0m, nine receivers, DX=9.0m).

References

1. Delima, G. R., Weglein, A. B., Porsani, M. J., and Ulrych, T. J., 1990, Robustness of a new source-signature estimation method under realistic data condition: A deterministic-statistical approach: 60th Ann. Internat. Mtg. Soc. Expl. Geophys, Expanded Abstract, 1658-1660

2. Weglein, A. B. and Secrest, G., 1990, Wavelet estimation for multidimensional acoustic or elastic earth: Geophysics, 55, P.902-913

General reading

1. Tan, T.H., 1992, Source signature estimation: Presented at the Internat. Conf. And Expo. Of Expl. And Development Geophys., Moscow, Russia

2. Tan, T.H., 1999, Wavelet spectrum estimation: Geophysics, **64**, 6, 1836-1846

Short note: G_0^{DD} and G_0^D integral equations relationships; The triangle relation is intact

Arthur B. Weglein[1] and Lasse Amundsen[2]
[1] University of Houston, [2] Statoil Research Center

Abstract

Weglein and Secrest (1990) established a relationship between the total pressure wavefield measured on the cable, the vertical derivative of that wavefield and the source signature. Amundsen et al (1995) and Corrigan et al (1991) use the triangle relationship to solve for $\frac{dP}{dn}$ from $A(\omega)$ and P along the cable. Tan (1992, 1999) and Osen et al. (1998) establish a relationship between the pressure wavefield along the cable, a single pressure measurement, between the free-surface and the cable, and the wavelet. We demonstrate how these two formulations relate to each other, and in that process establish that, in fact, they correspond to the same relationship between P and P', along the cable, and the wavelet, $A(\omega)$.

1 Definition

We present this analysis for a 1D version of these extinction theorem applications, for estimating the wavelet, since we understand that a Fourier transform over the lateral spatial variables in 2D and 3D leads to this precise 1D form (where $k_z = \sqrt{(\omega/c_0)^2 - k_x^2 - k_y^2}$ would substitute for $k = \omega/c_0$ in this paper) and z and z' would be depth variables.

We begin by defining G_0, G_0^D and G_0^{DD} as the causal whole space Green's function, the Green's function with Dirichlet boundary conditions on the free-surface, and the "double Dirichlet" Green's function vanishing on the free-surface and cable, respectively.

$G_0(z, z', \omega)$ satisfies the differential equation

$$\left(\frac{d^2}{dz^2} + k^2\right) G_0(z, z', \omega) = \delta(z - z') \tag{1}$$

for $0 \leq z, z' \leq a$ where $z = a$ is the measurement surface and $z = 0$ is the free surface. G_0^{DD} is the solution to equation (1) that vanishes at $z = 0$ and $z = a$. The general solution to (1) for any boundary conditions is

$$Ae^{ikz} + Be^{-ikz} + \frac{e^{ik|z-z'|}}{2ik} = G_0(z, z', \omega) \tag{2}$$

for $0 \leq z, z' \leq a$ and imposing

$$G_0(0, z', \omega) = 0 \tag{3}$$
$$G_0(a, z', \omega) = 0 \tag{4}$$

we find $G_0^{DD}(z, z', \omega)$ (the double D superscript denotes Dirichlet boundary conditions on two surfaces, $z = 0$ and $z = a$) to be

$$\begin{aligned} G_0^{DD}(z, z', \omega) = & \frac{1}{2ik}\left[\frac{e^{ik(z'-a)} - e^{-ik(z'-a)}}{e^{ika} - e^{-ika}}\right] e^{ikz} \\ & -\frac{1}{2ik}\left[\frac{e^{ika}\left(e^{ikz'} - e^{-ikz'}\right)}{e^{ika} - e^{-ika}}\right] e^{-ikz} + \frac{e^{ik|z-z'|}}{2ik}. \end{aligned} \tag{5}$$

Equation (5) can be combined

$$G_0^{DD} = \frac{1}{2ik}\frac{e^{ik(z-z')}}{1 - e^{2ika}}\left(1 - e^{2ikz'}\right)\left(1 - e^{2ik(a-z)}\right). \tag{6}$$

The last expression for G_0^{DD} is only for field point, z, below the source point z'. The Weglein-Secrest (1990) G_0^D result is

$$\begin{aligned} P(z, z_s, \omega) = & A(\omega) G_0^D(z, z_s, \omega) \\ & + P(a, z_s, \omega)\left[\frac{d}{dz'} G_0^D(z, z', \omega)\right]_{z'=a} \\ & - P'(a, z_s, \omega)\, G_0^D(z, a, \omega) \end{aligned} \tag{7}$$

where $G_0^D(z, z', \omega)$ vanishes only at $z = 0$.

2 The Osen et al. and H. Tan result using G_0^{DD}

For $0 < z < a$

$$P(z, z_s, \omega) = A(\omega) G_0^{DD}(z, z_s, \omega) + P(a, z_s, \omega)\left[\frac{d}{dz'} G_0^{DD}(z, z', \omega)\right]_{z'=a} \tag{8}$$

If we take the limit as $z \to a$ in (8) we find $P(a, z_s, \omega) = P(a, z_s, \omega)$ since

$$\lim_{z \to a}\left[\frac{d}{dz'} G_0^{DD}(z, z', \omega)\right]_{z'=a} = 1.$$

For the multi D case, it means that as the point above the cable approaches the cable, the G_0^{DD} vanishes and the $\frac{d}{dn}G_0^{DD}$ becomes δ-like. Hence, the field above the cable will only depend on one point that approaches the cable. This is a reassuring result!

If we differentiate (8) by z

$$P'(z, z_s, \omega) = A(\omega)\frac{dG_0^{DD}(z, z_s, \omega)}{dz} + P(a, z_s, \omega)\frac{d}{dz}\left[\frac{d}{dz'}G_0^{DD}(z, z', \omega)\right]_{z'=a} \tag{9}$$

and then take the limit as $z \to a$

$$P'(a, z_s, \omega) = A(\omega)\left[\frac{dG_0^{DD}(z, z_s, \omega)}{dz}\right]_{z=a} + P(a, z_s, \omega)\left[\frac{d}{dz}\left[\frac{d}{dz'}G_0^{DD}(z, z', \omega)\right]_{z'=a}\right]_{z=a} \tag{10}$$

Equation (10) is a relationship between $P(a, z_s, \omega)$, $P'(a, z_s, \omega)$ and $A(\omega)$. From (7), we can evaluate as $z \to a$

$$\begin{aligned} P(a, z_s, \omega) &= A(\omega)G_0^D(a, z_s, \omega) + P(a, z_s, \omega)\left[\frac{d}{dz'}G_0^D(a, z', \omega)\right]_{z'=a} \\ &\quad -P'(a, z_s, \omega)\, G_0^D(a, a, \omega) \end{aligned} \tag{11}$$

Hence (10) and (11) are both relations between $P(a, z_s, \omega)$, $P'(a, z_s, \omega)$ and $A(\omega)$. Are equations (10) and (11) independent relationships between P, P' and $A(\omega)$? E.g., if true, we could derive an exact relationship for $A(\omega)$ directly in terms of P. Or P' from P exactly.

It is useful in comparing (10) and (11) to notice that

$$\frac{G_0^D(a, z_s, \omega)}{G_0^D(a, a, \omega)} = \left(\frac{d}{dz}G_0^{DD}(z, z_s, \omega)\right)_{z=a}$$

where

$$G_0^D(z, z', \omega) = \frac{e^{ik(z-z')}}{2ik}\left(1 - e^{2ikz'}\right),$$

again for $z > z'$; it shows that these two integral expressions (11) and (10) are identical.

Hence, the triangle holds!

References

1. Amundsen, L., B.G. Secrest and B. Arntsen, 1995, Extraction of the normal component of the particle velocity from marine pressure data: Geophysics, **60**, 212-222.

2. Corrigan, D., Weglein, A. B., and Thompson, D. D. "Method and apparatus for seismic survey including using vertical gradient estimation to separate downgoing seismic wavefields." (Estimation of the vertical gradient of the wavefield from the wavefield and wavelet) Assignee: Atlantic Richfield Co., (1991) U.S. Patent No. 5,051,961.

3. Osen, A., B.G. Secrest, L. Admundsen and A. Reitan, 1998, Wavelet estimation from marine pressure measurements: Geophysics, **63**, 2108-2119.

4. Tan, T.H., 1992, Source signature estimation: Presented at the Internat. Conf. And Expo. Of Expl. And Development Geophys., Moscow, Russia

5. Tan, T.H., 1999, Wavelet spectrum estimation: Geophysics, **64**, 6, 1836-1846

6. Weglein, A.B., and Secrest, B.G., 1990, Wavelet estimation for a multidimensional acoustic or elastic earth. Geophysics, **55**, 902-913.

Subtraction working team review and update

Arthur B. Weglein†, Ray Abma*, Ken H. Matson*, Kristopher A. Innanen‡ and Simon A. Shaw*†
†University of Houston, *BP, ‡University of British Columbia

Abstract

The M-OSRP subtraction working team serves as an industry-academic forum for discussing issues and ideas related to the prediction and subtraction of multiples. There are a number of issues that impact our ability to remove multiples from seismic data. The effectiveness of multiple removal algorithms can be analyzed both on the basis of the method's underlying physics, and by the degree to which the method's prerequisites are satisfied.

In March 2002, the subtraction working team met at the University of Houston. Weglein introduced the meeting by dividing the issues of multiple attenuation into two categories: in-model and out-of-model. In-model issues need to be addressed even when the method's underlying physics are satisfied (e.g., source wavelet, dehosting, etc.). Out-of-model issues arise when the method's underlying physics are not realized (e.g., near source extrapolation, 2-D algorithms). The objective of adaptive subtraction methods is to remove multiples that have been imperfectly predicted. Talks on pattern recognition and a comparison study between least-squares and pattern recognition were presented by external speakers Simon Spitz (CGG) and Ray Abma (BP), respectively.

M-OSRP will continue the subtraction working team, serving as a forum for communication and an agent for generating new approaches to this important problem.

1 Introduction

In principle, the inverse scattering free surface multiple series algorithm *removes* all orders of free surface multiple, and the inverse scattering internal multiple series *attenuates* all orders of internal multiple. Both algorithms predict the correct times of the multiple events for a multi-dimensional (3-D) heterogeneous Earth, and neither require any subsurface information, event picking or interpretive intervention.

In the free surface multiple case, if all the prerequisites of the method are satisfied, then all free surface multiples, including diffracted multiples, will be eliminated from the input data. In order for these multi-dimensional algorithms to work most effectively, the dimension of the

algorithm must match the dimension of the experiment. In other words, multiples generated in a 3-D Earth, require a 3-D implementation of the algorithm, which in turn demands a truly 3-D data acquisition (e.g., areal shooting).

Two important prerequisites of the inverse scattering multiple attenuation series algorithms are

1. the source wavelet, amplitude and phase
2. source and receiver deghosted input data

In addition to these two prerequisites, the internal multiple attenuation algorithm requires that free surface multiples have been removed. Methods that provide the prerequisites for multiple attenuation have their own strengths and limitations. Frequently in practice, deghosting, an unknown source wavelet, and higher order multiple amplitude errors that arise when the series algorithms are truncated, are all handled through the energy minimization criterion in an adaptive subtraction procedure.

Table 1 breaks the problem of multiple subraction into two categories: in-model issues and out-of-model issues. In-model issues are present when all the assumptions of the method (and when the assumptions of the procedures employed to satisfy the prerequisites) are realized. Out-of-model issues arise when the assumptions of the underlying physics model are violated.

2 In-model issues

2.1 Prediction

In practice, the removal of free surface and internal multiples are prediction and subtraction methods. Even when the physics model of the theory is realized, then there are still in-model issues to address.

In-model issues include getting a good estimate of the source wavelet, performing deghosting and using sufficient terms in the series to properly predict the amplitudes of second and higher order multiples in the data. It is neccesary to calculate the appropriate number of terms in the series in order to correctly predict the amplitudes of all orders of free-surface multiples in the data.

Table 1: Issues that impact multiple removal can be separated into two categories: in-model and out-of-model.

In-model issues	Out-of-model issues
When underlying assumptions of physics are satisfied	When underlying assumptions of physics are *not* satisfied
• deghosting • wavelet estimation by energy minimization • truncation of the series • attenuation vs. elimination of internal multiples	• all in-model issues plus ... • missing data, especially crossline and near-source • wavelet estimation when energy minimization fails • depth sensitive deghosting

When the dimensions of the algorithm and of the acquired data are correct, then there are techniques to determine deghosted data and source wavelet directly from towed streamer data. Alternatively, we may use near field measurements and far field extrapolation to determine the wavelet.

There are a number of projects within M-OSRP that are designed to improve our ability to satisfy the prerequisites for multiple attenuation series algorithms. For example, variants of the Extinction Theorem provide methods for estimating the source wavelet and performing deghosting (e.g., Guo et al., 2003, Zhang and Weglein, 2003).

3 Out-of-model issues

3.1 Prediction

The quality of the prediction may be measured by the amplitude and phase of the predicted multiples compared to those in the input data. Timing errors are the most serious because they can result in us adding back multiples to the data. These errors are most frequently attributed to the use of a 2-D algorithm for an earth that is 3-D.

The physics of the free surface and internal multiple attenuation series assumes that the dimension of the algorithm and the dimension of the acquisition are consistent with the dimension of the subsurface structure that generates the multiples.

When the dimension is incorrect, this is the over-riding issue to address since it will impact timing errors. For example, Fig. 1 shows an example of a free-surface multiple prediction generated for synthetic data from a model with inline and crossline dip. When a 3-D algorithm is used, then the multiples are predicted at the correct time.

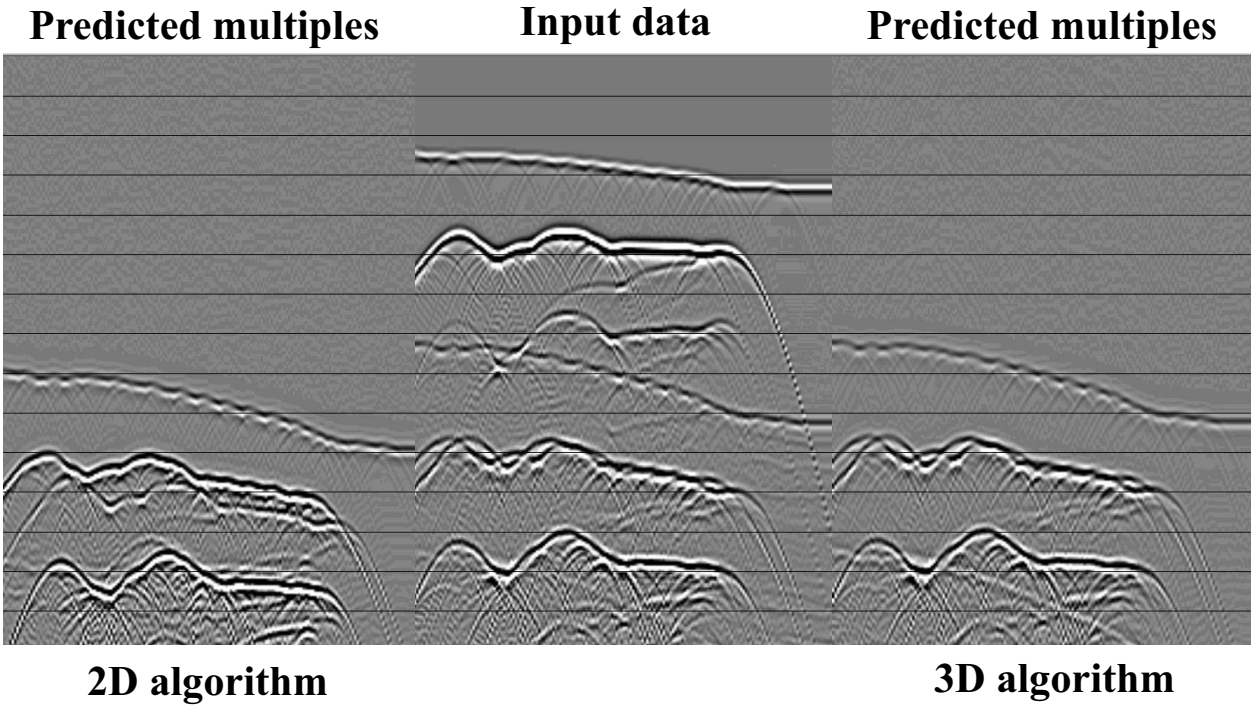

Figure 1: The middle pannel shows input data from a synthetic dataset that has both inline and crossline dip (i.e., from a 3-D Earth). The first and third panels are the results of 2-D and 3-D free surface multiple prediction, respectively. The timing errors introduced in using the 2-D algorithm are evident. All panels are common offset displays.

The project of data interpolation and extrapolation within M-OSRP is designed to improve our ability to provide the algorithms with adequately sampled data in the cases when data acquisition has not.

3.2 Comparison of adaptive subtraction techniques

3.2.1 Introduction

When predicted multiples have some (time and amplitude) errors with respect to the multiples in the data, then they need to be be *adaptively subtracted.* Adaptive subtraction techniques are designed to compensate for these errors. Methods that fit into the class of adaptive subtraction techniques include match filtering (e.g., Robinson and Trietel, 1980) and pattern recognition (e.g., Spitz 1999, 2000). In general, these methods assume that the predicted multiples are in some sense close to the multiples in the data. Match filtering techniques assume that the multiple estimate is close in time (and, e.g., offset for 2-D filters) and pattern recognition techniques assume that the multiple estimate is close in dip.

The current industry standard match filtering methods employ the least-squares (L2) criterion. For the adaptive subtraction of multiples, this assumes that when the multiples have been successfully removed, the energy within a window is minimized. The L1 criterion, assumes that the absolute value of the amplitudes is minimized.

Adaptive subtraction techniques have the potential to compensate for the unknown source wavelet, and account for other errors, such as those errors in the multiple estimate generated by using a 2-D implentation of the algorithm.

3.2.2 Methods

Non-deterministic adaptive subtraction methods are described and compared. Simple 1-D match-filter adaptive subtraction is compared to a pattern-matching subtraction method and to a 2-D filtering subtraction.

The pattern-matching approach suggested by Spitz (1999, 2000) was implemented as f-x domain filters where each frequency slice in the multiple estimate has a filter designed to remove the estimated multiples at that frequency. This filter was then applied to the data to remove the actual multiples. This pattern-matching method filters out events with dips found in the multiple estimate without regard to amplitude or timing. This technique allows more independence from amplitude errors in the multiple estimate and frees the subtraction from the least-squares constraints of the match-filtering approach.

In an effort to combine the match-filter and pattern-matching approaches to adaptive subtraction, we attempted to separate the signal and multiple with multi-dimensional filters.

In the examples in the next section, a shaped 2-D filter is used to provide prediction within a trace as well as predictions across traces (Abma, 1995, and Abma and Claerbout, 1995). The 2-D filter is similar to the combined set of Spitz's f-x filters, but it is a filter that is shorter in time. The 2-D filter collapsed to one column is equivalent to a 1-D filter. This suggests that a 2-D filter could retain advantages of both approaches.

When the free surface multiple removal series is truncated, as is often done in practice, then different orders of multiples have different relative amplitudes. In this case, the 1-D match-filter subtraction is inaccurate when different orders of multiples exist within one design window. Pattern-matching and 2-D filtering, which are independent of the relative amplitudes, are shown to attenuate the primaries as well as the multiples. Furthermore, while the data is unavailable for presentation, it has been found that L1 subtraction provides generally similar results to L2 subtraction, although small improvements have been found in some parts of the data.

The pattern-matching filter used here is similar, but not identical to the approach used by Spitz (1999). While Spitz uses a set of filters in the f-x domain, we use an approach that is more like a projection filter, in that we take the multiple estimate in the f-k domain, generate a weighting function in that domain to remove the multiples, and apply that weighting function to the data in the f-k domain. This approach has similar dip-attenuation characteristics to the f-x approach. The 2-D filter subtraction is done by designing a 2-D t-x annihilation filter on the multiple estimate, then applying that filter to the data.

3.2.3 Examples

Comparisons of 1-D match-filter, pattern-matching, and 2-D filter adaptive subtraction methods are made using a simple synthetic and on the Pluto 1.5 dataset (Stoughton et al., 2001). Figure 2 shows an example of linear signal and noise. In this case, the signal is the horizontal event and the noise, which would correspond to multiples, is the set of dipping events in Fig. 2(b). Note that the amplitudes of the two dipping events differ; the steepest event's amplitude is twice that of the event with the smaller slope.

Figure 2(b) is an approximation to the noise in Fig. 2(a). The two events in Fig. 2(b) are equal in amplitude, while the amplitudes of the corresponding noise events in Fig. 2(a) differ. The noise events in Fig. 2(b) are shifted slightly in time with respect to the corresponding events in Fig. 2(a).

The least-squares match-filter subtraction method shown in Fig. 2(c) demonstrates the limitations of this method. While the signal has been well preserved, the steepest event has

been only partially attenuated, while the event with lower dip has been over attenuated and now has a negative amplitude. This is the result of trying to fit the two equal amplitude events seen in Fig. 2(b) to the unequal amplitude events in Fig. 2(a) with a 1-D filter. This issue of matching events of different amplitude ratios is important for the multiple attenuation problem, particularly when different orders of multiples are scaled as a function of their order in the surface-related multiple prediction routines commonly used.

Figure 2(d) shows the result of pattern-matching subtraction. The result in this case is superior to that of the 1-D match filter. The amplitudes of the events are relatively unimportant for pattern-matching, whereas the discrimination in the patterns of the dip is more significant. The result is an almost perfect separation. In Fig. 2(e), the separation of signal and noise was done with a 2-D annihilation filter calculated on the noise. The result is excellent, with almost complete removal of the noise.

In a second synthetic example, Fig. 3(a) shows the data, the sum of a horizontal signal and a diffraction-like noise event. Figure 3(b) shows the predicted noise. Once again, the noise events in Fig. 3(b) are shifted slightly in time with respect to the corresponding event in Fig. 3(a).

The 1-D least-squares technique does an excellent job of attenuating the multiple, as seen in Fig. 3(c). This example is particularly suited to a 1-D match-filter since the filter only needs to produce a small shift in the modeled noise to match the noise in the data, and the signal is poorly correlated with the noise in time. The pattern-matching result shown in Fig. 3(d) is unsatisfactory. Both the noise and the signal are removed. The pattern-matching removed both the noise and the signal in an effort to remove all the dips contained in the diffraction-like event in the predicted noise. The signal dip overlaps the dip range of the noise. The 2-D match-filter result in Fig. 3(e) shows both the signal and noise attenuated. This is basically the same effect seen in the pattern-matching result in Fig. 3(d), except that the small t-x filter size limited the amount of attenuation in the presence of the large range of dips to be removed.

Finally, these methods were applied to the Pluto 1.5 dataset. The dataset is a 2-D elastic finite-difference synthetic that is significantly more complicated than the previous examples. Figure 4(a) shows a common-offset data section, which contains significant multiple energy. The predicted multiples are seen in Fig. 4(b). The water bottom multiple appears with a specular part and a multiple diffraction part. Figure 4(c) shows a least-squares subtraction. The multiples are very well attenuated, and there is no obvious weakening of the primary energy.

The pattern-matching result seen in Fig. 4(d) shows the specular component to be well attenuated, but the diffracted multiples still remain. The multiples of the diffractions remain, since the specular components of the multiples dominate the filter calculations. The 2-D filter result in Fig. 4(e) shows similar effects. The pattern-matching result shows attenuation of the signal near the multiple energy. The 2-D filter result also shows attenuation of the signal, but the attenuation of the multiples of the diffractions is poorer than that seen in the pattern-matching result. In the pattern-matching and the 2-D filter methods, the independence of the amplitudes of the estimated multiples from the amplitudes of the events in the data is both a strength and a weakness. The independence from the amplitude of the predicted multiples allows these methods to avoid the dependence on the exact amplitudes of the estimated multiples, making the subtraction more robust. Unfortunately, this independence also allows signal to be attenuated regardless of how the pattern of amplitudes on the multiple estimate matches the pattern in the data.

3.2.4 L1 versus L2 subtraction

Calculating adaptive subtraction filters can be done using a least-squares method, but in the presence of spiky noise, an L1 method might be preferable (Guitton and Verschuur, 2002). Although we found there was some improvement in the results on real data, the differences were generally small, at least on the dataset we tried it on. Since the subtraction is significantly more expensive with the L1 norm, it seems impractical at present. There may be cases where noise other than the multiples contaminates the matching filter enough that the L1 method is practical, but generally the multiples being considered are strong enough to dominate the match filter calculations.

4 Discussion

At some cost, data acquisition can improve our ability to remove free surface and internal multiples from seismic data. Recording near offsets, and having receivers positioned to collect wider aperture data are two examples of this. A third is to use near-field measurements of the source to estimate its signature. In short, money can improve prediction and lessen the burden on subtraction techniques.

None of the adaptive subtraction methods tested will remove multiples under all conditions, without modifying the primaries. While pattern-matching and multidimensional filtering

methods offer the promise of independence from the requirement that the amplitudes of the estimated multiples match those in the real data, these methods tend to attenuate signal as well as multiples. Of the three methods tested, the 1-D match-filter is the most robust under many conditions.

There are other possible approaches to adaptive subtraction. In particular, the 2-D f-x method and the 2-D filtering method may be extended into higher dimensions. The filters may be designed as annihilation filters or as multi-dimensional match-filters. Another possibility would be to use local slant stacks, or Radon transformations, to separate the multiples and the data into dip components and compare the amplitudes in that domain. There are more sophisticated methods that use inversion for the separation (Abma, 1995, Brown and Clapp, 2000, and Guitton et al., 2001). Inversion methods tend to be expensive, and in some cases they suffer from instabilities and sensitivities to weights applied as part of the inversion.

The subtraction working team will continue to act as a forum for discussing issues related to the prediction and subtraction of multiples.

Acknowledgements

The authors would like to thank BP for permission to publish some of the material in this note. Bill McLain, Nurul Kabir and Scott Michell are thanked for valuable discussions.

References

Abma, R., 1995, Least-squares separation of signal and noise with multidimensional filters, Ph.D. thesis, Stanford University.

Abma, R. and Claerbout, J., 1995, Lateral prediction for noise attenuation by t-x and F-X techniques: Geophysics, Soc. of Expl. Geophys., **60**, 1887-1896.

Brown, M. and Clapp, R., 2000, T-x domain, pattern-based ground-roll removal, 70th Ann. Internat. Mtg: Soc. of Expl. Geophys., 2103-2106.

Guitton, A., Brown, M., Rickett, J. and Clapp, R., 2001, Multiple attenuation using a t-x pattern-based subtraction method, 71st Ann. Internat. Mtg: Soc. of Expl. Geophys., 1305-1308.

Guitton, A., and Verschuur, E., 2002, Adaptive subtraction of multiples with the L1-norm: Stanford Exploration Project Report 111, 157-169.

Guo, Z., Tan, H. and Weglein, A.B. 2003, Source wavelet estimation: Mission-Oriented Seismic Research Program **2**, 4-12.

Robinson, E.A., and Treitel, S., 1980, Geophysical Signal Analysis: Prentice Hall.

Stoughton, D., Stefani, J., and Michell, S., 2001, 2D elastic model for wavefield investigations of subsalt Gulf of Mexico: 71st Annual Meeting of the SEG, 1269-1272.

Zhang, J., and Weglein, A.B., 2003, Initial tests on deghosting: Mission-Oriented Seismic Research Program **2**, 13-26.

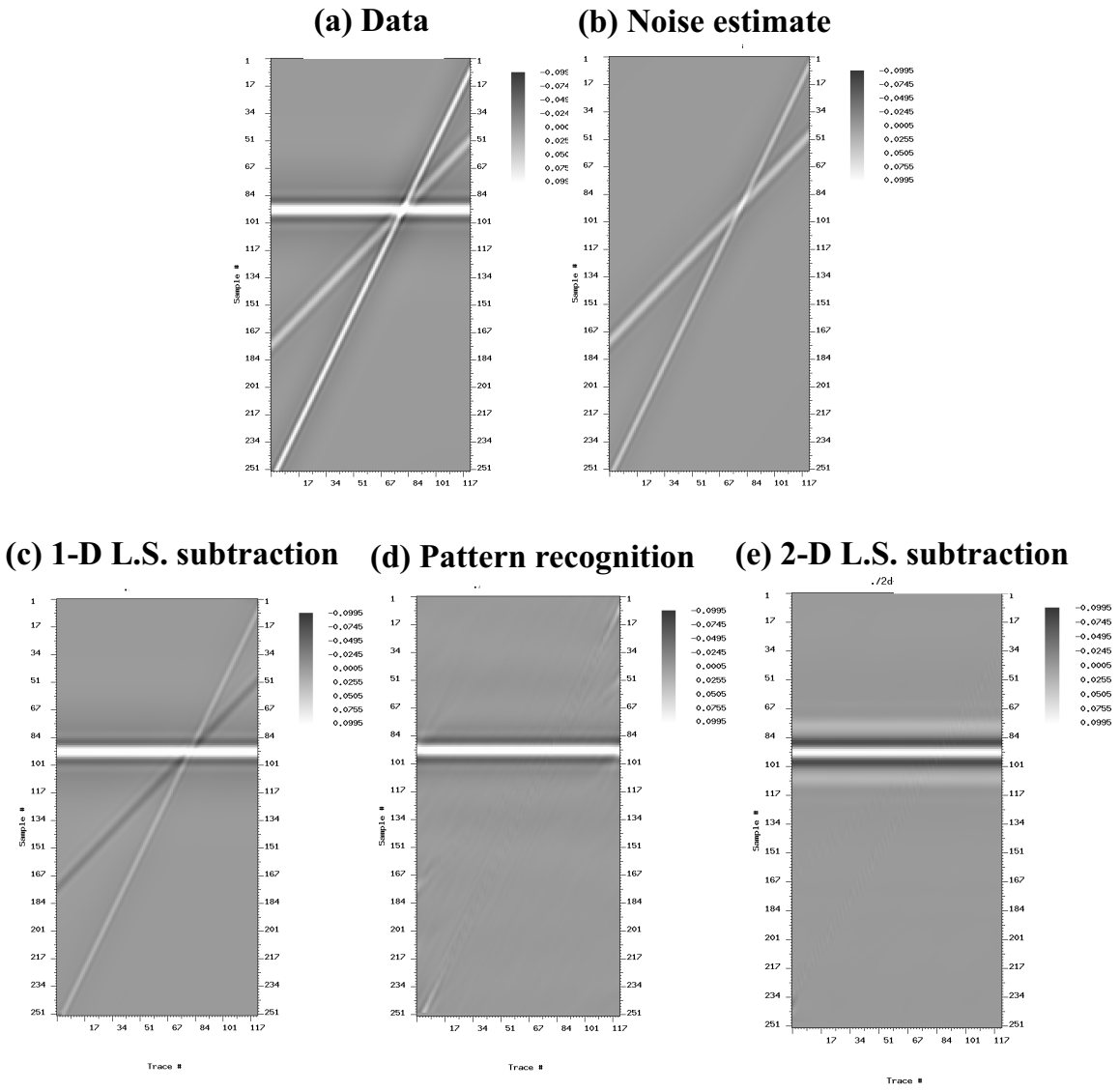

Figure 2: A simple synthetic example comparing different adaptive subtraction techniques.

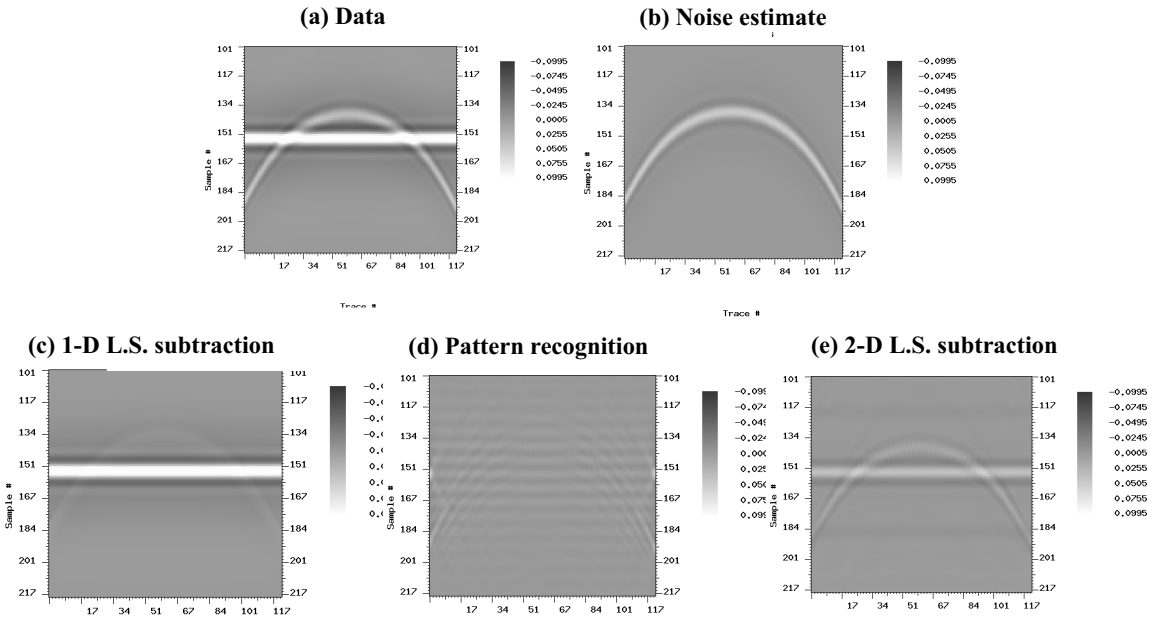

Figure 3: Comparison of different subtraction techniques for data with horizontal signal and diffraction-like noise.

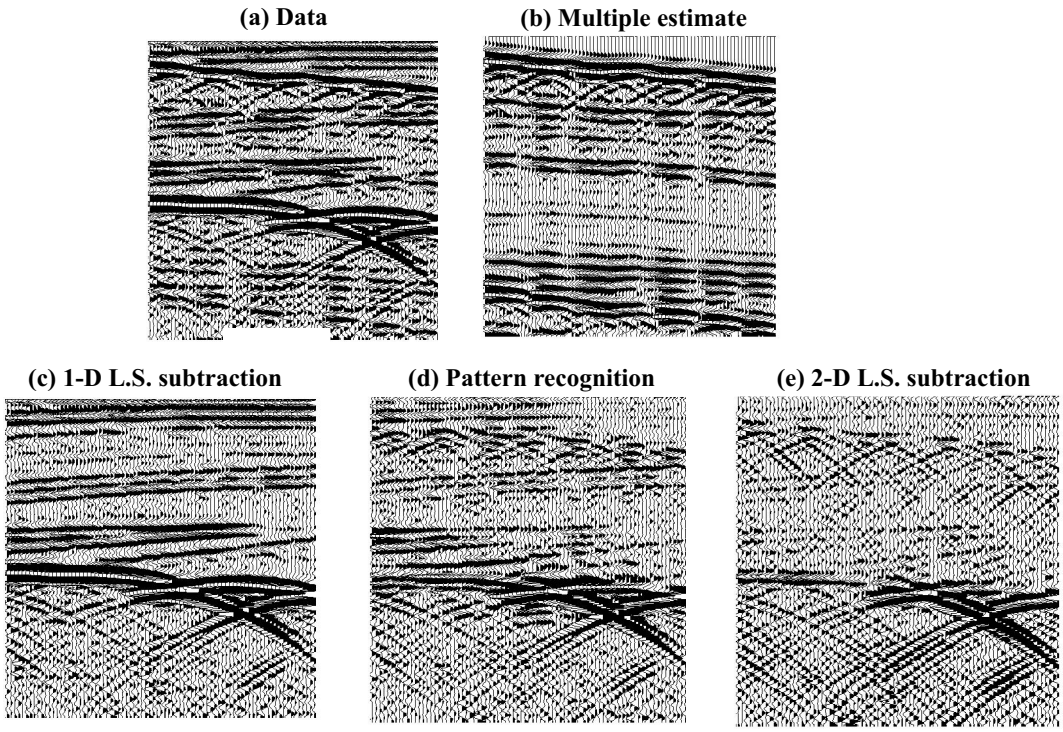

Figure 4: Comparison of different subtraction techniques on a common offset section from the SMAART Pluto 1.5 dataset.

Topical Review: Inverse-scattering series and seismic exploration

Arthur B. Weglein[1], Fernanda V. Araujo[2], Paulo M. Carvalho[3], Robert H. Stolt[4], Kenneth H. Matson[5], Richard Coates[6], Dennis Corrigan[7], Douglas J. Foster[8], Simon A. Shaw[1,5] and Haiyan Zhang[1]

[1] Department of Physics, University of Houston, 617 Science and Research Bldg 1, Houston, TX 77204-5005, U.S.A.

[2]Formerly Universidade Federal da Bahia, PPPG, Brazil; presently Exxon Production Research Co., P.O. Box 2189, Houston, TX 77252.

[3] Petrobras S.A., R. Acre 2504 Bloco M sala 12, 49080-010 Aracaju−SE, Brazil

[4] Conoco Inc., Geoscience and Reservoir Res. 5RDW, 1000 S. Pine, Ponca City, OK 74602-1267

[5] BP, 200 Westlake Park Blvd., Houston, TX 77079, U.S.A.

[6] Schlumberger Doll Research Ridgefield, CT.

[7] Retired from ARCO, 5821 SE Madison St., Portland, OR 97215, U.S.A.

[8] Conoco Phillips, 600 N. Dairy Ashford, P.O. Box 2197, Houston, TX 77252.

Abstract

This paper presents both an overview and a more detailed description of the key logic steps and mathematical-physics framework behind the development of practical algorithms for seismic exploration derived from the inverse scattering series.

We present both the rationale for seeking and methods of identifying uncoupled task specific subseries that accomplish: (1) free-surface multiple removal; (2) internal-multiple attenuation; (3) imaging primaries at depth; and (4) inverting for earth material properties. A combination of forward series analogue and physical intuition are employed to locate those subseries. We show that the sum of the four task specific subseries does not correspond to the original entire inverse series since terms with coupled tasks are never considered or computed. This aspect of the program, i.e., inversion in stages, with an isolated task followed by restarting the problem, provides tremendous practical advantage, since the achievement of a task is a form of useful information exploited in the redefined problem; and, the latter represents a critically important step in the logic and overall strategy.

There are both tremendous symmetries and critical and subtle differences between the forward scattering series construction and the inverse scattering series processing of seismic events. These similarities and differences help explain the efficiency and effectiveness of different inversion objectives. The individual subseries are analyzed

and their strengths, limitations and prerequisites exemplified with analytic, numerical, and field data examples.

1 Introduction and background

In exploration seismology, a man−made source of energy on (or near) the surface of the earth (or in the ocean, in marine exploration) generates a wave that propagates into the subsurface. When the wave reaches a rapid change in earth material properties, (i.e., a reflector) a portion of the wave is reflected back upward the surface; and, in the marine case, is recorded at numerous receivers along a towed streamer in the water column near the air-water boundary.

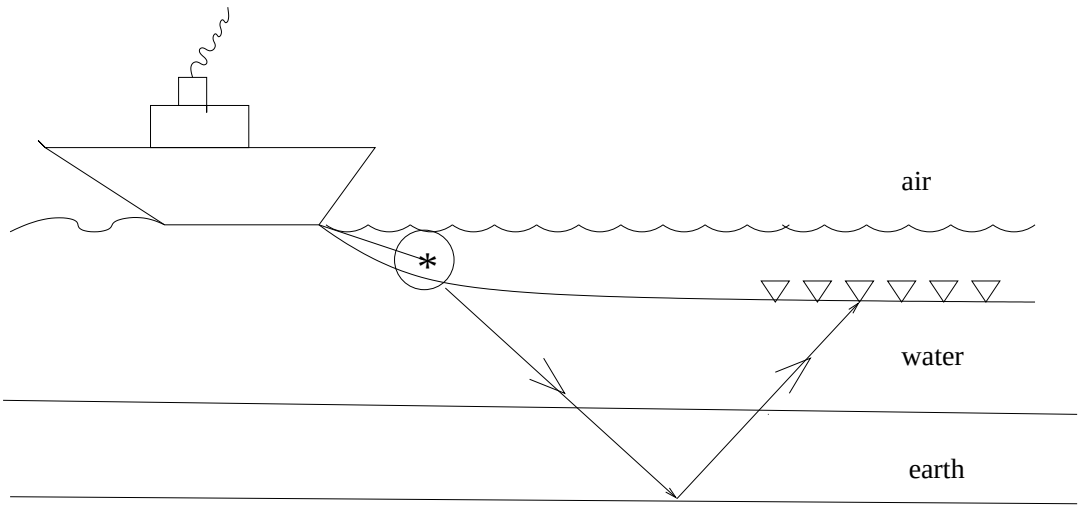

Figure 1: Marine Seismic Exploration Geometry: $*$ and $\bigtriangledown$ indicate source and receiver, respectively. The boat moves through the water with the source and receivers, and the experiment is repeated. The collection of the different source-receiver wave field measurements defines the seismic reflection data.

The objective of seismic exploration is to determine subsurface earth properties from the recorded wavefield. The ultimate objective is to determine subsurface targets and then to estimate the type and extent of rock and fluid properties for hydrocarbon potential.

The need for more effective and liable techniques for extracting information from seismic data is driven by several factors including (1) the higher acquisition and drilling cost and risk associated with the industry trend to explore and produce in deeper water; and (2) the

serious technical challenges associated with either deep water, or imaging beneath a complex and ill-defined overburden, above the target.

An event is a distinct arrival of seismic energy. Seismic reflection events are catalogued as primary or multiple depending on whether the energy arriving at the receiver has experienced one or more upward reflections, respectively. Multiples or multiply reflected events are further classified by the location of the downward reflection between two upward reflections. For marine data, multiples that have experienced at least one downward reflection at the air-water (free) surface are called free surface multiples. Multiples that have all of their downward reflections below the free surface are called internal multiples. (See Fig.2). Methods for extracting subsurface information from seismic data typically assume that the

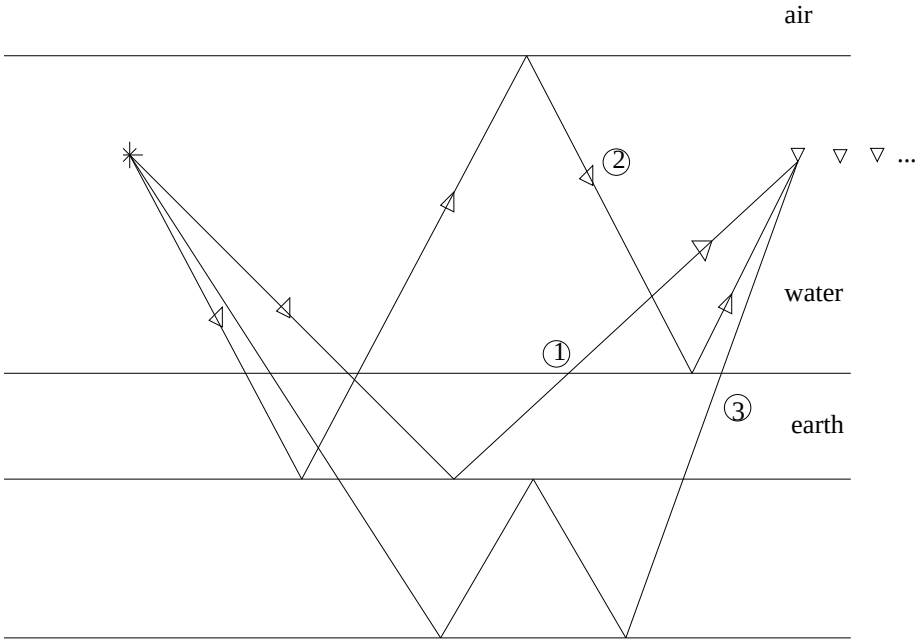

Figure 2: 1, 2 and 3 are examples of primaries, free-surface multiples and internal multiples, respectively.

data consists of primaries, since that model allows essentially one reflection process to be associated with each recorded event. The latter primaries-only assumption simplifies the processing of seismic data for determining the spatial location of reflectors and the local change in earth material properties across a reflector. Hence, multiple removal is a requisite to seismic processing. It is a long-standing problem and while significant progress has been achieved over the past decade, conceptual and practical challenges remain. The inability to remove multiples can lead to multiples masquerading or interfering with primaries causing false or misleading interpretations; and, ultimately poor drilling decisions. The assump-

tion of singly reflected (or scattered) data in seismic data analysis is an assumption shared with other fields of inversion and non-destructive evaluation, e.g., it is common to medical imaging, and ground penetrating radar, environmental hazards, and the violation of this assumptions in practice, can lead to deleterious and serious consequences for medical diagnosis, hazard detection, and buried object and fluid location/identification, for tunnels and caves. Even if multiples were to be removed from seismic reflection data, the challenges for accurate imaging (locating) and inversion across reflectors are significant, especially when the medium of propagation and the geometry of the target are complex and the contrast in earth material properties is large. The latter large contrast property condition is all by itself enough to cause linear inverse methods to bump up hard against their assumptions.

Specifically, the location and definition of hydrocarbon targets beneath salt, basalt, volcanics, and karsted sediments are of high economic moment in the petroleum industry today, and serious challenges to current imaging and inversion techniques that go beyond the daunting issues concerning the removal of multiples. For the latter geologic circumstances the requirement of all current methods for the imaging-inversion of primaries for an accurate (or at least adequate) model of the medium above the target, can often not be achievable in practice, leading to erroneous, ambivalent or misleading prediction. These difficult imaging conditions often occur in, e.g., the deep water Gulf of Mexico, where the confluence of large hydrocarbon reserves beneath salt and the high cost of drilling in deep water, drives the demand for more effective and reliable methods. In this Topical Review, we will describe how the inverse scattering series has provided the promise of an entire new vision and level of seismic capability and effectiveness. That promise has already been delivered for the removal of free surface and internal multiples. We will also describe the recent research progress and results on the inverse series for the processing of primaries. Our objectives in writing this Topical Review are: (1) To provide both an overview and a more comprehensive mathematical-physics description of these new seismic processing concepts and practical industrial production strength algorithms, that derive from the inverse series and (2) To describe and exemplify the strengths and limitations of these seismic processing algorithms; and to discuss open issues and challenges. (3) To explain how this work reflects a general philosophy, and approach (strategy and tactics) to defining, prioritizing and choosing, and then solving significant real-world problems, from developing new fundamental theory, to issues with limitations with field-data, to satisfying practical prerequisites and computational requirements.

The problem of determining earth material properties from seismic reflection data is an inverse scattering problem; and, specifically, a non-linear inverse scattering problem. Although,

an overview of all seismic methods is well beyond the scope of this paper, it is accurate to say that prior to the early 1990s, (when non-linear inverse scattering series methods were first applied) (Weglein, Boyse and Anderson (1981) and practical algorithms first demostrated Weglein *et al.* (1997)) all deterministic methods used in practice in exploration seismology could be viewed as different realizations of a linear approximation to inverse scattering, the inverse-Born approximation (see, e.g., Cohen and Bleistein (1997), Stolt and Weglein (1985), Morley and Claerbout (1983)).

All scientific methods assume a model that starts with assumptions that include some (and ignore other) phenomena and components of the reality. Among earth models used in seismic exploration are: acoustic, elastic, heterogeneous, anisotropic and anelastic, and the experimental description model for the characteristics of the man-made source, and the resultant incident field, the character of the receivers, the dimension of variability of the earth and geometry of reflectors. The configuration and extent of the experiment, and the sampling rate of sources and receivers that comprise the recorded seismic wave field need to be included in the model and subsequent theory and algorithms.

Although 2D, 3D closed form complete integral equation solutions exist for the Schrodinger equation (see, Newton (2002)) - there is no analogous closed form complete multi-dimensional inverse solution for the acoustic or elastic equation. The push to develop complete multi-dimensional non-linear seismic inversion methods came from a several directions: (1) The need to remove multiples from a complex multidimentional earth and (2) the interest in a more realistic model for primaries.

This absence of a closed form exact inverse (for a 2D acoustic or elastic earth) shifted attention to non-closed or series forms. An inverse series can be written, at least formally, for any differential equation expressed in a perturbative form.

This paper describes and illustrates the development of concepts and practical methods from the inverse scattering series for multiple attenuation and, provides some recent new promising conceptual and algorithmic results for primaries.

2 Seismic data and scattering theory

2.1 The scattering equation

Scattering theory is a form of perturbation analysis. In broad terms it describes how a perturbation in the properties of a medium relates a perturbation to a wave field that experiences

that perturbed medium. It is customary to consider the original unperturbed medium as the reference, and, to consider the perturbation or alteration of properties turning the reference into the actual. The difference between the actual and reference media is characterized by the perturbation operator. The corresponding difference between the actual and reference wavefields is called the scattered field. Forward scattering takes as input the reference medium, the reference field, and the perturbation operator, and outputs the actual wavefield. Inverse scattering takes as input the reference medium, the reference field and values of the actual field on the measurement surface, and outputs the difference between actual and reference medium properties, through the perturbation operator. Inverse-scattering-theory methods typically assume the support of the perturbation to be on one side of the measurement surface. In seismic application this condition translates to a requirement that the difference between actual and reference media be non-zero only below the source-receiver surface. Consequently, inverse scattering methods require, for seismic application, that the reference medium agrees with the actual at and above the measurement surface.

For marine application the sources and receivers are located within the water column and the simplest reference medium is a half-space of water bounded by a free surface at the air-water interface. Since scattering theory relates the difference between actual and reference wavefields to the difference between their medium properties, it is reasonable that the mathematical description begin with the differential equations governing wave propagation in these media. Let

$$\mathbf{LG} = -\delta(\mathbf{r} - \mathbf{r}_s) \tag{1}$$

and

$$\mathbf{L}_0\mathbf{G}_0 = -\delta(\mathbf{r} - \mathbf{r}_s) \tag{2}$$

where $\mathbf{L}$, $\mathbf{L}_0$ and $\mathbf{G}$, $\mathbf{G}_0$ are the actual and reference differential operators and Greens functions, respectively, for a single temporal frequency. Equations (1) and (2) assume that the source and receiver signatures have been deconvolved. The impulsive source is ignited at $t = 0$. $\mathbf{G}$ and $\mathbf{G}_0$ are the matrix elements of the Greens operator, $\mathbf{G}$ and $\mathbf{G}_0$, in the spatial coordinates and temporal frequency representation. $\mathbf{G}$ and $\mathbf{G}_0$ satisfy $\mathbf{LG} = -\mathbf{1}$ and $\mathbf{L}_0\mathbf{G}_0 = -\mathbf{1}$, where $\mathbf{1}$ is the unit operator. The perturbation operator, $\mathbf{V}$, and the scattered field operator, Ψ_s, are defined as follows:

$$\mathbf{V} = \mathbf{L} - \mathbf{L}_0 \ , \tag{3}$$

$$\Psi_s = \mathbf{G} - \mathbf{G}_0 \ . \tag{4}$$

Ψ_s is not itself a Green's operator. The Lippmann-Schwinger equation, the fundamental equation of scattering theory, is an operator identity that relates Ψ_s, $\mathbf{G}_0$, $\mathbf{V}$ and $\mathbf{G}$, (see, e.g., Taylor, 1972),

$$\Psi_s = \mathbf{G} - \mathbf{G}_0 = \mathbf{G}_0\mathbf{V}\mathbf{G} \ . \tag{5}$$

In the coordinate representation, Eq. (5) is valid for all positions of $\mathbf{r}$ and $\mathbf{r}_s$ whether or not they are outside the support of $\mathbf{V}$. A specific simple example of $\mathbf{L}$, $\mathbf{L}_0$, and $\mathbf{V}$, when $\mathbf{G}$ corresponds to a pressure field in an inhomogeneous acoustic medium (see, e.g., Clayton and Stolt, (1981))

$$\mathbf{L} = \frac{\omega^2}{\kappa} + \nabla \cdot \left(\frac{1}{\rho}\nabla\right) \ ,$$

$$\mathbf{L}_0 = \frac{\omega^2}{\kappa_0} + \nabla \cdot \left(\frac{1}{\rho_0}\nabla\right) \ ,$$

and

$$\mathbf{V} = \omega^2 \left(\frac{1}{\kappa} - \frac{1}{\kappa_0}\right) + \nabla \cdot \left[\left(\frac{1}{\rho} - \frac{1}{\rho_0}\right) \nabla\right] \ , \tag{6}$$

where κ, κ_0, ρ and ρ_0 are the actual and reference bulk modulus and densities, respectively; ω is the temporal frequency. Other forms that are appropriate for elastic isotropic media and a homogeneous reference, begin with the generalization of equations Eqs. (1), (2) and (5) where matrix operators e.g.:

$$G = \begin{pmatrix} G_{pp} & G_{ps} \\ G_{sp} & G_{ss} \end{pmatrix}$$

and

$$G_0 = \begin{pmatrix} G_p^0 & 0 \\ 0 & G_s^0 \end{pmatrix}$$

express the increased channels available for propagation and scattering and

$$V = \begin{pmatrix} V_{pp} & V_{ps} \\ V_{sp} & V_{ss} \end{pmatrix}$$

is the perturbation in an elastic world. (see,e.g., Stolt and Weglein, 1985).

2.2 Forward series in operator form

Equation (5) can be expanded in an infinite series

$$\Psi_s \equiv \mathbf{G} - \mathbf{G}_0 = \mathbf{G}_0\mathbf{V}\mathbf{G}_0 + \mathbf{G}_0\mathbf{V}\mathbf{G}_0\mathbf{V}\mathbf{G}_0 + \dots \tag{7}$$

for Ψ_s in orders of the perturbation operater, $\mathbf{V}$. Then Eq. (7) can be rewritten as

$$\Psi_s = (\Psi_s)_1 + (\Psi_s)_2 + (\Psi_s)_3 + \dots \tag{8}$$

where $(\Psi_s)_n \equiv \mathbf{G}_0(\mathbf{V}\mathbf{G}_0)^n$, and is the portion of Ψ_s that is n-th order in $\mathbf{V}$. The inverse series of Eq. (7) (or Eq. (8)) is an expansion for $\mathbf{V}$ in orders (or powers) of the measured values of $\Psi_s \equiv (\Psi_s)_m$. The measured values of $\Psi_s = (\Psi_s)_m$ constitute the data, D. Expand $\mathbf{V}$ as a series

$$\mathbf{V} = \mathbf{V}_1 + \mathbf{V}_2 + \mathbf{V}_3 + \dots \tag{9}$$

where $\mathbf{V}_n$ is the portion of $\mathbf{V}$ that is nth order in the data, D.

To find $\mathbf{V}_1$, $\mathbf{V}_2$, $\mathbf{V}_3$, ... and, hence, $\mathbf{V}$, first substitute the inverse form Eq. (9) into the forward Eq. (5)

$$\begin{aligned}\Psi_s \;=\; & \mathbf{G}_0(\mathbf{V}_1 + \mathbf{V}_2 + \dots)\mathbf{G}_0 + \mathbf{G}_0(\mathbf{V}_1 + \mathbf{V}_2 + \dots)\mathbf{G}_0(\mathbf{V}_1 + \mathbf{V}_2 + \dots)\mathbf{G}_0 \\ & + \mathbf{G}_0(\mathbf{V}_1 + \mathbf{V}_2 + \dots)\mathbf{G}_0(\mathbf{V}_1 + \mathbf{V}_2 + \dots)\mathbf{G}_0(\mathbf{V}_1 + \mathbf{V}_2 + \dots)\mathbf{G}_0 \\ & + \dots \; .\end{aligned} \tag{10}$$

Evaluate both sides of Eq. (10) on the measurement surface and set terms of equal order in the data equal. The first order terms are

$$(\Psi_s)_m = D = (\mathbf{G}_0\mathbf{V}_1\mathbf{G}_0)_m \; , \tag{11}$$

the second order terms

$$0 = (\mathbf{G}_0\mathbf{V}_2\mathbf{G}_0)_m + (\mathbf{G}_0\mathbf{V}_1\mathbf{G}_0\mathbf{V}_1\mathbf{G}_0)_m \tag{12}$$

and the third order

$$\begin{aligned}0 \;=\; & (\mathbf{G}_0\mathbf{V}_3\mathbf{G}_0)_m + (\mathbf{G}_0\mathbf{V}_1\mathbf{G}_0\mathbf{V}_2\mathbf{G}_0)_m \\ & + (\mathbf{G}_0\mathbf{V}_2\mathbf{G}_0\mathbf{V}_1\mathbf{G}_0)_m + (\mathbf{G}_0\mathbf{V}_1\mathbf{G}_0\mathbf{V}_1\mathbf{G}_0\mathbf{V}_1\mathbf{G}_0)_m + \dots\end{aligned} \tag{13}$$

and to n-th order

$$\begin{aligned}0 \;=\; & (\mathbf{G}_0\mathbf{V}_n\mathbf{G}_0)_m + (\mathbf{G}_0\mathbf{V}_1\mathbf{G}_0\mathbf{V}_{n-1}\mathbf{G}_0)_m + \dots \\ & + (\mathbf{G}_0\mathbf{V}_1\mathbf{G}_0\mathbf{V}_1\mathbf{G}_0\mathbf{V}_1 \dots \mathbf{G}_0\mathbf{V}_1\mathbf{G}_0)_m \; .\end{aligned} \tag{14}$$

$(\Psi_s)_m$ are the measured values of the scattered field Ψ_s. To solve these equations, start with Eq. (11) and invert the $\mathbf{G}_0$ operators that sandwich $\mathbf{V}_1$. Then substitute $\mathbf{V}_1$ into Eq. (12) and perform the same inversion operation as in Eq. (11) to invert the $\mathbf{G}_0$ operators that sandwich $\mathbf{V}_2$. Now substitute $\mathbf{V}_1$ and $\mathbf{V}_2$ found from equations (11) and (12), into Eq. (13) and again invert the $\mathbf{G}_0$ operators that bracket $\mathbf{V}_3$ and in this manner continue this program to compute any $\mathbf{V}_n$. This method for determining $\mathbf{V}_1$, $\mathbf{V}_2$, $\mathbf{V}_3$, ... and, hence, $\mathbf{V} = \sum_{n=1}^{\infty} \mathbf{V}_n$ is an explicit direct inversion formalism that, in principle, can accommodate a wide variety of physical phenomena, and concomitant differential equations, including multidimensional acoustic, elastic, an certain forms of anelastic wave propagation. Because a closed or integral equation solution is currently not available for the multidimensional forms of the latter equations, and a multidimensional earth model is a minimal required realism to develop relevant and differential technology, the inverse scattering series became a focus of attention for those seeking significant added completeness and effectiveness beyond linear, 1D, or small contrast techniques.

In the derivation of the inverse series equations (11)–(14) there is no assumption about the closeness of $\mathbf{G}_0$ to $\mathbf{G}$, nor of the closeness of $\mathbf{V}_1$ to $\mathbf{V}$, nor is $\mathbf{V}$ or $\mathbf{V}_1$ assumed to be small in any sense. $\mathbf{V}_1$ is the portion of $\mathbf{V}$ that is linear in the data. That is all that is assumed. Equation (11) is an exact equation for $\mathbf{V}_1$. If one were to assume that $\mathbf{V}_1$ is close to $\mathbf{V}$, and then treat Eq. (11) as an approximate solution for $\mathbf{V}$, then that would then correspond to the inverse Born approximation. The latter assumption of $\mathbf{V} \approx \mathbf{V}_1$ is never made in the formalism of the inverse scattering series. The inverse Born approximation inputs the data D, and $\mathbf{G}_0$, and outputs $\mathbf{V}_1$ which is then treated as $\mathbf{V}$.

All of current seismic processing methods for imaging and inversion are different incarnations of using Eq. (11) to find an approximation for $\mathbf{V}$(see Stolt and Weglein (1985)), hence, the understandable and sustained effort to build ever more realism and completeness into the reference differential operator, $\mathbf{L}_0$ and its impulse response, $\mathbf{G}_0$. As with all technical approaches, the latter road (and current mainstream seismic thinking) eventually leads to a stage of maturity where further sustained effort will no longer bring a commensurate benefit. The inverse series methods provides a vennato achieve objectives beyond the reach of linear methods for a given level of a-priori information. Several additional comments: (1) the forward and inverse Born approximations are two separate and distinct methods: the forward Born approximation for the scattered field, Ψ_s, uses a linear truncation of Eq. (7) (and Eq. (8)) to estimate Ψ_s

$$\Psi_s \cong \mathbf{G}_0\mathbf{V}\mathbf{G}_0$$

and inputs $\mathbf{G}_0$ and $\mathbf{V}$ to find an approximation to Ψ_s; the inverse Born approximation inputs

D and $\mathbf{G}_0$ and solves for $\mathbf{V}_1$ as $\mathbf{V}$ which it approximates by inverting

$$(\Psi_s)_m = D \cong (\mathbf{G}_0 \mathbf{V} \mathbf{G}_0)_m$$

(2) the inverse series is a separate and distinct procedure from iterative linear inversion.

Iterative linear inversion would start with Eq. (11) and solve for $\mathbf{V}_1$. Then a new reference operator, $L_0' = L_0 + \mathbf{V}_1$; impulse response, $\mathbf{G}_0'$ (where $\mathbf{L}_0'\mathbf{G}_0' = -\delta$); and data, $D' = (\mathbf{G} - \mathbf{G}_0')_m$ are input to a new linear inverse form

$$D' = (\mathbf{G}_0' \mathbf{V}_1' \mathbf{G}_0')_m$$

where a new operator,$\mathbf{G}_0'$, has to now be removed (inverted) from both sides of $\mathbf{V}_1'$. These linear steps are iterated, note that at each step a new and, in general, more complicated operator (or matrix or frechetderivative) is required to be inverted. In contrast, the inverse-scattering series Eqs. (11)–(14) inverts the same and original input operator, $\mathbf{G}_0$, at each step. The inverse-scattering series methods were first developed by Moses (1956), Prosser (1969), Razavy (1975), and transformed for application to a multi-dimensional Earth and exploration seismic reflection data by Weglein, Boyse and Anderson (1981) and Stolt and Jacobs (1980). The first question in considering a series solution is the issue of convergence and if encouraging, followed closely by the question of rate of convergence. The important pioneering work on convergence criteria for the inverse series by Prosser (1969) is given as a condition which is difficult to translate into a statement on the size and duration of the contrast between actual and reference media. Faced with that lack of theoretical guidance, empirical tests of the inverse series were performed (Carvalho (1992)) for a 1D acoustic medium, which indicated that, starting with no a-priori information, convergence was observed but appeared to be restricted to small contrasts and duration (e.g., $< 11\%$ difference between actual earth acoustic velocity and water (reference) speed).

Since the acoustic wave speed in the earth quickly gets further than 11% from the acoustic wave speed in water (1500 m/sec) the practical value of the entire series, without a priori information, appeared to be quite limited.

A reasonable response might seem to be to use seismic methods that estimate the velocity trend of the earth to try to get the reference medium proximal to the actual, and that in turn could allow the series to possibly converge.

The problem with that thinking was that velocity trend estimation methods assumed that multiples were removed prior to that analysis. Furthermore, concurrent with these technical strategic decisions (around 1990) was the loud and clear message heard from petroleum

industry operating units that multiple removal was on increasingly prioritized and serious problem and impediment to effectiveness.

Methods for removing multiples (at that time) assumed either: (1) the earth was 1D, (2), the velocity model was known, (3) reflectors generating the multiples could be defined, different patterns could be identified in waves from primaries and multiples, and (5) primaries were random and multiples periodic. All of these assumptions were seriously violated in deep-water and/or complex geology, and the methods based upon them often enough outright failed to perform, or produced erroneous or misleading results.

This interest in multiples came in large part from the industry trend to explore in deep water where the depth alone ($> 1km$) can cause, e.g., multiple removal methods based on periodicity arguments to seriously violate their assumptions. Complex multidimensional heterogeneous and hard to estimate geologic conditions and targets provided additional challenges for multiple removal methods that relied on having 1D assumptions or access to inaccessible details about the reflectors that were the source of these multiples.

The inverse scattering series was (and remains) the only multi-dimensional direct inversion formalism that could accommodate arbitrary heterogeneity directly in terms of $\mathbf{G}_0$ with estimated rather than actual propagation properties.

The confluence of these factors lead to the development of thinking that viewed inversion as a series of tasks or stages, and to view one of these as multiple removal.

2.3 Subseries

A combination of factors: (1) that the inverse series represent the only multidimensional direct seismic inversion; (2) numerical tests that suggested an apparent lack of robust convergence of the overall series, (when starting with no a-priori information), and, (3) the interest in extracting something of value from this only formalism for complete multi-dimensional inversion; and, (4) the industry need for more effective methods for removing multiply reflected events (multiples) from data collected over an unknown heterogeneous earth, all came together to imagine inversion in terms of steps or stages with intermediate objectives towards the ultimate goal of identifying earth material properties. The stages were each defined as achieving a task or objective: (1) removing free-surface multiples; (2) removing internal multiples; (3) imaging (locating) reflectors in space; and (4) determining the changes in earth material properties across those reflectors. The idea was to seek to identify within the overall series, and specific distinct subseries that performed these focused tasks and to evaluate

those subseries for convergence, rate of convergence, data requirements and theoretical and practical prerequisites. Perhaps a subseries for one specific task would have a more favorable attitude towards, e.g., convergence in comparison to the entire series. These tasks, if achievable, could bring practical benefit on their own terms, and, if achievable, could be realized from the inverse-scattering series directly in terms of the data, D, and reference wave propagation, $\mathbf{G}_0$ and where $\mathbf{G}_0$ is not assumed to be proximal to the actual. At the outset, many important issues were open (and some remain open) that could cause a pause or hesitation in pursuing such a new task separation strategy. Among them are (1) does the series in fact uncouple in terms of tasks, (2) if it does uncouple, then how to identify those uncoupled task-specific subseries; (3) will the inverse series view multiples as noise to be removed, or as signal to be used for helping to image/invert the target; and (4) will the subseries derived require different algorithms (and computer codes) for different earth model types (e.g., acoustic version and elastic version) how can you know or determine, in a given application, how many terms in a subseries will be required to achieve a certain degree of effectiveness. We will address and respond to these questions in this paper and list others that are outstanding or the subject of current investigation. How to identify a task specific subseries? The pursuit of task specific subseries used several different types of analysis with testing of new concepts to evaluate, refine and develop embryonic thinking largely based on analogues and physical intuition. To begin, the forward and inverse series Eqs. (7) (8), and Eqs. (11)–(14) have a tremendous symmetry. The forward series produces the scattered wavefield, Ψ_s from a sum of terms each of which is composed of the operator, $\mathbf{G}_0$ acting on $\mathbf{V}$. When evaluated on the measurement surface, the forward series creates all of the data, $(\Psi_s)_m = D$ and contains all recorded primaries and multiples. The inverse series produces $\mathbf{V}$ from a series of terms each of which can be interpreted as the operator $\mathbf{G}_0$ acting on the recorded data, D. Hence, in scattering theory the same engine, $\mathbf{G}_0$, that acts on $\mathbf{V}$ to create data, acts on D to invert data. If we consider

$$< \mathbf{G}_0\mathbf{V}\mathbf{G}_0 >_m = < \mathbf{G}_0(\mathbf{V}_1 + \mathbf{V}_2 + \mathbf{V}_3 + \dots)\mathbf{G}_0 >_m$$

and use equations (12)–(14) we find

$$< \mathbf{G}_0\mathbf{V}\mathbf{G}_0 >_m = < \mathbf{G}_0\mathbf{V}_1\mathbf{G}_0 >_m - < \mathbf{G}_0\mathbf{V}_1\mathbf{G}_0\mathbf{V}_1\mathbf{G}_0 >_m + \dots \tag{15}$$

there is a remarkable symmetry between the inverse series Eq. (15) and the forward series Eq. (7)

$$(\Psi_s)_m = < \mathbf{G}_0\mathbf{V}\mathbf{G}_0 >_m + < \mathbf{G}_0\mathbf{V}\mathbf{G}_0\mathbf{V}\mathbf{G}_0 >_m + \dots \tag{7}$$

In terms of diagrams, the inverse series for $\mathbf{V}$, Eq. (15) can be represented as

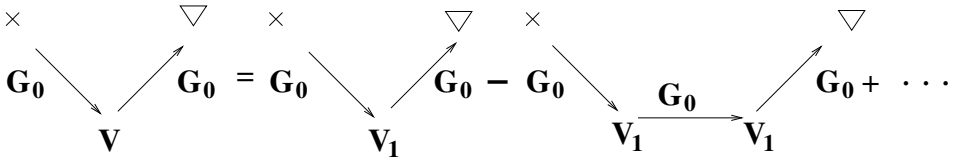

while the forward series, Eq. (7) for the data, $(\Psi_s)_m \equiv D$, can be represented as

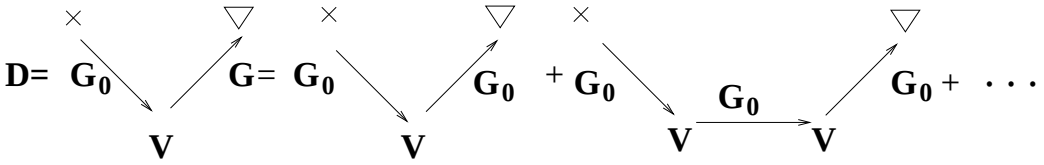

and, therefore, this diagram comparison indicates further opportunities for relating forward and inverse processes. The symbols $\times$ and $\bigtriangledown$ indicate a source and receiver, respectively. However, we know that the forward and inverse problems are not "inverses" in some more formal sense - meaning that the forward creates data but the inverse doesn't annihilate data, it inverts data. Never-the-less, the inverse scattering task specific subseries were thought to act on only specific subsets of the data, e.g., free surface multiples, internal multiples, and, imaging and inverting primaries. Hence, the guess was that if we could figure out how those events were created in the forward series in terms of $\mathbf{G}_0$ and $\mathbf{V}$, perhaps we could figure out how those events were processed in the inverse series when once again $\mathbf{G}_0$ was acting on D. That intuitive leap was later provided with a somewhat rigorous basis for free surface multiples, but the more challenging internal multiple attenuation subseries and the distinct subseries that image and invert primaries at depth without the velocity model while having attracted some insightful mathematical-physics rigor (Ten Kroode (2002)), remain with certain key steps in their logic based on plausibility, empirical tests, and physical intuition. In fact, for internal multiples understanding how the forward scattering series produces an event only hints at where the inverse process might be located. That 'hint' required and presently remains indebted to intuition, testing and subtle refinement of concepts to go to the location of the inverse operation. This is further internal. This last statement is neither an apology nor an expression of hubris, but a normal and expected stage in the development and evolution of new fundamentally concepts.

3 The marine case

For the marine case, with sources and receivers in the water column, the simplest reference medium is a half-space of water bound by a free surface at the air-water interface. The reference Green's function, $\mathbf{G}_0$, consists of two parts

$$\mathbf{G}_0 = \mathbf{G}_0{}^d + \mathbf{G}_0{}^{FS} \ , \tag{16}$$

where $\mathbf{G}_0{}^d$ is the direct propagating, causal, whole-space Green's function in water and $\mathbf{G}_0{}^{FS}$ is the additional part of the Green's function due to the presence of the free surface (see Fig. 3). $\mathbf{G}_0{}^{FS}$ corresponds to a reflection off the free surface. In the absence of a free

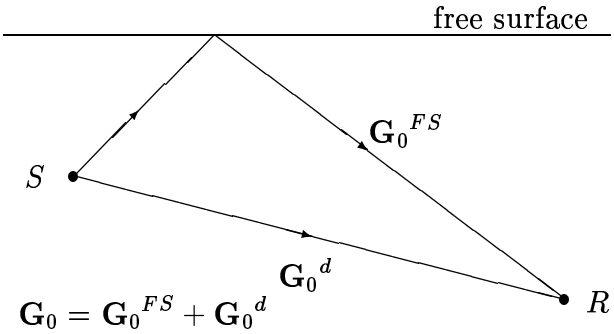

Figure 3: The marine configuration and reference Green's function.

surface, the reference medium is a whole-space of water and $\mathbf{G}_0{}^d$ is the reference Green's function. In this case, the forward series equation (7) describing the data is constructed from the direct propagating Green's function, $\mathbf{G}_0{}^d$, and the perturbation operator, $\mathbf{V}$. With our choice of reference medium, the perturbation operator characterizes the difference between earth properties and water; hence, the support of $\mathbf{V}$ begins at the water bottom. With the free surface present, the forward series is constructed from $\mathbf{G}_0 = \mathbf{G}_0{}^d + \mathbf{G}_0{}^{FS}$ and the same perturbation operator, $\mathbf{V}$. Hence, $\mathbf{G}_0{}^{FS}$ is the sole difference between the forward series with and without the free surface; therefore $\mathbf{G}_0{}^{FS}$ is responsible for generating those events that owe their existence to the presence of the free surface, i.e., ghosts and free-surface multiples. Ghosts are events that either start their history propagating from the source up to (and reflecting down from) the free-surface or end their history as the downgoing portion of the recorded wavefield at the receiver, having its last experience as a downward reflection at the free surface (see Fig.3).

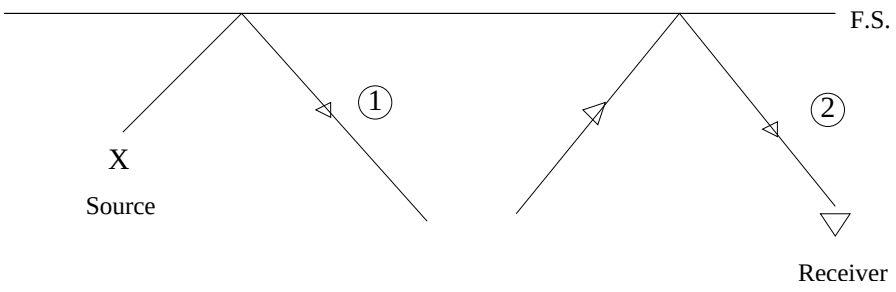

Figure 4: 1 and 2 correspond to source and receiver ghosts, respectively.

In the inverse series, equations (11)–(14), it is reasonable to infer that $\mathbf{G_0}^{FS}$ will be responsible for all the extra tasks that inversion needs to perform when starting with data containing ghosts and free-surface multiples rather than data without those events. Those extra inverse tasks include deghosting and the removal of free-surface multiples. In the section on the free-surface demultiple subseries that follows, we describe how the extra portion of the reference Green's function due to the free surface, $\mathbf{G_0}^{FS}$, performs deghosting and free-surface multiple-event removal.

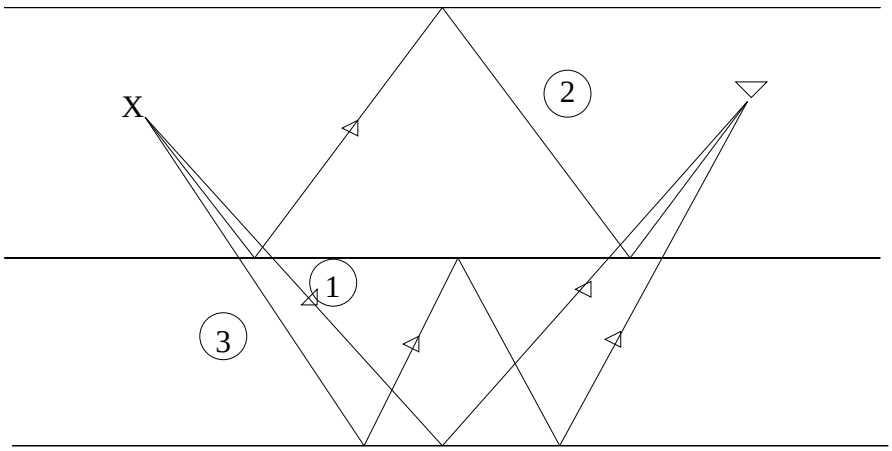

Figure 5: Deghosted Marine Data: 1, 2 and 3 represent deghosted primaries, free surface multiples and internal multiples, respectively.

Once the events associated with a free surface are removed, the remaining measured field consists of primaries and internal multiples. For a marine experiment absent of a free surface, the scattered field, Ψ'_s, can be expressed as a series in terms of a reference medium consisting of a whole-space of water, the reference Green's function, $\mathbf{G_0}^{d}$, and the perturbation, $\mathbf{V}$, as

follows:

$$\begin{aligned}\Psi'_s &= \mathbf{G_0}^d\mathbf{V}\mathbf{G_0}^d + \mathbf{G_0}^d\mathbf{V}\mathbf{G_0}^d\mathbf{V}\mathbf{G_0}^d + \mathbf{G_0}^d\mathbf{V}\mathbf{G_0}^d\mathbf{V}\mathbf{G_0}^d\mathbf{V}\mathbf{G_0}^d + \dots \\ &= (\Psi'_s)_1 + (\Psi'_s)_2 + (\Psi'_s)_3 \dots \end{aligned} \tag{17}$$

The values of Ψ'_s on the measurement surface, D', are the data, D, absent of free-surface events; i.e., D' consists of primaries and internal multiples

$$D' = D'_1 + D'_2 + D'_3 + \dots + D'_n + \dots$$

where D'_m is the projection of $(\Psi'_s)_m$ on the measurement surface. Unfortunately, the free-space Green's function, $\mathbf{G_0}^d$, doesn't separate into a part responsible for primaries and a part responsible for internal multiples; a new concept was necessary to be introduced to separate the tasks associated with $\mathbf{G_0}^d$ (Weglein *et al.*, (1997)).

A seismic event represents the measured arrival of energy that has experienced a specific set of actual reflections, R, and transmissions, T, at reflectors and propagation, p, governed by medium properties between reflectors. A complete description of an event would typically consist of a single-term expression with all the actual episodes of R, T, and p in its history. The classification of an event in D' as a primary or an internal multiple depends on the number and type of actual reflections it has experienced.

In contrast, forward scattering describes data, D', in terms of a series. Each term of the series corresponds to a sequence of *reference* medium propagations, $\mathbf{G_0}^d$, and scatterings off the perturbation, $\mathbf{V}$. The scattering theory description of any specific event in D' also requires an infinite series necessary to build the actual R, T, and p's in terms of reference propagation, $\mathbf{G_0}^d$, and the perturbation operator, $\mathbf{V}$. That is, R, T, and p are nonlinearly related to $\mathbf{G_0}^d$ and $\mathbf{V}$. We will illustrate this with a simple example later in this section. Hence two chasms need to be bridged to determine e.g., the subseries that removes internal multiples. The first requires a map between primary and internal multiples in D' and their description in the language of forward scattering theory, $\mathbf{G_0}^d$ and $\mathbf{V}$; the second requires a map between the construction of internal multiple events in the forward series and the removal of these events in the inverse series.

The internal multiple attenuation concept requires the construction of these two dictionaries: one relates seismic events to a forward-scattering description, the second relates forward construction to inverse removal. The task separation strategy requires that those two maps to be determined . Both of these multidimensional maps were originally derived using arguments of physical intuition and mathematical reasonableness. Subsequently, Matson

(1996) provided, for 1-D constant-density acoustic media, a mathematically rigorous map of the relationship between seismic events and the forward scattering series. Recent work by Nita *et al.* (2003), and Innanan and Weglein (2003), extend that work to prestack analysis and absorptive media, respectively. Within the context of the important Matson paper, his results agree with and confirm the original intuitive arguments. The second map, relating forward construction and inverse removal, remains largely based on its original foundation of reasonableness. Recently, Ten Kroode (2002) presented a formal mathematical map for certain important aspects of the forward to inverse internal multiple map based on a leading order definition of internal multiples. For the purpose of this paper, we present only the key logical steps of the original arguments that lead to the required maps; the argument of the first map is presented here; the second map, relating forward construction and inverse removal, is presented in the next section.

To understand how the forward scattering series describes a particular event, it is useful to recall that the forward series for D' is a generalized Taylor series in the scattering operator, $\mathbf{V}$ (Keys and Weglein, 1983). But what is the forward scattering subseries for a given event in D'? Since a specific event consists of a set of actual R, T, and p factors, it is reasonable to start by asking how these individual factors are expressed in terms of the perturbation operator. Consider the simple example of one-dimensional acoustic medium consisting of a single interface and a normal-incidence plane wave, e^{ikz}, illustrated in Fig. 6.

Let the reference medium be a whole-space with acoustic velocity, c_0. The actual and reference differential equations describing the actual and reference wave fields, P and P_0, are:

$$\left[\frac{d^2}{dz^2} + \frac{\omega^2}{c^2(z)}\right] P(z,\omega) = 0 \ ,$$

and

$$\left[\frac{d^2}{dz^2} + \frac{\omega^2}{c_0^2}\right] P_0(z,\omega) = 0 \ ,$$

where $c(z)$ is the actual velocity.

The perturbation operator, $\mathbf{V}$, is

$$\mathbf{V} = L - L_0 = \frac{\omega^2}{c^2(z)} - \frac{\omega^2}{c_0^2} \ .$$

Characterize $c(z)$ in terms of c_0 and the variation in index of refraction, α,

$$\frac{1}{c^2(z)} = \frac{1}{c_0^2}[1 + \alpha(z)] \ .$$

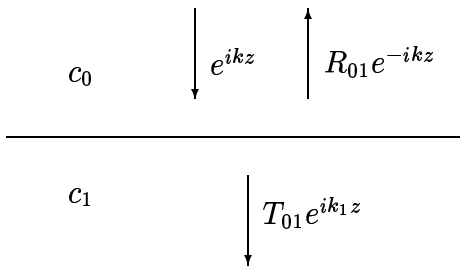

Figure 6: The 1-D plane-wave normal-incidence acoustic example.

In the lower half-space

$$\frac{1}{c_1^2} = \frac{1}{c_0^2}[1+\alpha] \ ,$$

α_1 essentially represents (within a constant factor of ω^2/c_0^2) the change in the perturbation operator at the interface. The reflection and transmission coefficients and the transmitted wave propagating in the lower half-space are

$$R_{01} = \frac{c_1 - c_0}{c_1 + c_0} \ ,$$
$$T_{01} = \frac{2c_1}{c_1 + c_0} \ ,$$

and

$$P_1 = T_{01}e^{i\frac{\omega}{c_1}z} = T_{01}p_1$$

Using

$$c_1 \equiv \frac{c_0}{(1+\alpha)^{\frac{1}{2}}} \cong c_0\left[1 - \frac{1}{2}\alpha + h.p.(\alpha)\right] \ ,$$

these R, T, and p quantities are expandable as power series in the perturbation, α_1 ($h.p.$ denotes "higher powers of").

$$\begin{aligned} R_{01} &= -\frac{1}{4}\alpha + h.p.(\alpha) \ , \\ T_{01} &= 1 + h.p.(\alpha) \ , \\ p_1 &= e^{i\frac{\omega}{c_1}z} = e^{i\frac{\omega}{c_0}z} + h.p.(\alpha) \\ &= p_0 + h.p.(\alpha) \ . \end{aligned}$$

Thus, to lowest order in an expansion in the local perturbation, the actual reflection is proportional to the local change in the perturbation, the transmission is proportional to 1, and the actual propagation is proportional to the reference propagation. An event in D' consists of a combination of R, T and p episodes. The first term in the series that contributes to this event is determined by collecting the leading-order contribution (in terms of the local change in the perturbation operator) from each R, T and p factor in its history. Since the mathematical expression for an event is a *product* of all these actual R, T and p factors, it follows that the lowest order contribution, in the powers of the perturbation operator, will equal the number of R factors in that event. The fact that the forward series, Eq. (17), is a power series in the perturbation operator then allows us to identify the term in Eq. (3) that provides the first contribution to the construction of an event. Since by definition all primaries have only one R factor, their leading contribution comes with a single power of the perturbation operator; hence, from the first term of the series for D'. First-order internal multiples, with three factors of reflection, have their leading contribution with three factors of the perturbation operator; hence, the leading-order contribution to a first-order internal multiple comes from the third term in the series for D'. All terms in the series beyond the first make second-order and higher contributions for the construction of the R, T and p's of primaries; similarly, all terms beyond the third provide higher-order contributions for constructing the actual reflections, transmissions and propagations of first-order internal multiples. How do we separate the part of the third term in the forward series that provides a third-order contribution to primaries from the portion providing the leading-term contribution to first-order internal multiples?

The key to the separation resides in recognizing that the three perturbative contributions in D'_3 are located at the spatial *location* of reflectors. For a first-order internal multiple the leading-order contribution (illustrated on the right-hand-member of Fig. 7), consists of perturbative contributions located at the spatial location (depth) of the three reflectors where reflections occur. Specifically for the example in Fig. 7, the three linear approximations to R_{12}, R_{10}, R_{12}, that is, $\alpha_2 - \alpha_1$, α_1, $\alpha_2 - \alpha_1$ are located at depths z_1, z_2, z_3 where $z_1 > z_2$ and $z_3 > z_2$. In this single layer example $z_1 = z_3$. In general, D'_3 consists of the sum of all three perturbative contributions from any three reflectors at depths z_1, z_2, and z_3. The portion of D'_3 where the three reflectors satisfy $z_1 > z_2$ and $z_3 > z_2$ corresponds to the leading order construction of a first-order internal multiple involving those three reflectors. The part of D'_3 corresponding to the three perturbative contributions at reflectors that do not satisfy both of these inequalities, provide third-order contribution to the construction of primaries. A simple example is illustrated in Fig. 8.

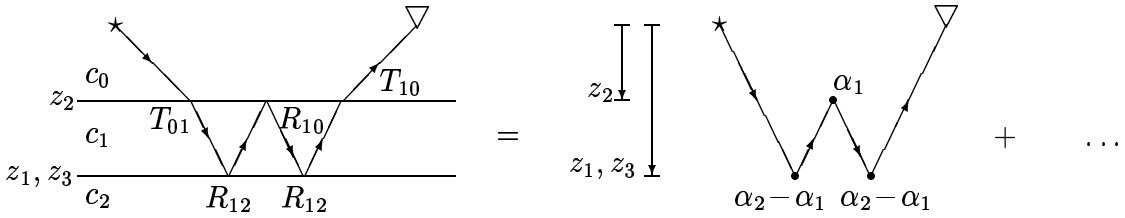

Figure 7: The left-hand-member of this diagram represents a first-order internal multiple; and the right-hand-member illustrates the first series contribution, from D_3', to its construction. α_1 and $\alpha_2 - \alpha_1$ are the perturbative contributions at the two reflectors; c_0, c_1 and c_2 are the acoustic velocities and $1/c_2^2 = 1/c_0^2(1+\alpha_2)$, $1/c_1^2 = 1/c_0^2(1+\alpha_1)$.

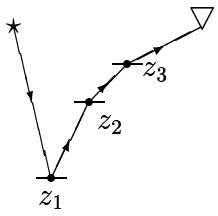

Figure 8: Diagram representing a portion of D_3' that makes a third-order contribution to the construction of a primary.

The *sum* of *all* the contributions in D_3' that satisfy $z_1 > z_2$ and $z_3 > z_2$ for locations of the three successive perturbations, is the sum of the leading contribution term for *all* first-order internal multiples. Similarly, second, third, $\cdots$, n-th order internal multiple find their initial contribution in the fifth, seventh, $\cdots$, $(2n+1)$-th term of the forward series. We use this identified leading-order contribution to all internal multiples of a given order in the forward series to suggest a map to the corresponding leading-order *removal* of all internal multiples of that order in the inverse series.

The forward map between the forward scattering series Eqs. (7) and (8) for $(\Psi_s)_m$ and the primaries and multiples of seismic reflection data works as follows. The scattering series builds the wavefield as a sum of terms with propagations $\mathbf{G}_0$ and scattering off $\mathbf{V}$. Scattering occurs in all directions from the scattering point $\mathbf{V}$ and the relative amplitude in a given direction determined by the isotropy (or anisotropy) of the scattering operator. An scattering operator being anisotropic is distinct from physical anisotropy, the latter of course means that the wave speed in the actual medium at a point is a function of the direction of propagation of the wave at that point. A two-parameter acoustic (isotropic) medium has an anisotropic scattering operator. (see Eq. (6)). In any case, since primaries and multiples are defined in terms of reflections, we imagine that primaries and internal multiples will be distinguished by the number of reflection like scatterings in their forward description. A reflection-like scattering is where the incident wave moves away from and the wave emerging from the scattering point moves towards the measurement surface. Every reflection event in

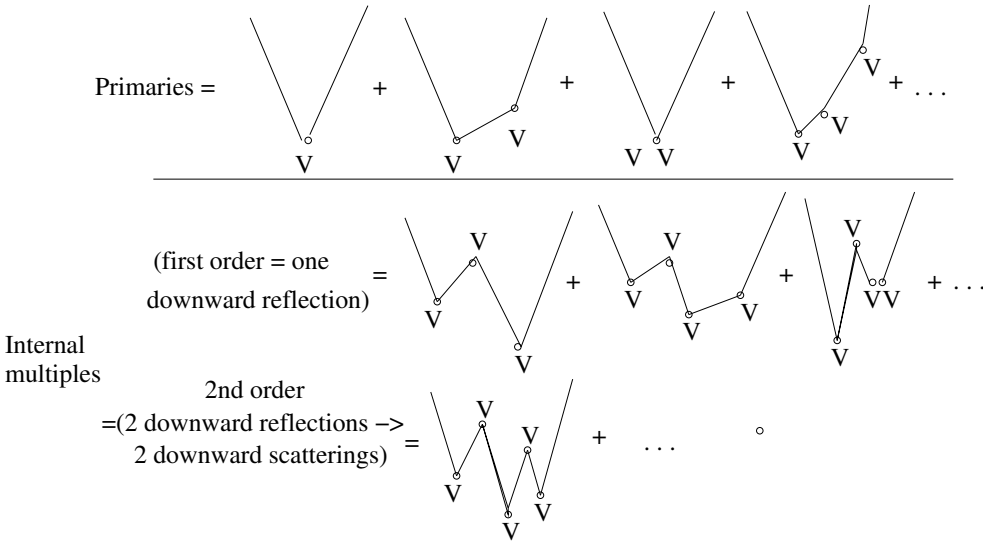

Figure 9: A scattering series description of primaries and internal multiples.

seismic data requires contributions from an infinite number of terms in the scattering theory

description. Even with water as reference speed the simplest primaries, i.e., the water bottom reflection, requires an infinite number of contributions to take the scattering ingredients $\mathbf{G}_0$ and $\mathbf{V}$ into $\mathbf{G}_0$ and $\mathbf{R}$ where $\mathbf{V}$ and $\mathbf{R}$ correspond to the perturbation operator change and reflection coefficient at the water bottom, respectively. For a sub-water bottom primary the series has further issues to deal with beyond turning the local value of $\mathbf{V}$ into the local reflection coefficient, $\mathbf{R}$. For the latter case the reference Green's function, $\mathbf{G}_0$, no longer corresponds to the propagation down to and back from the reflector ($\mathbf{G} \neq \mathbf{G}_0$) , and the terms in the series beyond the first, $\mathbf{G}_0\mathbf{V}\mathbf{G}_0$, are required to correct, e.g., for the timing errors, and for ignoring transmission coefficients, in addition to taking $\mathbf{V}$ into $\mathbf{R}$.

The remarkable fact is that all primaries are constructed in the forward series by portions of every term in the series. The contributing part has one and only one upward reflection-like scattering. Furthermore, internal multiples of a given order (order is defined by the number of downward reflections, independent of the location of that reflector) have contributions from all terms that have exactly a number of reflection-like scatterings corresponding to the order of that internal multiple.

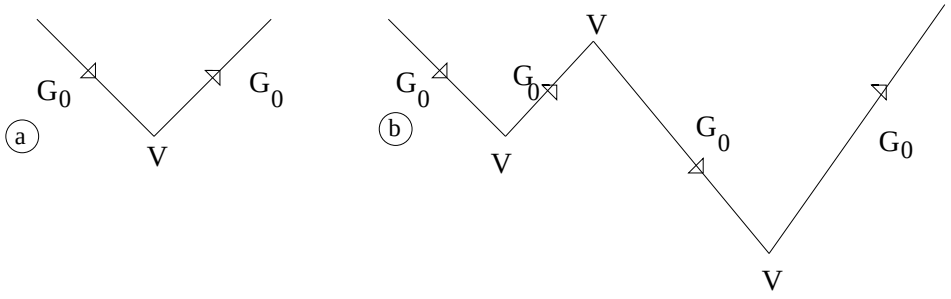

Figure 10: a)A reflection-like scattering for a primary. b)Three reflection-like scatterings contributing to a first order internal multiple.

The first term in the forward series for the data equations Eqs. (7) and (8),

$$((\Psi_s)_m)_1 = (\mathbf{G}_0\mathbf{V}\mathbf{G}_0)_m$$

where

$$(\Psi_s)_m = \sum_{n=1}^{\infty}[(\Psi_s)_m]_n$$

is an integral over the entire subsurface, where $\mathbf{V}$ resides, and approximates all primaries at once, as well as a single scattering model case, independent of depth. Of course the quality of the approximation represented by $(\Psi_s)_1$, depends on how many issues (e.g., phase,

transmission coefficients and reflection coefficient) starting with $\mathbf{G}_0$, $\mathbf{V}$ into $\mathbf{G}$ and $\mathbf{R}$ are required by any particular event.

All internal multiples of first order begin their creation in the scattering series in the portion of the third term of $[(\Psi)_s]_m, [[(\Psi)_s]_m]_3$, with three reflection like scatterings. All terms in the fourth and high terms of $(\Psi_s)_m$ that consist of three and only three reflection−like scattering, plus any number of transmission−like and self−interactions also contribute to the construction of first order internal multiples.

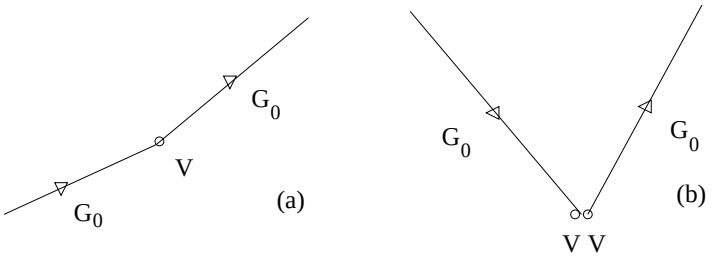

Figure 11: Examples of transmission (a) and self-interaction (b) scattering diagrams.

As mentioned, all of these conclusions were originally deduced based on physically intuitive arguments and later confirmed by analysis of the relationship between seismic events and the forward series for 1D media (Matson, 1996). Further research in the scattering theory descriptions of seismic events is warranted, and underway, and will strengthen the first of the two key logic links (maps) required for developments of more effective and better understood task specific inversion procedures.

Map I takes data into scattering series forward description. Map II takes scattering series description of seismic events to the inverse scattering series processing that are performed on those events. If you know how $\mathbf{G}_0$ and $\mathbf{V}$ make primaries and multiples, then perhaps you can figure out how $\mathbf{G}_0$ and $D(t)$ processes those same events.

4 The inverse series and task separation: terms with coupled and uncoupled tasks

As we mentioned, the fact that: (1) in the forward series ${\mathbf{G}_0}^{FS}$ is the agent that creates all events that come into existence due to the presence of the free surface (i.e., ghosts and free-surface multiples) and (2) that the inverse series starting with data that includes those free-surface related events - has additional tasks to perform (i.e., deghosting and free surface

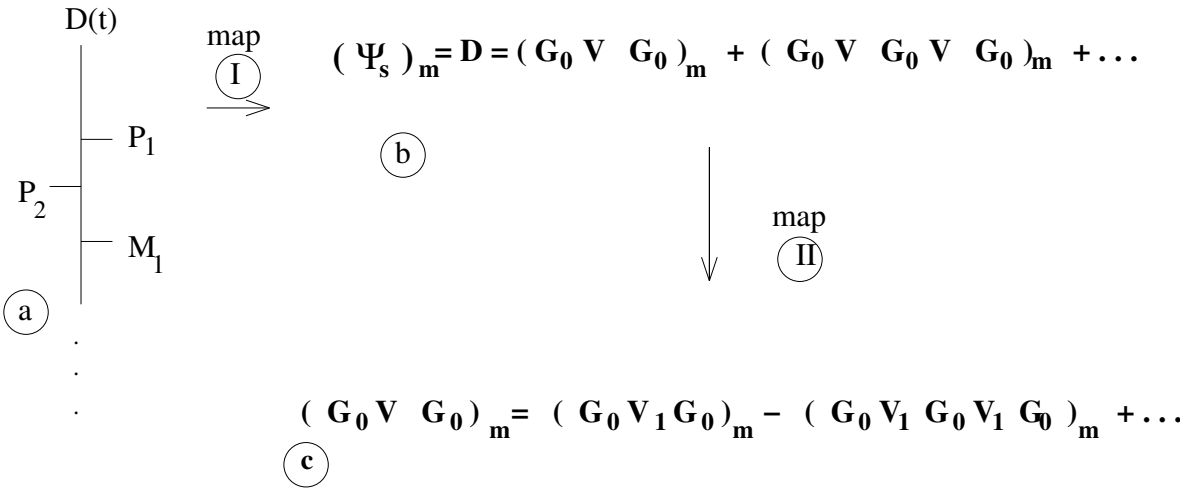

Figure 12: Two maps for inverse scattering subseries. a) $D(t) = (\Psi_s)_m$ consisting of primaries P_1, P_2, ... and multiples, M_1, ... b) $(\Psi_s)_m = D(t)$ as a forward series in terms of $\mathbf{G}_0$ and $\mathbf{V}$. c) The inverse series for $< \mathbf{G}_0\mathbf{V}\mathbf{G}_0 >_m = < \mathbf{G}_0\mathbf{V}_1\mathbf{G}_0 >_m - < \mathbf{G}_0\mathbf{V}_1\mathbf{G}_0\mathbf{V}_1\mathbf{G}_0 >_m + \ldots$ Map (I) takes seismic events to a scattering series description. Map (II) takes forward construction of events to inverse processing of those events.

multiple removal) on the way to constructing the perturbation, $\mathbf{V}$, and (3) that the forward and inverse engine, the reference Green's function, $\mathbf{G}_0$, consists of $\mathbf{G}_0{}^d$ plus $\mathbf{G}_0{}^{FS}$, for the marine case, would be taken together imply that $\mathbf{G}_0{}^{FS}$ would, in the inverse series, be the removal machine for the events it is responsible for having created in the forward series.

How to go from that thought to a deghosting and free surface multiple removal subseries? The inverse series expansions (11)-(14), in the marine case, consists of terms $< \mathbf{G}_0\mathbf{V}_n\,\mathbf{G}_0 >_m$ with $\mathbf{G}_0 = \mathbf{G}_0{}^d + \mathbf{G}_0{}^{FS}$. Deghosting is realized by removing the two outside $\mathbf{G}_0 = \mathbf{G}_0{}^d + \mathbf{G}_0{}^{FS}$ functions and replacing them with $\mathbf{G}_0{}^d$, a downgoing wave from source to $\mathbf{V}$ and an upgoing wave from $\mathbf{V}$ to the receiver. Details are provided in section 10.

After that deghosting operation $D =< \mathbf{G}_0\mathbf{V}_1\,\mathbf{G}_0 >_m$ to $\tilde{D} =< \mathbf{G}_0{}^d\mathbf{V}_1\,\mathbf{G}_0{}^d >_m$ where D and $\tilde{D}$ are $(\Psi_s)_m = (G - \mathbf{G}_0)_m$ and the source and receiver deghosted data, respectively. The objective is to remove free surface multiples from the deghosted data, $\tilde{D}$.

The terms in the series equations (11)-(14), with input $\tilde{D}$ replacing D, contain both $\mathbf{G}_0{}^d$ and $\mathbf{G}_0{}^{FS}$ between the operators $\mathbf{V}_1$. The terms in the series are of three types, e.g.,

$$\begin{aligned} Type1 &: \left(\mathbf{G}_0{}^d\mathbf{V}_1\mathbf{G}_0{}^{FS}\mathbf{V}_1\mathbf{G}_0{}^{FS}\mathbf{V}_1\mathbf{G}_0{}^d\right)_m; \\ Type2 &: \left(\mathbf{G}_0{}^d\mathbf{V}_1\mathbf{G}_0{}^{FS}\mathbf{V}_1\mathbf{G}_0{}^d\mathbf{V}_1\mathbf{G}_0{}^d\right)_m; \end{aligned}$$

and

$$Type3 \quad : \quad \left(\mathbf{G}_0{}^d\mathbf{V}_1\mathbf{G}_0{}^d\mathbf{V}_1\mathbf{G}_0{}^d\mathbf{V}_1\mathbf{G}_0{}^d\right)_m .$$

From an isolated task point of view we interpret these types of terms as: Type (1) when only $\mathbf{G}_0{}^{FS}$ appears between two $\mathbf{V}_1$ contributions then the term removes free surface multiples (when added to $\tilde{D}$) and no other task is to be performed; Type (2): when both $\mathbf{G}_0{}^d$ and $\mathbf{G}_0{}^{FS}$ appear between two $\mathbf{V}_1$ contributions, then a free surface multiple removal plus a task associated with $\mathbf{G}_0{}^d$ are *both* to be performed and; Type (3), when only $\mathbf{G}_0{}^d$ appears between two $\mathbf{V}_1$ contributions, then no free surface multiples are removed by that term. The two outside G_0^d merely denotes that the data has been deghosted.

The idea behind task separated subseries is two fold: (1) isolate the terms in the overall series that perform a given task *as if no other task exists* (i.e., Type 1 above) and (2) do not return to the original inverse series with its coupled tasks involving $\mathbf{G}_0{}^{FS}$ and $\mathbf{G}_0{}^d$, but rather restart the problem with an input data, D', (equation (11")), absent of free surface multiples. Collecting all Type 1, $\mathbf{G}_0{}^{FS}$ terms we have

$$\begin{aligned}
D_1' &\equiv \tilde{D} = \left(\mathbf{G}_0{}^d\mathbf{V}_1\mathbf{G}_0{}^d\right)_m && (11') \\
D_2' &= -\left(\mathbf{G}_0{}^d\mathbf{V}_1\mathbf{G}_0{}^{FS}\mathbf{V}_1\mathbf{G}_0{}^d\right)_m && (12') \\
D_3' &= +\left(\mathbf{G}_0{}^d\mathbf{V}_1\mathbf{G}_0{}^{FS}\mathbf{V}_1\mathbf{G}_0{}^{FS}\mathbf{V}_1\mathbf{G}_0{}^d\right)_m && (13') \\
&\vdots
\end{aligned}$$

and $D' = \sum_{i=1}^{\infty} D_i'$ is the deghosted and free-surface multiple removed data. The data D' consists of primaries and internal multiples and an inverse series for $\mathbf{V} = \sum_{i=1}^{\infty}\mathbf{V}_i'$ where $\mathbf{V}_i'$ is the portion of $\mathbf{V}$ first order in primaries and internal multiples

$$\begin{aligned}
D' &= \left(\mathbf{G}_0{}^d\mathbf{V}_1{}'\mathbf{G}_0{}^d\right)_m && (11'') \\
\left(\mathbf{G}_0{}^dV_2'\mathbf{G}_0{}^d\right)_m &= -\left(\mathbf{G}_0{}^d\mathbf{V}_1{}'\mathbf{G}_0{}^d\mathbf{V}_1{}'\mathbf{G}_0{}^d\right)_m && (12'') \\
\left(\mathbf{G}_0{}^dV_3'\mathbf{G}_0{}^d\right)_m &= -\left(\mathbf{G}_0{}^d\mathbf{V}_1{}'\mathbf{G}_0{}^d\mathbf{V}_1{}'\mathbf{G}_0{}^d\mathbf{V}_1{}'\mathbf{G}_0{}^d\right)_m \\
&\quad -\left(\mathbf{G}_0{}^d\mathbf{V}_1{}'\mathbf{G}_0{}^dV_2'\mathbf{G}_0{}^d\right)_m \\
&\quad -\left(\mathbf{G}_0{}^d\mathbf{V}_2{}'\mathbf{G}_0{}^d\mathbf{V}_1{}'\mathbf{G}_0{}^d\right)_m && (13'') \\
&\quad \vdots \quad .
\end{aligned}$$

$\mathbf{G}_0{}^d$ creates primaries and internal multiples in the forward series and is responsible for inverse tasks on the same events in the inverse.

We repeat this process for removing internal multiples seeking to isolate terms that only care about this one and only responsibility of ${\mathbf{G}_0}^d$. No coupled task terms (e.g., that involve tasks concerned with both internal multiples and primaries) are included.

After that is accomplished and internal multiples are attenuated, restart the problem, once again, to write an inverse series whose input consists only of primaries. This task isolation and restarting the definition of the inversion procedure strategy has several advantages over a rigid fixation with the original series. Those advantages includes the recognition that a task has already been accomplished is a form of new information and makes subsequent tasks in our list that are often progressively more difficult, considerably less daunting, especially compared to the original all-inclusive data series approach. For example, after removing multiples with a reference medium of water speed, it is easier to estimate a variable background to aid. Transforming to a simpler data with fewer tasks to perform has serious advantages over the strict adherence to the original series for

$$\mathbf{V} = \sum_{i=1}^{\infty} \mathbf{V}_i.$$

Note that the $\mathbf{V}$ the difference between water and earth properties is the same in $\mathbf{V} = \sum_{i=1}^{\infty} \mathbf{V}_i$ and $\mathbf{V} = \sum_{i=1}^{\infty} \mathbf{V}'_i$, but $\mathbf{V}_i \neq \mathbf{V}'_i$ since $\mathbf{V}_i$ assumes the data is D (primaries and all multiples) and ${\mathbf{V}_i}'$ assumes the data is D' (primaries and only internal multiples),e.g., $\mathbf{V}_1$ is linear in all primaries, free surface and internal multiples, while $\mathbf{V}'_1$ is linear in all primaries and internal multiples.

5 An analysis of the Earth model-type and the inverse series and sub-series

To invert for medium properties requires choosing a set of parameters that you seek to identify. The chosen set of parameters (e.g. P and S wave velocity and density) defines an Earth model-type (e.g. acoustic, elastic, isotropic, anisotropic earth), and the details of the inverse series will depend on that choice. Choosing an earth model-type defines the form of L, L_0 and $\mathbf{V}$.

On the way towards identifying the earth properties, (for a given model type), intermediate tasks are performed, such as the removal of free surface and internal multiplies and the location of reflectors in space.

It will be shown below that the free surface and internal multiple attenuation sub-series not only do not require subsurface information for a given model type, they are even independent of earth model type for a very large class of models. The meaning of model type independent task specific subseries is that the defined task is achievable with precisely the same algorithm for an entire class of earth model-types. The members of the model type class we are considering satisfy the convolution theorem, and include acoustic, elastic and certain anelastic media.

In this section, we provide a more general and complete formalism for the inverse series and especially the sub-series that has appeared in the literature to-date. That formalism allows us to examine the issue of model-type and inverse scattering objectives. Finally, when we discuss the imaging and inversion subseries in §7, we use this general formalism as a framework for defining and addressing the new challenges we face in developing subseries that perform imaging at depth without the velocity and inverting large contrast complex targets. All inverse methods for identifying an objective function or medium properties require specification of the parameters to be determined, i.e., of the assumed earth-model type that has generated the scattered wavefield.

To understand how the free surface multiple removal and internal multiple attenuation task specific subseries avoid this requirement, it is instructive to examine the mathematical-physics and logic behind the classic inverse series and see precisely the role model type plays in the derivation.

References for the inverse series include: *Moses, H. E. 1956, Razavy, M., 1975, Weglein, A.B., Boyse, W.E., and Anderson, J.E., 1981, Stolt, R.H., and Jacobs, B., 1980.* In an outline: the inverse series paper by Razavy (1975) is a lucid and important paper relevant to seismic exploration. In that paper, Razavy considers a normal plane wave incident on a one dimensional acoustic medium. We follow the Razavy (1975) development to see precisely how model type enters, and, to glean further physical insight from the mathematical procedure. Then we introduce a perturbation operator, $\mathbf{V}$, general enough in structure to accommodate the entire class of earth model types under consideration.

Finally, if a process (i.e., a subseries) can be performed without specifying how $\mathbf{V}$ depends on the earth property changes, (i.e., what set of earth properties are assumed to vary inside $\mathbf{V}$), the process itself is independent of earth model type.

5.1 Inverse series for a 1-D acoustic constant density medium

Start with the 1-D variable velocity, constant density acoustic wave equation, where $c(x)$ is the wave speed and $\Psi(x,t)$ is a pressure field at location x at time t. The equation that $\Psi(x,t)$ satisfies is

$$\left(\frac{\partial^2}{\partial x^2} - \frac{1}{c^2(x)}\frac{\partial^2}{\partial t^2}\right)\Psi(x,t) = 0 \tag{18}$$

and after a temporal Fourier transform, $t \to \omega$,

$$\left(\frac{d^2}{dx^2} + \frac{\omega^2}{c^2(x)}\right)\Psi(x,\omega) = 0. \tag{19}$$

Characterize the velocity configuration $c(x)$ in terms of a reference velocity, c_0, and perturbation, V

$$\frac{1}{c^2(x)} = \frac{1}{c_0^2}\left(1 - V(x)\right) \ . \tag{20}$$

The experiment consists of a plane wave e^{ikx} where $k = \frac{\omega}{c_0}$ incident upon $V(x)$ from the left (see Fig. (13)). Assume here that V has compact support and that the incident wave approaches $V(x)$ from the same side of $V(x)$ that the scattered field is measured.

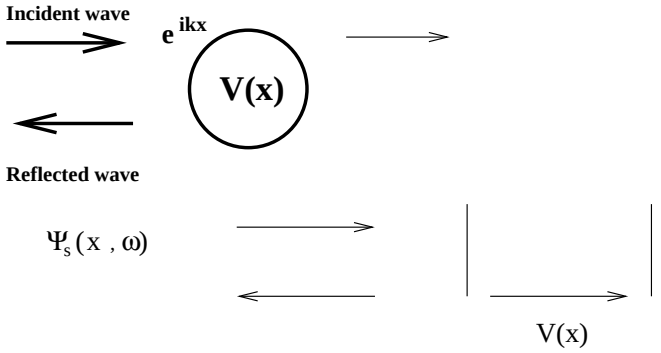

Figure 13: The scattering experiment: a plane wave incident upon the perturbation, V.

Let $b(k)$ denote the overall reflection coefficient for $V(x)$. It is determined from the reflection data at a given frequency ω. e^{ikx} and $b(k)e^{-ikx}$ are the incident and the reflected waves respectively. Rewrite (19) and (20) and the incident wave boundary condition as an integral equation,

$$\Psi(x,\omega) = e^{ikx} + \frac{1}{2ik}\int e^{ik|x-x'|}k^2 V(x')\Psi(x',\omega)dx' \tag{21}$$

and define the scattered field Ψ_s

$$\Psi_s(x,\omega) \equiv \Psi(x,\omega) - e^{ikx}.$$

Also, define the T matrix

$$T(p,k) \equiv \int e^{-ipx} V(x) \Psi(x,k) dx \tag{22}$$

and the Fourier sandwich of the parametrization, V

$$V(p,k) \equiv \int e^{-ipx} V(x) e^{ikx} dx \ .$$

The scattered field, Ψ_s takes the form

$$\Psi_s(x,\omega) = b(k) e^{-ikx} \tag{23}$$

for values of x less than the support of $V(x)$.

From equations (21), (22) and (23) it follows that

$$T(-k,k)\frac{k}{2i} = b(k). \tag{24}$$

Multiply Eq. (21) by $V(x)$ and then Fourier transform over x to find

$$T(p,k) = V(p,k) - k^2 \int_{-\infty}^{\infty} \frac{V(p,q)T(q,k)}{q^2 - k^2 - i\epsilon} dq \tag{25}$$

where p is the Fourier conjugate of x. Razavy (1975) also derives another integral equation by exchanging the roles of unperturbed and perturbed with L_0 viewed as a perturbation of $-V$ upon L,

$$V(p,k) = T(p,k) + k^2 \int_{-\infty}^{\infty} \frac{T^*(k,q)T(p,q)}{q^2 - k^2 - i\epsilon} dq \ . \tag{26}$$

Finally, define $W(k)$ as essentially the Fourier transform of the sought after perturbation, V

$$W(k) \equiv V(-k,k) = \int_{-\infty}^{\infty} e^{2ikx} V(x) dx \tag{27}$$

and recognize that predicting $W(k)$ for all k produces $V(x)$.

From Eq. (26) we find after setting $p = -k$,

$$W(k) = V(-k,k) = T(-k,k) + k^2 \int_{-\infty}^{\infty} \frac{T^*(k,q)T(-k,q)}{q^2 - k^2 - i\epsilon} dq \ . \tag{28}$$

The left hand member of Eq. (28) is the desired solution, $W(k)$, but the right hand member requires both $T(-k,k)$ (that we determine from $\frac{2i}{k}b(k)$) and $T^*(k,q)T(-k,q)$ for all q.

We cannot directly determine $T(k,q)$ for all q from measurements outside V.

If we could determine $T(k,q)$ for all q, then (28) would represent **a closed form** solution to the (multidimensional) inverse problem. If $T(-k,k)$ relates to the reflection coefficient, then what does $T(k,q)$ mean for all q?

Let us start with the integral form for the scattered field

$$\Psi_s(x,k) = \frac{1}{2\pi}\int\int \frac{e^{ik'(x-x')}}{k^2-k'^2}dk'k^2V(x')\Psi(x',k)dx' \tag{29}$$

and Fourier transform (29) going from the configuration space variable, x, to the wave number p to find

$$\Psi_s(p,k) = \int\int \frac{\delta(k'-p)e^{-ik'x'}}{k^2-k'^2-i\epsilon}dk'k^2V(x')\Psi(x',k)dx' \tag{30}$$

and if integrate over k' to find

$$\Psi_s(p,k) = \frac{k^2}{k^2-p^2-i\epsilon}\int e^{-ik'x'}V(x')\Psi(x',k)dx'. \tag{31}$$

The integral in Eq. (31) is recognized from equation (22) as

$$\Psi_s(p,k) = k^2\frac{T(p,k)}{k^2-p^2-i\epsilon}. \tag{32}$$

Therefore to determine $T(p,k)$ for all p for any k is to determine $\Psi_s(p,k)$ for all p and any k ($k=\frac{w}{c_0}$).

But to find $\Psi_s(p,k)$ from $\Psi_s(x,k)$ you need to compute

$$\int_{-\infty}^{\infty} e^{-ipx}\Psi_s(x,k)dx \tag{33}$$

i.e. it requires $\Psi_s(x,k)$ at every x, (not just at the measurement surface, i.e. a fixed x value outside of V).

Hence (28) would provide $W(k)$ and therefore $V(x)$, if we provide not only reflection data $b(k)=T(-k,k)\frac{2i}{k}$ but the scattered field, Ψ_s, at all depths, x.

Since knowledge of the scattered field, Ψ_s (and, hence, the total field), at all x could be used in equation (19) to directly compute $c(x)$, at all x, there is not much point or value in treating Eq. (28) in its pristine form as a complete and direct inverse solution.

Moses (1956) first presented a way around this dilemma. His thinking resulted in the inverse scattering series and consisted of two necessary and sufficient ingredients:

(1) model type combined with (2) A solution for $V(x)$, (and all quantities that depend on V) order by order in the data, $b(k)$.

Expand $V(x)$ as series in orders of the measured data

$$V = V_1 + V_2 + V_3 + \cdots = \sum_{n=1}^{\infty} V_n \tag{34}$$

where V_n is $n-$th order in the data D. When the inaccessible $T(p,k)$, $|p| \neq |k|$ are ignored, Eq. (28) becomes the Born-Heitler approximation and a comparison to the inverse Born approximation (the Born approximation ignores the entire second term of the right hand member of Eq. (28)) was analyzed in Devaney and Weglein (1985).

It follows that all quantities that are power series (starting with power one) in V are also power series in the measured data.

$$T(p,k) = T_1(p,k) + T_2(p,k) + \ldots \tag{35}$$

$$W(k) = W_1(k) + W_2(k) + \ldots \tag{36}$$

$$V(p,k) = V_1(p,k) + V_2(p,k) + \ldots . \tag{37}$$

The model type, in this simple acoustic case, provides a key relationship

$$V(p,k) = W\left(\frac{k-p}{2}\right) \tag{38}$$

that constrains the Fourier sandwich, $V(p,k)$, to be a function of only the difference between k and p. This model-type (acoustic constant density model), combined with order by order construction of the $T(p,k)$ for $p \neq k$ required by the series, provides precisely what we need to solve for $V(x)$.

Start with the measured data, $b(k)$, and substituting $W = \sum W_n$, $T = \sum T_n$ from equations (35) and (36) into Eq. (28) we find

$$\sum_{n=1}^{\infty} W_n(k) = \frac{2i}{k} b(k) + k^2 \int \frac{dq}{q^2 - k^2 - i\epsilon} \left(\sum_{n=1}^{\infty} T_n^* \sum_{n=1}^{\infty} T_n \right) \ . \tag{39}$$

To first order in the data, $b(k)$, $k > 0$ (note that $b^*(+k) = b(-k)$, $k > 0$)

$$W_1(k) = \frac{2i}{k} b(k) \tag{40}$$

and Eq. (40) determines $W_1(k)$ for all k. From Eq. (40) together with Eq. (27) to first order in the data

$$W_1(k) = V_1(-k, k) = \int_{-\infty}^{\infty} V_1(x) e^{2ikx} dx \tag{41}$$

we find $V_1(x)$. The next step towards our objective of constructing $V(x)$ is to find $V_2(x)$.

From $W_1(k)$ we can determinate $W_1(\frac{k-p}{2})$ for all k and p and from Eq. (38) to first order in the data

$$V_1(p, k) = W_1\left(\frac{k-p}{2}\right) \tag{42}$$

which in turn provides $V_1(p, k)$ for all p, k.

(Here is model type in action: The acoustic model with variable velocity and constant density).

Next we go to Eq. (26) to first order $V_1(p, k) = T_1(p, k)$ for all p and k, and substituting in (28) we get the second order in the data

$$W_2(k) = k^2 \int_{-\infty}^{\infty} \frac{dq}{q^2 - k^2 - i\epsilon} T_1^*(k, q) T_1(-k, q) \tag{43}$$

and

$$W_2(k) = \int_{-\infty}^{\infty} e^{2ik} V_2(x) dx. \tag{44}$$

After finding $V_2(x)$ we can repeat the steps to determine the total V order by order

$$V = V_1(x) + V_2(x) + \ldots$$

Order-by-order arguments and model type allow

$$T_1(p, k) = V_1(p, k)$$

although

$$T(p, k) \neq V(p, k) \ .$$

From a physics and information content point-of-view what has happened? The data D collected at e.g. $x = 0$, $\Psi_s(x = 0, \omega)$ determines $b(k)$. This in turn allows the construction of $T(p, k)$, $(k = \omega/c_0)$ for all p order by order in the data. Hence the required scattered wavefield at depth, represented by $T(p, k)$, $k = \omega/c_0$, for all p, for Eq. (28) is constructed order-by-order, for a single temporal frequency, ω, using the model type constraint. The data at one depth for all frequencies is traded for the wavefield at all depths at one frequency. This observation, that in constructing the perturbation, $V(x)$, order-by-order in the data, the actual wavefield at depth is constructed, represents an alternate path or strategy for seismic inversion (see Weglein *et al.* (2000)).

If the inverse series makes these model type requirements for its construction how do the free surface and internal multiple sub-series work independent of earth model type? What can we anticipate about the attitude of the imaging and inversion at depth sub-series with respect to these model type dependence issues?

5.2 The operator V for a class of earth-model types

Consider, once again, the variable velocity, variable density acoustic wave equation

$$\left(\frac{\omega^2}{K} + \nabla \cdot \frac{1}{\rho}\nabla\right) P = 0 \tag{45}$$

where K and ρ are the bulk modulus and density, and can be written in terms of reference values and perturbations a_1 and a_2

$$\frac{1}{K} = \frac{1}{K_r}(1 + a_1) \qquad \frac{1}{\rho} = \frac{1}{\rho_r}(1 + a_2)$$

$$L_0 = \frac{\omega^2}{K_r} + \nabla \cdot \frac{1}{\rho_r}\nabla \tag{46}$$

$$\mathbf{V} = \frac{\omega^2}{K_r}a_1(\vec{r}) + \left(\nabla \cdot \frac{a_2(\vec{r})}{\rho_r}\nabla\right) \ . \tag{47}$$

We will assume a 2-D earth with line sources and receivers, (the 3-D generalization is straightforward). A Fourier sandwich of this $\mathbf{V}$ is

$$V(\vec{p}, \vec{k}; \omega) = \int e^{-i\vec{p}\cdot\vec{r}} V e^{i\vec{k}\cdot\vec{r}} d\vec{r} = \frac{\omega^2}{K_r}a_1(\vec{k} - \vec{p}) + \frac{\vec{k}\cdot\vec{p}}{\rho_r}a_2(\vec{k} - \vec{p}) \tag{48}$$

where $\vec{p}$ and $\vec{k}$ are arbitrary 2D vectors. Green's Theorem and the compact support of a_1 and a_2 help Eq. (47) to Eq. (48). For an isotropic elastic model, equation (48) generalizes for $\mathbf{V}_{pp}$ (see Stolt and Weglein (1985), Boyse (1986), and Boyse and Keller (1986))

$$V_{pp}(\vec{p},\vec{k};\omega) = \frac{\omega^2}{K_r}a_1(\vec{k}-\vec{p}) + \frac{\vec{k}\cdot\vec{p}}{\rho_r}a_2(\vec{k}-\vec{p}) - \frac{2\beta_0^2}{\omega^2}|\vec{k}\times\vec{p}|^2 a_3(\vec{k}-\vec{p}) \tag{49}$$

where a_3 is the relative change in shear modulus and β_0 is the shear velocity in the reference medium.

The inverse series procedure can be extended for perturbation operators (48) or (49), but the detail will differ for these two models. The model-type and order-by-order arguments still hold. Hence 2-D (3-D) general perturbative form will be

$$V(\vec{p},\vec{k};\omega) = V_1(\vec{p},\vec{k};\omega) + \cdots$$

where $\vec{p}$ and $\vec{k}$ are two dimensional (or 3D) independent wave-vectors (that can accommodate a set of earth model types that include acoustic, elastic and certain anelastic forms).

- **ACOUSTIC**
$$\mathbf{V} = \frac{\omega^2}{\alpha_0^2}a_1$$
- **ACOUSTIC** (density variable)
$$\mathbf{V} = \frac{\omega^2}{\alpha_0^2}a_1 + \vec{k}\cdot\vec{k'}a_2$$
- **ELASTIC** isotropic (p-p)
$$\mathbf{V} = \frac{\omega^2}{\alpha_0}a_1 + \vec{k}\cdot\vec{k'}a_2 - 2\frac{\beta_0^2}{\omega^2}|\vec{k}\times\vec{k'}|^2 a_3$$

$a_1 \equiv$ Relative change in the bulk modulus.

$a_2 \equiv$ Relative change in density.

$a_3 \equiv$ Relative change in shear modulus. What can we compute in the inverse series without specifying how $\mathbf{V}$ depends on $(a_1), (a_1, a_2), \cdots$? If we can achieve a task in the inverse series without specifying what parameters $\mathbf{V}$ depends on, then that task can be attained with the same identical algorithm **independent** of earth-model type.

5.3 Free surface and internal multiple subseries and model-type independence

In equations (11)–(14), we presented the general inverse scattering series without specifying the nature of the reference medium that determines $\mathbf{L}_0$ and $\mathbf{G}_0$ and the class of earth model types that relate to the form of $\mathbf{L}$, $\mathbf{L}_0$ and $\mathbf{V}$. In this section, we present the explicit inverse scattering series for the case of marine acquisition geometry. This will also allow the issue of model-type independence to be analyzed in the context of marine exploration.

The reference medium is a half-space, with the acoustic properties of water, bounded by a free surface at the air-water interface, located at $z = 0$. We consider a 2-D medium, and assume that a line source and receivers are located at (x_s, ϵ_s) and (x_g, ϵ_g), where ϵ_s and ϵ_g are the depths below the free surface of the source and receivers, respectively.

The reference operator, $\mathbf{L}_0$, satisfies

$$\begin{aligned} \mathbf{L}_0\mathbf{G}_0 &= \left(\frac{\nabla^2}{\rho_0} + \frac{\omega^2}{\kappa_0}\right)\mathbf{G}_0(x,z,x',z';\omega) \\ &= -\delta(x-x')\big\{\delta(z-z') - \delta(z+z')\big\}\ , \end{aligned} \tag{50}$$

where ρ_0 and κ_0 are the density and bulk modulus of water, respectively. The two terms on the right member of Eq. (10), correspond to the actual source located at (x', z') and the image of this source, across the free surface, at $(x', -z')$, respectively; (x, z) is any point in 2-D space.

The actual medium is a general earth model with associated wave operators, $\mathbf{L}$, and Green's function, $\mathbf{G}$. Fourier transforming Eq. (10) with respect to x, we find:

$$\begin{aligned} &\left[\frac{1}{\rho_0}\frac{d^2}{dz^2} + \frac{q^2}{\kappa_0}\right] G_0(k_x,z,x',z';\omega) = \\ &\quad -\frac{1}{(2\pi)^{1/2}} e^{-ik_x x'}\big\{\delta(z-z') - \delta(z+z')\big\}\ . \end{aligned} \tag{51}$$

The causal solution of Eq. (11) is

$$G_0(k_x,z,x',z';\omega) = \frac{\rho_0}{\sqrt{2\pi}}\frac{e^{-ik_x x'}}{-2iq}\left(e^{iq|z-z'|} - e^{iq|z+z'|}\right)\ , \tag{52}$$

where the vertical wave number, q, is defined as

$$q = \text{sign }(\omega)\sqrt{(\omega/c_0)^2 - k_x^2}\ ,$$

and c_0 is the acoustic velocity of water

$$c_0 = \sqrt{\kappa_0/\rho_0} \ .$$

With G_0 given by Eq. (12), the linear form equation (11) can be written as

$$D(k_g, \epsilon_g, k_s, \epsilon_s; \omega) = \frac{\rho_0^2}{q_g q_s} \sin(q_g \epsilon_g) \sin(q_s \epsilon_s) V_1(k_g, q_g, k_s, q_s, \omega) \ , \tag{53}$$

where $V(\vec{k_g}, \vec{k_s}, \omega) = V_1(\vec{k_g}, \vec{k_s}, \omega) + V_2(\vec{k_g}, \vec{k_s}, \omega) + \ldots$ and $\vec{k_g}, \vec{k_s}$ are arbitrary two dimensional vectors. The variable k_z is defined as

$$k_z = -(q_g + q_s) \ ,$$

where

$$q_g = \text{sign } (\omega) \sqrt{(\omega/c_0)^2 - k_g^2} \ , \tag{54}$$

and

$$q_s = \text{sign } (\omega) \sqrt{(\omega/c_0)^2 - k_s^2} \ . \tag{55}$$

The first term in the inverse series (in two dimensions) in equation (11') in terms of deghosted data, $\tilde{D}$ is

$$\frac{D}{(e^{2iq_g\epsilon_g} - 1)(e^{2iq_s\epsilon_s} - 1)} = \mathbf{G_0}^d \mathbf{V_1} \mathbf{G_0}^d = \tilde{D}(k_g, \epsilon_g, k_s, \epsilon_s; \omega) \tag{56}$$

Using the bilinear form for $\mathbf{G_0}^d$ on both sides of $\mathbf{V_1}$ in Eq. (56) and Fourier transforming both sides of this equation with respect to x_s and x_g we find

$$e^{iq_g\epsilon_g} e^{iq_s\epsilon_s} \frac{V_1(\vec{k_g}, \vec{k_s}; \omega)}{q_g q_s} = D(k_g, \epsilon_g, k_s, \epsilon_s; \omega) \tag{57}$$

where $\vec{k_g}$ and $\vec{k_s}$ are now constrained by $|\vec{k_g}| = |\vec{k_s}| = \frac{\omega}{c_0}$ in the left-hand member of Eq. (57).

In a 2D world only the three dimensional projection of the five dimensional $V_1(\vec{p}, \vec{k}; \omega)$ is recoverable from the surface measurements $D(k_g, \epsilon_g, k_s, \epsilon_s; \omega)$ which is a function of three variables, as well.

It is important to recognize that you cannot determine $\mathbf{V_1}$ for a general operator $\mathbf{V_1}(\vec{r_1}, \vec{r_2}; \omega)$ or $\mathbf{V_1}(\vec{k'}, \vec{k}; \omega)$ from surface measurements on m, and only the three dimensional projection of $\mathbf{V_1}(\vec{k'}, \vec{k}; \omega)$ with $|\vec{k}| = |\vec{k'}| = \frac{\omega}{c_0}$ is recoverable.

However this three dimensional projection of $\mathbf{V}_1$ is more than enough to compute the first order changes in any number of two dimensional earth model parameters; $a_i^1(\vec{r})$ for a given earth model type. ($a_i^1 \equiv$ First order approximation to a_1, a_2, a_3 ...).

After solving for $a_1^1(\vec{r})$, $a_2^1(\vec{r})$, $a_3^1(\vec{r})$ ... ... , you could then use $a_1^1, a_2^1, a_3^1, \ldots$ to compute $\mathbf{V}_1(\vec{k'}, \vec{k}, \omega)$ for all $\vec{k'}, \vec{k}, \omega$ where $a_i'(\vec{r}) \equiv$ linear (or Born) inversion of $a_i(\vec{r})$.

This is the direct extension of the first step of the Moses (1956) procedure where model type is exploited.

Consider $\mathbf{V}_2$ for the operator $\mathbf{V}$ and its linear approximate $\mathbf{V}_1$ (from equation (12))

$$(\mathbf{G}_0\mathbf{V}_2\mathbf{G}_0)_m = -(\mathbf{G}_0\mathbf{V}_1\mathbf{G}_0\mathbf{V}_1\mathbf{G}_0)_m \tag{12}$$

written for the general $\mathbf{V}_1$ form

$$\begin{aligned} & V_2(\vec{k_g'}, \vec{k_s}, \omega) = -\int\int\int\int e^{-i\vec{k_g'}\cdot\vec{r_1}} V_1(\vec{r_1}, \vec{r_2}, \omega) G_0(\vec{r_2}, \vec{r_3}; \omega) \times \\ & V_1(\vec{r_3}, \vec{r_4}; \omega) e^{i\vec{k_s}\cdot\vec{r_4}} d\vec{r_1} d\vec{r_2} d\vec{r_3} d\vec{r_4} \\ = & -\int\int V_1(\vec{k_g'}, \vec{r_2}, \omega) G_0(\vec{r_2}, \vec{r_3}, \omega) V_1(\vec{r_3}, \vec{k_s}, \omega) d\vec{r_2} d\vec{r_3}. \end{aligned} \tag{58}$$

Expressing G_0 as a Fourier transform over $x_2 - x_3$ we find

$$\mathbf{G}_0(x_2 - x_3, z_2, z_3; \omega) = \int dk \mathbf{G}_0(k, z_2, z_3; w) e^{ik(x_2 - x_3)} \tag{59}$$

and

$$\mathbf{G}_0(k, z_2, z_3; \omega) = \int e^{-ikx} dx \mathbf{G}_0(x, z_2, z_3; \omega) \tag{60}$$

for $\mathbf{G}_0 = \mathbf{G}_0{}^d$, Eq. (60) reduces to

$$\mathbf{G}_0{}^d(k, z_2, z_3; \omega) = \frac{e^{iq|z_2 - z_3|}}{2iq} \tag{61}$$

where

$$q = \sqrt{\left(\frac{\omega}{c_0}\right)^2 - k^2}.$$

For the marine case where there is a free surface, the Green's function $\mathbf{G}_0$ satisfies:

$$\left(\nabla^2 + \frac{\omega^2}{c_0^2}\right) \mathbf{G}_0 = \delta(\vec{r_2} - \vec{r_3}) - \delta(\vec{r_2} - \vec{r_3^i}) \tag{62}$$

$$\left(\frac{d^2}{dz_2^2} - k_x^2 + \frac{\omega^2}{c_0^2}\right)\mathbf{G}_0 = \delta(z_2 - z_3) - \delta(z_2 - z_3^i) \tag{63}$$

where z_3^i is the image across the free surface of z_3 (with the free surface at $z = 0, z_3^i = -z_3$. The solution to Eq. (63) is

$$\mathbf{G}_0(k_x, z_2, z_3, \omega) = \frac{e^{iq|z_2 - z_3|} - e^{iq|z_2 + z_3|}}{2iq} = G_0^d + G_0^{FS}$$

The contribution to $\mathbf{V}_2$ from the additional portion of the Green's function due to the free surface, ${\mathbf{G}_0}^{FS}, -\frac{e^{iq|z_2+z_3|}}{2iq}$, will be from equation (58)

$$\int \mathbf{V}_1(\vec{k_g}, \vec{r_2}; \omega)d\vec{r_2} \cdot \int\int dk \frac{e^{iq|z_2+z_3|}}{2iq} e^{ik(x_2 - x_3)}\mathbf{V}_1(\vec{r_3}, \vec{k_s}; \omega)d\vec{r_3} \tag{64}$$

Using the convention

$$\mathbf{V}_1(\vec{k_1}, \vec{k_2}; \omega) \equiv \int e^{-i\vec{k_1}\cdot\vec{r_1}}\mathbf{V}_1(\vec{r_1}, \vec{r_2}; \omega)e^{i\vec{k_2}\cdot\vec{r_2}}d\vec{r_1}d\vec{r_2}$$

where

$$\vec{k_1} \equiv \vec{k_{out}}$$

and

$$\vec{k_2} \equiv \vec{k_{in}}$$

. The portion of $\mathbf{V}_2$ due to ${\mathbf{G}_0}^{FS}$ has the form

$$\int dk \mathbf{V}_1(k_g, -q_g, k, q, \omega)\mathbf{V}_1(k, -q, k_s, q_s, \omega) = -\mathbf{V}_2(k_g, -q_g, k_s, q_s, \omega) \tag{65}$$

where $\vec{k'} \equiv \vec{k_{out}} and \vec{k} \equiv \vec{k_{in}}$ (Fig.14).

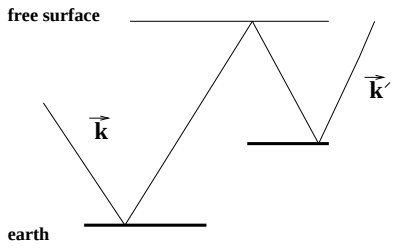

Figure 14: $\vec{k}$ and $\vec{k'}$.

The computation of the portion of $\mathbf{V}_2$ only due to ${\mathbf{G}_0}^{FS}$, ${\mathbf{V}_2}^{FS}$, is computable with $\mathbf{V}_1(\vec{k_g}, \vec{k_s}; \omega)$ where $|\vec{k_g}| = |\vec{k_s}| = \frac{\omega}{c_0}$; which is directly related to $\tilde{D}$ without assumption concerning the

relationship between $\mathbf{V}_1$ and relative changes in earth material properties. It is that portion of the inverse series that forms the free surface de-multiple sub-series.

Therefore the free surface demultiple algorithm is independent of the earth model type for the class of models we are considering.

The summary of the free surface demultiple algorithm (from Weglein *et al.*, 1997 and Carvalho, 1992) is as follows:

1. The data, D, is computed by subtracting the reference field, $\mathbf{G}_0 = \mathbf{G}_0{}^d + \mathbf{G}_0{}^{FS}$, from the total field, G, on the measurement surface.

2. Compute the deghosted data, $\tilde{D}$ where
   $\tilde{D} = D/[(e^{2iq_g\epsilon_g} - 1)(e^{2iq_s\epsilon_s} - 1)]$
   from D and the source and receiver deghosting factors in the $k-\omega$ domain, $\mathbf{G}_0{}^d/\mathbf{G}_0 = 1/(e^{2iq\epsilon} - 1)$. q_s, q_g and ϵ_s, ϵ_g are the vertical wavenumbers and the depths below the free-surface of the source and receiver, respectively.

3. The series for deghosted and free-surface demultipled data, D', is given in terms of the deghosted data D'_1 as follows:

$$\begin{aligned} D'_n(k_g, k_s, \omega) &= \frac{1}{i\pi\rho_r B(\omega)} \int_{-\infty}^{\infty} dk q e^{iq(\epsilon_g+\epsilon_s)} D'_1(k_g, k, \omega) \\ &\quad \times D'_{n-1}(k, k_s, \omega) \qquad n = 2, 3, 4, \ldots \end{aligned} \tag{66}$$

and

$$D'(k_g, k_s, \omega) = \sum_{n=1}^{\infty} D'_n(k_g, k_s, \omega) \ . \tag{67}$$

where $D'(k_g, k_s, \omega) \equiv D'(k_g, \epsilon_g, k_s, \epsilon_s, \omega)$, $B(\omega)$ and ρ_r are the source signature and reference density, respectively. The data D' consist of deghosted primaries and internal multiples only and $D'_1 = \tilde{D}$. Hence, D' represents the deghosted data without free-surface multiples. The mathematical details of equations (66) and (67) follow from equations (11*ı*), (12*ı*) and (13*ı*) and are provided in Carvalho *et al.* (1992) and Weglein *et al.* (1997). Equations (66) and (67) are the prestack multidimensional generalizations of the one-dimensional, normal-incidence free-surface-elimination map presented in the appendix of Ware and Aki (1969).

6 Internal multiple attenuation

In the previous section, we described how to achieve the goal of separating the removal of surface multiples from the other three tasks of inversion. We now address the more difficult issue of separating the task of attenuating internal multiples from the last two goals of migration and inversion.

When we separated surface multiples from the other three goals we were able to isolate a portion of the Green's function, $\mathbf{G}_0$, namely $\mathbf{G}_0{}^{FS}$, whose purpose in the forward and inverse series was to produce and remove, respectively, events due to the presence of the free surface. Unfortunately, for internal multiples, we don't have that relatively straightforward road to follow.

If we attempt to repeat the reasoning that proved useful with surface multiples, we seek an example that has neither surface *nor* internal multiples. We can imagine a problem where we have two half-spaces; that is, we wish to invert a model that has only a single horizontal reflector. In that case, the scattered field, the primary, requires for its description a complete forward scattering series in terms of $\mathbf{G}_0{}^d$ and the exact perturbation, $\mathbf{V}$. The inverse series for $\mathbf{V}$ in terms of the data, the primary, requires the full series and $\mathbf{G}_0{}^d$. The lesson, from this single reflector example, is that the complete $\mathbf{G}_0{}^d$ is required in the inverse series when the only tasks are locating reflectors and estimating parameters. Hence, we *cannot* separate $\mathbf{G}_0{}^d$ into an extra part that exists only in the presence of internal multiples, but which is not present when internal multiples are absent. Thus, a fundamentally different approach is required for the attenuation of internal multiples.

We next present the logical path that leads to this new approach. The forward series generates primaries and internal multiples through the action of $\mathbf{G}_0{}^d$ on $\mathbf{V}$. The inverse series constructs $\mathbf{V}$ from the action of $\mathbf{G}_0{}^d$ on the recorded data. The action of $\mathbf{G}_0{}^d$ on data must remove internal multiples on the way to constructing $\mathbf{V}$. In an earlier section, we presented an analysis and interpretation of the forward series and specifically, how $\mathbf{G}_0{}^d$ generates primaries and internal multiples of a given order. However, before we focus on the internal-multiple issue, it is important to note an essential difference between the scattering theory pictures of free-surface and internal multiple generation.

Given data, D', without free-surface events, the forward series generates data, D, with free-surface events by the action of $\mathbf{G}_0{}^{FS}$ on D'. Each term in that series generates one order of free-surface multiple; that is, all events that have reflected from the free surface a given number of times. The modelling that $\mathbf{G}_0{}^{FS}$ provides is an exact description of a wave

propagating in the water and reflecting from the free surface. Hence, $\mathbf{G}_0{}^{FS}$ generates in the forward series, and removes in the inverse series, one order of free-surface multiple with each term.

The situation for primaries and internal multiples is quite different. For those events, we adopt a point-scatterer model, and every term in that forward series contributes to (but does not by itself fully describe) either primary or internal multiples. Each primary or internal multiple requires an infinite series for its construction. We adopt the simpler surface reflection model when describing wave phenomena associated with reflectors at or above the measurement surface; we adopt the point-scatterer model for waves associated with sub-receiver/source structure. The former is our model of choice when we have accurate or nearly accurate information about velocities and structure, and the latter is our model when that information is unavailable or unreliable.

The location and properties of the free surface are captured in $\mathbf{G}_0{}^{FS}$ and it is that specific and well defined experience (or its absence) which allows free surface multiples to be separated from primaries and internal multiples with one term creating (in the forward series) and one term removing (in the inverse series) all events that have experienced the free surface a given number of times. The number of $\mathbf{G}_0{}^{FS}$ factors in a term in the subseries equations (12*ı*-13*ı*) correspond to the order of free surface multiples it removes. The internal multiples have (by definition) all of their downward reflections below the free surface and since we assume absolutely no subsurface information those reflectors are assumed to be completely unknown in both location and character.

This makes the problem of distinguishing the generation (and removal) of internal multiples from primaries more difficult in terms of direct propagation through water $\mathbf{G}_0{}^{d}$ and the difference between earth and water properties, $\mathbf{V}$. As mentioned earlier a series is required to generate any primary or any internal multiple in terms of $\mathbf{G}_0{}^{d}$ and $\mathbf{V}$ and new concepts required to distinguished this forward subseries.

It is no surprise that the first term in the generation and first term in the removal of internal multiples are approximate. The efficiency of the first term in the removal subseries of internal multiples is remarkably higher than the first term in the forward creation, e.g., it takes an infinite series to get the important time prediction (phase) of any internal multiple in the forward series (in terms of $\mathbf{G}_0{}^{d}$ and $\mathbf{V}$) whereas, as we will demonstrate, the first term in the removal series (of an internal multiple of a given order) predicts the time precisely and well approximates the amplitude (in terms of $\mathbf{G}_0{}^{d}$ and D') of all multiples of that order - from all reflectors at all depths at once. The efficiency of the inverse subseries accounts for its practical value and impact.

The fact that generating primaries and internal multiples of a given order requires an infinite series suggests that an infinite series of terms, each involving operations with $\mathbf{G_0}^d$ on D', is required to remove internal multiples of a given order. The particular inverse-scattering subseries for attenuating all internal multiples, described here, chooses only the leading and most significant contribution from the removal series of each order of multiple, forming a series that well attenuates, rather than eliminates, all internal multiples.

In our earlier discussion of the forward series for primaries and internal multiples we argued that primaries are constructed starting with the first term in the series, and first-order internal multiples have their leading contribution in the third term. Similarly, second-order internal multiples are generated by contributions starting with the fifth term in the forward series. In general, n-th order internal multiples have contributions from all terms starting at term $2n+1$. In addition, the portion of the third term that starts to build the first-order internal multiple was distinguished from the part that has a third-order contribution to constructing primaries. The leading-term contribution to constructing a class of multiples in the forward series suggests the leading-term contribution for their removal in the inverse series (Fig. 15).

The first two terms in the forward series don't contribute to generating first-order internal multiples. Similarly, it's argued that the first two terms in the inverse series don't contribute to their removal. The mathematical realization of Fig. 15a, is the leading contribution to the generation of first-order internal multiples; it suggests the corresponding mathematical expression for the leading-order attenuation of those multiples. To realize Fig. 15b select the portion of the third term of the inverse series with $z_1 > z_2$ and $z_3 > z_2$.

With this purpose in mind we examine $\mathbf{V}_3$, the third term in the inverse series. In contrast with the subseries generated by $\mathbf{G_0}^{FS}$, for free-surface multiple attenuation, the three terms in $\mathbf{V}_3$ do not sum to a single term when the inverse series is generated with the direct propagating Green's function, $\mathbf{G_0}^d$. From the fact that $\mathbf{G_0}^{FS}$ can be viewed as the Green's function due to an image source above the free surface and is therefore *outside* the volume, it follows that for all z, z' inside the volume (i.e., below the free surface) $\mathbf{G_0}^{FS}$ satisfies the homogeneous differential equation

$$\left(\frac{\nabla^2}{\rho_0} + \frac{\omega^2}{\kappa_0}\right) \mathbf{G_0}^{FS} = 0 \ .$$

The fact that $\mathbf{G_0}^{FS}$ satisfies a homogeneous differential equation leads in turn to the math-

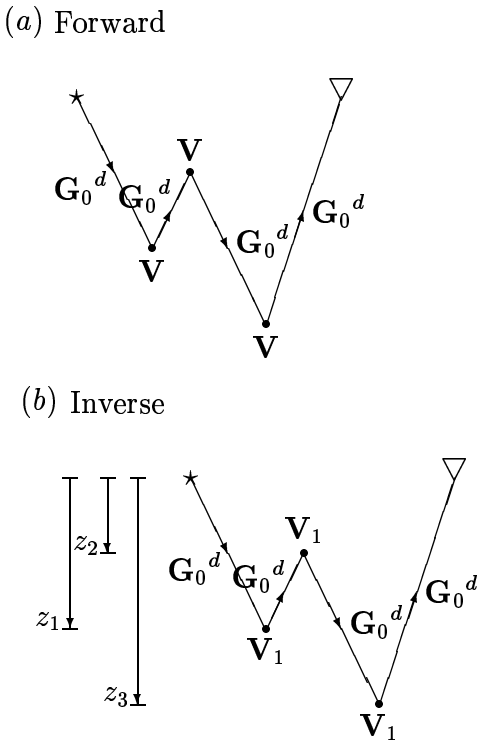

Figure 15: The leading term contribution to the generation of first-order internal multiples is represented in (a) and suggests the leading term contribution, in the inverse series, to the removal of first-order internal multiples represented in (b). $\mathbf{G_0}^d$, $\mathbf{V}$ and $\mathbf{V}_1$ are the whole-space Green's function, the perturbation operator and the "migrated data-like" first-order approximation to $\mathbf{V}$, respectively.

ematical simplification

$$\begin{aligned}\left(\mathbf{G_0}^d\mathbf{V}_1\mathbf{G_0}^{FS}\mathbf{V}_1\mathbf{G_0}^{FS}\mathbf{V}_1\mathbf{G_0}^d\right)_m &= -\left(\mathbf{G_0}^d\mathbf{V}_1\mathbf{G_0}^{FS}\mathbf{V}_2\mathbf{G_0}^d\right)_m \\ &= -\left(\mathbf{G_0}^d\mathbf{V}_2\mathbf{G_0}^{FS}\mathbf{V}_1\mathbf{G_0}^d\right)_m \ . \end{aligned} \tag{68}$$

$\mathbf{G_0}^{FS}$ doesn't require off-shell $\vec{k} \neq \vec{k'}$ contribution as long it is in integrals over the volume V_1, and its effective source, the image source is outside the volume. This is another way to understand why the free-surface demultiple algorithm is automatically model-type independent. Model type was needed in Razavy (1975), to provide $T_1(k,p)$ for $k \neq p$. Since $\mathbf{G_0}^{FS}$ never requires $\vec{k} \neq \vec{p}$ in its integrations with V_1 it doesn't depend upon the inverse series model type argument to generate this subseries. Hence the free-surface multiple removal subseries is independent of earth model type. In contrast, $\mathbf{G_0}^d$ satisfies the inhomogeneous differential equation

$$\left(\frac{\nabla^2}{\rho_0} + \frac{\omega^2}{\kappa_0}\right)\mathbf{G_0}^d = -\delta(z-z')\delta(x-x') \ .$$

From Eq. (13"), and using $\mathbf{G_0}^d$, we have:

$$\begin{aligned}\left(\mathbf{G_0}^d\mathbf{V}_3\mathbf{G_0}^d\right) &= -\left(\mathbf{G_0}^d\mathbf{V}_1\mathbf{G_0}^d\mathbf{V}_2\mathbf{G_0}^d\right) \\ &\quad -\left(\mathbf{G_0}^d\mathbf{V}_2\mathbf{G_0}^d\mathbf{V}_1\mathbf{G_0}^d\right) - \left(\mathbf{G_0}^d\mathbf{V}_1\mathbf{G_0}^d\mathbf{V}_1\mathbf{G_0}^d\mathbf{V}_1\mathbf{G_0}^d\right) \\ &= \left(\mathbf{G_0}^d\mathbf{V}_{31}\mathbf{G_0}^d\right) + \left(\mathbf{G_0}^d\mathbf{V}_{32}\mathbf{G_0}^d\right) + \left(\mathbf{G_0}^d\mathbf{V}_{33}\mathbf{G_0}^d\right) \ , \end{aligned} \tag{69}$$

where

$$\mathbf{V}_{31} \equiv -\mathbf{V}_1\mathbf{G_0}^d\mathbf{V}_2 \ , \tag{70}$$

$$\mathbf{V}_{32} \equiv -\mathbf{V}_2\mathbf{G_0}^d\mathbf{V}_1 \ , \tag{71}$$

and

$$\mathbf{V}_{33} \equiv -\mathbf{V}_1\mathbf{G_0}^d\mathbf{V}_1\mathbf{G_0}^d\mathbf{V}_1 \ . \tag{72}$$

In contrast to the case of $\mathbf{G_0}^{FS}$, these three terms $\mathbf{V}_{31}, \mathbf{V}_{32}$ and $\mathbf{V}_{33}$ make distinct contributions. The first two terms, $\left(\mathbf{G_0}^d\mathbf{V}_{31}\mathbf{G_0}^d\right)$ and $\left(\mathbf{G_0}^d\mathbf{V}_{32}\mathbf{G_0}^d\right)$, on the right member can be shown (Araújo, 1994) to consist of a refraction-like scattering component, and are thus not chosen for the task of removing internal multiples. These contribute to the other inversion tasks (migration and inversion) that act on primaries. The third term on the right hand side,

$$\left(\mathbf{G_0}^d\mathbf{V}_{33}\mathbf{G_0}^d\right) = -\left(\mathbf{G_0}^d\mathbf{V}_1\mathbf{G_0}^d\mathbf{V}_1\mathbf{G_0}^d\mathbf{V}_1\mathbf{G_0}^d\right) \ ,$$

Figure 16: Diagrams corresponding to different portions of $\Lambda_s \mathbf{G}_0{}^d \mathbf{V}_1 \mathbf{G}_0{}^d \mathbf{V}_1 \mathbf{G}_0{}^d \mathbf{V}_1 \mathbf{G}_0{}^d \Lambda_g$. Only (d), with $z_1 > z_2$ and $z_2 < z_3$, contributes to the attenuation of first-order internal multiples (see also Fig. 15b).

can be broken up into four parts corresponding to the four diagrams in Fig. 16.

Choose the portion of $\left(\mathbf{G_0}^d\mathbf{V}_{33}\mathbf{G_0}^d\right)_m$ corresponding to Fig. 16d; a diagram that represents a contribution to multiple *reflection* attenuation. $\left(\mathbf{G_0}^d\mathbf{V}_{31}\mathbf{G_0}^d\right)_m$ and $\left(\mathbf{G_0}^d\mathbf{V}_{32}\mathbf{G_0}^d\right)_m$ do not support a diagram of the Fig. 16d variety, and therefore were not selected for that task. The mathematical and algorithmic realizations of Fig. 16d takes place by requiring a lower-higher-lower relationship between the successive vertical locations of the data in the integral. Using this criterion, the appropriate portion of each of the odd terms in the series is selected. The generalization of the diagram found in Fig. 16d is used to select the appropriate portion of the leading-order contribution to removing higher-order internal multiples.

7 Internal multiple attenuation and model-type dependence

For $\mathbf{G_0}^d$, the direct propagating Green's function we have from Eq. (61)

$$\frac{e^{iq|z_2-z_3|}}{2iq} = \frac{1}{2\pi}\int_{-\infty}^{\infty}\frac{e^{iq'(z_2-z_3)}}{q^2-q'^2+i\epsilon}dq'$$

and separating the integral into a principal value and a contribution from contours around the poles $q' = \pm q$ as

$$\begin{aligned}\frac{1}{q^2-q'^2+i\epsilon} &= P.V.\left(\frac{1}{q^2-q'^2}\right) + i\pi\delta\left(q'^2-q^2\right)\\ &= P.V.\left(\frac{1}{q^2-q'^2}\right) + \frac{1}{2\pi}\left(i\pi\frac{1}{2\left|q\right|}\left(\delta(q'-q)+\delta(q'+q)\right)e^{iq'(z_2-z_3)}\right)\end{aligned}$$

This contour around the pole contribution leads to:

$$\int_{-\infty}^{\infty}dk\left[\frac{V_1\left(k_g,-q_g,k,q\right)V_1\left(k,q,k_s,q_s\right)}{2iq}+\frac{V_1\left(k_g,-q_g,k,-q\right)V_1\left(k,-q,k_s,q_s\right)}{2iq}\right]$$

and is computable directly from $\mathbf{V}_1\left(k_g,q_g,k_s,q_s\right)$.

The portion of V_2 that depends on the principal value part of the contribution to G_0^d is not computable from $\Psi_s\left(x_g,\epsilon_g,x_s,\epsilon_s,\omega\right)$ without assuming a model-type. Since the internal multiple algorithm derives from the analogous $i\pi\delta$ contributions from the $\mathbf{V}_1\mathbf{V}_1\mathbf{V}_1$ or V_{33} (equation (72)) contribution from the third term in the series (equation (13"))

$$\int dkdk'\left[\frac{\mathbf{V}_1\left(k_g,-q_g,k,q\right)\mathbf{V}_1\left(k,q,k',-q'\right)}{2iq}.\frac{\mathbf{V}_1\left(k',-q',k_s,q_s\right)}{2iq'}+\ldots\right]$$

is once again computable directly from surface data without assumption of model type.

An important point to recognize in deriving the internal multiple algorithm, not emphasized in previous publication, is that although the "W" or lower-higher-lower relationship from the forward series provides a guide for the examination of a similar diagram in the inverse, to actually realize an internal multiple algorithm the quantity taken through the diagram was not $\mathbf{V}_1$ but rather

$$b_1\left(k_g,\epsilon_g,k_s,\epsilon_s,q_g+q_s\right)=\left(-2iq_s\right)D'\left(k_g,\epsilon_g,k_s,\epsilon_s,\omega\right)=\frac{\mathbf{V}_1\left(k_g,q_g,k_s,q_s,\omega\right)}{-2iq_g}$$

the effective data generated by a single frequency plane-wave incident field. This was originally deduced (see Araujo (1994) and Weglein *et al.* (1997)) through empirical evaluation and testing of different candidate quantities (e.g. a first and natural guess of taking $\mathbf{V}_1$ through "W" doesn't lead to an attenuation algorithm) that, in turn, allow different subdivisions of the $\mathbf{V}_{33}$ term in terms of a "W" diagram.

The fact that this quantity, b_1, results in a localized incident wavefront in every dimension (without the wake behind the front that the impulse response in 1D and 2D experience) is the only and best (although meager) 'understanding' or hint we have for this fact, to-date. Hence, the forward construction and inverse removal symmetry for the internal multiple went only so far and the fact that, $b_1=\frac{\mathbf{V}_1(k_g,q_g,k_s,q_s,\omega)}{-2iq_g}$ is the quantity that when transformed to (k_g,q_g,z) and broken into lower-higher-lower contributions results in the internal multiple algorithm remains partly intuitive and empirical in its foundation and invites further analysis for better understanding. That algorithm operates in a 1D, 2D or 3D earth. A deeper awareness and comprehension of the workings of the inverse series will, of course, also benefit the current research on imaging and inverting primaries.

The internal multiple algorithm is independent of model type because if derives from a algorithm depending on the portion of $\mathbf{V}_1$ that only requires $|\vec{k_g}|=|\vec{k_s}|=\frac{\omega}{c_0}$.

8 Internal multiple algorithm

The first term in the internal multiple-attenuation subseries is the data, D', consisting of primaries and internal multiples. The second term in the attenuation series comes from a portion of the third term in the series (equations (69) and (72)). This portion of the third

term,

$$\begin{aligned} b_3 =& \frac{1}{(2\pi)^2}\int_{-\infty}^{\infty}\int_{-\infty}^{\infty} dk_1 e^{-iq_1(\epsilon_g-\epsilon_s)} dk_2 e^{iq_2(\epsilon_g-\epsilon_s)} \\ &\times \int_{-\infty}^{\infty} dz_1 e^{i(q_g+q_1)z_1} b_1(k_g,k_1,z_1) \\ &\times \int_{-\infty}^{z_1} dz_2 e^{i(-q_1-q_2)z_2} b_1(k_1,k_2,z_2) \\ &\times \int_{z_2}^{\infty} dz_3 e^{i(q_2+q_s)z_3} b_1(k_2,k_s,z_3) \ , \end{aligned} \tag{73}$$

is chosen to satisfy $z_1 > z_2$ and $z_2 < z_3$. b_1 is defined in terms of the original prestack data with free-surface multiples eliminated, D', and is defined by

$$D'(k_g,k_s,\omega) = (-2iq_s)^{-1} B(\omega)\ b_1(k_g,k_s,q_g+q_s) \ . \tag{74}$$

b_1 is the data that would result from a single-frequency incident plane wave and $B(w)$ is the source signature. The data with internal multiples attenuated, D^{IM}, is

$$D^{IM}(k_g,k_s,\omega) = (-2iq_s)^{-1} B(\omega) \sum_{n=0}^{\infty} b_{2n+1}(k_g,k_s,q_g+q_s). \tag{75}$$

A recursive relationship that generalizes Eq. (75) and provides b_{2n+1} in terms of b_{2n-1} for $n = 1,2,3,\ldots$ is given in Araújo (1994) as

$$\begin{aligned} b_{2n+1}(k_g,k_s,q_g+q_s) =& \frac{1}{(2\pi)^{2n}}\int_{-\infty}^{\infty} dk_1 e^{-iq_1(\epsilon_g-\epsilon_s)} \\ &\times \int_{-\infty}^{\infty} dz_1 e^{i(q_g+q_1)z_1} b_1(k_g,k_1,z_1) A_{2n+1}(k_1,k_s,z_1) \\ & \qquad\qquad n = 1,2,3,\ldots \end{aligned} \tag{76}$$

where

$$\begin{aligned} A_3(k_1,k_s,z_1) =& \int_{-\infty}^{\infty} dk_2 e^{iq_2(\epsilon_g-\epsilon_s)} \int_{-\infty}^{z_1} dz_2 e^{i(-q_1-q_2)z_2} \\ &\times\ b_1(k_1,k_2,z_2) \int_{z_2}^{\infty} dz_3 e^{i(q_2+q_s)z_3} b_1(k_2,k_s,z_3) \end{aligned}$$

and

$$A_{2n+1}(k_1,k_s,z_1) = \int_{-\infty}^{\infty} dk_2 e^{iq_2(\epsilon_g-\epsilon_s)} \times \int_{-\infty}^{z_1} dz_2 e^{i(-q_1-q_2)z_2} b_1(k_1,k_2,z_2) \times \int_{-\infty}^{\infty} dk_3 e^{-iq_3(\epsilon_g-\epsilon_s)} \int_{z_2}^{\infty} dz_3 e^{i(q_2+q_3)z_3} \times \; b_1(k_2,k_3,z_3) A_{2n-1}(k_3,k_s,z_3) \qquad n = 2,3,4,\ldots \; .$$

As we mentioned, the full series for $\mathbf{V}$ can have restrictive convergence properties and a sensitivity to missing low-frequency information, (see, e.g., Carvalho, 1992). In contrast, tests indicate (see Araújo, 1994; Araújo et al., 1994a; Araújo et al., 1994b) that the multiple attenuation subseries in Eq. (76) always converges and is insensitive to missing low frequency information.

Free-surface multiple attenuation methods operate one temporal frequency at a time (see equations (66) and (67)); in contrast, the attenuation of an internal multiple from a single frequency of data requires data at all frequencies [see equations 75 – 76]. This requirement derives from the integral over temporal frequency in the transform of $q_g + q_s$ to z. With bandlimited data this transform is only approximate; nevertheless, the truncated integral remains effective in attenuating multiples. As in the case of the surface-removal algorithm each term in the series, Eq. (75), attenuates a given order of internal multiple, and prepares the higher order internal multiples for the higher demultiple terms in the series. Since $e^{ik_z z} b_1(k_g,k_s,\omega)$ is a downward continuation of shots and receivers to depth z in the reference medium, and subsequent integration over k_z is a simple constant Jacobian away from integration over ω ($t = 0$ imaging condition), it follows that $b_1(k_g,k_s,z)$ corresponds to uncollapsed-migration (Stolt and Weglein, 1985; Weglein and Stolt, 1999). Indeed, the algorithm can be interpreted as a sequence of these uncollapsed migrations restricted to lower-higher-lower, pseudo-depth, which is essentially vertical travel time, since the reference is constant water speed. Uncollapsed-migration is a generalization of the original migration concept; sources and receivers are downward continued to a common-depth level z, time is evaluated at zero, and information at $x_g \neq x_s$ is retained. The latter retention of $x_g \neq x_s$ distinguishes uncollapsed-migration from migration; it provides local angle-dependent reflection coefficients rather than the angle-averaged reflection coefficient of the traditional $x_g = x_s$ imaging condition(see Weglein and Stolt, 1999).

When free-surface and internal multiples are present: (1) apply the free-surface demultiple algorithm to D and output D', then (2) input D' to the internal multiple attenuation algorithm, to produce primaries.

9 Purposeful perturbation concept and examples of free surface and internal multiple attenuation

9.1 Purposeful perturbation

As we have described, the response to the apparent lack of robust convergence of the entire inverse series, without a-priori information, and the recognition that it nevertheless represented the only complete inversion formalism for the multidimensional acoustic and elastic waves combined to encourage seeking task specific subseries that would have more favorable properties. However, another issue that these task specific (well-converging) subseries faced was how many terms would you require in practice to achieve a certain level of effectiveness. The concept of purposeful perturbation was developed to address the latter issue.

The idea was to identify the specific purpose or role that each term within a task specific subseries performs independent of the subsurface or target over which the recorded data was collected.

The terms of the series perform tasks and coupled tasks; the task specific subseries perform isolated, uncoupled tasks; and, we define the purposeful perturbation concept to know precisely what each term within a given task specific subseries is designed to accomplish. For example, a term in the inverse scattering subseries for eliminating free surface multiples removes precisely one order of free-surface multiple completely independent of the depth of the water or any other property or characteristic of the Earth.

9.2 1D free surface demultiple algorithm

For the simplest illustration of this purposeful perturbation concept, consider the generation of free-surface multiples for a 1-D Earth, whose primary reflections and internal multiples have a response $R(\omega)$; and, where the free surface is characterized by a reflection coefficient of -1 (see Fig. 17).

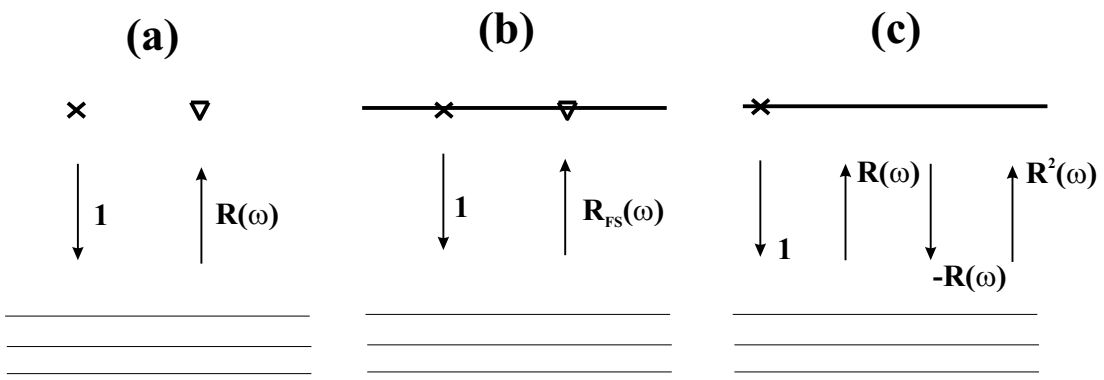

Figure 17: Illustration of the free surface multiple removal series: (a) Data without a free surface, (b) the total upgoing field in the presence of a free surface R_{FS}, and (c) the series for R_{FS}.

If the subseries we isolate are defined for accomplishing one of the four broad tasks we earlier defined, purposeful perturbation seeks to determine, or further define, the specific role or sub-task that individual terms in the sub-series perform. Then, e.g., if you estimate the range of depths of potential hydrocarbon reservoirs in a given setting, and the depth to the water-bottom, then you have a good way to determine the highest order of water-bottom multiple you need to be concerned with and precisely the number of terms in the free surface demultiple subseries (equations (66) and (67)) that can accomplish that objective.

For source and receiver deghosted data, and a source wavelet with unit amplitude, the upgoing field in the presence of a free surface R_{FS} is able to be written in terms of $R(\omega)$ by imagining (see Fig (17)c) the wave first leaving the source moving down into the Earth; that incident unit pressure wave generates a reflected response from the Earth, $R(\omega)$, consisting of primaries and internal multiples. This in turn propagates as a train up in the water column until it hits the free-surface, where it experiences a (-1) reflection coefficient and heads down through the water columns as $-R(\omega)$. The impulse response of the Earth $R(\omega)$ times this effective downgoing "wavelet", $-R(\omega)$ produces a new wave moving up from the Earth through the water column towards the free surface. This process continues and results in the total upgoing wave in the presence of the free surface, $R_{FS}(\omega)$ in terms of the primary and internal multiple wavefield, $R(\omega)$ as follows

$$\begin{aligned} R_{FS} &= R - R^2 + R^3 - \dots \\ &= \frac{R}{1+R} \end{aligned} \tag{77}$$

Each term in Eq. (77) generates all free surface multiples of a given order independent of any detail of the subsurface. The order of a free surface multiple corresponds to the number

of times that event has experienced a reflection at the free surface. Since each successive term in Eq. (77) comes from one additional reflection at the free-surface, it generates one additional order of free-surface multiple. Solving Eq. (77) for the data without free-surface multiples, R, we have

$$\begin{aligned} R &= \frac{R_{FS}}{1 - R_{FS}} \\ &= R_{FS} + R_{FS}^2 + R_{FS}^3 + \dots \end{aligned} \tag{78}$$

The first term in Eq. (78), R_{FS}, is the upgoing portion of the reflection data that contains all free-surface multiples. When the second term, R_{FS}^2, is added to R_{FS} two things happen: (1) all free-surface multiples that have reflected once (and only once) from the free-surface are removed and (2) all higher-order free-surface multiples are altered in preparation for higher terms, e.g., R_{FS}^3, to remove them order-by-order, as well. This well-defined action of the terms in the free-surface demultiple series is totally independent of any water-bottom or subsurface detail (of course, within an assumed 1D, 2D or 3D dimension of the Earth variation).

This is an example of purposeful perturbation; and, it has enormous practical significance. For example, if you estimate that for a given depth of water and target, that only a certain order of multiples could be troublesome, then you know precisely how many terms in the series you need to use in your processing algorithm for that data. Eq. (78) is the 1-D normal incidence special case of the general multi-dimensional inverse scattering subseries for free-surface multiple removal equations (66) and (67) (see also Carvalho *et al.*, 1992 and Weglein *et al.*, 1997).

Equation (78) is the 1D antecedent of equations (11*ı*- 13*ı*) and (66) and (67) for free surface multiple removal. Several observations about equations (77) and (78) are worth noting.

First, the role of $\mathbf{G_0}^{FS}$, the extra portion of $\mathbf{G_0}$ due to the free-surface, is played by the (-1) reflection coefficient in deriving (77) and its inverse (78). Second, the forward construction series was a guide (and in this simple instance, more than a guide) to the inverse process. Only the free-surface reflection coefficient (-1) i.e., $\mathbf{G_0}^{FS}$ terms enter confirms the forward and removal series (77), (78). Focussing on the one task, and only one task, this simple consistent strategy we described, i.e., no $\mathbf{G_0}^{FS}, \mathbf{G_0}^{D}$ coupled terms appear in the analogous and transparently simple equations (77) and (78).

Regarding some practical issues, exemplified by equations (77) and (78), if instead of 1, a unit incident pulse, a wavelet $A(w)$ was the source signature, then equation (77) would

become

$$R_{FS} = \frac{A(w)R}{1+R} \tag{79}$$

and Eq. (78) becomes

$$R = \frac{\frac{R_{FS}}{A(w)}}{1-\frac{R_{FS}}{A(w)}} = \frac{R_{FS}}{A(w)} + (\frac{R_{FS}}{A(w)})^2 + \dots \tag{80}$$

and, hence, the wavelet is a critical requirement for the free-surface removal and all subseries application.

A similar process of purposeful perturbation occurs (and has been identified) for the internal multiple removal series. Understanding the specific purpose, within an overall task, that each term accomplishes not only reveals what has (and has not) been achieved for a given finite number of terms and this significantly mitigates issues of overall convergence and rate of convergence.

9.3 1D analytic example of the internal multiple attenuation algorithm

The 2D internal multiple algorithm described in equations (73-76)

$$b(k_g, k_s, q_g + q_s) = -2iq_s D'(k_g, k_s, \omega)$$

where D' is the free-surface multiple removed data resulting from an impulsive source. The second term in the internal multiple attenuation series, b_3, is given by

$$\begin{aligned} b_3(k_g, k_s, q_g + q_s) &= \frac{1}{(2\pi)^2} \int_{-\infty}^{\infty} \int_{-\infty}^{\infty} dk_1 e^{iq_1(\epsilon_s - \epsilon_g)} dk_2 e^{iq_2(\epsilon_g - \epsilon_s)} \\ &\times \int_{-\infty}^{\infty} dz_1 e^{i(q_g+q_1)z_1} b_1(k_g, -k_1, z_1) \\ &\times \int_{-\infty}^{z_1} dz_2 e^{i(-q_1-q_2)z_2} b_1(k_1, -k_2, z_2) \\ &\times \int_{z_2}^{\infty} dz_3 e^{i(q_2+q_s)z_3} b_1(k_2, -k_s, z_3) \end{aligned}$$

The first two terms in the multiple attenuation series, $(-2iq_s)(b_1 + b_3)$, Eq. (75), attenuate all first order internal multiples. For a 1D earth and a normal incidence plane wave, Eq.

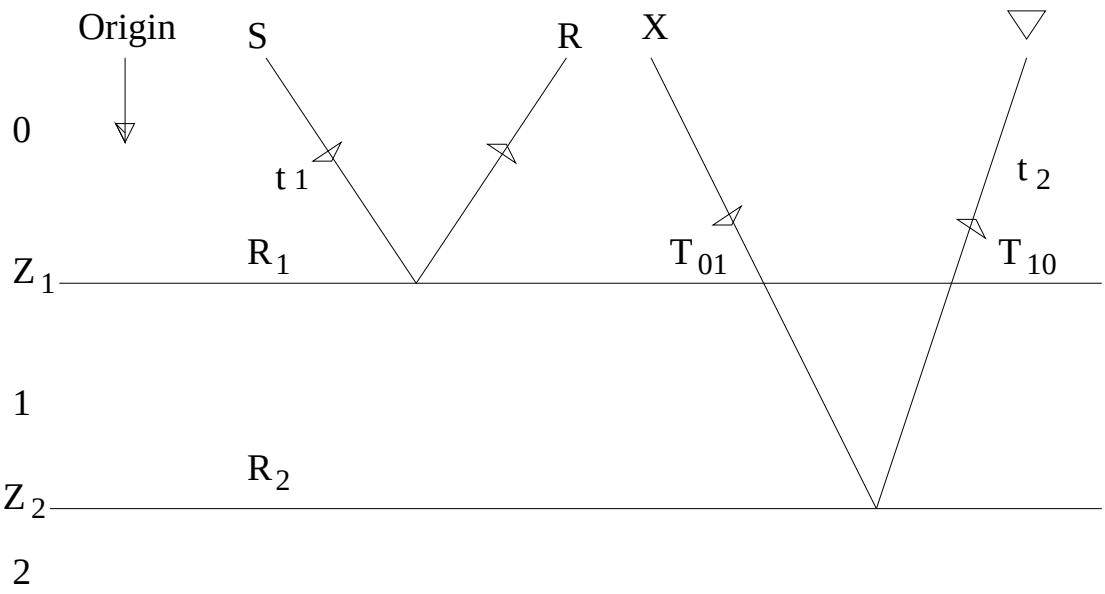

Figure 18: One dimensional model with 2 interfaces.

(73) reduces to:

$$b_3(k) = \int_{-\infty}^{\infty} dz_1 e^{ikz_1} b(z_1) \int_{\infty}^{z_1} dz_2 e^{-ikz_2} b(z_2) \int_{z_2}^{\infty} dz_3 e^{ikz_3} b(z_3) \tag{81}$$

To explicitly demonstrate how the internal multiple attenuation algorithm works and to examine its properties, we will consider the simplest model that can produce an internal multiple. For the model shown in Fig. (18) the reflection data due to an impulsive incident wave $\delta(t - \frac{z}{c})$ is

$$D(t) = R_1 \delta(t - t_1) + T_{01} R_2 T_{10} \delta(t - t_2) + \dots$$

where t_1, t_2, R_1, R_2 are the two way times and reflection coefficients from the two reflectors and T_{01} and T_{10} are the transmission coefficients between 0 and 1 and 1 and 0, respectively.

$$D(\omega) = R_1 e^{i\omega t_1} + T_{01} R_2 T_{10} e^{i\omega t_2} + \dots \tag{82}$$

where $D(w)$ is the temporal former transform of $D(t)$.

Note that the $(-2iq_s)$ factor that multiples D' in the internal multiple theory is not required in this example since we assume that the incident wave is an impulsive plane wave. The role of the $(-2iq_s)$ is to transform an incident (or reference field) $\mathbf{G}_0$, into a plane wave in the Fourier domain. The internal multiple algorithm inputs the data with primaries and internal multiples, b and is the first term in the multiple attenuated series, b_1.

$$b^{IM}(k) = b_1(k) + b_3(k) + b_5(k) + \dots$$

where $b_1 = b$, the input data.

The vertical wave number

$$k_z = \sqrt{(\omega/C_0)^2 - k_{x_g}^2} + \sqrt{(\omega/C_0)^2 - k_{x_s}^2}$$

for 1D medium and normal incident wave is $k_z = 2\frac{\omega}{C_0}$ and

$$b(k_z) = D(\omega) \ . \tag{83}$$

The reflection data from Eq. (82) and (83) is expressed in terms of k_z

$$b(k_z) = R_1 e^{i(\frac{2\omega}{C_0})(\frac{C_0 t_1}{2})} + T_{01} R_2 T_{10} e^{i(\frac{2\omega}{C_0})(\frac{C_0 t_2}{2})} + \dots \tag{84}$$

and define the pseudo-depths z_1 and z_2 in the reference medium as:

$$z_1 \equiv \frac{C_0 t_1}{2}$$

$$z_2 \equiv \frac{C_0 t_2}{2} \ .$$

The input data is now expressed in terms of $k = k_z$ and z_1 and z_2 as

$$b(k) = R_1 e^{ikz_1} + T_{01} R_2 T_{10} e^{ikz_2} + \dots \tag{85}$$

ready for the internal multiple algorithm.

Substitute the data from Eq. (85) into the algorithm (b_3, equation (81)). After transforming from $k = k_z$ to z.

$$b(z) = \int_{-\infty}^{\infty} e^{-ikz} b(k) dk \tag{86}$$

The first integral in Eq. (81) towards computing b_3 is

$$\int_{z_2'+\epsilon_1}^{\infty} dz_3 e^{ikz_3} (R_1 \delta(z_3' - z_1) + R_2' \delta(z_3' - z_2) + \dots) \tag{87}$$

where

$$R_2' \equiv T_{01} R_2 T_{10} \ .$$

ϵ_1 is a small positive parameter chosen to insure that the $'W'$ diagram is strictly lower-higher-lower and avoids the lower than or equal to contribution. In actual seismic field data application the parameter ϵ is chosen to be the width of the source wavelet and speaks two the fact that subresolution (i.e., thin bed multiples) will not be attenuated. The integral (87) evaluates to:

$$H(z_1-(z_2'+\epsilon_1))R_1e^{ikz_1}+H(z_2-(z_2'+\epsilon_1))R_2'e^{ikz_2}\ .$$

The second integral in Eq. (81) is:

$$\begin{aligned}
&\int_{-\infty}^{z_1'-\epsilon_2}(R_1\delta(z_2'-z_1)+R_2'\delta(z_2'-z_2))(H(z_1-(z_2'+\epsilon_1))R_1e^{ikz_1}+ \qquad (88)\\
&H(z_2-(z_2'+\epsilon_1))R_2'e^{ikz_2})e^{-ikz_2'}dz_2'\\
&=R_1^2H((z_1'-\epsilon_2)-z_1)\underline{H(z_1-(z_1+\epsilon_1))}e^{ikz_1}e^{-ikz_1}\\
&+R_1R_2'H((z_1'-\epsilon_2)-z_2)\underline{H(z_1-(z_2+\epsilon_1))}e^{ikz_1}e^{-ikz_2}\\
&+R_1R_2'H((z_1'-\epsilon_2)-z_1)H(z_2-(z_1+\epsilon_1))e^{ikz_2}e^{-ikz_1}\\
&+(R_2')^2H((z_1'-\epsilon_2)-z_2)\underline{H(z_2-(z_2+\epsilon_1))}e^{ikz_2}e^{-ikz_2}
\end{aligned}$$

where ϵ_2 is a positive parameter with the same function as G_1 and all the underlined terms are zero.

The third (and last) integral is:

$$\begin{aligned}
b_3(k)=&\int_{-\infty}^{\infty}dz_1'e^{-ikz_1'}(R_1\delta(z_1'-z_1)+R_2'\delta(z_1'-z_2))\\
&(R_1R_2'H((z_1'-\epsilon_2)-z_1)H(z_2-(z_1+\epsilon_1))e^{ikz_2}e^{-ikz_1})\\
=&e^{ikz_1}R_1^2R_2'\underline{H(-\epsilon_2)}H(z_2-z_1+\epsilon_1)e^{ikz_2}e^{-ikz_1}\\
&+e^{ikz_2}R_1(R_2')^2H(z_2-z_1-\epsilon_2)H(z_2-z_1-\epsilon_1)e^{ikz_2}e^{-ikz_1}
\end{aligned}$$

and the underlined function is zero. Then, since

$$R_2'=T_{01}R_2T_{10},$$

the prediction is:

$$b_3(k)=R_1R_2^2T_{01}^2T_{10}^2\ e^{2ikz_2}\ e^{2ikz_2}e^{-ikz_1}$$

and

$$\rightarrow b_3(t)=R_1R_2^2T_{01}^2T_{10}^2\delta(t-(2t_2-t_1))$$

From the example it is easy to compute the actual first order internal multiple precisely

$$-R_1 R_2^2 T_{01} T_{10} \delta(t - (2t_2 - t_1)) \ .$$

Hence the key prediction of time is perfect and the amplitude of the prediction has an extra power of $T_{01}T_{10}$ thus defining exactly the difference between the attenuation represented by b_3 and elimination.

Since $T_{01}T_{10}$ is less than one, the method always attenuates and, furthermore, the residual after adding b_1 to b_3 has the same sign as the multiple. Therefore, the internal multiple algorithm has well-defined amplitude prediction properties. If $R = 1/4$ (a large reflection coefficient) then $R^2 = 1/16$ and $T^2 = 15/16 (R^2 + T^2 = 1)$, and $T = \sqrt{15/16} \sim 31/32$.

So even with large R, T^2 is still not far from 1 and that explains the remarkable efficiency of the leading order term for removing first order multiples. It produces the precise timing of all internal multiples of first order, independent of where the upward and downward reflections occur and well approximates their amplitudes, always less than the actual, the precise relationship between the internal multiple amplitude and the b_3 prediction is quantified. Since the difference in amplitude is related to transmission information the internal multiple predictor can provide indirect useful effective, overbunden transmission estimation, as well. Hence, while it is precise to say that the internal multiple algorithm doesn't predict the exact amplitude it is not accurate to say that no significant useful amplitude information is predicted by the internal multiple algorithm.

9.4 Synthetic and field data examples

Figure 19 shows an example of the internal multiple attenuation series algorithm applied to a 2-D synthetic dataset. From left to right, the three panels show the input data, the predicted internal multiples and the result of inverse scattering internal multiple attenuation, respectively.

Figures 20–22 illustrate the free surface and internal multiple attenuation algorithms applied to a dataset from the Gulf of Mexico over a complex salt body. Seismic imaging beneath salt is a challenging problem due to the complexity of the resultant wavefield. In Figure 20, the left panel is a stack section of the input data, and the right panel shows the result of the inverse scattering free surface multiple removal algorithm. Figure 21 is a cartoon that illustrates the events that are used by the algorithm to predict the free surface multiples in the data. Figure 22 illustrates the internal multiple attenuation method applied to the

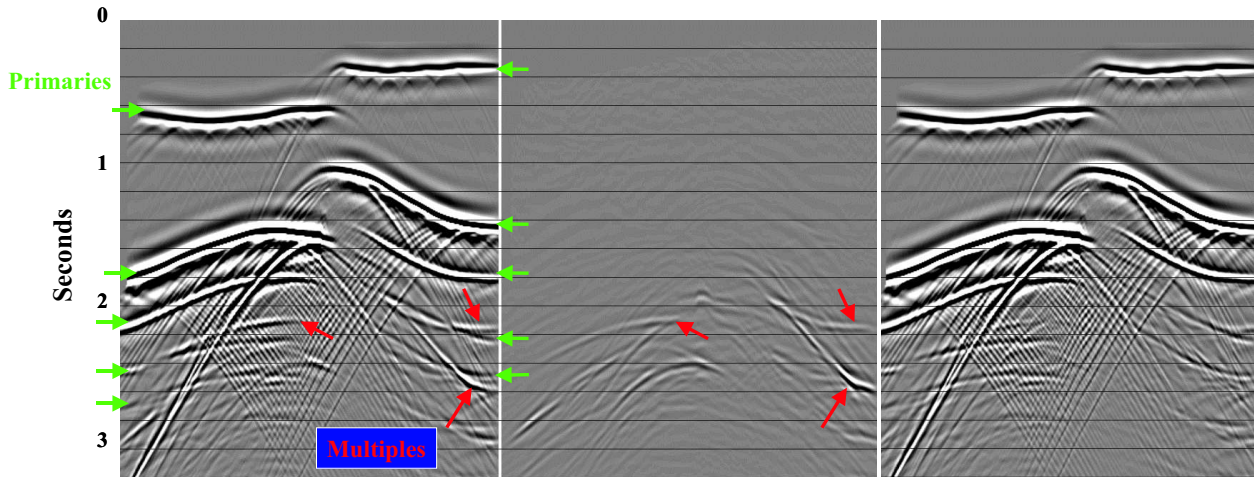

Figure 19: The left panel shows a common offset display from a 2-D synthetic dataset. The middle panel shows the predicted internal multiples. The right-hand panel is the result of subtracting the multiples from the input dataset.

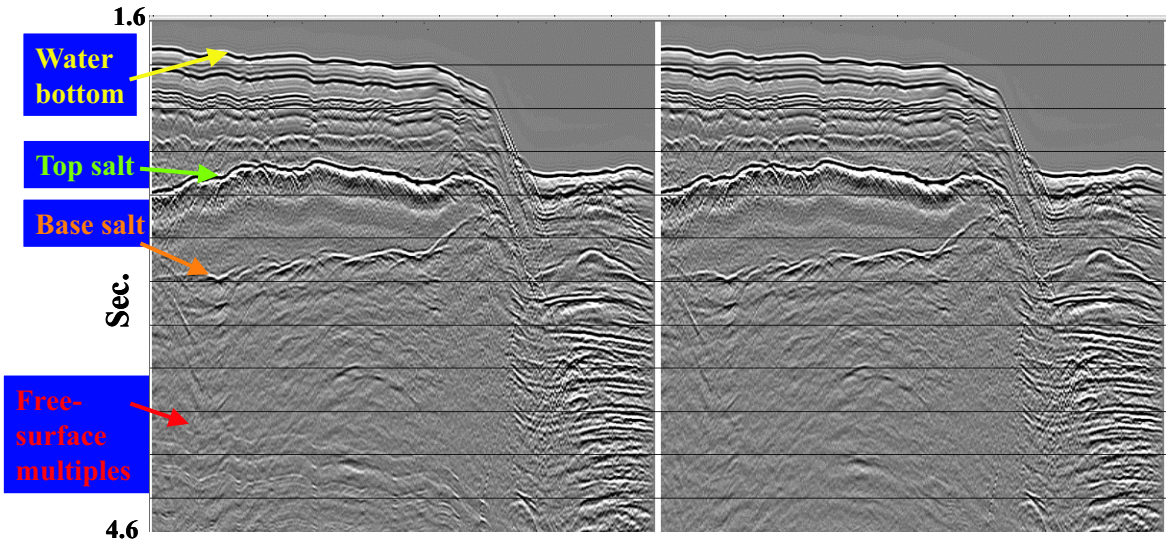

Figure 20: The left panel is a stack of a field dataset from the Gulf of Mexico. The right panel is the result of free surface demultiple. Data are courtesy of WesternGeco.

same Gulf of Mexico dataset. An internal multiple that has reverberated between the top of the salt body and the water bottom, is well attenuated through this method. The cartoons in Fig. 23 illsutrate the subsevents that are used by the algorithm to predict the internal multiples.

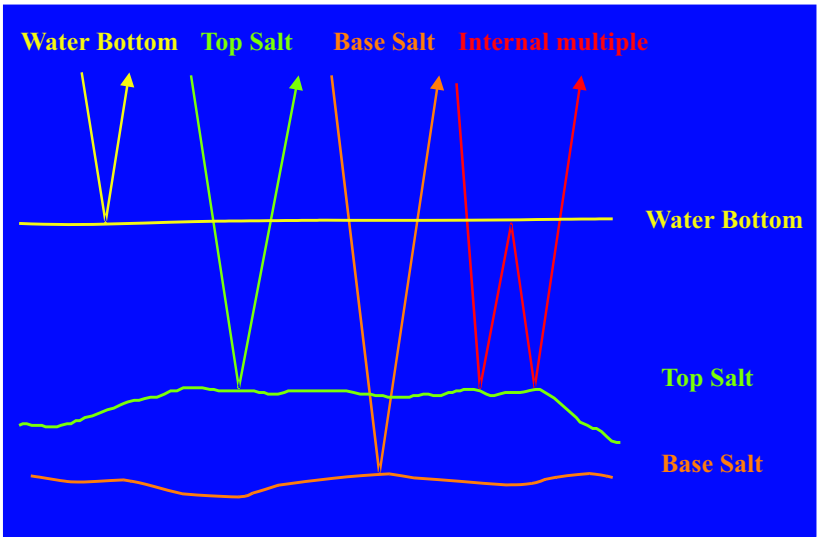

Figure 21: A cartoon illustrating the events that are used by the algorithm to predict free surface multiples.

10 Inverse subseries for imaging and inversion at depth without the velocity model for large contrast complex targets

Initial analysis for identifying the imaging and inversion tasks associated with primaries within the series have recently been reported by Weglein *et al.* (2002). Starting with the acoustic Eq. (6), and defining

$$\frac{1}{k} = \frac{1}{k_r}(1+\alpha)$$

$$\frac{1}{\rho} = \frac{1}{\rho_r}(1+\beta)$$

for a one dimensional variable velocity and density acoustic medium with point sources and receivers at depth ϵ_s and ϵ_g, respectively, Eq. (11$\prime$) becomes

$$\begin{aligned}\widetilde{D}(q_g,\theta,\epsilon_g,\epsilon_s) &= -\frac{\rho_r}{4}e^{-iq_g(\epsilon_s+\epsilon_g)}[\frac{1}{\cos^2\theta}\widetilde{\alpha_1}(-2q_g) \\ &\quad +(1-\tan^2\theta)\widetilde{\beta}_1(-2q_g)] \end{aligned} \tag{89}$$

where the subscripts s and g denote source and receiver respectively, and q_g, θ and $k=\omega/c_0$ are shown in Fig. (24), and they have the following relations:

$$q_g = q_s = k\cos\theta$$

$$k_g = k_s = k \sin\theta \ .$$

Similarly, from Eq. (12*I*) we can get the solution for $\alpha_2(z)$ and $\beta_2(z)$ as a function of $\alpha_1(z)$ and $\beta_1(z)$

$$\begin{aligned}\frac{1}{\cos^2\theta}\alpha_2(z) + (1-\tan^2\theta)\beta_2(z) = &-\frac{1}{2\cos^4\theta}\alpha_1^2(z) \\ &+ \frac{1}{\cos^4\theta}\alpha_1(z)\beta_1(z) \\ &- (\frac{3}{2} + \tan^2\theta + \frac{1}{2}\tan^4\theta)\beta_1^2(z) \\ &- \frac{1}{2\cos^4\theta}\alpha_1^{'}(z)\int_0^z dz^{'}[\alpha_1(z^{'}) - \beta_1(z^{'})] \\ &+ \frac{1}{2}(\tan^4\theta - 1)\beta_1^{'}(z)\int_0^z dz^{'}[\alpha_1(z^{'}) - \beta_1(z^{'})] \ . \qquad (90)\end{aligned}$$

For a single reflection between two acoustic half-spaces where the upper half space corresponds to the reference medium the data consists of primaries and the inversion tasks they face are simply to locate the reflector and to invert for acoustic property charges across the reflector. When the primary data from this two half space model is substituted into Eq. (89) and (90), then the two terms involving integrals on the right hand side become zero. If the model would allow a second reflector, and a two primary wavefield, then those same terms involving the integrals are not zero. From an inversion point-of-view, the primary from the second reflector has more tasks to perform, (in comparison with the first primary) since the first event actually travelled through the reference medium. In addition to estimating changes in earth material properties, the second primary will be imaged where it is placed by the reference medium. From this type of observation and the detailed analysis formed in Weglein *et al.*, (2002) and Shaw and Weglein (2003), it is deduced that the last two terms in Eq. 90 assist in moving the second (deeper) primary to its correct location and the first three terms of Eq. 90 are associated with improving the linear inversion (Eq. 89).

The first three terms on the right-hand-side of equation (90) have two objectives. The first objective: for a primary off the shallower reflector, those first three terms start the nonlinear process of turning that events reflection coefficient into the earth property changes α and β. The reflection coefficient is a non-linear series in α and β; and, conversely, α and β are themselves nonlinear series in the reflection coefficient. For the second (deeper) primary, the first objective is more complicated, since the event amplitude is a function of both the reflection coefficient at the second reflector and the transmission coefficient down-through and up-past the first reflector. The communication between the two events allowed in e.g., α_1^2 can be shown to allow the reflection coefficient of the shallower reflector to work towards removing

the transmission coefficients impeding the amplitude of the second event from inverting for local properties at the second reflector. Hence, specific communication between primaries from different reflectors work together to remove the extraneous transmission coefficients on deeper primaries that are suffering from being given the wrong velocity.

Similarly, the integral terms on the right-hand-side of equation (90) represent a recognition that the reference velocity will give an erroneous image, and asks for an integral of $\alpha_1 - \beta_1$, the linear approximation to the change in acoustic velocity, from the onset of $\alpha_1 - \beta_1$, down to the depth needing the imaging help. Two important observations: (1) When the actual velocity doesn't change across an interface, $R(\theta)$ is not a function of θ and from equation (89) it can be shown that

$$\alpha_1 - \beta_1 = (\frac{\Delta V}{V})_1 = 0 \ .$$

Therefore, when the actual velocity doesn't change then the linear approximation to the change in velocity is zero. Therefore, when the velocity is equal to the reference across all reflectors (e.g., when density changes but not velocity) then these equations understand and don't correct the location from where the reference velocity locates those events, which in that case is correct; and (2) the error in locating reflectors caused by an error in velocity depends on both the size of the error and the duration of the error. Hence, the integral of $\alpha_1 - \beta_1$ represents an amplitude and duration correction to the originally mislocated primary. This is a general principle, when an inversion task has a duration aspect to the problem being addressed, the response has an integral in the solution. The inverse series empowers the primary events in the data to speak to themselves for non linear inversion and to speak to each other to deal with the effect of erroneous velocity on amplitude analysis. The analogous "discussion between events" for multiple removal is described in the conclusions.

Figures (25) and (26) illustrate the imaging portion of the inverse series for a 1-D constant density, variable velocity acoustic medium. The depth that the reference velocity images the second reflector at is $z_{b'}$=136m. The band-limited singular functions of the imaging subseries act to extend the interface from $z_{b'}$ to z_b (Fig. (25)). The cumulative sum of these imaging subseries terms is illustrated in Fig. 26. After summing five terms, the imaging subseries has converged and the deeper reflector has moved towards its correct depth $z_b = 140$ m.

Figures (28)–(31) are a comparison of linear and non-linear prediction for a two-parameter acoustic medium and for a 1-D single interface example (Fig. 27). Figure (28) shows α_1 as a function of two different angles of incidence for a chosen set of acoustic parameters. Figure (29) shows the sum of α_1+α_2, and shows a clear improvement, for all precritical angles, as

an estimate for α. Figure (31) illustrates similar improvements for the second parameter β over the linear estimate given in Fig. (30).

Early analysis and tests are encouraging demonstrating intrinsic potential for the of task specific subseries of the inverse series to perform imaging at the correct depth (Shaw *et al.*, 2003) and improving upon linear estimation of earth material properties (Zhang and Weglein, 2003), without an adequate velocity model. Furthermore, tests point to convergence for imaging for large error and duration of error in velocity and rapid improvement in estimates of earth material properties beyond the industry standard linear techniques.

11 Conclusions and Summary

The forward series begins with the reference propagator, $\mathbf{G}_0$, and the perturbation operator, $\mathbf{V}(\vec{r},\omega)$, the difference between actual and reference medium properties as a function of space, $\vec{r}$. The inverse series inputs data, $D(t)$, in time, and the reference propagator, $\mathbf{G}_0$.

Since the forward series inputs the perturbation, $\mathbf{V}(\vec{r},w)$, and rapid variation of $\mathbf{V}$ correspond to the exact spatial location of reflectors it follows that space is the domain of comfort of the forward series.

On the contrary, the computation of time of arrival of any (and every)seismic event for which the actual propagation path is not described by $\mathbf{G}_0$ requires an infinite series to get the correct time from the forward series. Time is the domain of discomfort for the forward series for seismic events.

For the inverse series the input is data, $D(t)$,in time, and processes that involve transforming, $D(t)$, to another function of time, e.g., the data without free-surface multiples, $D'(t)$,are simpler to achieve than tasks such as imaging primaries in space that require a map from $D(t)$ to $\mathbf{V}(\vec{r},\omega)$.

In addition, if accurate a-priori information can be provided for the localization and separation of a given task (as in the case of a free-surface reflection coefficient or ${\mathbf{G}_0}^{FS}$) e.g., for the removal of ghosts and free-surface multiples, where the task is defined in terms of separating events that have a well defined experience (from those events that have not) then further efficiency can derive from subseries that involve time to time maps. In table (1), we summarize the amount of effort required to achieve a certain level of effectiveness for each of the four task-specific subseries.

The strategy is to accomplish one task at a time, in the order listed, and then restart the problem as though the already achieved task never existed. This avoids the coupled task terms in the series. Further more, the achievement of these tasks, in order, can enhance the ability of subsequent tasks to reach their objective. For example, the removal of free-surface and internal multiples significantly improves the ability to estimate the overburden velocity model and subsequently aids the efficacy and efficiency of the imaging and inversion subseries for primaries.

Since the rate of convergence of both multiple removal subseries doesn't benefit at all from anything closer to the earth than water speed, and the cost of the algorithms quickly increase with complexity of the reference medium, the idea is to perform tasks that prefer simple, cheap reference propagation with what they want. Then restart the problem with certain issues in the data addressed, i.e., with new data (e.g., primaries) that require proximal velocity information, with more complex and more costly subseries for tasks that appreciate that assistance for practical efficacy and efficiency. If you don't like the 'Isolated Task and Restart the Problem Strategy', and you wanted to be a purist and start and end with one inverse scattering series, you would need the single complex reference that would allow the toughest task to have an opportunity to succeed. Two issues with the latter approach: (1) where would you get the proximal velocity if troublesome multiples are in your input data; and (2) the one series, one time for all data is an "all or nothing at all" strategy that doesn't allow for stages to succeed and provide benefit, when the overall series or more ambitious goals are beyond reach.

Although both primaries and multiples have experienced the subsurface; and, hence, carry information encoded in their character, the indisputable attitude of the only multidimensional direct inversion method for acoustic and elastic media, the inverse scattering series, is to treat multiples as coherent noise to be removed and primaries as the provider of subsurface information. That doesn't mean that one could never use multiples in some inclusive method that seeks to exploit the information that both primaries and multiples contain. If simply means that an inclusive theory, starting with realistic a-priori information, doesn't now exist, and, further, that the inverse series definitely adopts the exclusive view.

While the ability to directly achieve seemingly impossible inversion objectives from data, $D(t)$, and only an estimated reference propagator, $\mathbf{G}_0$, (which can be inadequate) certainly follows from Eq. (11-14) (see also Weglein *et al.* (1997)) there is value in providing an understanding from an information content point of view, as well.

What basically happens in each task specific subseries is that specific conversations take place between events in the data as a whole that allows, e.g., multiple prediction or accurate

depth imaging to take place without an accurate velocity model. "Non-linear in the data" is the key, and means that quadratic terms enter the picture (data times data, at least) and that allows different events to have multiplicative communication.

For example, if you provide the medium in detail you can readily determine whether any event in the data is a primary or multiple. However, if you provide only an isolated event, without the medium properties, then there is no way to determine if it is a primary or multiple, in fact it can be either for different models. So how does the inverse series figure out whether the event is a primary or multiple with out any subsurface information? Since it is a series there is a "conversation" set up with other events and then a yes or no to whether an event is a primary or multiple is completely achievable without any information about the medium. In Fig. (32) we show an internal multiple (dashed line), SABCR. Primaries SABE, DBCR and DBE have a phase relationship with the internal multiple SABCR such that.

$$(\text{SABE})_{\text{time}} + (\text{DBCR})_{\text{time}} - (\text{DBE})_{\text{time}} = (\text{SABCR})_{\text{time}}. \tag{91}$$

Hence, if the overall data contains three events such that two are longer time events and if the sum of the time of the two longer events *minus* one smaller time event corresponds to the time of the event under investigation, the event is an internal multiple and, if so, it is removed. This is the reason the third term in the inverse series, that involves three $D(t)$ data terms, starts the process of internal multiple removal and why the "W" diagram (see Fig (32)) is as the heart of the internal multiple prediction from the data procedure; and, finally, why the time prediction of all internal multiples is precise.

In the subseries for imaging at depth without the velocity the first term is current linear migration and places each events exactly where the input reference velocity dictates. The latter imaging process is linear in the data and events are not asked their individual view or opinion of the input velocity non are they allowed to discuss it amongst themselves.

The second term in the inverse series has integral terms (e.g., Eq. 90) that start to move the incorrectly imaged events (from using the reference velocity) towards their correct location. There is a quadratic dependence on the data, allowing multiplicative conversations between two events and they are empowered to have an opinion about the input velocity. If they decide together that (at least) one of the events has been provided with a velocity model not consistent with those two events, the troubled event (usually deeper) asks for assistance from a shallower event to help it use its amplitude and the degree of dissatisfaction to move the deeper primary towards its correct location.

Hence, the inverse series and the task-specific subseries concept, represent as fundamentally a new and potentially impactful way of thinking about imaging and inverting primaries as it represented for the earlier (and now mature and standard algorithms for) removal of multiples. There were serious conceptual and practical hurdles in the theoretical evolution, development and robust industrial application.

We anticipate that in bringing the subseries for imaging and inverting primaries through that same process, that higher hurdles and tougher prerequisites will be addressed. The potential benefits for exploration and production of hydrocarbons are great. We would be delighted if this paper would serve to encourage other fields of non-destructive evaluation e.g., medical imaging, environmental monitoring, and defense detection and identification, and earth quake deep earth definition, application to benefit from these efforts as well.

Acknowledgments

We would like to thank Craig Cooper at BP and Larry Pinksy and Art Vailas at UH. The support of the M-OSRP sponsors is gratefully acknowledged. Johana Diaz and Gino Ananos are thanked for typing.

References

Araújo, F. V., 1994, Linear and nonlinear methods derived from scattering theory: Backscattered tomography and internal multiple attenuation: Ph.D. thesis, Universidade Federal da Bahia, Brazil, (in Portuguese).

Araújo, F. V., Weglein, A. B., Carvalho, P. M., and Stolt, R. H., 1994a, Internal multiple attenuation: EAEG Abstracts.

Araújo, F. V., Weglein, A. B., Carvalho, P. M., and Stolt, R. H., 1994b, Inverse scattering series for multiple attenuation: An example with surface and internal multiples: 64th Ann. Internat. Mtg., Soc. Expl. Geophys., Expanded Abstracts, 1039-1041.

Boyse, W. E., Wave propagation and inversion in slightly inhomogeneous media, p.40. (1986)

Boyse, W.E. and Keller J.B., Inverse elastic scattering in three dimensions, 1986: J. Acoust. Soc. Am., **79**, 215–218.

Carvalho, P. M., 1992, Free-surface multiple reflection elimination method based on nonlinear inversion of seismic data: Ph.D. thesis, Universidade Federal da Bahia, Brazil, (in Portuguese).

Robert W. Clayton and Robert H. Stolt: Geophysics, **46**, 1559-1567.

Jack K. Cohen and Bleistein N.: SIAM Journal of Applied Math (1977), **32**, 784-799.

Devaney, A. J., and Weglein A. B., Inverse scattering using the Heitler equation, Inverse Problems (December, 1989) **5**, 3, p49–52.

Innanen, K.A. and Weglein, A.B., Viscoacoustic Born Series Continued: Toward Scattering-based Q Compensation /Estimation, 2003, (in preparation).

Keys, R. G., and Weglein, A. B., 1983, Generalized linear inversion and the first Born theory for acoustic media, J. Math. Phys., **24(6)**, 144-149.

ten Kroode, F., 2002, Prediction of internal multiples, Wave Motion 35, p.315-338.

Matson, K., 1996, The relationship between scattering theory and the primaries and multiples of reflection seismic data: J. Seis. Expl., **5**, 63-78.

Morley, L., and J. Claerbout: Geophysics, **48**, 515-531.

Moses, H. E., 1956, Calculation of scattering potential from reflection coefficients: Phys. Rev., **102**, 559-567.

Newton, R.G., 2002, Scattering Theory of Waves and Particles, Dover Publishing.

Nita, B., Matson, K. and Weglein, A. B., 2003, Forward scattering series seismic events: high frequency approximations, critical and postcritical reflections. Journal of Mathematical Physics.

Prosser, R. T., 1969, Formal solutions of inverse scattering problems: J. Math. Phys., **10**, 1819-1822.

Razavy, M., 1975, Determination of the wave velocity in an inhomogeneous medium from reflection data: J. Acoust. Soc. Am., **58**, 956-963.

Shaw, S.A. and Weglein, A.B., Imaging seismic reflection data at the correct depth without specifying an accurate velocity model: initial numerical examples of an inverse scattering subseries, 2003 in Frontiers of remote sensing information processing, C.H. Chen (ed.), World scientific publishing co. (in press).

Shaw, S.A., Weglein, A.B., Foster, D.J., Matson, K.H., and Keys, R.G., Isolation of a leading order depth imaging series and analysis of its convergence properties, 2003, (in preparation).

Stolt, R. H. and Weglein, A. B., 1985, Migration and inversion of seismic data: Geophysics, **50**, 2458-2472.

Stolt, R. H. and Jacobs, B., 1980, Inversion of seismic data in a laterally heterogeneous medium: SEP Report, **24**, 135-152.

Ware, J. A. and Aki, K., 1969, Continuous and discrete inverse-scattering problems in a stratified elastic medium. I. Plane waves at normal incidence: J. Acoust. Soc. Am., **45**, 911-921.

Weglein, A. B., Boyse, W. E. and Anderson, J. E., 1981, Obtaining three-dimensional velocity information directly from reflection seismic data: an inverse scattering formalism: Geophysics, **46**, 116-1120.

Weglein, A.B., D.J. Foster, K.H. Matson, S.A. Shaw, P.M. Carvalho and D. Corrigan, Predicting the correct spatial location of reflectors without knowing or determining the precise medium and wave velocity: initial concept, algorithm and analytic and numerical example, Journal of Seismic Exploration 10, 367-382 (2002).

Weglein, A.B., Gasparotto, F.A., Carvalho, P.M. and Stolt, R.H., 1997. An inverse scattering series method for attenuating multiples in seismic reflection data. Geophysics, 62: 1975-1989.

Weglein, A.B., Matson, K.H., Foster, D.J., Carvalho, P.M., Corrigan, D. and Shaw, S.A., 2000. Imaging and inversion at depth without a velocity model. 70th Ann. Internat. SEG Mtg., Calgary, Alberta.

Weglein, A.B. and Stolt, R.H., 1999. Migration-inversion revisited (1999). The Leading Edge, **18**, 8: 950-952.

Zhang, H. and Weglein, A.B., Target identification using the inverse scattering series; inversion of large-contrast, variable velocity and density acoustic media, 2003, (in preparation).

Further Reading

References

Carvalho, P. M., Weglein, A. B., and Stolt, R. H., 1991, Examples of a nonlinear inversion method based on the T matrix of scattering theory: application on multiple suppression: 61st Ann. Internat. Mtg., Soc. Expl. Geophys., Expanded abstracts, 1319-1322.

Carvalho, P. M., Weglein, A. B., and Stolt, R. H., 1992, Nonlinear inverse scattering for multiple suppression: application to real data, Part I: 62nd Ann. Internat. Mtg., Soc. Expl. Geophys., Expanded abstracts, 1093-1095.

Coates, R. T., and Weglein, A. B., 1996, Internal multiple attenuation using inverse scattering: Results from prestack 1 & 2D acoustic and elastic synthetics, 66th Ann. Internat. Mtg., Soc. Expl. Geophys., Expanded abstracts, 1522-1525.

Dragoset, W. H., 1992, Surface multiple attenuation - theory, practical issues, examples: EAEG Abstracts, BO27.

Fokkema, J. T. and van den Berg, P. M., 1993, Seismic applications of acoustic reciprocity: Elsevier Science Publ. Co., Inc.

Ikelle, L. T., Roberts, G., and Weglein, A. B., 1995, Source signature estimation based on the removal of first order multiples: 65th Ann. Internat. Mtg., Soc. Expl. Geohys., Expanded Abstracts, 1478-1481.

Kennett, B. L. N., 1979, The suppression of surface multiples on seismic records: Geophys. Prosp., **27**, 484-600.

Matson, K., and Weglein, A. B., 1996, Free-surface elastic multiple removal using inverse scattering: Canad. SEG Expanded Abstracts.

Newton, R. G., 1981, Inversion of reflection data for layered media: a review of exact methods: Geophys. J. Roy. Astr. Soc., **65**, 191-215.

Riley, D. C., and Claerbout, J. F., 1976, 2D multiple reflections: Geophysics, **41**, 592-620.

Stolt, R. H. and Jacobs, B., 1981, An approach to the inverse seismic problem: SEP Report, **25**, 121-132.

Stolt, R. H. and Weglein, A. B., 1985, Migration and inversion of seismic data: Geophysics, **50**, 2458-2472.

Taylor, J. R., Scattering Theory, John Wiley and Sons, Inc., New York.

Verschuur, D. J., Berkhout, A. J. and Wapenaar, C. P. A., 1992, Adaptative surface-related multiple elimination: Geophysics, **57**, 1166-1177.

Weglein, A. B., 1985, The inverse scattering concept and its seismic application, *in* Fitch, A. A., Developments in Geophysical Exploration Methods: Elsevier Science Publ. Co., Inc, **6**, 111-138.

Weglein, A. B., 1995, Multiple attenuation: Recent advances and the road ahead: 65th Ann. Internat. Mtg., Soc. Expl. Geohys., Expanded Abstracts, 1492-1495.

Carvalho, P.M. and Weglein, A.B., 1994. Wavelet estimation for surface multiple attenuation using a simulated annealing algorithm. Expanded Abstr., 64th Ann. Internat. SEG Mtg., Los Angeles.

Manin, M. and Spitz, S., 1995. 3-D attenuation of targeted multiples with a pattern recognition technique. Expandede Abstr., 57th EAGE Conf., Glasgow, BO46.

Matson, K.H., 2000. An overview of wavelet estimation using free-surface multiple removal. The Leading Edge, 19: 50-55. Matson, K.H. and Weglein, A.B., 1996. Removal of elastic interface multiples from land and ocean bottom data using inverse scattering. Expanded Abstr., 66th Ann. Internat. SEG Mtg., Denver: 1526-1529.

Matson, K.H., Paschal, D. and Weglein, A.B., 1999. A comparison of three multiple attenuation methods applied to a hard water-bottom data set. The Leading Edge, 18: 120-126.

Osen, A., Secrest, B.G., Amundsen, L. and Reitan, A., 1998. wavelet estimation from marine pressure measurements. Geophysics, 63: 2108-2119.

Tan, T.H., 1999. Wavelet spectrum estimation. Geophysics, 64: 1836-1846.

Snieder, R., The role of the Born approximation in nonlinear inversion, 1990: Inverse Problems, **6**, 247–266.

Snieder, R., An extension of Backus-Gilbert theory to nonlinear inverse problems, 1991: Inverse Problems, **7**, 409–433.

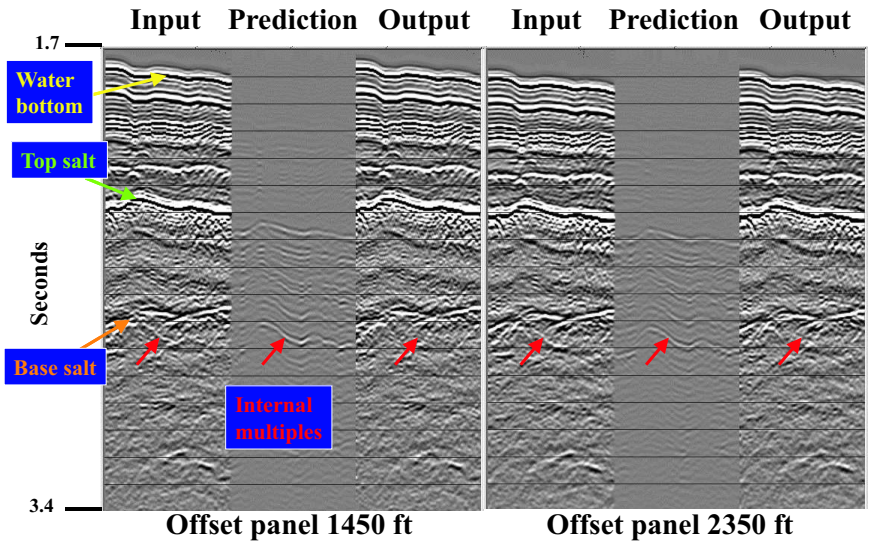

Figure 22: An example of internal multiple attenuation from the Gulf of Mexico. Data are courtesy of WesternGeco.

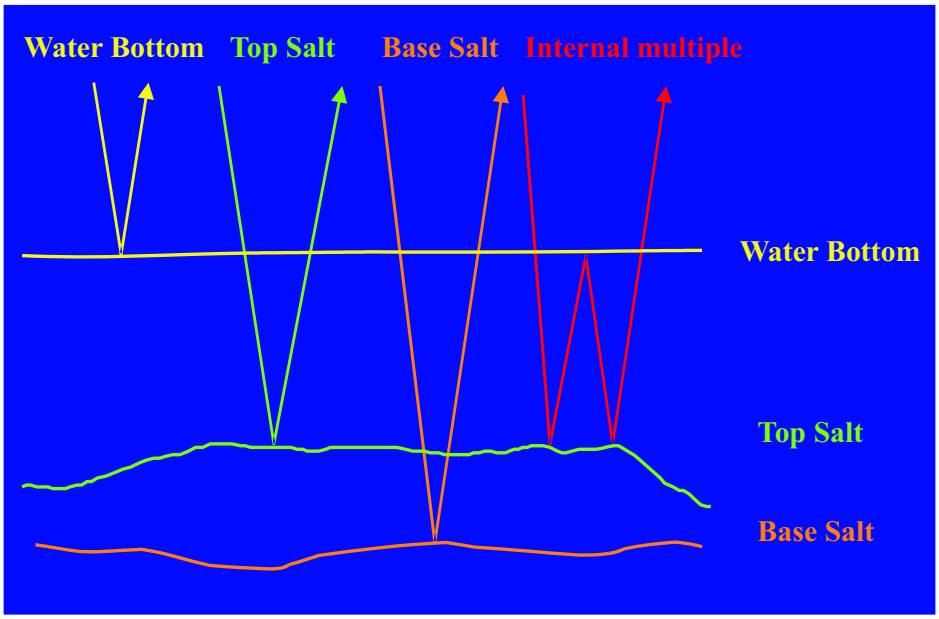

Figure 23: A cartoon illustrating the events that are used by the algorithm to predict a subsalt internal multiple.

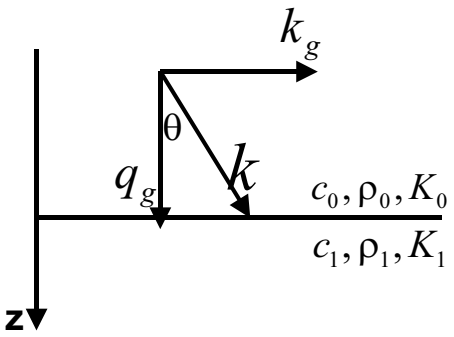

Figure 24: The relationship between q_g, k_g and θ

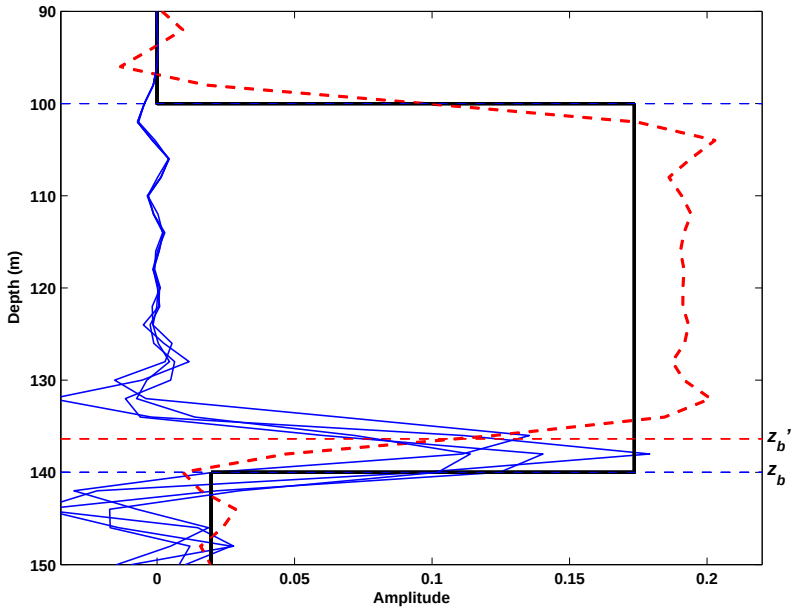

Figure 25: Five terms in the leading order imaging subseries. The solid black line is the actual perturbation α and the dashed red line is α_1, the first approximation to α. The blue lines are the leading order imaging subseries terms. The cumulative sum of these imaging terms is shown in Figure 26.

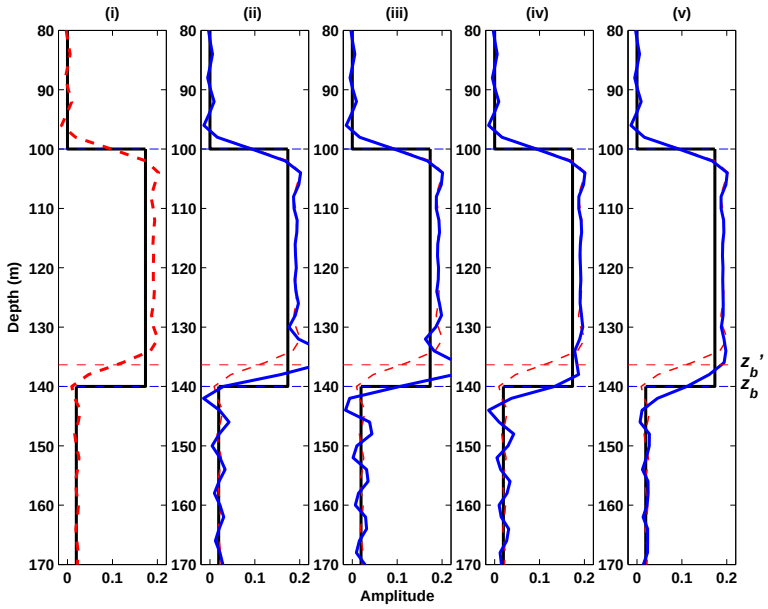

Figure 26: Cumulative sum of five terms in the leading order imaging subseries. The solid black line is the perturbation α and the red line is the first approximation to α or the first term in the inverse series, α_1. The blue line is the cumulative sum of the imaging subseries terms, e.g. in panel (ii) the sum of two terms in the subseries is shown, and in panel (v) the sum of five terms in the subseries is displayed.

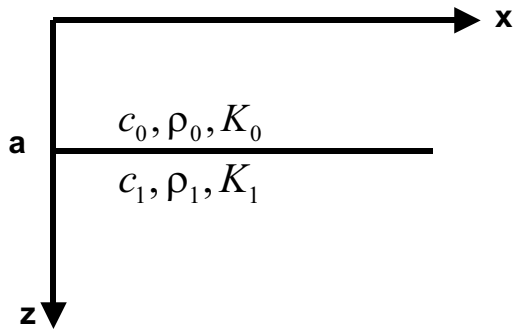

Figure 27: One-dimensional acoustic model.

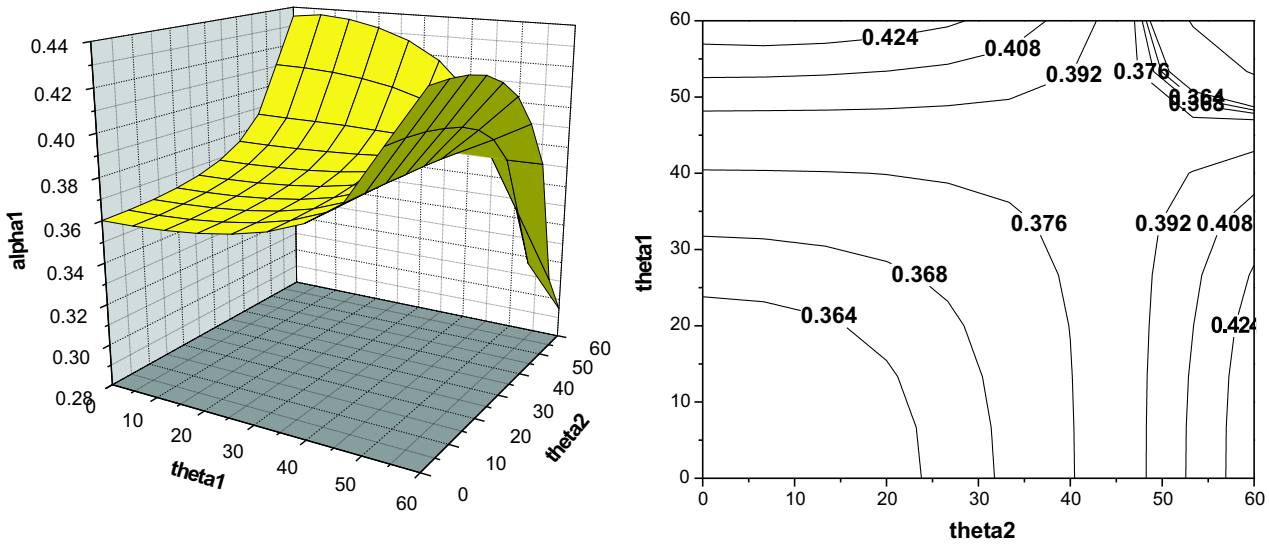

Figure 28: α_1 displayed as a function of two angles. The graph on the right is a contour plot of the graph on the left. In this example, the exact value of α is 0.292.

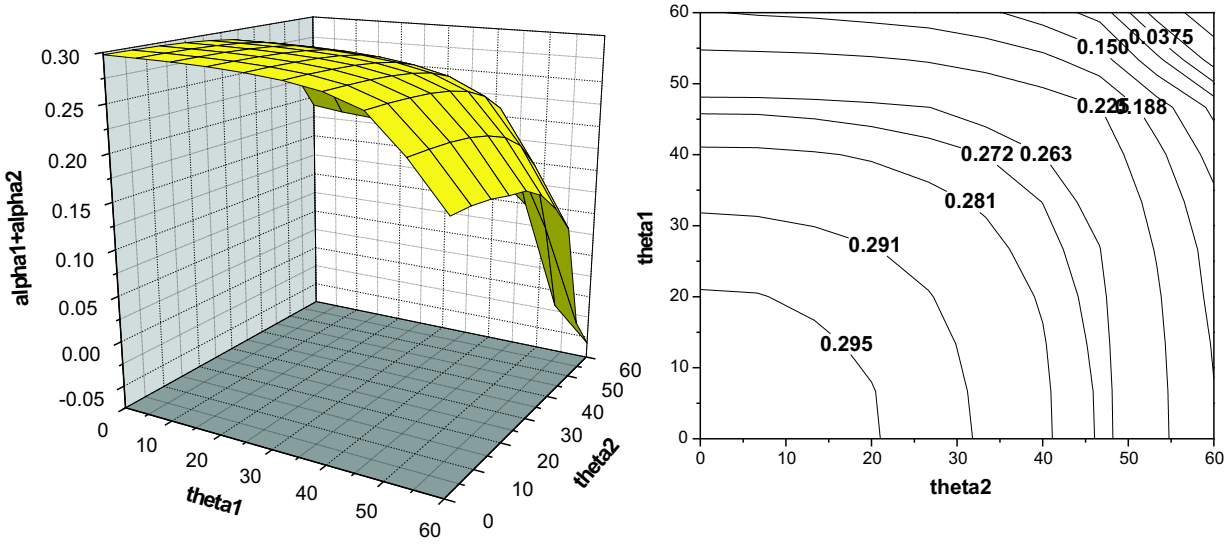

Figure 29: The sum of $\alpha_1 + \alpha_2$ displayed as a function of two angles for the same example as in Fig. 28.

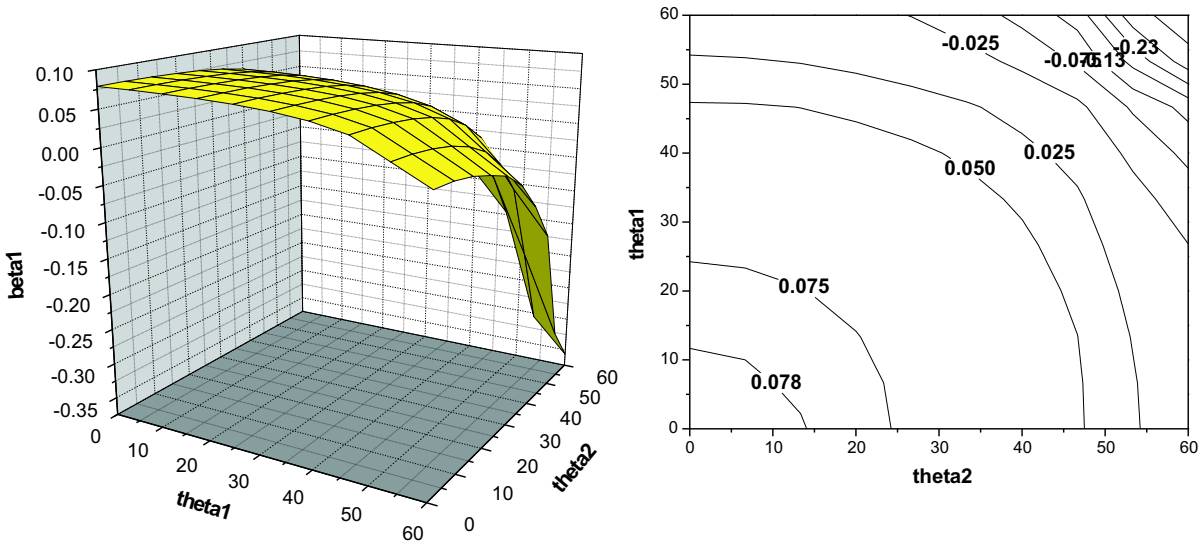

Figure 30: β_1 displayed as a function of two angles. The graph on the right is a contour plot of the graph on the left. In this example, the exact value of β is 0.09.

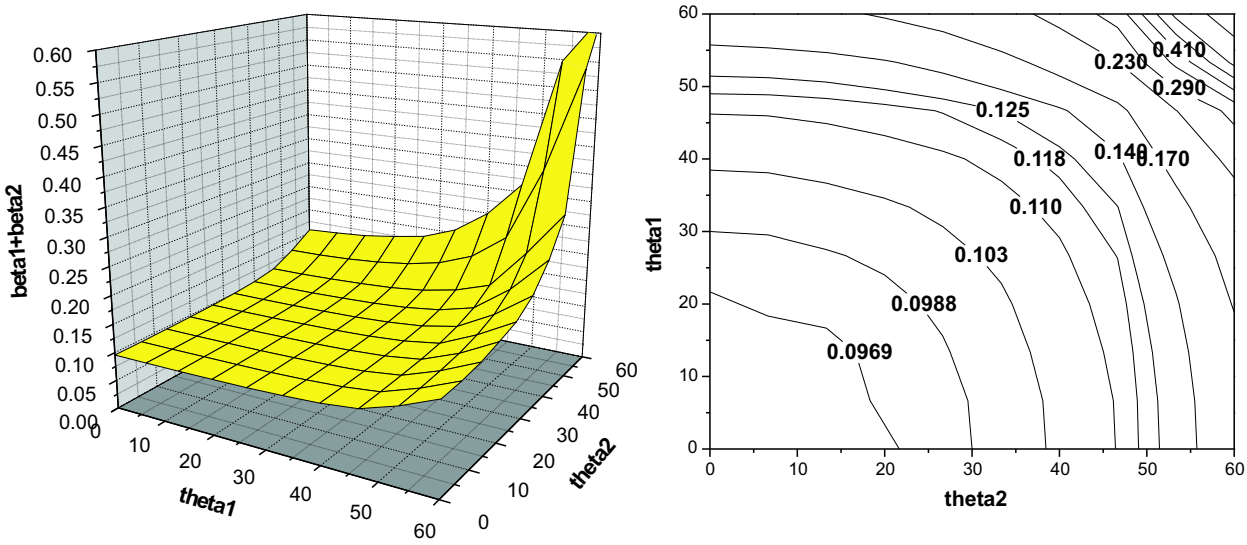

Figure 31: The sum of $\beta_1 + \beta_2$ displayed as a function of two angles for the same example as in Fig. 30.

TASK	PROPERTIES.
Free-surface multiple elimination	One term in the subseries predicts precisely the time and amplitude of all free-surface multiples of a given order independent of the rest of the history of the event. Order is defined as number of times the multiple has a downward reflection at the free-surface.
Internal multiple attenuation	One term in the inverse series predicts the precise time and approximate amplitude of all internal multiples of a given order. The order of an internal multiple is defined by the number of downward reflections from any subsurface reflector at any depth.
Imaging at depth without the precise velocity	First term in series corresponds to current migration or migration − inversion. To achieve a well-estimated depth-map requires an infinite series directly in terms of an inadequate velocity model. A priori velocity estimate will aid rate of convergence.
Inversion at depth without the precise overburden	First term in subseries corresponds to current linear amplitude analysis. For improvement to linear estimates of earth property changes and to account for inadequate overburden requires infinite series. Tests indicate rapid convergence for the first non-linear parameter estimation objective.

Table 1: Summary of task-specific subseries.

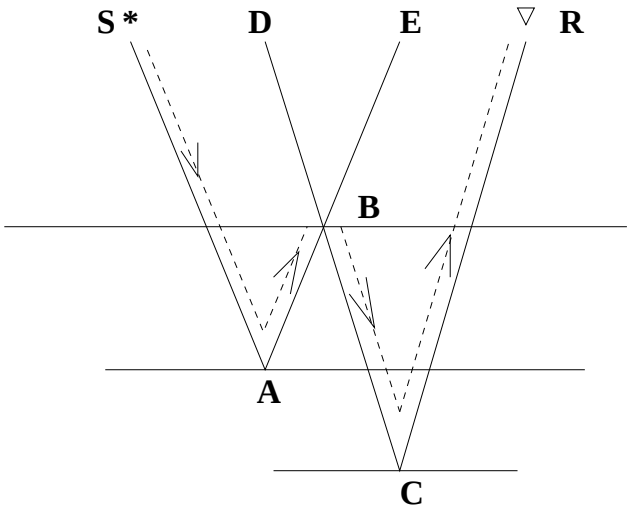

Figure 32: Subevents for an internal multiple.

Viscoacoustic Born Series Continued: Toward Scattering-based Q Compensation/Estimation

Kristopher A. Innanen† and Arthur B. Weglein‡
†University of British Columbia, ‡University of Houston

Abstract

The forward scattering series in 1D has available to it a mapping (Matson, 1996) which allows one to follow terms, or groups of terms, from their individual computation through to their overall effect on the closed form wave field expression. This provides a tool to gain insight into the likely behaviour of the inverse scattering series, and the subseries' which have elsewhere been identified and separated as means to eliminate/attenuate multiples, and image and invert primaries. Here this tool is used to (1) gain basic understanding of the types of scattering interaction which give rise to macroscopic properties of the viscoacoustic wave field, and (2) gain focused understanding of where in the inverse scattering series the machinery for Q compensation and estimation must reside. In casting the problem with an acoustic reference medium a conceptually compelling result is obtained: a viscoacoustic wave field, attenuated and dispersed, is correctly computed through the scaled, nonlinear, combination of propagations which all occur in a lossless (reference) medium. Beyond this, the key conclusion is that the "imaging subseries", which in the acoustic case is seen as an engine for moving reflectors to their correct depths, must be generalized to include the removal of all propagation effects. This includes the phase and amplitude distortions associated with attenuation. In other words, the imaging subseries is also the basic Q-compensation machine; it is to this subseries that we must direct our attention in devising scattering-based processing strategies.

1 Introduction: Viscoacoustic Scattering Potentials

This paper involves refining our understanding of how the forward scattering series, or Born series, functions in media which attenuate the wave field. The first section develops some ideas of how various types of scattering diagram conspire to construct aspects of the viscoacoustic wave field – for instance, the absorptive propagation effects, and the negative of the direct wave. The second section is more focused on predicting the nature of an inverse scattering-based scheme for Q compensation and estimation. In it we consider the role of the so-called "separated" and "self-interacting" scatter-type comparatively, contrasting a purely

acoustic case with a purely absorptive one. The results suggest where in the inverse series we must look for tools to accomplish these tasks of estimation and compensation.

To begin, we review the Born series for viscoacoustic media, and construct some appropriate scattering potentials.

The Born series representation of a wave field arises from a perturbation of the coefficients of the wave equation around a reference value. For instance, in a 1D constant density acoustic medium, the equation

$$\left[\frac{d^2}{dz^2} + \frac{\omega^2}{c(z)^2}\right] \psi(z|z_s;\omega) = \delta(z - z_s), \tag{1}$$

which describes the behaviour of the wave field $\psi(z|z_s;\omega)$, measured at z and due to an impulsive source at z_s, in a medium characterized by the wavespeed profile $c(z)$, is re-written

$$\left[\frac{d^2}{dz^2} + k_0^2(1 - \alpha(z))\right] \psi(z|z_s;k_0) = \delta(z - z_s), \tag{2}$$

where $k_0^2 = \omega^2/c_0^2$. Usually the reference model, here represented by the constant wavespeed c_0, is assumed to be known, so the perturbation $\alpha(z) = 1 - \frac{c_0^2}{c^2(z)}$ is the *de facto* model. The scattering potential $V(k_0, z)$ is the difference between the "true" and reference wave operators:

$$V(k_0, z) = \left[\frac{d^2}{dz^2} + \frac{\omega^2}{c(z)^2}\right] - \left[\frac{d^2}{dz^2} + \frac{\omega^2}{c_0^2}\right] = k_0^2\alpha(z). \tag{3}$$

The acoustic Born series is a representation of the solution of equation (1) in orders of $V(k_0, z)$. A straightforward derivation involves placing the term $V(k_0, z)\psi(z|z_s;k_0)$, onto the right-hand side of equation (2), multiplying these "sources" by the Green's function $G_0(z|z_s;k_0)$, which satisfies

$$\left[\frac{d^2}{dz^2} + k_0^2\right] G_0(z|z_s;\omega) = \delta(z - z_s), \tag{4}$$

and integrating:

$$\psi(z|z_s;k_0) = G_0(z|z_s;k_0) + \int_{-\infty}^{\infty} G_0(z|z';k_0)V(k_0,z')\psi(z'|z_s;k_0)dz'. \tag{5}$$

Finally, equation (5), which is the 1D version of the Lippmann-Schwinger equation, is expanded to produce the Born series:

$$\psi(z|z_s;k_0) = \psi_0(z|z_s;k_0) + \psi_1(z|z_s;k_0) + \psi_2(z|z_s;k_0) + \psi_3(z|z_s;k_0) + ..., \tag{6}$$

where

$$\begin{aligned}
\psi_0(z|z_s;k_0) &= G_0(z|z_s;k_0), \\
\psi_1(z|z_s;k_0) &= \int_{-\infty}^{\infty} G_0(z|z';k_0)V(k_0,z')G_0(z'|z_s;k_0)dz', \\
\psi_2(z|z_s;k_0) &= \int_{-\infty}^{\infty} G_0(z|z';k_0)V(k_0,z')\int_{-\infty}^{\infty} G_0(z'|z'';k_0)V(k_0,z'')G_0(z''|z_s;k_0)dz''dz',
\end{aligned} \tag{7}$$

etc. Clearly, ψ_1 is first order in V, whereas ψ_2 is second order in V, and so forth. Because the Green's function $G_0(z|z';k_0)$ describes propagation in the reference medium from point z' to point z, the term ψ_N may be interpreted as a wave field which has propagated in the reference medium $N+1$ times, and has N times interacted with the perturbation $\alpha(z)$ via the scattering potential. Since the reference medium is characterized by constant wavespeed c_0, the Green's function is (e.g. DeSanto, 1993):

$$G_0(z|z_s;k_0) = \frac{e^{ik_0|z-z_s|}}{2ik_0}. \tag{8}$$

Therefore, having defined $V(k_0,z)$ via some desired Earth model, and knowing G_0, one may compute as many terms as desired in equation (6) to approximate the solution.

One may define a wide variety of scattering potentials, differing in what the "true" medium properties are with respect to the reference medium. Here we consider two variants on the acoustic case, each utilizing wavenumbers which permit attenuation to be modeled in addition to acoustic behaviour. This requires moving away from the acoustic $k_0 = \omega/c_0$, and adopting for the true medium:

$$k(z) = \frac{\omega}{c(z)}\left[1+\beta(\omega,z)\right], \tag{9}$$

where $\beta(\omega,z)$, a complex number, is the spatial distribution of an attenuation parameter which instills absorption and dispersion character into the wave field. From equation (9), and guided by equation (3), two related scattering potentials are defined. The first corresponds to media in which both wavespeed contrasts and attenuation contrasts are permitted:

$$\alpha_{cq}(z) = 1 - \frac{k^2(z)}{k_0^2} = 1 - \frac{c_0^2}{c^2(z)}\left[1+2\beta(\omega,z)\right], \tag{10}$$

neglecting terms quadratic in β. The second corresponds to a medium in which the wavespeed is constant throughout, and contrasts are only permitted in β. Since in such a case $c(z) = c_0$, from equation (10) the form is

$$\alpha_q(z) = 2\beta(\omega,z). \tag{11}$$

The remarkable simplicity of this perturbation and its association with the actual value of β arises partly because there is no attenuation in the reference medium, and also because of the attenuating wavenumber of equation (9) already resembles a perturbation away from the acoustic case. In this paper we consider only cases in which the reference medium is acoustic, and non-attenuative.

If we choose the constant Q model of Kjartansson (1979), for instance, we have

$$\beta(\omega, z) = \frac{i}{2Q(z)} - \frac{1}{\pi Q(z)} \ln\left(\frac{\omega}{\omega_r}\right), \tag{12}$$

where ω_r is a chosen reference frequency. This arises due to the form of a 1D constant Q wavenumber:

$$k_1 = \frac{\omega}{c_0}\left[1 + \frac{i}{2Q} - \frac{1}{\pi Q}\ln\left(\frac{\omega}{\omega_r}\right)\right]. \tag{13}$$

2 The Terms and Diagrams of the Born Series

The Born series, equation (6), is a decomposition of the full wave field into those components which have interacted with the non-reference portion of the medium a certain number of times; each interaction is separated by a propagation in the reference medium. Scattering diagrams, which, as used here, are the wave-theoretic analogues of the Feynman diagrams of quantum field theory (e.g. Weglein et al., 2002), arise from further decomposition of the terms in this series. In this section, the scattering diagrams associated with a simple 1D transmission case are developed from the form of the Born series integrals, and linked to the explicitly computed terms in the series.

The integrals which give rise to the terms ψ_n in equation (6) subdivide because of the geometric constraints on the propagation imposed by the Green's functions (equation 8). To see this, consider equations (7) with the condition that the source z_s is less than all z for which the perturbation is non-zero. Then:

$$\psi_0(z|z_s; k_0) = \frac{e^{ik_0(z-z_s)}}{2ik_0}. \tag{14}$$

Also,

$$\begin{aligned}\psi_1(z|z_s;k_0) &= \int_{-\infty}^{\infty} \frac{e^{ik_0|z-z'|}}{2ik_0} k_0^2\alpha(z')\frac{e^{ik_0(z'-z_s)}}{2ik_0}dz' \\ &= \int_{-\infty}^{z} \frac{e^{ik_0(z-z')}}{2ik_0} k_0^2\alpha(z')\frac{e^{ik_0(z'-z_s)}}{2ik_0}dz' + \int_{z}^{\infty} \frac{e^{ik_0(z'-z)}}{2ik_0} k_0^2\alpha(z')\frac{e^{ik_0(z'-z_s)}}{2ik_0}dz' \\ &= -\frac{1}{4}e^{ik_0(z-z_s)}\int_{-\infty}^{z}\alpha(z')dz' - \frac{1}{4}e^{-ik_0(z+z_s)}\int_{z}^{\infty} e^{i2k_0z'}\alpha(z')dz' \\ &= \psi_{11} + \psi_{12}.\end{aligned} \tag{15}$$

The integrals are likewise broken up in the computation of ψ_2:

$$\begin{aligned}\psi_2(z|z_s;k_0) &= \int_{-\infty}^{\infty} \frac{e^{ik_0|z-z'|}}{2ik_0} k_0^2\alpha(z')\int_{-\infty}^{\infty} \frac{e^{ik_0|z'-z''|}}{2ik_0} k_0^2\alpha(z'')\frac{e^{ik_0(z''-z_s)}}{2ik_0}dz''dz' \\ &= \psi_{21} + \psi_{22} + \psi_{23} + \psi_{24},\end{aligned} \tag{16}$$

where

$$\begin{aligned}\psi_{21}(z|z_s;k_0) &= \frac{1}{8}ik_0e^{ik_0(z-z_s)}\int_{-\infty}^{z}\alpha(z')\int_{-\infty}^{z'}\alpha(z'')dz''dz', \\ \psi_{22}(z|z_s;k_0) &= \frac{1}{8}ik_0e^{ik_0(z-z_s)}\int_{-\infty}^{z}e^{-i2k_0z'}\alpha(z')\int_{z'}^{\infty}e^{i2k_0z''}\alpha(z'')dz''dz', \\ \psi_{23}(z|z_s;k_0) &= \frac{1}{8}ik_0e^{-ik_0(z+z_s)}\int_{z}^{\infty}e^{i2k_0z'}\alpha(z')\int_{-\infty}^{z'}\alpha(z'')dz''dz', \\ \psi_{24}(z|z_s;k_0) &= \frac{1}{8}ik_0e^{-ik_0(z+z_s)}\int_{z}^{\infty}\alpha(z')\int_{z'}^{\infty}e^{i2k_0z''}\alpha(z'')dz''dz'.\end{aligned} \tag{17}$$

In the "new" series,

$$\psi(z|z_s;k_0) = \psi_0 + \psi_{11} + \psi_{12} + \psi_{21} + \psi_{22} + \psi_{23} + \psi_{24} + ..., \tag{18}$$

the terms have been divided into, first, the number of interactions, and second, the relative location of the interactions. For instance, the term ψ_{23} represents the totality of second order interactions in which $z' > z$ and $z' > z''$, whence arise the scattering diagrams, which symbolize this particular scattering geometry. Since the addition of a further order of interaction, e.g. going from second to third order, involves the inclusion of one further Green's function, which must be subdivided into two cases, in general the n'th order term produces 2^n sub-terms. In this way, the eight terms of ψ_3, followed by the 16 terms of ψ_4, and so forth may be produced. Scattering diagrams may now be drawn based on the terms in equation (18). This is preceded by a description of the chosen 1D model.

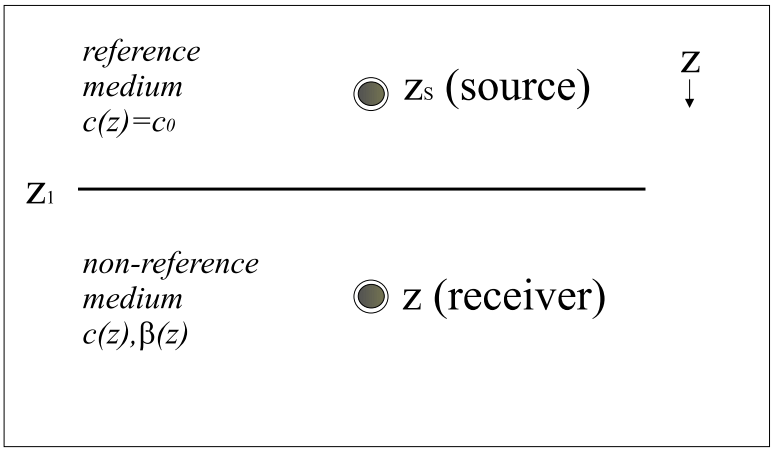

(a)

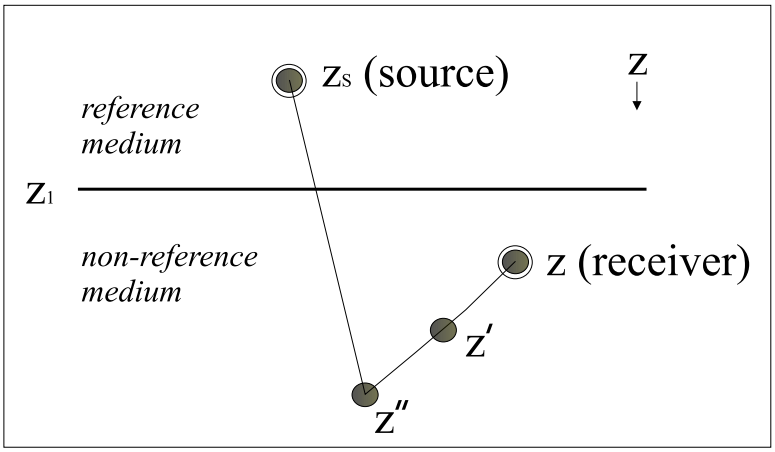

(b)

Figure 1: 1D transmission model and framework for scattering diagrams: (a) a homogeneous acoustic wholespace is chosen as the reference medium, in which the source is located; a homogeneous (visco-)acoustic half-space is chosen as the non-reference medium, in which the receiver is located; the step-like interface is located at z_1; (b) an example (ψ_{23}) of the form and construction of the scattering diagrams is superimposed on the chosen transmission model; the arrows and labels included in this example are assumed but omitted in subsequent diagrams.

The model is a 1D homogeneous acoustic whole-space, characterized by constant density and the wavespeed c_0. Overlaying this reference whole-space is the perturbation, a homogeneous half-space in which the medium parameters, i.e. $c(z)$ and/or $\beta(z)$, are constant and may or may not differ from that of the reference medium. A source is located at $z_s = 0$, in the reference medium, and a receiver is located at z, in the non-reference medium, thus mimicking a transmission experiment; the interface between the reference medium and the non-reference medium is at z_1. The model is illustrated in Figure 1a. This configuration is geometrically identical to one used by Matson (1996), such that the mapping developed therein, from Born series to closed-form, may be utilized. Figure 1b illustrates, as an example, the scattering diagram associated with ψ_{23}, within the context of the chosen model. In later diagrams the arrows are omitted, nevertheless, all propagations go from z_s to z. Further, it is worth mentioning that in this 1D model the lateral separation of scattering points has no meaning other than as an aid to visualization.

Figure 2 contains the scattering diagrams associated with ψ_0 (one diagram), ψ_1 (two diagrams), ψ_2 (four diagrams), and ψ_3 (eight diagrams), pictured without the context of the 1D model discussed above. As in Figure 1b, the the "top-left" endpoint is z_s, and the "bottom-right" is z.

The next step is to evaluate these integrals, given the chosen transmission model of Figure 1, and to use the Matson approach to produce the closed form expression for the transmitted wave field, all the while tracking the diagrams through the organization and collapsing of series. To remain general in the sense of acoustic/viscoacoustic perturbation, the perturbation $\alpha(z)$ is assigned the spatial dependence

$$\alpha(z) = \alpha_1 H(z - z_1), \tag{19}$$

such that the details of the contrast (i.e. acoustic or viscoacoustic) are hidden in the amplitude α_1, which could have a form like either of equations (10) or (11). The step-like behaviour is explicitly present in the Heaviside function $H(z - z_1)$. Substituting equation

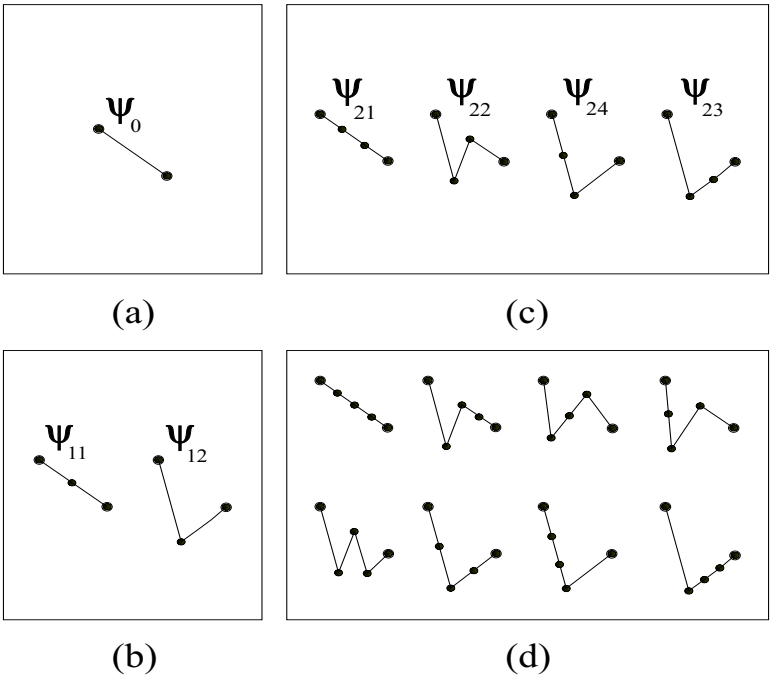

Figure 2: Scattering diagrams, for the 1D transmission example of Figure 1a, are illustrated up to third order in the perturbation α. (a) 0'th order, ψ_0; (b) 1st order, ψ_{11} – ψ_{12}; (c) 2nd order, ψ_{21} – ψ_{24}; (d) the eight diagrams of the 3rd order. Those diagrams associated with terms that have been explicitly computed in this paper are labelled as in the calculations.

(19) and $z_s = 0$ into the terms of equation (18) results in:

$$
\begin{aligned}
\psi_0(z|0;k_0) &= \frac{e^{ik_0 z}}{2ik_0}, \\
\psi_{11}(z|0;k_0) &= -\frac{\alpha_1}{4}\frac{e^{ik_0 z}}{2ik_0} 2ik_0(z-z_1), \\
\psi_{12}(z|0;k_0) &= \frac{\alpha_1}{4}\frac{e^{ik_0 z}}{2ik_0}, \\
\psi_{21}(z|0;k_0) &= -\frac{\alpha_1^2}{8}\frac{e^{ik_0 z}}{2ik_0}[ik_0(z-z_1)]^2, \\
\psi_{22}(z|0;k_0) &= -\frac{\alpha_1^2}{16}\frac{e^{ik_0 z}}{2ik_0} 2ik_0(z-z_1), \\
\psi_{23}(z|0;k_0) &= -\frac{\alpha_1^2}{16}\frac{e^{ik_0 z}}{2ik_0} 2ik_0(z-z_1), \\
\psi_{24}(z|0;k_0) &= \frac{\alpha_1^2}{16}\frac{e^{ik_0 z}}{2ik_0}.
\end{aligned}
\tag{20}
$$

The straightforward computation of the terms in equation (20) raises an issue that is of at least conceptual importance. The wave field associated with a single interface, whether reflected or transmitted, must ultimately consist of a local event due to that interface. Scattering series terms involve nested integrals over all (or much of) space. One might well ask why integrals over all space are necessary for the determination of the character of a local event. What, for instance, has the Earth at $100km$ depth got to say about a reflection coefficient at $50m$ depth? The answer is, not much, of course. The computation of equation (20) makes clear a more appropriate way of interpreting the "job" of these integrals which range over all space. The form of the perturbation places the interface at z_1 with a Heaviside function, which alters the integration limits of the integral to include z_1. In such a (definite) integral, then, the antiderivative is "picked out" at the limit z_1. This would happen anywhere an interface was placed in the form of $\alpha(z)$. As such the results are local terms, which depend on measurement location z and interface location z_1 only. So these integrals should be thought of as the process of *scanning* the model for discontinuities which give rise to local events in the series terms. This is the conceptual link – albeit simplified to include only stepwise constant media – between the integrals of the scattering series and the local nature of reflected and transmitted events.

Figure 3 contains an organization of the terms comprising the Born series representation of the wave field $\psi(z|0;k_0)$, including those of equations (20); above the low order terms, the associated scattering diagram is included. These terms are, together,

$$\begin{aligned}\psi(z|0;k_0) = \frac{e^{ik_0 z}}{2ik_0} + \frac{e^{ik_0 z}}{ik_0}\Bigg\{ & \frac{1}{8}\alpha_1 + \frac{1}{16}\alpha_1^2 + \frac{5}{128}\alpha_1^3 + ... \\ & - 2ik_0(z-z_1)\left[\frac{1}{8}\alpha_1 + \frac{1}{16}\alpha_1^2 + \frac{5}{128}\alpha_1^3 + ...\right] \\ & -k_0^2(z-z_1)^2\left[\frac{1}{16}\alpha_1^2 + \frac{3}{64}\alpha_1^3 + \frac{9}{256}\alpha_1^4 + ...\right] + ...\Bigg\}.\end{aligned} \tag{21}$$

Equation (21) makes use of two definitions:

$$R = 2\left\{\frac{1-\alpha_1/2-(1-\alpha_1)^{1/2}}{\alpha_1}\right\}, \tag{22}$$

and

$$\gamma = (1-\alpha_1)^{1/2} = \frac{k_1}{k_0}, \tag{23}$$

where k_1 is the wavenumber in the non-reference medium (which may describe acoustic or viscoacoustic propagation). Noting that γ may be expanded in Taylor series:

$$\gamma = (1-\alpha_1)^{1/2} = 1 - \frac{1}{2}\alpha_1 - \frac{1}{8}\alpha_1^2 - \frac{1}{16}\alpha_1^3 - \frac{5}{128}\alpha_1^4 - ..., \tag{24}$$

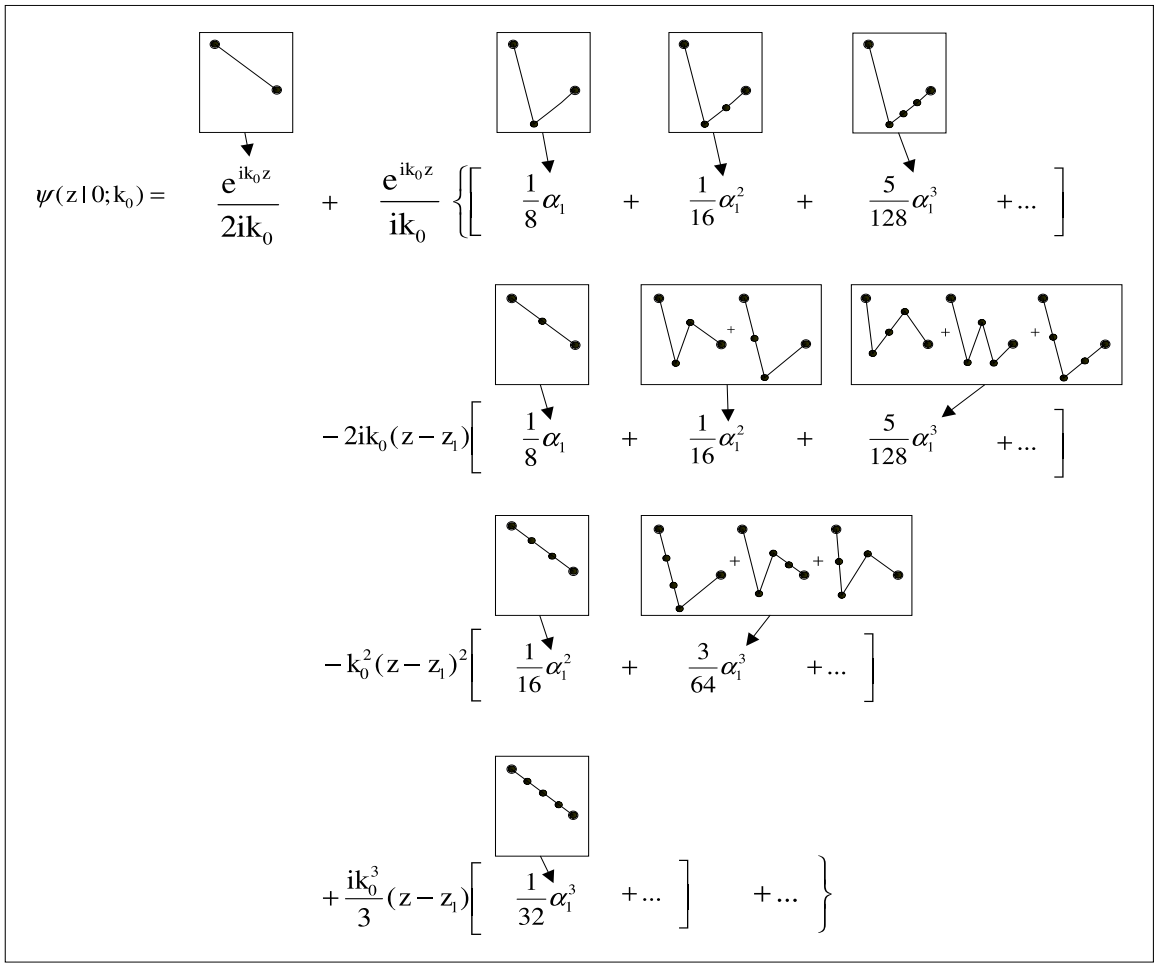

Figure 3: The Born series terms for the 1D transmission case of equation (20) are illustrated with their associated scattering diagrams.

and keeping in mind the terms found in Figure 3, one may write

$$\frac{1}{8}\alpha_1 + \frac{1}{16}\alpha_1^2 + \frac{5}{128}\alpha_1^3 + ... = \frac{R}{2}, \tag{25}$$

$$\frac{1}{16}\alpha_1^2 + \frac{3}{64}\alpha_1^3 + \frac{9}{256}\alpha_1^4 + ... = (1-\gamma)\frac{R}{2}, \tag{26}$$

and so on. The series' in powers of α_1, i.e. the rows of Figure 3, therefore collapse into single terms in R and $1-\gamma$. In fact:

$$\psi(z|0;k_0) = \frac{e^{ik_0 z}}{2ik_0} + \frac{e^{ik_0 z}}{ik_0}\frac{R}{1-\gamma}\left\{\frac{(1-\gamma)}{2} - ik_0(z-z_1)(1-\gamma) - \frac{k_0^2(z-z_1)^2}{2}(1-\gamma)^2 + ...\right\}. \tag{27}$$

These collapsed series' in α_1 are therefore coefficients of a further series in orders of $-ik_0(z-z_1)$. Notice that one may expand as a Taylor's series:

$$\begin{aligned} & e^{-ik_0(z-z_1)(1-\gamma)} - \frac{(1+\gamma)}{2} \\ &= \left[1 - \frac{(1+\gamma)}{2}\right] - ik_0(z-z_1)(1-\gamma) - \frac{k_0^2}{2}(z-z_1)^2(1-\gamma)^2 + ... \\ &= \frac{(1-\gamma)}{2} - ik_0(z-z_1)(1-\gamma) - \frac{k_0^2}{2}(z-z_1)^2(1-\gamma)^2 + ... \end{aligned} \tag{28}$$

This is the form of the series in equation (27). Substituting equation (28) into equation (27) produces the closed-form expression:

$$\begin{aligned} \psi(z|0;k_0) &= \frac{e^{ik_0 z}}{2ik_0} + \frac{e^{ik_0 z}}{ik_0}\frac{R}{1-\gamma}\left\{e^{-ik_0(z-z_1)(1-\gamma)} - \frac{(1+\gamma)}{2}\right\} \\ &= \frac{e^{ik_0 z}}{2ik_0} + \frac{k_0}{k_0+k_1}\frac{e^{ik_0 z_1}}{ik_0}e^{ik_1(z-z_1)} - \frac{e^{ik_0 z}}{2ik_0} \\ &= \frac{k_0}{k_0+k_1}\frac{e^{ik_0 z_1}}{ik_0}e^{ik_1(z-z_1)}, \end{aligned} \tag{29}$$

using the definitions of equations (22) and (23). This expression for the transmitted wave field, generalized to accomodate viscoacoustic or acoustic propagation, propagates according to k_1, which is the non-reference wavenumber.

Observing the process of collapsing the series, from the form of Figure 3 to that of equation (27), the roles of the types of scattering interaction in the construction of the eventual wave field become clear.

The wave field, propagating correctly in the non-reference medium via the term $e^{ik_0 z}e^{-ik_0(z-z_1)(1-\gamma)}$ $= e^{ik_0 z}e^{ik_0(k_1/k_0)(z-z_1)} = e^{ik_1(z-z_1)}$, is generated in the Born series by a weighted series in orders of $-ik_0(z-z_1)$, i.e. each row of equation (21) and Figure 3. Notice from Figure 3 that the leading terms in each order $n > 0$ of $[-ik_0(z-z_1)]^n$, arise due to the same scattering interaction-type, that is, those with no direction-change from source to receiver (see Figure 4a). It is therefore justifiable to attribute much of the burden of alteration of propagation (wavespeed and/or attenuation) to this type of scattering interaction in the Born series. Of course, to correctly alter k_0 to k_1 requires $\gamma = k_1/k_0$, which in turn requires terms at all orders of α_1; nevertheless, the leading terms are the most signficant, especially for small α_1.

Next consider the amplitude of the transmitted wave field, $k_0/(k_0+k_1) = R/(1-\gamma)$, which is correctly produced by the series of 0'th order in $-ik_0(z-z_1)$, i.e. the first "row" of equation (21) and Figure 3. While it is true that every order of $-ik_0(z-z_1)$ has such a series embedded

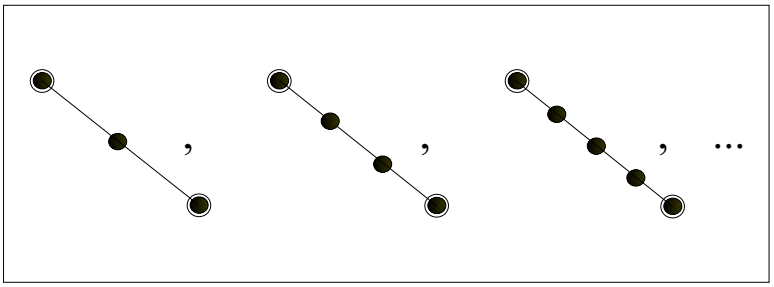

(a)

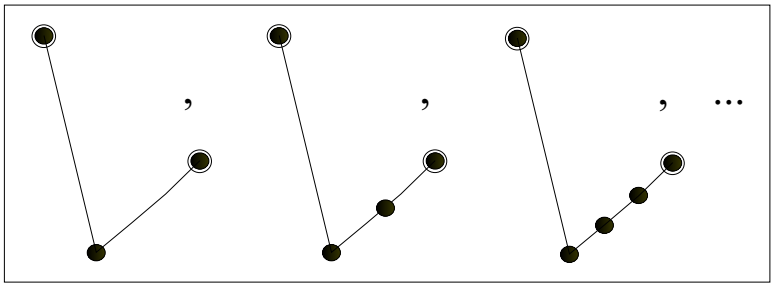

(b)

Figure 4: Certain scattering-types are seen to be associated with the generation of macroscopic properties of the transmitted wave field. (a) These interaction types contain all information necessary to properly alter the amplitude of the transmitted wave field; also, these interaction-types are solely responsible for producing the negative of the direct wave; (b) These interaction types are responsible for the leading order terms in the alteration of the propagation wavenumber, from k_0 (reference medium) to k_1 (true medium).

in it, so in truth the whole series produces the amplitude coefficient, the information required for its correct computation is laid down by this first row of equation (21). Inspection of Figure 3 reveals that this series is also characterized by scattering interactions of common type (see Figure 4b). This amplitude produces the expected transmission coefficient, as was noted in Matson (1996) for the acoustic case:

$$T = \frac{|\psi(z|0;k_0)|}{|G_0(z|0;k_0)|} = \frac{2k_0}{k_0 + k_1}; \tag{30}$$

and so one is justified in looking to these types of interaction as being central to amplitude adjustment.

In "mixed" terms, of order higher than $n = 1$ in $[\alpha_1]^n$ and $n = 0$ in $[-ik_0(z - z_1)]^n$, more than one type of scattering diagram is associated with each term. In other words, certain scattering interaction-types are not distinct in the solution. Inspection of Figure 3 suggests that these indistinct components of the solution are related in that they share the same number of "up-" and "down-"scattering directions. For instance, the term $-k_0^2(z - z_1)^2(3/64)\alpha_1^3$ has three contributing diagrams: from left to right, "down-down-down-up", "down-up-down-down", and "down-down-up-down". Since the source is fixed to be above all interactions, the first direction must be "down"; therefore, these three diagrams represent all permutations of "two downs + one up-" interaction type.

Finally, consider the third key task of the Born series: the elimination of the direct wave $\psi_0 = e^{ik_0 z}/2ik_0$. The series accomplishes this, in equation (28), concurrently to the wave field construction, by creating the negative of the direct wave such that they destructively interfere. This is also a conclusion of Matson (1996). This "task" is accomplished by the terms which are 0'th order in $-ik_0(z - z_1)$; the unit first term is split into two parts, $(1+\gamma)/2$ and $1 - (1 + \gamma)/2$, the former of which ultimately becomes the negative of the direct wave (equation 28). This direct wave eliminator, unlike the amplitude term, owes its existence *solely* to scattering interactions of the type seen in Figure 4b.

Lastly, we might underscore a remarkable aspect of the propagations and interactions which constitute the terms in the Born series. The reference Green's function propagates from interaction point to interaction point in every term – no other type of propagation ever occurs in this formalism. The reference Green's function is, here, the solution to the acoustic wave equation, yet the final wave field is viscoacoustic: this means that an attenuated and dispersed wave field is being correctly generated by a sophisticated interplay of non-attenuating wave propagations.

In this section the scattering potentials, generalized to permit viscoacoustic wave propagation, have been confirmed as producing the expected wave field expression for a simple 1D

transmission case. Concurrently, scattering diagrams, which are a byproduct of the subdivision of the Born series terms into computable units, are carried through the calculations. Thus, when the mapping of Matson (1996) is used to produce the closed form expression for the wave field, the "scattering interaction-types" that produced each term may be categorized as to their contribution to overall wave field properties, such as amplitude, phase (and attenuation), and the destruction of unwanted wave field components.

3 Toward Scattering-based Q Compensation/Estimation

In this section we utilize a different categorization of scattering diagram, that of "separated" vs. "self-interaction" (Weglein et al., 2002). The insight gained from such a categorization directly guides the search in the inverse series for task-oriented subseries.

The promise of the inverse scattering series, convergence issues notwithstanding, is to compute the model $\alpha(z)$ via certain nonlinear operations carried out upon the data. If the measured wave field is distorted and smoothed because it propagated through an attenuating medium that has sharp transitions, then the reconstruction of these sharp transitions *must* include some process of Q-compensation. Furthermore, since Q can be cast as part of the perturbation, the computation of the model *must* include Q-estimation. To determine how and where such processes take place in the inversion, it is, as ever, useful to turn to the forward scattering series.

It is particularly compelling to consider a 1D case in which only Q contrasts, and no wavespeed contrasts, exist. These contrasts produce reflections, but the wave never travels at a speed different from that of the reference medium. So, in the inverse, no beyond-Born imaging *per se* will be required. All events will be correctly located by imaging with the reference wavespeed. The only processing step necessary will be to remove the smoothing and distortion effects. Weglein et al. (2002) have identified a separable subseries responsible for imaging in the presence of wavespeed contrasts – will this subseries shut down in a Q-only case? How then will Q compensation occur? Let us next address these questions by looking at the forward analogue of the imaging subseries.

Consider the two models shown in Figures 5a and b, both of which represent 1D media. Both are geometrically identical, but the first (5a) represents a purely acoustic variation: the wave field propagates at wavespeed c_0 for $z < z_1$ and $z > z_2$, but at c_1 in the layer between (z_1, z_2). Meanwhile, the second corresponds to a situation akin to that described above: the wavespeed never changes, $c(z) = c_0$ everywhere. The absorption parameter Q,

which we assume obeys the dispersion relation associated with Kjartansson's constant Q model (1979), undergoes a contrast in this case (Figure 5b), from ∞ outside (z_1, z_2) to Q_1 within.

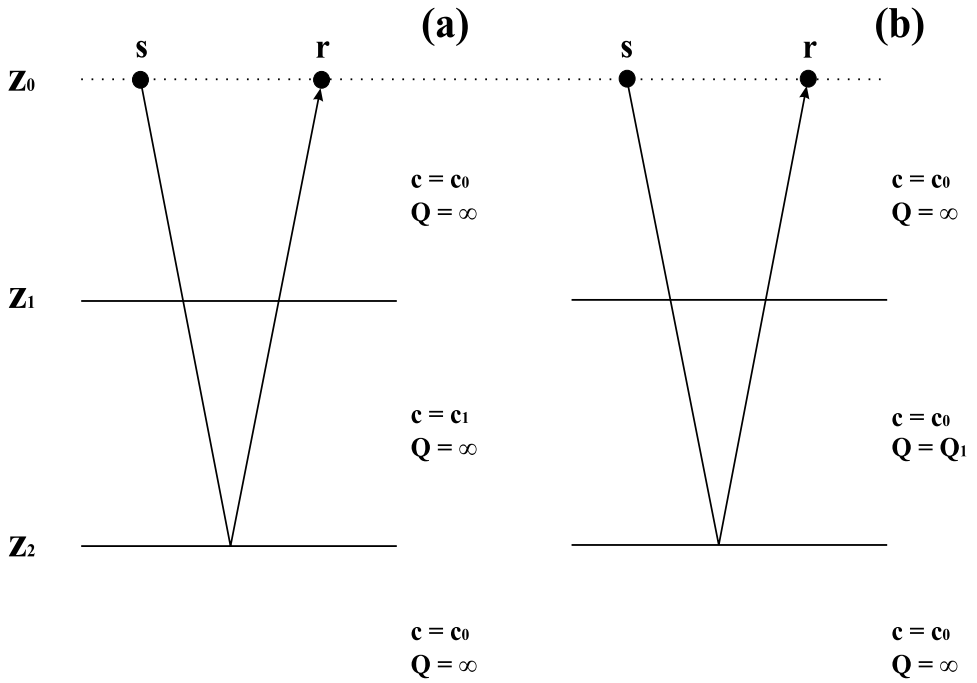

Figure 5: Schematic of two models for a 1D reflected wavefield. (a) The acoustic case: we consider the "second primary", i.e. that which has reflected at the z_2 interface, which in this case corresponds to a wavespeed contrast. (b) The viscoacoustic case: an identical geometry as that of (a), here we consider a contrast in Q only. This latter wave field travels everywhere with the wavespeed c_0, and hence no alteration of the Born approximate arrival time is required; we wish to ascertain what if any effect the "mover", or timing-related terms in the series have on the construction of this field.

Matson (1996) finds an expression for the primary reflection associated with the lower interface (z_2) in a model of this sort (whose ray-path is illustrated in Figures 5a and b). Previous work of Innanen (M-OSRP Report, 2001) has shown that the general form of Matson's expressions are the same for both the acoustic and viscoacoustic examples. After the amplitude

series' have been collapsed, we have

$$\begin{aligned}\psi_{pr2}(z<z_1|0;k_0) = \frac{e^{-ik_0z}e^{i2k_0z_2}}{2ik_0}R_2T_{10}T_{01}\left[1+ik_02(z_2-z_1)(\gamma-1)\right.\\ \left.-\frac{k_0^2}{2!}4(z_2-z_1)^2(\gamma-1)^2-\frac{ik_0^3}{3!}8(z_2-z_1)^3(\gamma-1)^3+...\right],\end{aligned} \tag{31}$$

which further collapses to

$$\psi_{pr2}(z<z_1|0;k_0) = \frac{e^{-ik_0z}e^{i2k_0z_2}}{2ik_0}R_2T_{10}T_{01}e^{i2k_0(z_2-z_1)(\gamma-1)}, \tag{32}$$

recalling that $\gamma = k_1/k_0$, i.e. the ratio of the reference and non-reference wavenumbers. The reflection and transmission coefficients (R_2, and T_{10} and T_{01}, for the reflection, transmission from medium 1 to 0 and transmission from medium 0 to 1 respectively) have been produced similarly to the amplitude of the transmitted wave field in the previous section.

The terms in the Born series which have conspired to produce the bulk of the $e^{i2k_0(z_2-z_1)(\gamma-1)}$ component in equation (32) correspond to "separated" diagrams, by virtue of the presence of powers of (z_2-z_1); hence this component is due to the forward analogue of the *imaging* subseries. We expect, therefore, that in the acoustic case, this term will do much of the work required to take the incorrectly-timed arrival of the Born approximation, and alter it such that it arrives having travelled everywhere at the correct wavespeed. Let us first see that this is the case.

In the acoustic case

$$\gamma = \frac{k_1}{k_0} = \frac{c_0}{c_1}, \tag{33}$$

so, expanding equation (32),

$$\psi_{pr2}(z<z_1|0;k_0) = \frac{e^{-ik_0z}}{2ik_0}R_2T_{10}T_{01}\left[e^{i2k_0z_2}e^{-i2k_0z_2}\right]e^{i2k_0z_1}e^{i2k_0(z_2-z_1)\frac{c_0}{c_1}}. \tag{34}$$

Consider first equation (32). The incorrect arrival time of the Born approximation appears in the uncorrected leftmost term $\frac{e^{-ik_0z}e^{i2k_0z_2}}{2ik_0}$, specifically in the part which produces a phase delay over the distance z_2 with wavenumber k_0: $e^{i2k_0z_2}$. Next consider equation (34). Notice that the -1 portion of $(\gamma-1)$ in the correction produces a term opposing this arrival (both are in square brackets $[\cdot]$) when the expression is expanded. So in the acoustic case, the first task of the series' "corrector" term, $e^{i2k_0(z_2-z_1)(\gamma-1)}$, is to delete the incorrectly timed event. Next,

$$\begin{aligned}\psi_{pr2}(z<z_1|0;k_0) &= \frac{e^{-ik_0z}}{2ik_0}R_2T_{10}T_{01}e^{i2k_0z_1}e^{i2[\frac{\omega}{c_0}\frac{c_0}{c_1}](z_2-z_1)}\\ &= \frac{e^{-ik_0z}}{2ik_0}R_2T_{10}T_{01}e^{i2k_0z_1}e^{i2k_1(z_2-z_1)}.\end{aligned} \tag{35}$$

Here, the second task of the series corrector is engaged: the remainder of $(\gamma - 1)$, namely c_0/c_1, multiplies the reference wavenumber k_0 in the square brackets, deleting the incorrect wavespeed and replacing it with the correct wavespeed and thus the correct wavenumber k_1.

In their totality, the "separated diagram" type terms therefore have the effect of (1) deleting the Born approximate arrival, and (2) replacing it with the correctly-timed true arrival. Thus arises the interpretation, in the inverse analogue, of these separated diagram terms as being "movers". One might indeed expect that, in the event of a true medium with no wavespeed variation, these terms would shut down. There are a number of problems with this expectation, however, not least of which is: they don't.

Let us proceed by examining the purely-Q contrast case. We have

$$\gamma = \frac{k_1}{k_0} = \frac{\frac{\omega}{c_0}\left[1 + \frac{i}{2Q_1} - \frac{1}{\pi Q_1}\ln\left(\frac{\omega}{\omega_r}\right)\right]}{\frac{\omega}{c_0}} = 1 + \frac{i}{2Q_1} - \frac{1}{\pi Q_1}\ln\left(\frac{\omega}{\omega_r}\right), \tag{36}$$

following the constant Q law of Kjartansson (1979). Once again expanding equation (32), but this time with the viscoacoustic γ, we have

$$\begin{aligned}\psi_{pr2}(z < z_1|0;k_0) &= \frac{e^{-ik_0 z}e^{i2k_0 z_2}}{2ik_0}R_2 T_{10}T_{01}e^{i2k_0(z_2-z_1)\left[1+\frac{i}{2Q_1}-\frac{1}{\pi Q_1}\ln\left(\frac{\omega}{\omega_r}\right)-1\right]} \\ &= \frac{e^{-ik_0 z}e^{i2k_0 z_2}}{2ik_0}R_2 T_{10}T_{01}e^{i2k_0(z_2-z_1)\left[\frac{i}{2Q_1}-\frac{1}{\pi Q_1}\ln\left(\frac{\omega}{\omega_r}\right)\right]}.\end{aligned} \tag{37}$$

So the correcting term doesn't become unity, or by any means vanish, even though there are no timing changes to be made – the imaging subseries analogue stays alive. What happens instead is that the form of the viscoacoustic γ extinguishes the -1 from $(\gamma - 1)$ – see equation (37). This was the mechanism in the acoustic case that deleted the incorrect arrival. The Born arrival time of this primary is kept! What is left in place of a "mover" term, that deletes and replaces primaries, is an operator, $e^{i2k_0(z_2-z_1)\left[\frac{i}{2Q_1}-\frac{1}{\pi Q_1}\ln\left(\frac{\omega}{\omega_r}\right)\right]}$, that distorts the amplitude and phase of the Born primary according to the Q model. We finally arrive at

$$\psi_{pr2}(z < z_1|0;k_0) = \frac{e^{-ik_0 z}}{2ik_0}R_2 T_{10}T_{01}e^{i2k_0 z_2\left[1+\frac{i}{2Q_1}-\frac{1}{\pi Q_1}\ln\left(\frac{\omega}{\omega_r}\right)\right]}e^{-i2k_0 z_1\left[\frac{i}{2Q_1}-\frac{1}{\pi Q_1}\ln\left(\frac{\omega}{\omega_r}\right)\right]}, \tag{38}$$

Here, via the term $e^{i2k_0 z_2\left[1+\frac{i}{2Q_1}-\frac{1}{\pi Q_1}\ln\left(\frac{\omega}{\omega_r}\right)\right]}$, the wave field propagates the entire distance $2z_2$, attenuating with Q_1. This is the correct arrival time, but the incorrect amount of attenuation – too much. The rightmost term, $e^{-i2k_0 z_1\left[\frac{i}{2Q_1}-\frac{1}{\pi Q_1}\ln\left(\frac{\omega}{\omega_r}\right)\right]}$, corrects this by deconvolving the attenuation effects (not the propagation effects) associated with the distance $2z_1$. The final result is that the second primary has experienced the expected amount of attenuation, that is, through the distance $2(z_2 - z_1)$.

The important point here is that the "separated diagram"-type terms have played an enormously important role in the Q contrast only case, in spite of the fact that no "moving" was required. It seems clear that a redefinition of the forward analogue of the imaging subseries is in order. We surmise that these terms are responsible for generating *propagation effects* rather than simply *timing changes* – with the former reducing to the latter in the acoustic case. The "movers", which correspond to the imaging subseries in the inverse case, must be generalized to "depropagators".

4 Conclusions

The work described in this paper reflects the course of the initial investigation into the use of scattering theory as a means to process data with non-negligible attenuation effects. It contains, first, the results of computing terms in the forward (or Born) series, and following the scattering diagram associated with each of these terms. Secondly, it concerns itself with the effect on a reflected primary of terms that involve "separated" interactions. These are the forward series analogues of the imaging terms of the inverse scattering series. We reach the conclusion that the meaning of the "moving" terms, those whose diagrammatical representation involves separated scattering interactions, must be generalized to accomodate the inclusion of all propagation effects into the true wave field.

The consequences with regards to how the inverse scattering series must treat attenuation are clear – we must look to the imaging subseries to remove the effects of Q. In an example pathologically created with no wavespeed changes, we may indeed find that the imaging series does only this. In such an example the inversion subseries (Zhang's work in this report) must therefore be involved with Q-estimation only.

Beyond ascertaining that this is the case, the next challenge is to cast the inverse scattering series problem with at least two parameters (perhaps c and Q), and use a pre-stack experimental milieu to investigate both the imaging (depropagation) and inversion (c and Q estimation) subseries.

Acknowledgments

This work was done in close association with Tad Ulrych (UBC) and CDSST and M-OSRP. The authors are grateful to Ken Matson, Simon Shaw, Gwenn Flowers and members of both consortia for their comments and advice.

References

DeSanto, J. A., Scalar wave theory, 1993: Springer-Verlag, Berlin.

Kjartansson, E., Constant q-wave propagation and attenuation, 1979: Journal of Geophysical Research, **84**, 4737–4748.

Matson, K. H., The relationship between scattering theory and the primaries and multiples of reflection seismic data, 1996: Journal of Seismic Exploration, **5**, 63–78.

Weglein, A. B., Foster, D. J., Matson, K. H., Shaw, S. A., Carvalho, P. M., and Corrigan, D., Predicting the correct spatial location of reflectors without knowing or determining the precise medium and wave velocity: initial concept, algorithm, and analytic and numerical example, 2002: Journal of Seismic Exploration, **10**, 367–382.

Forward scattering series and seismic events: high frequency approximations, critical and postcritical reflections

Bogdan G. Nita[1], Kenneth H. Matson[2] and Arthur B. Weglein[1]
[1]University of Houston, [2]BP

Abstract

In this paper we progress the analysis of the forward scattering series and seismic events for 1D normal incidence seismic data introduced by Matson (1996) and later extended to prestack data by Matson (1997). We show that the exchange of certain integrals in the prestack calculation of the forward scattering series terms in the later yield the same result as a high frequency approximation of the integrals, without the interchange. The reasonableness of this outcome is described from both a mathematical and a physical point of view. The convergence of the forward scattering series at the critical angle is also proved and an explanation is proposed for the divergence of the series for postcritical incident planewaves.

1 Introduction

Inverse scattering series is using the deghosted and demultipled recorded data to locate reflectors and invert for parameters that change at those locations. The present location and inversion algorithms, although successful, are written for smooth, horizontal interfaces and process either 1D data or 2D precritical data. If interfaces are considered to have a higher degree of realism (dipping, highly corrugated, diffractive etc.) then the data contains more and different information than expected by those algorithms (postcritical reflections, headwaves) even for simple incident planewaves. For both fundamental and practical advances, it is important to establish the attitude taken towards these returning signals (portions of the recorded scattered wavefield) as noise or as information bearing agents. The general objective of this particular research is to establish the scattering theory description and processing of more complicated waves. While analogies between forward and inverse processes are not maps, they never-the-less provide useful hints or at least point where certain activity resides in the inverse series. The forward series does not hint at whether events will be signal or noise in the inverse series, only suggests where one might look for that answer. Take multiples for example: it turns out that the inverse scattering subseries made of terms that mimic the

diagrams for multiples in the forward series is responsible for attenuating/removing them from the data. Precritical data has been studied by Matson (1997) who showed that the expected (from wave-theory) precritically reflected wavefield is constructed by the convergent forward scattering series in a 2D experiment. This study brings new understanding about the physical interpretation of Matson results; it also shows that the same forward series converges for critical angles as well. An explanation of the postcritical divergence is proposed.

2 The forward series and seismic reflection data

Matson (1996) and thesis (1997) describe the propagation of a wavefield in a given 1D or 2D medium respectively, using the forward scattering series. The actual medium is viewed as a perturbation of a reference medium; the propagation of the wavefield in the actual medium is given by the forward scattering (Born) series, a series of propagations in the reference medium separated by different orders of scattering interactions with a point scatterer perturbation

$$\begin{aligned} P(\vec{r}|\vec{r}_s;\omega) &= P_0(\vec{r}|\vec{r}_s;\omega) \\ &+ \int_{-\infty}^{\infty} P_0(\vec{r}|\vec{r}';\omega)V(\vec{r}')P_0(\vec{r}'|\vec{r}_s;\omega)d\vec{r}' \\ &+ \int_{-\infty}^{\infty} P_0(\vec{r}|\vec{r}';\omega)V(\vec{r}') \left(\int_{-\infty}^{\infty} P_0(\vec{r}'|\vec{r}'';\omega)V(\vec{r}'')P_0(\vec{r}''|\vec{r}_s,\omega)d\vec{r}'' \right) d\vec{r}' \\ &+ .... \end{aligned}$$

where all the position vectors are fully 3D and $\vec{r}_s$ represents the position of the source, $\vec{r}$ the position of the receiver and $\vec{r}'$ indicates the position of a point scatterer. For a two dimensional model, the propagations in the reference medium are given by the 2D Green's function

$$G_0(x,z|x_s,z_s) = \frac{1}{2\pi}\int_{-\infty}^{\infty} \frac{e^{ik_s(x-x_s)}e^{i\nu_{0s}|z_g-z_s|}}{2i\nu_{0s}}dk_s$$

where k_s and ν_{0s} are the horizontal and the vertical wavenumber of the reference medium respectively ($\nu_{0s}^2 + k_s^2 = \omega^2/c_0^2$). Rewriting G_0 as

$$G_0(x,z|x_s,z_s) = \frac{1}{2\pi}\int_{-\infty}^{\infty} \frac{e^{-ik_s x_s}}{2i\nu_{0s}}\phi_0(x_g,z_g|k_s,z_s;\omega)dk_s$$

with $\phi_0(x_g, z_g|k_s, z_s; \omega) = e^{i(k_s x_g + \nu_{0s}|z_g - z_s|)}$, it is apparent that G_0 represents a superposition of weighted plane waves. This motivates the use of a plane-wave as the incident wave with the remark that one can construct solutions for point sources from plane-wave solutions by performing the above mentioned weighted integration. The model used is a half-space earth with no lateral variance, with an interface at z_1 ; the scattering perturbation for this model is

$$V(z') = k_0^2 a_1 H(z' - z_1)$$

where $a_1 = 1 - c_0^2/c_1^2$, c_1 is the velocity in the second medium, c_0 the velocity in the reference medium with H being the Heaviside function. For simplicity consider the source location to be (0, 0); the Born series takes the form

$$\begin{aligned} P(\vec{r}|\vec{r}_s\,;\omega) \;=\; & e^{i(kx_g + \nu_0 z_g)} \\ & + \int_{-\infty}^{\infty}\int_{-\infty}^{\infty}\frac{1}{2\pi}\int_{-\infty}^{\infty}\frac{e^{ik_g(x_g - x')}e^{i\nu_0|z_g - z'|}}{2i\nu_0}dk_g k_0^2 a_1 H(z' - z_1)P_0(x', z'; \omega)dx'dz' \\ & + \int_{-\infty}^{\infty}\int_{-\infty}^{\infty}\frac{1}{2\pi}\int_{-\infty}^{\infty}\frac{e^{ik_g(x_g - x')}e^{i\nu_0|z_g - z'|}}{2i\nu_0}dk_g k_0^2 a_1 H(z' - z_1)P_1(x', z' > z_1|k, \omega)dx'dz' \\ & + ... \end{aligned}$$

Note that the incoming wave hits all the scatterers at once; each scatterer then emits a spherical wave which can propagate to the receiver or to another point scatterer. Each term in the forward series represents the response at the receiver after a certain number of interactions: the zeroth term represents the direct arrival, the first term represents the wavefield after one interaction with a point scatterer and so on. To construct even the simplest event, one needs an infinite number of terms in the forward series. To obtain the total wavefield at the receiver we have to solve the integrals in the previous expression. Following Matson (1997) we solve for the first term in the series

$$P_1 = \int_{-\infty}^{\infty}\int_{-\infty}^{\infty}\frac{1}{2\pi}\int_{-\infty}^{\infty}\frac{e^{ik_g(x_g - x')}e^{i\nu_0|z_g - z'|}}{2i\nu_0}dk_g k_0^2 a_1 H(z' - z_1)e^{i(kx' + \nu_0 z')}dx'dz'$$

Begin by switching the order of integration so that the integration with respect to dx' is performed first. Hence

$$P_1 = \frac{1}{2\pi}\int_{z_1}^{\infty}\int_{-\infty}^{\infty}\left(\int_{-\infty}^{\infty}e^{i(k - k_g)x'}dx'\right)e^{ikgx_g}e^{i\nu_{0g}|z_g - z'|}e^{i\nu_0 z'}\frac{k_0^2 a_1}{2i\nu_{0g}}dk_g dz'$$

Using

$$\int_{-\infty}^{\infty} e^{i(k-k_g)x'}dx' = 2\pi\delta(k_g - k)$$

P_1 becomes

$$P_1 = \int_{z_1}^{\infty}\int_{-\infty}^{\infty} \delta(k_g - k)e^{ikgx_g}e^{i\nu_{0g}|z_g - z'|}e^{i\nu_0 z'}\frac{k_0^2 a_1}{2i\nu_{0g}}dk_g dz'.$$

Using the properties of the delta function we see that the inside integral switches $k_g \to k$ and hence $\nu_{0g} \to \nu_0$ so the expression becomes

$$P_1 = \frac{k_0^2 a_1}{2i\nu_0}e^{ikx_g}\int_{z_1}^{\infty} e^{i\nu_0|z_g - z'|}e^{i\nu_0 z'}dz'.$$

There are two cases to be considered at this point: $z_g < z_1$ for the reflected P_1 and $z_g > z_1$ for the transmitted part. The first enters into the series for the total reflected field while the second is used either into the series for transmitted wavefield or for the calculation of P_2 (reflected or transmitted).
We have

$$P_1(x_g, z_g < z_1|k;\omega) = \frac{k_0^2 a_1}{2i\nu_0}e^{ikx_g}e^{-i\nu_0 z_g}\int_{z_1}^{\infty} e^{i\nu_0 2z'}dz'.$$

Integrating and considering that, due to some small dissipation, the wave at infinity vanishes, we obtain

$$P_1(x_g, z_g < z_1|k;\omega) = \frac{k_0^2 a_1}{4\nu_0^2}e^{ikx_g}e^{i\nu_0(2z_1 - z_g)}.$$

Same integration procedure is used for the calculation of P_2 , P_3 etc. The calculated terms

$$P(x_g, z_g < z_1|k;\omega) = e^{ikx_g}e^{i\nu_0(2z_1 - z_g)}\left[\frac{1}{4}\frac{k_0^2 a_1}{\nu_0^2} + \frac{1}{8}\left(\frac{k_0^2 a_1}{\nu_0^2}\right)^2 + \frac{5}{64}\left(\frac{k_0^2 a_1}{\nu_0^2}\right)^3 + \frac{7}{128}\left(\frac{k_0^2 a_1}{\nu_0^2}\right)^4 + ...\right]$$

indicate certain regularity: the series is recognized to be the Taylor series for $\sqrt{1 - \frac{k_0^2 a_1}{\nu_0^2}}$ about $\frac{k_0^2 a_1}{\nu_0^2} = 0$ after some algebraic operations performed on it. The ratio test indicates

that the series converges for $\left|\frac{k_0^2 a_1}{\nu_0^2}\right| < 1$. By writing $\nu_0 = k_0 \cos\theta$, with θ being the incidence angle of the plane wave, this condition becomes

$$\sin\theta < \frac{c_0}{c_1} < \left(1 + \cos^2\theta\right)^{1/2} \tag{1}$$

This last relation can be viewed in two ways:

1. First, for a fixed incidence angle θ, this is a restriction on the velocity contrast between the reference and the actual medium. For $\theta = 0$ (normal incidence) the left inequality is satisfied for any 2 velocities; the right hand inequality becomes $c_0 < \sqrt{2} c_1$ (Matson 1996).

2. Second, for a fixed velocity model, the restriction is on the incident angle. Note that given any two velocities c_0 and c_1, one of the two inequalities is automatically satisfied. For $c_0 > c_1$, the condition reads $\frac{c_0}{c_1} < (1 + \cos^2\theta)^{1/2}$ or $\sin^2\theta < 1 + a_1$ with $a_1 < 0$.

For $c_0 < c_1$, the condition becomes $\sin\theta < \frac{c_0}{c_1}$ or $\theta < \theta_c$ where θ_c is the critical angle $\theta_c = \sin^{-1}(c_0/c_1)$. When the series converges, the limit is

$$2\frac{\nu_0^2}{k_0^2 a_1}\left[1 - \sqrt{1 - \frac{k_0^2 a_1}{\nu_0^2}}\right] - 1 = \frac{\nu_0 - \nu_1}{\nu_0 + \nu_1}$$

so the final expression for the total field is

$$P = \frac{\nu_0 - \nu_1}{\nu_0 + \nu_1} e^{ikx_g} e^{i\nu_0(2z_1 - z_g)}$$

which is the expected result from Wave Theory.

3 Comments about the calculation of terms in the forward scattering series

The calculation of

$$P_1 = \int_{-\infty}^{\infty}\int_{-\infty}^{\infty} \frac{1}{2\pi}\left(\int_{-\infty}^{\infty} \frac{e^{ik_g(x_g - x')} e^{i\nu_0|z_g - z'|}}{2i\nu_0} dk_g\right) k_0^2 a_1 H(z' - z_1) e^{i(kx' + \nu_0 z')} dx' dz' \tag{2}$$

contains a reordering of integrals: in the original expression the dk_g integral should be solved first since it is the inner most one then the dx' integral and finally the dz' one.

The calculations are greatly simplified if the dx' integration is performed first, then the dk_g and finally the dz' integration. However this kind of operation has to be performed with great care since it might change the result obtained from solving the integrals in the original order. In this section we show that the interchange of integrals is only valid in the high frequency approximation. To get a feeling why this statement is true even before proving it mathematically, study the equation (2) in detail. Recall that Fubini theorem gives sufficient conditions for interchanging integrals. It states that when a function f is integrable (continuity or boundedness imply integrability) on $R^n = R^k \times R^m$ then the iterated integrals of f over R^k and R^m exist and

$$\int\limits_{R^n} f = \int\limits_{R^k}\int\limits_{R^m} f(x,y)dydx = \int\limits_{R^m}\int\limits_{R^k} f(x,y)dxdy.$$

Note that the inner most integrand in (2) is neither continuous nor bounded due to $\nu_0 = \sqrt{\frac{\omega^2}{c_0^2} - k_g^2}$ in the denominator. When k_g runs from $-\infty$ to ∞, the integrand blows up at $\pm\frac{\omega}{c_0}$. However, in the high frequency approximation, we have

$$\int\limits_{-\infty}^{\infty} \frac{e^{ik_g(x_g-x')}e^{i\nu_0|z_g-z'|}}{2i\nu_0}dk_g \sim \int\limits_{-\omega/c_0}^{\omega/c_0} \frac{e^{ik_g(x_g-x')}e^{i\nu_0|z_g-z'|}}{2i\nu_0}dk_g \tag{3}$$

and the integrand is now continuous hence integrable everywhere. The Fubini theorem applies and the interchange of integrals, and hence Matson's derivation, is valid. Next, we recalculate P_1 using saddle point approximations for the two integrals involved without switching the order of integration and show that the result is the one obtained by Matson. Saddle point or stationary phase approximation gives the leading asymptotic behavior of generalized Fourier integrals, i.e. of the form $\int\limits_{-\infty}^{\infty} F(p)e^{\omega f(p)}dp$, having stationary points, i.e. points p_s such that $f'(p_s) = 0$. The idea of the method is to use the analyticity of the integrand to justify deforming the path of integration to a new path on which $f(p)$ has a constant imaginary path. How the contour is deformed depends on the singularities and branch cuts of the integrand. Once this has been done the integral may be found asymptotically ($\omega \to \infty$) to be

$$\int\limits_{-\infty}^{\infty} F(p)e^{\omega f(p)}dp \sim \left|\frac{2\pi}{\omega f''(p_s)}\right|^{1/2} F(p_s)e^{isign(f''(p_s))\frac{\pi}{4}} \exp\left[\omega f(p_s)\right]. \tag{4}$$

To calculate P_1 start by rewriting

$$G_0 = \frac{1}{2\pi}\int\limits_{-\infty}^{\infty} \frac{e^{ik_g(x_g-x')}e^{i\nu_0|z_g-z'|}}{2i\nu_0}dk_g$$

as

$$G_0 = \frac{1}{2\pi} \int_{-\infty}^{\infty} F(p) e^{\omega f(p)} dp$$

where

$$F(p) = \frac{1}{2i\sqrt{1/c_0^2 - p^2}}$$

and

$$f(p) = i \left[p(x_g - x') + \sqrt{\frac{1}{c_0^2} - p^2}\, |z_g - z'| \right].$$

Note that, due to the square root, $F(p)$ defines two branch cuts in the complex p plane; the branch cuts are hyperbolas in the first and third quadrant and are running very close to the coordinate axis (for a full discussion of the branch cuts of F see Aki and Richards (1980) Box 6.2). By definition, branch cuts are lines of discontinuities for $F(p)$ and here are given by $\mathrm{Im}\sqrt{1/c_0^2 - p^2} = 0$. This means that when the new integration path (see Figure 6.6 in Aki and Richards) intersects these branch cuts, $F(p)$ is discontinuous hence not analytic. This apparent problem can be avoided if we relax the condition $\mathrm{Im}\sqrt{1/c_0^2 - p^2} \geq 0$ along the integration path. Instead we allow $\mathrm{Im}\sqrt{1/c_0^2 - p^2}$ to change sign at each branch cut intersection which, for the integration path, is equivalent to a transition to a different Riemann sheet. The integrand looses physical interpretation while on another Riemann sheet but gains analyticity. However, the two intersections with the branch cut insure two sign changes and the emergence of the integrand with the correct sign at the saddle point (eventually the integrand is going to be expanded in a Taylor series at that point and the rest of the path is going to be discarded). To calculate the location of the saddle point equate the derivative of f with zero; we find

$$p_s = \frac{x_g - x'}{c_0 d'}$$

with $d' = \sqrt{(z_g - z')^2 + (x_g - x')^2}$. Calculate

$$f(p_s) = i \frac{d'}{c_0}$$

$$f''(p_s) = -\frac{i c_0 d'^3}{|z_g - z'|^2}$$

$$F(p_s) = \frac{c_0 d'}{2i\,|z_g - z'|}$$

and plug them into the above formula (4) to obtain

$$G_0 \sim \frac{1}{2\pi i}\left(\frac{\pi c_0}{2\omega d'}\right)^{1/2} e^{ik_0 d'}. \tag{5}$$

This last expression shows that, in the high frequency approximation, the main contribution from each point scatterer comes along the line connecting the scatterer with the receiver. The coefficient accounts for the dismissed directions of propagation. In time domain the G_0 from equation (5) is

$$G_0 = \frac{1}{i}\sqrt{\frac{c_0}{2id'}}\frac{1}{\sqrt{t - \frac{d'}{c_0}}} H\left(t - \frac{d'}{c_0}\right). \tag{6}$$

With this approximation, the expression for P_1 becomes

$$P_1 = \frac{1}{2\pi i}\int_{z_1}^{\infty}\int_{-\infty}^{\infty} e^{ik_0 d'}\left(\frac{\pi c_0}{2\omega d'}\right)^{1/2} k_0^2 a_1 e^{i(kx' + \nu_0 z')} dx' dz' \tag{7}$$

or

$$P_1 = \frac{k_0^{3/2} a_1}{2\pi i}\sqrt{\frac{\pi}{2}}\int_{z_1}^{\infty} e^{i\nu_0 z'}\int_{-\infty}^{\infty}\frac{e^{i\omega\left(\frac{d'}{c_0} + \frac{k}{\omega}x'\right)}}{\sqrt{d'}} dx' dz'. \tag{8}$$

Again, the inner most integral has the form

$$I = \int_{-\infty}^{\infty} F(x') e^{\omega f(x')} dx'$$

with $F(x') = \frac{1}{\sqrt{d'}}$ and $f(x') = i\left(\frac{d'}{c} + \frac{k}{\omega}x'\right)$. Note that the integrand has no branch cuts this time since $d' = \sqrt{(z_g - z')^2 + (x_g - x')^2}$ is always positive; the saddle point is x'_s such that

$$x_g - x'_s = |z_g - z'|\,\frac{k'}{\nu_0}$$

and so we have

$$f(x'_s) = \left(\frac{\nu_0}{\omega}|z_g - z'| + \frac{k}{\omega}x_g\right),$$

$$f''(x'_s) = \frac{ic_0^2\nu_0^3}{\omega^3\,|z_g - z'|}$$

and

$$F(x_s') = \frac{1}{\sqrt{|z_g - z'|}} \sqrt{\frac{c_0 \nu_0}{\omega}}.$$

Using the same high frequency approximation (4) we find

$$\int_{-\infty}^{\infty} \frac{e^{i\omega\left(\frac{d'}{c} + \frac{k}{\omega}x'\right)}}{\sqrt{d'}} dx' \sim \frac{1}{\nu_0} \sqrt{\frac{2\pi\omega}{c_0}} e^{i(\nu_0 |z_g - z'| + k x_g)}. \tag{9}$$

Plugging this into the expression (8) for P_1 we obtain

$$P_1 = \frac{k_0^2 a_1}{2i\nu_0} e^{ikx_g} \int_{z_1}^{\infty} e^{i\nu_0 |z_g - z'|} e^{i\nu_0 z'} dz'$$

which is the same result as obtained before by switching the order of integration. The rest of the terms in the series for P can be similarly shown to resemble the expressions given by Matson (1997).

4 Physical interpretation of the approximations

The two high frequency approximations made in the previous derivation have an easy to understand physical interpretation. The approximation of the first integral represents the most important contribution coming to the receiver from each point scatterer (see Figure 1).

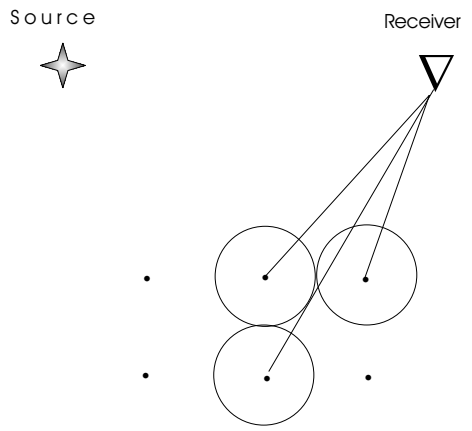

Figure 1: The physical interpretation of the approximation of G_0 - the inner most integral in the expression of P_1.

The result,

$$G_0 \sim \frac{1}{2\pi i}\left(\frac{\pi c_0}{2\omega d'}\right)^{1/2} e^{ik_0 d'},$$

represents the ray from the scatterer to the receiver multiplied by a coefficient which accounts for the dismissal of all the other directions of propagations.

The approximation of the second integral looks at the totality of the rays arriving at the receiver. Again the most important contribution is picked out to be the one coming from the rays that make an angle equal to the incident's plane wave angle with the vertical (see Figure 2); this can also be seen from the expression of the saddle point

$$x_g - x'_s = |z_g - z'|\,\frac{k'}{\nu_0}. \tag{10}$$

The last integral in the expression of P_1 is a one dimensional integral along the bold line

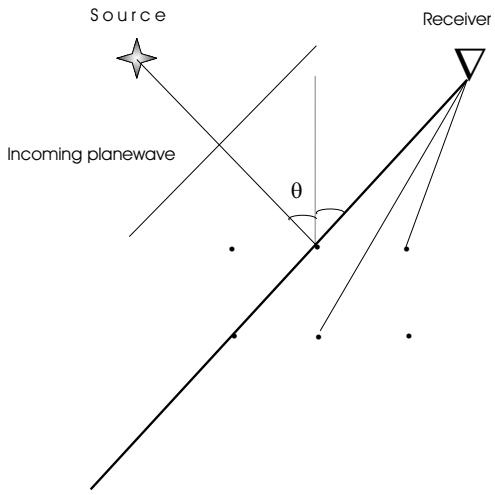

Figure 2: The physical interpretation of the approximation of the second integral in the calculation of P_1.

showed in Figure 2. Even though the parameter of integration is z', there is a certain relation between z' and x', given by (10), so that the direction of integration is tilted at angle equal to the incident angle and not vertical.

5 Convergence at the critical angle

The forward scattering series for the model discussed in this paper is (see Matson (1997))

$$P(x_g, z_g < z_1|k;\omega) = e^{ikx_g} e^{i\nu_0(2z_1 - z_g)} \left[\frac{1}{4}\frac{k_0^2 a_1}{\nu_0^2} + \frac{1}{8}\left(\frac{k_0^2 a_1}{\nu_0^2}\right)^2 + \frac{5}{64}\left(\frac{k_0^2 a_1}{\nu_0^2}\right)^3 + \frac{7}{128}\left(\frac{k_0^2 a_1}{\nu_0^2}\right)^4 + ... \right]. \tag{11}$$

The ratio test shows convergence for $\left|\frac{k_0^2 a_1}{\nu_0^2}\right| < 1$, divergence for $\left|\frac{k_0^2 a_1}{\nu_0^2}\right| > 1$ and it is inconclusive for $\left|\frac{k_0^2 a_1}{\nu_0^2}\right| = 1$. When $c_0 < c_1$ this last condition is equivalent to $\frac{k_0^2 a_1}{\nu_0^2} = 1$ which in turns is equivalent to $\theta = \theta_c$, i.e. the incident angle is the critical angle. In other words, the forward series is convergent for precritical incidence and divergent for postcritical incidence; no information is found about the critical incidence. For a critical incident planewave, the series becomes

$$P(x_g, z_g < z_1|k;\omega) = e^{ikx_g} e^{i\nu_0(2z_1 - z_g)} \left[\frac{1}{4} + \frac{1}{8} + \frac{5}{64} + \frac{7}{128} + ... \right]. \tag{12}$$

Rewrite

$$R = \frac{1}{4} + \frac{1}{8} + \frac{5}{64} + \frac{7}{128} + ... = \sum_{n=2}^{\infty} \frac{1}{n!} \frac{1 \cdot 3 \cdot 5 .... (2n-3)}{2^{n-1}} = \sum_{n=1}^{\infty} \frac{\Gamma(n+1/2)}{(n+1)!\Gamma(1/2)}.$$

Note that the series has the form $\sum_{n=2}^{\infty} a_n$ with $a_n = \frac{1}{n!}\frac{1 \cdot 3 \cdot 5 .... (2n-3)}{2^{n-1}}$ and so

$$\lim_{n\to\infty} n\left(\frac{a_n}{a_{n+1}} - 1\right) = \lim_{n\to\infty} n\left(\frac{2n+2}{2n-1} - 1\right) = \frac{3}{2} > 1$$

hence Raabe's Convergence Test shows convergence (for a full discussion of this convergence test see Bromwich (1965)). The conclusion is that the forward scattering series for this model converges at the critical angle as well. Note that the sum of the series, which corresponds to the reflection coefficient, is $R = 1$.

6 Postcritical divergence

For a $c_0 < c_1$ model, the forward series converges for precritical and critical incidence and diverges for postcritical incidence. From wave theory, the reflection coefficient R which should be constructed by the forward scattering series is:

- $R = \frac{\nu_0 - \nu_1}{\nu_0 + \nu_1} < 1$ for precritical incidence. In this case both ν_0 and ν_1 are real.
- $R = 1$ for critical incidence. In this case $\nu_1 = 0$.
- $R = \frac{\nu_0 - \nu_1}{\nu_0 + \nu_1}$ for postcritical incidence. In this case ν_1 is purely imaginary and hence R is complex. However $|R| = 1$ and the complexity of R is attributed to a phase-shift of the emerging wave after hitting the interface due to the evanescent waves created in the second medium.

The term $\frac{a_1 k_0^2}{\nu_0^2} = 1 - \frac{\nu_1^2}{\nu_0^2}$ is grater than one exactly when ν_1 becomes imaginary. In fact if for this case one writes $R = e^{i\epsilon}$, where ϵ is the phase-shift of the wavefield, then $\frac{a_1 k_0^2}{\nu_0^2} = 1 + \tan^2 \frac{\epsilon}{2}$ enforcing the earlier statement that the divergence is due to the phase-shift of the reflected wave. In other words, it is the impossibility of constructing a complex number ν_1 as a series of real numbers (powers of ν_0) which leads to the divergence of the series. The graph of ν_1 as a function of $\frac{a_1 k_0^2}{\nu_0^2}$ is shown in Figure 3. For $c_0 < c_1$ we have that $a_1 > 0$ so we are looking at

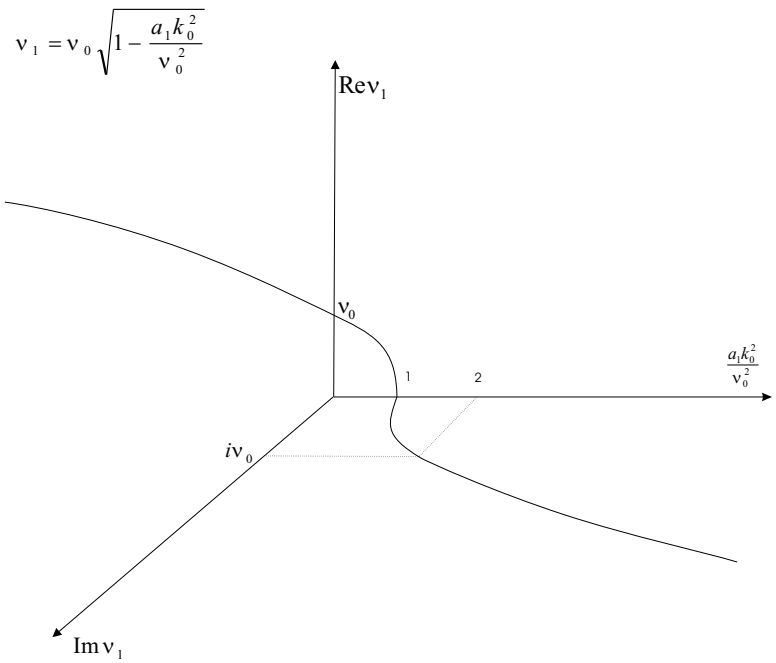

Figure 3: The graph of ν_1 as a function of $\frac{a_1 k_0^2}{\nu_0^2}$.

the positive x-axis of the graph; if the velocity model is fixed, $a_1 k_0^2$ is a constant. The vertical wavenumber of the propagating wave in the actual medium, ν_1, is equal to ν_0 when $\frac{a_1 k_0^2}{\nu_0^2} = 0$, i.e. at normal incidence. When $\frac{a_1 k_0^2}{\nu_0^2} = 1$ (at critical incidence), ν_1 is zero showing that there is no propagation into the second medium. When $\frac{a_1 k_0^2}{\nu_0^2} > 1$ (post-critical incidence), ν_1 is

complex and it becomes unrecoverable by a Taylor series written at $\frac{a_1 k_0^2}{\nu_0^2} = 0$; the series is now divergent. For $c_0 > c_1$ it seems like this problem does not exist. In this case there is no critical angle and so the vertical wavenumber ν_1 never becomes complex. However the series inherits the divergent behavior for $\frac{a_1 k_0^2}{\nu_0^2} < -1$ due to the singularity at $\frac{a_1 k_0^2}{\nu_0^2} = 1$. For any value of $\frac{a_1 k_0^2}{\nu_0^2}$ outside the unit sphere centered at the origin the series will diverge due to that same singularity.

References

Aki, K. and Richards, P. G. (1980). Quantitative seismology, theory and methods. W. H. Freeman, New York.

Bromwich, T. J. I'A. (1965). An Introduction to the theory of infinite series. Macmillian & Co. Ltd., London.

Matson, K. H. (1996). The relationship between scattering theory and the primaries and multiples of reflection seismic data. J. Seis. Expl. 5, p 63-78.

Matson, K. H. (1997). An inverse scattering series method for attenuating elastic multiples from multicomponent land and ocean bottom seismic data. Ph.D. Thesis, University of British Columbia, Canada.

Isolation of a leading order depth imaging series and analysis of its convergence properties

Simon A. Shaw*†, Arthur B. Weglein†, Douglas J. Foster§, Kenneth H. Matson* and Robert G. Keys‡
*BP, †University of Houston, §ConocoPhillips, ‡ExxonMobil

Abstract

The objective of seismic depth imaging is to produce a spatially accurate map of the reflectivity below the Earth's surface. Current methods for depth imaging require an accurate velocity model in order to place reflectors at their correct locations. Existing techniques to derive the velocity model can fail to provide this information with the necessary degree of accuracy, especially in areas that are geologically complex.

Recently, Weglein et al. (2000) have proposed using the inverse scattering series, a direct non-linear inverse procedure, to perform the task of imaging reflectors at depth without needing to specify the exact velocity. The primary objective of the research described here is to derive and develop a practical inverse series algorithm to perform the task of imaging without accurate velocity information. The strategy employed is to isolate a subseries of the inverse series with the purpose of imaging reflectors in space (Weglein et al., 2002).

In this paper, a leading order imaging subseries is isolated and its convergence properties are analyzed. It is shown analytically that this imaging subseries converges for any finite contrast between the actual and reference medium, and for band-limited data with a finite maximum frequency. The rate of convergence is greater for small contrasts and smaller maximum frequencies.

1 Introduction

At its core, seismic data processing is an inverse method; the data are inverted for the Earth's subsurface properties. These properties include the spatial location of reflectors and the contrasts in density and elastic properties at these reflectors. In practice, the processing of seismic data is carried out in a sequence of steps, e.g., random noise attenuation, source wavelet deconvolution, removal of free surface multiples, removal of internal multiples, imaging (also called migration), and inversion for changes in Earth properties. The order in which these steps are carried out can be important because most algorithms assume that the data have been preconditioned by the preceding processes. The research described here concerns

the single step of imaging primaries. Primaries are events in the measured wavefield that have experienced a single upward reflection in the subsurface and are distinguished from multiples which have experienced more than one upward reflection. Imaging may be thought of as a process that transforms the recorded primary seismic wavefield into a spatially accurate picture of the Earth's subsurface reflectivity.

The research described here represents progress in a long-term project to develop multi-dimensional algorithms that have a greater ability to achieve the goals of seismic processing while lowering the demands on (often inaccessible) a-priori information about the subsurface. As with earlier analysis of algorithms for multiple attenuation, the evaluation of new concepts and theory progresses from simple, analytic examples to complex, numerical models and ultimately to field data. To avoid numerical, stability or discreteness issues, testing is first conducted with analytic data for one-dimensional examples. This ensures that the results are attributed to the inverse procedure only.

The following section explains the motivation for addressing the problem of imaging when the exact velocity model is unknown. Then, in the next section, the inverse scattering series is derived and the strategy for isolating subseries of the inverse series that perform seismic processing tasks is described. In the remaining sections, a leading order imaging subseries is derived and its convergence properties are studied analytically and numerically.

2 Motivation for an accurate imaging algorithm when the velocity is unknown

Reflectors exist where there are sharp contrasts in Earth material properties that are usually attributed to boundaries between different types of rocks and fluids. Oil and gas are often trapped below the surface by impermeable rocks. Seismic imaging produces a map of subsurface reflectors. The accuracy of this reflector map has a direct impact on our ability to predict the location, volume and even type of hydrocarbons trapped below the surface. Hence seismic imaging plays a key role in exploration and production of natural resources.

Current methods for imaging can be derived using Green's Theorem and the wave equation to predict the wavefield inside the Earth from measurements on its surface (e.g., Schneider 1978; Stolt 1978; Berkhout and Palthe 1981; Wapenaar et al. 1989). For example, for a constant density acoustic medium, if P is the wavefield due to the seismic source, and G is

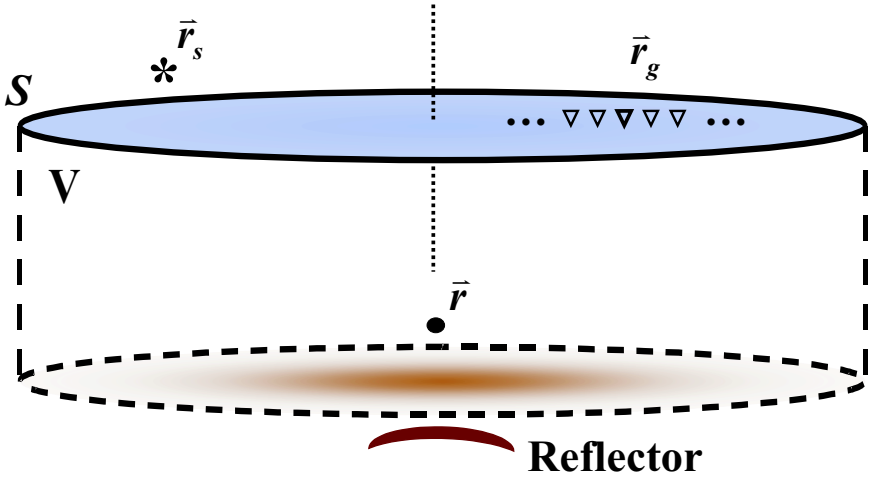

Figure 1: Current imaging algorithms may be derived using Green's Theorem and the wave equation to predict the wavefield in the Earth from measurements on its surface. Knowledge of the Earth's properties inside the volume V is required.

the Green's function that satisfies

$$\left(\nabla^2 + \frac{\omega^2}{c^2(\vec{r})}\right) G(\vec{r}|\vec{r}\,';\omega) = \delta(\vec{r} - \vec{r}\,'), \tag{1}$$

where c is the velocity inside the volume V defined in Figure 1, then the wavefield prediction formula can be shown to be

$$P(\vec{r}|\vec{r}_s;\omega) = \oint_{\vec{r}\,'\in S} \left(P(\vec{r}\,'|\vec{r}_s;\omega)\nabla G(\vec{r}|\vec{r}\,';\omega) - G(\vec{r}|\vec{r}\,';\omega)\nabla P(\vec{r}\,'|\vec{r}_s;\omega)\right)\cdot\hat{n}dS \tag{2}$$

where $\vec{r}$ is the location at which the wavefield is predicted and $\vec{r}_s$ is the source location. The need for the measurement of ∇P is avoided by making G satisfy Dirichlet boundary conditions on the measurement surface. The requirement of current imaging algorithms for the velocity comes from the need to compute the Green's function G inside the volume V.

The wavefield predicted in the Earth is transformed into a map of reflectivity using an imaging condition. Usually, the imaging condition asks for the seismic amplitude recorded in the limit of a small recording time for a hypothetical experiment where a source and receiver are coincident in the Earth (e.g., Claerbout 1971). If a reflector exists immediately below the source and receiver in the Earth, then the imaging condition will output a measure of the reflector's strength.

As mentioned, traditional methods for imaging require the precise velocity model in order to compute the Green's function that back-propagates the measured wavefield into the Earth.

Without the true propagation velocity, the wavefield in the Earth will not be correctly predicted, and the imaging condition will fail to locate the reflectors. It is for this reason that the quality of the results from current methods for depth imaging are critically dependent on the accuracy of the velocity model.

Velocity information itself can be derived from seismic reflection data by picking reflection travel times (Taner and Koehler, 1969) or using reflection tomography (e.g., Stork and Clayton 1991). In practice, the seismic interval velocities can be in error by 5-10% (Gray et al., 2001) depending on data quality, geologic complexity, and the sophistication and robustness of the algorithm being used to derive them.

The failure of current methods to produce accurate depth images below complex overburdens, such as below salt, basalt, and karsted or gas-saturated sediments, is the motivation for the research proposed here. Under these geologic conditions, current velocity estimation procedures fail to yield the velocity model with the necessary degree of accuracy to place reflectors at their correct locations. The objective of this research is to develop a new method to accurately image seismic data that is less dependent on our ability to describe the precise velocity model.

3 Scattering theory and seismic data processing

The research described here applies inverse scattering theory to the seismic inverse problem. In scattering theory, the difference in the behavior of an incident wave in two media (referred to as the *reference* medium and the *actual* medium) is described in terms of the difference between the physical properties of these two media.

The wave equations for the actual and reference wavefields are expressed by

$$L\psi = A(\omega)\delta(\vec{r}_g - \vec{r}_s) \tag{3}$$

$$L_0\psi_0 = A(\omega)\delta(\vec{r}_g - \vec{r}_s) \tag{4}$$

where L and L_0 are the differential operators that describe wave propagation in the actual and reference media, respectively, and $A(\omega)$ is the source wavelet. The variables $\vec{r}_g$ and $\vec{r}_s$ are the receiver and source position vectors, respectively. The Green's functions for the actual medium, G, and the reference medium, G_0, satisfy

$$LG = \delta(\vec{r}_g - \vec{r}_s) \tag{5}$$

$$L_0G_0 = \delta(\vec{r}_g - \vec{r}_s) \tag{6}$$

and so $\psi = A(\omega)G$ and $\psi_0 = A(\omega)G_0$. The scattering potential and the scattered wavefield are defined by

$$V \equiv L_0 - L \tag{7}$$

$$\psi_s \equiv \psi - \psi_0, \tag{8}$$

respectively. The equation that relates the actual and reference wavefields to the scattering potential is the Lippmann-Schwinger equation

$$\psi(\vec{r}_g\,|\vec{r}_s\,;\omega) = \psi_0(\vec{r}_g\,|\vec{r}_s\,;\omega) + \int_{-\infty}^{\infty} G_0(\vec{r}_g\,|\vec{r}'\,;\omega)V(\vec{r}'\,;\omega)\psi(\vec{r}'\,|\vec{r}_s\,;\omega)d\vec{r}'\,. \tag{9}$$

This equation can be successively iterated for ψ on the right-hand side resulting in the forward, or Born, series for the actual wavefield ψ

$$\psi = \psi_0 + \psi_1 + \psi_2 + \ldots \tag{10}$$

where

$$\psi_1(\vec{r}_g\,|\vec{r}_s\,;\omega) = \int_{-\infty}^{\infty} G_0(\vec{r}_g\,|\vec{r}'\,;\omega)V(\vec{r}'\,;\omega)\psi_0(\vec{r}'\,|\vec{r}_s\,;\omega)d\vec{r}' \tag{10a}$$

$$\psi_2(\vec{r}_g\,|\vec{r}_s\,;\omega) = \int_{-\infty}^{\infty} G_0(\vec{r}_g\,|\vec{r}'\,;\omega)V(\vec{r}'\,;\omega) \times \int_{-\infty}^{\infty} G_0(\vec{r}'\,|\vec{r}''\,;\omega)V(\vec{r}''\,;\omega)\psi_0(\vec{r}''\,|\vec{r}_s\,;\omega)d\vec{r}'\,d\vec{r}'' \tag{10b}$$

$$\vdots$$

The forward series is a solution for ψ in terms of G_0, ψ_0 and V. The wavefield that propagates in the *actual* medium is described in terms of an infinite series of propagations in a chosen *reference* medium and interactions with the potential V. Conversely, the inverse series is a solution for V in terms of the scattered field on the measurement surface $(\psi - \psi_0)_m = (\psi_s)_m$ and G_0. The inverse series can be derived by first writing V as the sum of constituent components (Moses, 1956)

$$V = V_1 + V_2 + V_3 + \ldots = \sum_{n=1}^{\infty} V_n \tag{11}$$

where V_n is the portion of V that is n^{th} order in the measured values of the scattered field, $(\psi_s)_m$. Substitution of equation (11) into the forward series (equation 10) and matching

terms that are equal order in $(\psi_s)_m$ yields the inverse series:

$$(G_0 V_1 \psi_0)_m = (\psi_s)_m \tag{11a}$$

$$(G_0 V_2 \psi_0)_m = -(G_0 V_1 G_0 V_1 \psi_0)_m \tag{11b}$$

$$(G_0 V_3 \psi_0)_m = -(G_0 V_1 G_0 V_1 G_0 V_1 \psi_0)_m - (G_0 V_2 G_0 V_1 \psi_0)_m - (G_0 V_1 G_0 V_2 \psi_0)_m \tag{11c}$$

$$\vdots$$

See, for example, Weglein et al. (1981) for references to the development of the inverse series. To calculate only the first term in the inverse series (i.e., solving equation 11a) and to treat $V_1 \approx V$ is to make the inverse Born approximation. However, the inverse series does not make that assumption. V_1 is assumed to be the first order approximation to V and equation (11a) is the exact equation for that quantity. The inverse Born approximation forms the basis of all current techniques employed to perform seismic inversion (Clayton and Stolt, 1981), i.e., normal moveout (NMO) stack, amplitude variation with offset (AVO) analysis, migration (imaging) and migration-inversion (Stolt and Weglein, 1985). Linear approximate inverse methods are also the basis of medical imaging and other non-destructive evaluation methods. For the seismic problem, the inverse Born is a reasonable approximation for precritical primary reflections, for small contrasts in material properties, and for a reference medium that is close to the actual medium. Second and higher terms in the inverse series can be viewed as correcting V_1 towards V when the series convergences. The tasks of removing multiples, imaging primaries at their correct depth, and inverting for large changes in Earth properties reside in the second and higher order terms in the inverse series.

The inverse scattering series (equation 11) is a multi-dimensional direct inversion procedure. The scattering medium's properties are directly determined from the recorded data without iterative updating of the reference medium towards the actual medium. Alternative approaches, e.g., iterative linear inversion, involve updating the reference model so that the reference wavefield, in some sense, fits the observed data (Tarantola, 1987). The inverse series is a distinct and separate method from iterative linear inversion. Equation (11) solves for $V_1, V_2 \ldots$ and hence for $V = V_1 + V_2 + \ldots$ directly in terms of $(\psi_s)_m$ and G_0.

Empirical tests of the *entire* inverse series for a simple acoustic model suggested that it does not converge for contrasts between actual and reference medium properties greater than about 11 % (Carvalho, 1992). Based on these tests, it was believed that the radius of convergence is too small to be of direct practical use when no a-priori information is supplied. Rather than abandon the inverse series, research has been undertaken to isolate convergent subseries that perform individual tasks associated with inversion. Inversion of seismic data can be viewed as performing a sequence of four tasks:

1. Removal of free-surface multiples;
2. Removal of internal multiples;
3. Positioning reflectors at their correct spacial locations (imaging); and
4. Inverting reflectivity for changes in Earth parameters (target identification).

The inverse series accomplishes these tasks using only measured data and reference medium properties. Isolating specific subseries that perform these tasks is less ambitious than directly inverting for Earth properties in one step and so convergence properties may be more favorable. Also, by carrying out these tasks in sequence, tasks 2–4 benefit from the fact that previous tasks have already been performed which constitutes valuable *a priori* information. At each step, the simplest possible reference medium is chosen that allows rapid convergence of the specific subseries.

This strategy of task separation first produced a multi-dimensional free surface multiple removal algorithm. Free surface multiples are events that have reflected in the subsurface, traveled back up, hit the free surface at least once, and traveled back into the Earth. These events usually have large amplitudes and can obscure reflection events that have traveled further into the Earth but arrive at the same time as the multiples. The presence of multiples often precludes accurate estimation of reference medium properties. The second task-specific subseries to be isolated was the one that predicts and attenuates internal multiple reflections. Internal multiples are events that have all their downgoing reflections below the free surface.

The multiple removal algorithms derived using the inverse series (Weglein et al., 1997) have the unique property that they expect the recorded seismic data and the source wavelet as input, but do not require the propagation velocity or any other subsurface information. For marine seismic data, both the free surface and internal multiple subseries converge for a homogeneous acoustic reference medium – water – which makes the algorithms computationally efficient. More importantly, they predict and attenuate multiples generated by actual Earth model types that are much more complicated than the homogeneous acoustic reference medium and include elastic, heterogeneous, anisotropic and certain forms of anelastic media.

An important prerequisite of these inverse scattering algorithms is knowledge of the source wavelet. Methods for estimating the wavelet include direct near-field measurements (Ziolkowski, 1991) or an estimation from the recorded data (Weglein and Secrest, 1990; Osen et al., 1998; Tan, 1999).

The strategy employed in this research is to first remove the multiples with their task-specific subseries, and then to use the demultipled data with its source wavelet deconvolved, as input to the subseries that act on primaries. This represents a staged approach where tasks are carried out in an order that progresses from relatively easy to more challenging and that uses the successful completion of earlier tasks to improve the chances of subsequent tasks being successful.

Recently, Weglein et al. (2000) have proposed using the inverse scattering series to perform the third and fourth tasks of imaging reflectors in depth and inverting for Earth parameters, both in terms of reference medium information. The concepts surrounding the task of imaging using the inverse series have been set out by Weglein et al. (2002). The next section summarizes how the inverse series performs imaging illustrated using 1-D analytic and numerical examples.

4 Imaging using the inverse series

4.1 1-D inverse series and task separation

Wave propagation in a 1-D constant density variable velocity acoustic medium is described by the equation

$$\left(\frac{d^2}{dz^2} + k^2(z)\right)\psi(z;\omega) = 0 \tag{12}$$

where $k(z) = \omega/c(z)$, ω is the angular frequency, $c(z)$ is the velocity, and z is the field point of the wavefield. Assume that the region that equation (12) describes does not contain the source. If the reference medium is chosen to be an acoustic wholespace with velocity c_0, then the perturbation has the form

$$\begin{aligned} V &= L_0 - L \\ &= k_0^2 - k^2 \\ &= k_0^2\alpha \end{aligned} \tag{13}$$

where $\alpha(z) = 1 - c_0^2/c^2(z)$ and $k_0 = \omega/c_0$. In this context, the inverse problem is to solve for α where

$$\alpha = \alpha_1 + \alpha_2 + \alpha_3 + \ldots = \sum_{n=1}^{\infty} \alpha_n \tag{14}$$

The first term in the inverse series (equation 11a) is then

$$\psi_s(z_m;\omega) = \int_{-\infty}^{\infty} \frac{e^{ik_0|z_m - z'|}}{2ik_0} k_0^2 \alpha_1(z')\psi_0(z';k_0)dz' \tag{15}$$

where z_m is the measurement depth and the reference wavefield is $\psi_0 = e^{ik_0(z'-z_m)}$. Solving for α_1 (see appendix 6) yields

$$\alpha_1(z) = 4\int_0^z \psi_s(z_m;z')dz' \tag{16a}$$

where $z' = c_0 t/2$ and t is the travel time. Time zero ($t = 0$) corresponds to when the downgoing incident wave passes z_m. Equation (16a), which in this 1-D case amounts to trace integration, is a conventional migration-inversion. The second term in the inverse series (Equation 11b) can be broken up in to two terms (see appendix 6):

$$\alpha_2(z) = -\frac{1}{2}\left(\alpha_1^2(z) + \left[\frac{d\alpha_1(z)}{dz}\right]\int_0^z \alpha_1(z')dz'\right). \tag{16b}$$

These two terms in α_2 correspond to "self-interaction" (α_1^2) and "separated" ($\alpha_1' \int \alpha_1$) scattering diagrams represented in Fig. 2. All higher order inverse series terms can be broken up in a similar manner. As has been reported by Weglein et al. (2002), separated diagram terms with a single upward scattering point contribute to a subseries that images reflectors at their correct spatial location, and self-interaction terms form the subseries that corrects the amplitude of α_1 towards α. The third term in the inverse series (Equation 11c) is broken up as follows (see appendix 6):

$$\begin{aligned}
\alpha_3(z) =& \frac{3}{16}\alpha_1^3(z) + \frac{1}{8}\left[\frac{d^2}{dz^2}\alpha_1(z)\right]\left(\int_0^z \alpha_1(z')dz'\right)^2 \\
&- \frac{1}{8}\left[\frac{d}{dz}\alpha_1(z)\right]\int_0^z \alpha_1^2(z')dz' \\
&+ \frac{3}{4}\left[\frac{d}{dz}\alpha_1(z)\right]\alpha_1(z)\int_0^z \alpha_1(z')dz' \\
&- \frac{1}{16}\int_0^z\int_0^z \left[\frac{d}{dz'}\alpha_1(z')\right]\left[\frac{d}{dz''}\alpha_1(z'')\right]\alpha_1(z''+z'-z)dz''dz'
\end{aligned} \tag{16c}$$

Consider that the inverse series can be separated into subseries so that

$$\begin{aligned}
\alpha &= \alpha_1 + \alpha_2 + \alpha_3 + \ldots \\
&= \alpha_1 + \left(\alpha^{IS} - \alpha_1\right) + \left(\alpha^{AO} - \alpha_1\right) + \left(\alpha^{IM} - \alpha_1\right) + \ldots
\end{aligned} \tag{17}$$

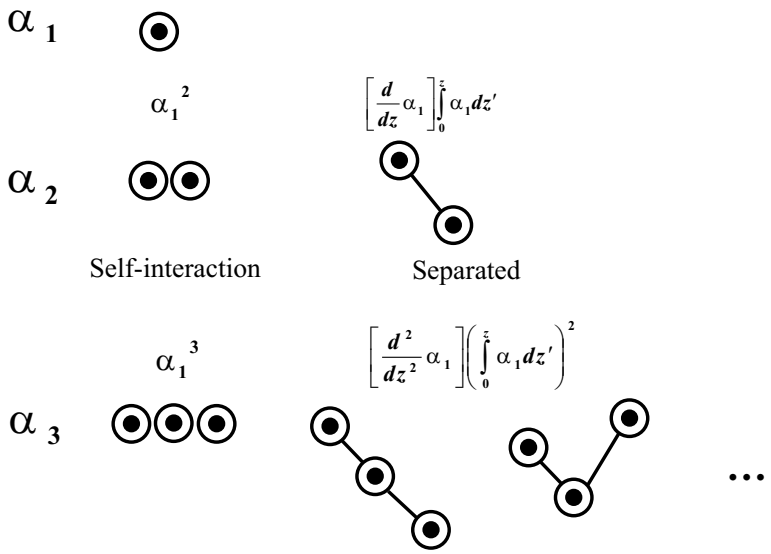

Figure 2: The terms in the inverse series can be interpreted using scattering diagrams. The circles represent α_1 and the line represents a propagation in the reference medium. Self-interaction occurs when two or more scattering points are at the same location. Separated diagrams refer to scattering between points that are at different locations. Diagrams shown here perform inverse tasks on primary events.

where

$$\begin{aligned}
\alpha^{IS} &= \text{Imaging subseries} \\
\alpha^{AO} &= \text{Subseries that inverts amplitudes only} \\
\alpha^{IM} &= \text{Subseries that removes internal multiples} \\
&\quad \text{(Note that each of the subseries in} \\
&\quad \text{equation (17) have been written to include } \alpha_1.)
\end{aligned}$$

The residual "$+\ldots$" in equation (17) includes terms that correct the amplitude between where α_1 places reflectors, and where α^{IS} locates them. Coupled tasks such as these will be the subject of future reports.

The removal of internal multiples begins in the third term in the inverse series (Weglein et al., 1997) and, in this context, is written

$$\begin{aligned}
\alpha^{IM}(z) &= \alpha_1(z) \\
&\quad - \frac{1}{16}\int_0^z \int_0^z \left[\frac{d}{dz'}\alpha_1(z')\right]\left[\frac{d}{dz''}\alpha_1(z'')\right]\alpha_1(z''+z'-z)dz''dz' + \ldots
\end{aligned} \tag{18}$$

The self-interaction terms that correct amplitude only, and not location, can be grouped and written

$$\alpha^{AO}(z) = \alpha_1(z) - \frac{1}{2}\alpha_1^2(z) + \frac{3}{16}\alpha_1^3(z) - \dots \tag{19}$$

The imaging subseries terms do not alter the amplitude of α_1 but act to correctly locate the interfaces that are mislocated in α_1. The imaging subseries can be considered in two parts: leading order (LO) and higher order (HO) contributions. Leading order terms are those that correspond to purely separated scattering diagrams with a single upward scattering point, whereas the higher order imaging terms consist of separated diagrams that also have self-interaction components (see Fig. 3) above the deepest scattering point.

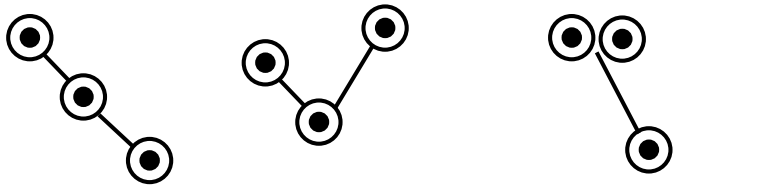

Figure 3: Examples of leading order and higher order imaging terms from the third term in the inverse series.

$$\alpha^{IS}(z) = \alpha^{IS_{LO}}(z) + \alpha^{IS_{HO}}(z) \tag{20}$$

More will be said about the leading and higher order contributions in the next section with an analytic example. The leading order contributions to the imaging subseries are

$$\begin{aligned}\alpha^{IS_{LO}}(z) =& \alpha_1(z) - \frac{1}{2}\left[\frac{d\alpha_1(z)}{dz}\right]\left(\int_0^z \alpha_1(z')dz'\right) \\ &+ \frac{1}{8}\left[\frac{d^2\alpha_1(z)}{dz^2}\right]\left(\int_0^z \alpha_1(z')dz'\right)^2 + \dots \\ =& \sum_{n=0}^{\infty}\left(\frac{(-1/2)^n}{n!}\right)\left[\frac{d^n\alpha_1(z)}{dz^n}\right]\left(\int_0^z \alpha_1(z')dz'\right)^n\end{aligned} \tag{21}$$

Equation (21) is the leading order imaging subseries and was originally derived through an analysis of the first three terms in the inverse series, and the recognition of a general form that predicts the expected fourth and higher order series coefficients in the case of a simple analytic example (given in the next section). This analysis is typical of the kind used to derive inverse series algorithms in the past. The forward series gives us clues as to which terms

in the inverse series perform a particular task. Then we isolate those terms of the inverse series and study their behavior for simple analytic examples deliberately chosen so that the inverse task is clear. For the task of imaging, a logical example to study a two-interface model where we only know the velocity to the first interface. The first term in the inverse series will properly locate the shallower interface and mislocate the deeper one. If the series converges, then the higher order terms will neccesarily act to correct the depth of the deeper interface. It was this type of analysis that yielded the leading order imaging algorithm, which was subsequently tested on more complicated analytic and numerical examples with good results.

In the next two sections, analytic and numerical examples are used to illustrate how this algorithm works. Notice that equation (21) can be simplified as follows

$$\begin{aligned}\alpha^{IS_{LO}}(z) =& \sum_{n=0}^{\infty}\left(\frac{(-1/2)^n}{n!}\right)\left[\frac{1}{2\pi}\int_{-\infty}^{\infty}(ik_0)^n\tilde{\alpha}_1(k_0)e^{ik_0z}dk_0\right]\left(\int_0^z\alpha_1(z')dz'\right)^n \\ =&\frac{1}{2\pi}\int_{-\infty}^{\infty}\sum_{n=0}^{\infty}\frac{1}{n!}\left(-ik_0\frac{1}{2}\int_0^z\alpha_1(z')dz'\right)^n\tilde{\alpha}_1(k_0)e^{ik_0z}dk_0.\end{aligned}$$

Recognizing that

$$\sum_{n=0}^{\infty}\frac{1}{n!}\left(-ik_0\frac{1}{2}\int_0^z\alpha_1(z')dz'\right)^n = \exp\left(-ik_0\frac{1}{2}\int_0^z\alpha_1(z')dz'\right) \tag{22}$$

for any finite k_0 and $\int_0^z\alpha_1 dz'$, then we can write a closed form of the leading order imaging subseries

$$\alpha^{IS_{LO}}(z) = \frac{1}{2\pi}\int_{-\infty}^{\infty}\tilde{\alpha}_1(k_0)e^{ik_0\left(z-\frac{1}{2}\int_0^z\alpha_1(z')dz'\right)}dk_0 \tag{23}$$

$$= \alpha_1\left(z-\frac{1}{2}\int_0^z\alpha_1(z')dz'\right) \tag{24}$$

Equation (23) has the form of a phase-shift migration, where the shift is equal to $\frac{1}{2}\int_0^z\alpha_1(z')dz'$. In the absence of the actual velocity function, this algorithm extracts the neccesary information from the amplitudes and depth information in α_1 through an integral. The closed form expression will be used to discuss the convergence properties after the analytic and numerical examples.

4.2 Analytic example

In this section, the ability of the inverse series to perform the task of imaging without needing to specify the velocity is illustrated using a simple 1-D acoustic example. Consider

the experiment illustrated in Figure 4 with a source and receiver at the surface $z_m = 0$. The reference velocity is chosen to be constant c_0, whereas the actual Earth velocity is an unknown function $c(z)$.

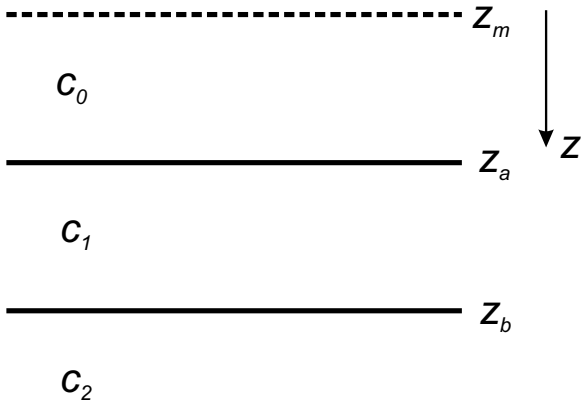

Figure 4: A single layer with velocity c_1 between two homogeneous half-spaces with velocity c_0 and c_2. The depth of the first interface is z_a and the depth of the second interface is z_b.

In accordance with the strategy, all multiples (i.e., free-surface and internal multiples) have been removed from the input data. Hence, for this example, the data consist of two primary reflections that arrive at times t_1 and t_2

$$D(t) = R_1\delta(t - t_1) + \hat{R}_2\delta(t - t_2). \tag{25}$$

R_1 is the reflection coefficient for a downgoing wave at the first interface and $\hat{R}_2 = T_{01}R_2T_{10}$ where R_2 is the downgoing reflection coefficient at the second interface and T_{01} and T_{10} are the transmission coefficients for a wave propagating down and up, respectively through the first interface. The equations for the reflection and transmission coefficients are

$$R_1 = \frac{c_1 - c_0}{c_1 + c_0} \tag{26}$$

$$T_{01} = 1 - R_1 \tag{27}$$

$$T_{10} = 1 + R_1 \tag{28}$$

$$\text{and } R_2 = \frac{c_2 - c_1}{c_2 + c_1}. \tag{29}$$

The data D differ from the scattered field ψ_s in equation (16a) in that multiples having been removed from D. Substitution of equation (25) into equation (16a) yields a primaries-only α_1:

$$\alpha_{1_p}(z) = 4R_1H(z - z_a) + 4\hat{R}_2H(z - z_{b'}) \tag{30}$$

where $z_{b'}$ is the pseudo depth at which the event with travel time t_2 images with velocity c_0. This pseudo depth can be written

$$z_{b'} = z_a + \gamma(z_b - z_a) \tag{31}$$

where $\gamma = c_0/c_1$. Figure 5 illustrates α_1 for the case where $c_0 < c_1$. The second reflector is imaged at a depth that is too shallow because the reference velocity is less than the actual velocity in the layer. Furthermore, the amplitude of α_1 is different from that of α. These differences between α_1 and α are corrected by the higher order terms in the inverse series.

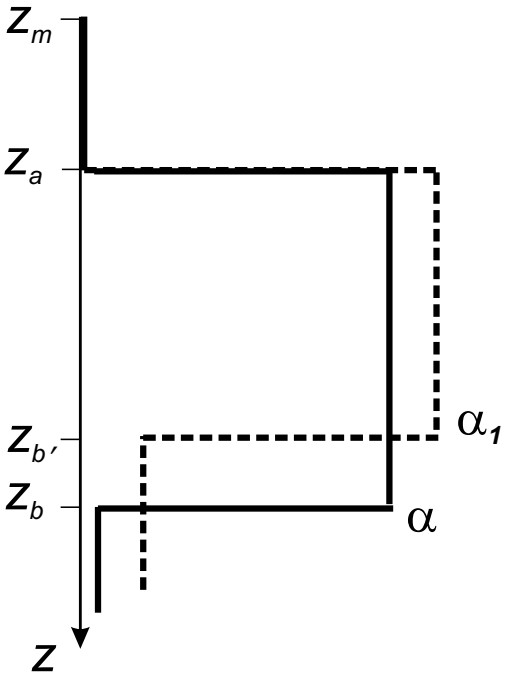

Figure 5: Given the reference velocity c_0, the first term in the inverse series, α_1, places the second interface at the incorrect depth $z_{b'}$ rather than the actual depth z_b. For the case where $c_0 < c_1$, $z_{b'}$ will be shallower than z_b. The task of imaging is the process of moving the interface from $z_{b'}$ to z_b whereas the last remaining task in the inversion for α must correct the amplitude of α_1. Both of these tasks reside in the higher order terms of the inverse series.

Evaluating the second and higher order terms in the leading order imaging subseries (equa-

tion 21) leads to

$$\alpha_{2_p}^{IS_{LO}}(z) = -2R_1(z-z_a)4\hat{R}_2\delta(z-z_{b'}) \tag{32}$$
$$\alpha_{3_p}^{IS_{LO}}(z) = 2R_1^2(z-z_a)^2 4\hat{R}_2\delta'(z-z_{b'}) \tag{33}$$
$$\alpha_{4_p}^{IS_{LO}}(z) = -\frac{4}{3}R_1^3(z-z_a)^3 4\hat{R}_2\delta''(z-z_{b'}) \tag{34}$$
$$\vdots$$

In this example, the task of imaging is to shift the deeper interface from $z_{b'}$ to z_b. The imaging subseries accomplishes this shift through a Taylor series for the difference of two Heaviside functions expanded about the mislocated interface. This shift is a scaled box $B(z)$ where

$$\begin{aligned} B(z) =& H(z-z_{b'}) - H(z-z_b) \\ =& (z_b - z_{b'})\delta(z-z_{b'}) - \frac{(z_b-z_{b'})^2}{2!}\delta'(z-z_{b'}) + \frac{(z_b-z_{b'})^3}{3!}\delta''(z-z_{b'}) - \dots \end{aligned} \tag{35}$$

The δ functions and their derivatives relate to those in equations (32)–(34). The coefficients of the Taylor series contain the correct depth to the interface, z_b. In the inverse series, these coefficients are constructed order by order in the data D, and are a function of the amplitudes and travel times (or pseudo depths) down to the reflector being imaged. Combining equations (26) and (31) provides the coefficients

$$(z_b - z_{b'}) = -2(z_{b'}-z_a)\left(R_1 + R_1^2 + R_1^3 + \dots\right) \tag{36}$$
$$\frac{(z_b-z_{b'})^2}{2!} = 2(z_{b'}-z_a)^2\left(R_1^2 + 2R_1^3 + 3R_1^3 + \dots\right) \tag{37}$$
$$\frac{(z_b-z_{b'})^3}{3!} = -\frac{4}{3}(z_{b'}-z_a)^3\left(R_1^3 + 3R_1^4 + 6R_1^5 + \dots\right) \tag{38}$$
$$\vdots$$

The contributions to these coefficients that are *leading order* in the data are

$$(z_b - z_{b'})^{LO} = -2(z_{b'}-z_a)R_1 \tag{39}$$
$$\left(\frac{(z_b-z_{b'})^2}{2!}\right)^{LO} = 2(z_{b'}-z_a)^2 R_1^2 \tag{40}$$
$$\left(\frac{(z_b-z_{b'})^3}{3!}\right)^{LO} = -\frac{4}{3}(z_{b'}-z_a)^3 R_1^3 \tag{41}$$
$$\vdots$$

These coefficients correspond to those predicted by the leading order imaging subseries terms in equations (32)–(34). The higher order imaging subseries terms predict the remaining coefficients in equations (36)–(38). For $|R_1| << 1$ the leading order contributions will be more significant than the higher order ones. Careful analysis of the relative significance of these terms will be the subject of future work.

In the next subsection, numerical examples illustrate how the imaging subseries terms act to shift the reflectors towards the correct depth for band-limited synthetic input data.

4.3 Numerical Examples

Consider the 1-D model depicted in Fig. 4 with the following parameters: c_0 =2000 m/s, c_1 =2200 m/s, c_2 =2020 m/s, z_a =100 m and z_b=140m. Choosing a reference velocity c_0 =2000 m/s, and simulating data for a $0-125$ Hz band-limited source, then the computed α_1 is shown as the dashed red line in Fig. 6.

The depth that the reference velocity images the second reflector at is $z_{b'}$=136m. The band-limited singular functions of the imaging subseries act to extend the interface from $z_{b'}$ to z_b. The cumulative sum of these imaging subseries terms is illustrated in Fig. 7. After summing five terms, the imaging subseries has converged and the deeper reflector has moved towards its correct depth z_b.

Figure 8 illustrates the result of the closed form of the leading order imaging subseries for a four-layer example. For this example, the leading order contributions to the imaging series are seen to shift the interfaces (in α_1) most of the distance towards their actual depths.

5 Convergence properties of the leading order imaging subseries

The essence of the leading order imaging series for the 1-D acoustic case has been shown to reduce to the Taylor series for e^x (equation 22), i.e.,

$$e^x = \sum_{n=0}^{\infty} \frac{x^n}{n!} \tag{42}$$

where

$$x = \left(-ik_0 \frac{1}{2} \int_0^z \alpha_1(z')dz' \right). \tag{43}$$

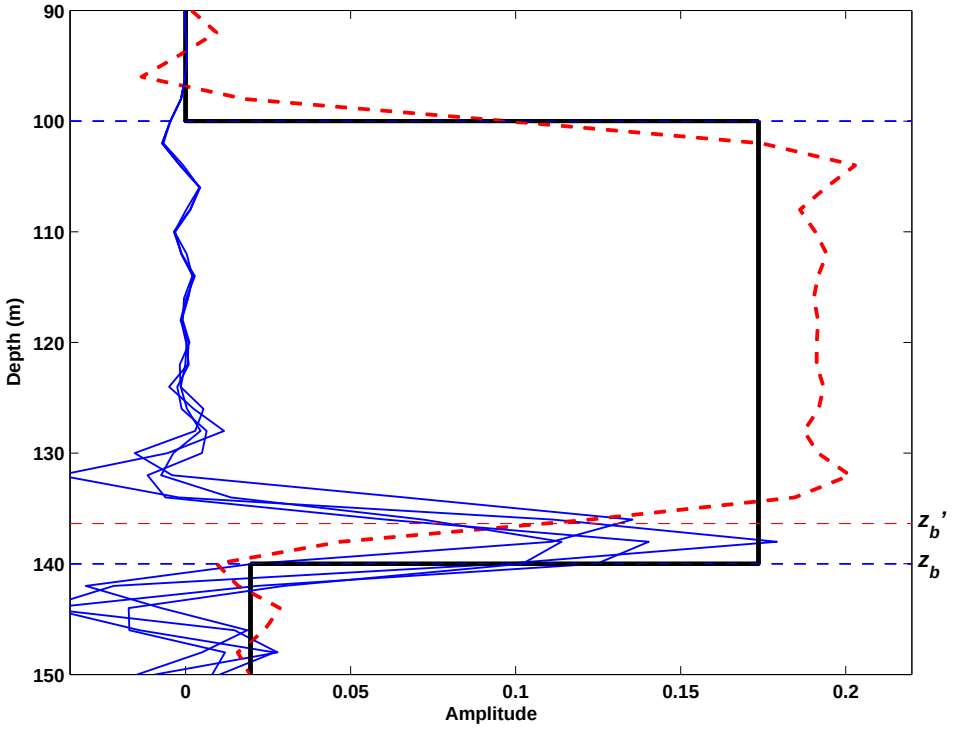

Figure 6: Five terms in the leading order imaging subseries. The solid black line is the actual perturbation α and the dashed red line is α_1, the first approximation to α. The blue lines are the leading order imaging subseries terms. The cumulative sum of these imaging terms is shown in Fig. 7.

k_0 is the reference wavenumber (ω/c_0) and α_1 is a migration-inversion, or linear estimate of α.

This series for e^x is known to converge for any finite x, and hence the leading order imaging subseries will converge as long as both the maximum frequency ω, and the "cumulative" perturbation are both finite. Both of these conditions are realizable in practice.

Concerning the rate of convergence, the series will converge more rapidly for smaller perturbations and for smaller values of ω. Hence, the closer the reference medium velocity is to the actual medium velocity, the faster the series will converge. Since the strategy is to remove multiples before processing primaries, then velocity analysis can be employed to derive a velocity model that is proximate to the actual model, thereby making the contrast between the reference medium and the actual medium as small as possible. Also, lower resolution data (small ω) will image more quickly using this imaging series.

As might be expected, the leading order imaging subseries will not converge to the exact

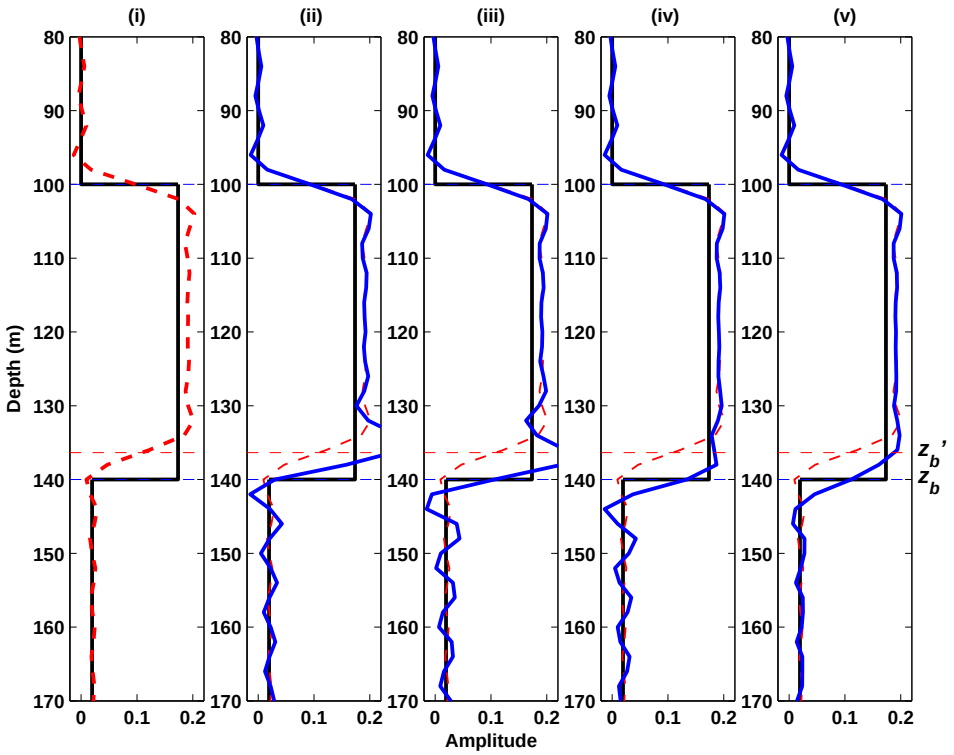

Figure 7: Cumulative sum of five terms in the leading order imaging subseries. The solid black line is the perturbation α and the red line is the first approximation to α or the first term in the inverse series, α_1. The blue line is the cumulative sum of the imaging subseries terms, e.g. in panel (ii) the sum of two terms in the subseries is shown, and in panel (v) the sum of five terms in the subseries is displayed.

depth because the higher order terms are not included in the series. Returning to the simple analytic example in Fig. 4, where the data is expressed by Eq. (25), then Eq. (24) provides for the leading-order imaged data:

$$\begin{aligned}\alpha_p^{IS_{LO}} =& 4R_1 H\left(z - 2R_1(z-a)H(z-a) - a - 2\hat{R}_2(z-z_{b'})H(z-z_{b'})\right) \\ &+ 4\hat{R}_2 H\left(z - 2R_1(z-a)H(z-a) - b' - 2\hat{R}_2(z-z_{b'})H(z-z_{b'})\right)\end{aligned} \tag{44}$$

Studying this expression, we find that for $|R_1| < 1/2$

$$\alpha_p^{IS_{LO}} = 4R_1 H\left(z-a\right) + 4\hat{R}_2 H\left(z - b^{LO}\right) \tag{45}$$

where the second interface has shifted from b' to the leading order approximation to b,

$$b^{LO} = a + \frac{(b'-a)}{(1-2R_1)}. \tag{46}$$

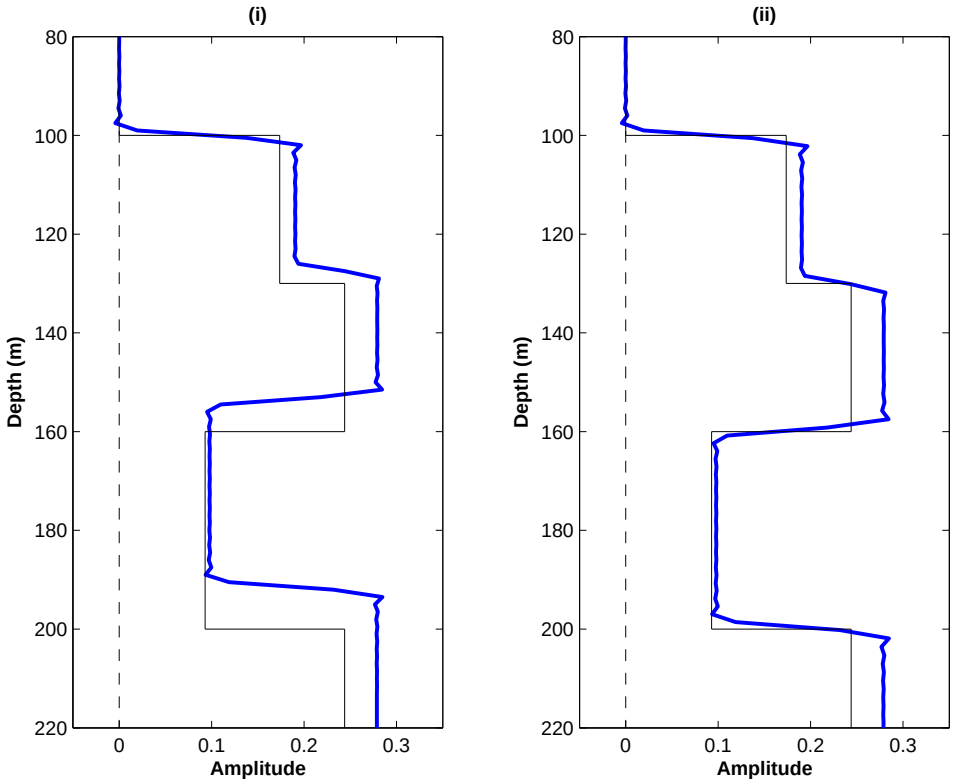

Figure 8: The thin black line shows α for a four layer example where $c_0 = 1500$ m/s, $c_1 = 1650$ m/s, $c_2 = 1725$ m/s, $c_3 = 1575$ m/s and $c_4 = 1725$ m/s. The thick blue line in panel (i) is α_1 generated using the constant velocity $c_0 = 1500$ m/s for 0-125 Hz band-limited synthetic data. The thick blue line in panel (ii) shows the closed form result of the leading order imaging subseries $\alpha_p^{IS_{LO}}$. The interfaces have shifted from the incorrect depths towards their correct ones.

The actual depth b is (from equation 31)

$$b = a + \frac{(1 - R_1)}{(1 + R_1)}(b' - a). \tag{47}$$

For small R_1, b^{LO} is a good approximation to b. Analysis of more complicated analytic examples, including the effects of transmission in the overburden, will the subject of future work.

6 Discussion and Conclusions

The free surface multiple removal subseries predicts the correct time of all orders of multiple with just one term. It then takes a series to get the amplitudes of the second and higher order multiples correct. The internal multiple removal series takes one term to predict the right time, but a whole series to *approximate* the amplitudes of the multiples. Extending this analogue, we have now isolated an imaging subseries that requires an infinite number of terms to get the approximate depth. Clearly the subseries become more demanding the closer we get to reaching the ultimate objectives of direct inversion.

The derivation of the 1-D acoustic leading order imaging subseries algorithm presented in this paper constitutes a blueprint for deriving the algorithms in multi-D and extending them for more complicated Earth models. Significant progress has already been made in deriving the equations for variable velocity and density acoustic Earth models, and for a depth-varying reference medium (Zhang and Weglein, 2003; Liu and Weglein, 2003).

In conclusion, we have isolated a subseries of the inverse scattering series that images seismic data in depth in the absence of adequate velocity information. We have found analytically and numerically that this series' convergences properties are extremely favorable. The series images the reflectors directly at depths that are the leading order approximations to their precise locations. In 1-D, and for a constant density, varible velocity acoustic medium, there exists a closed form solution to this imaging subseries.

Acknowledgments

The first author would like to express his appreciation to Craig Cooper for his encouragement of this research. Kris Innanen and Tad Ulrych are thanked for valuable technical discussions. The support of the M-OSRP sponsors is gratefully acknowledged.

References

Berkhout, A. J. and D. W. V. Palthe (1981). Migration in terms of spatial deconvolution. *Geophysical Prospecting 27*, 261–291.

Carvalho, P. M. (1992). *Free-surface multiple reflection elimination method based on non-linear inversion of seismic data.* Ph. D. thesis, Universidade Federal da Bahia. in Portuguese.

Claerbout, J. F. (1971). Toward a unified theory of reflector mapping. *Geophysics 36*(3), 467–481.

Clayton, R. W. and R. H. Stolt (1981). A Born-WKBJ inversion method for acoustic reflection data. *Geophysics 46*(11), 1559–1567.

Gray, S. H., J. Etgen, J. Dellinger, and D. Whitmore (2001). Seismic migration problems and solutions. *Geophysics 66*(5), 1622–1640.

Liu, F. and A. B. Weglein (2003). Inverse series for a v(z) background. *Mission-Oriented Seismic Research Program 2*, 210–225.

Matson, K. H. (1997). *An inverse scattering series method for attenuating elastic multiples from multicomponent land and ocean bottom seismic data.* Ph. D. thesis, University of British Columbia.

Moses, H. (1956). Calculation of scattering potential from reflection coefficients. *Phys. Rev.* (102), 559–567.

Osen, A., B. G. Secrest, L. Amundsen, and A. Reitan (1998). Wavelet estimation from marine pressure measurements. *Geophysics 63*(6), 2108–2119.

Schneider, W. A. (1978). Integral formulation for migration in two-dimensions and three-dimensions. *Geophysics 43*(1), 49–76.

Stolt, R. H. (1978). Migration by Fourier transform. *Geophysics 43*(1), 23–48.

Stolt, R. H. and A. B. Weglein (1985). Migration and inversion of seismic data. *Geophysics 50*(12), 2458–2472.

Stork, C. and R. W. Clayton (1991). Linear aspects of tomographic velocity analysis. *Geophysics 56*(4), 483–495.

Tan, T. H. (1999). Wavelet spectrum estimation. *Geophysics 64*(6), 1836–1846.

Taner, M. T. and F. Koehler (1969). Velocity spectra - Digital computer derivation and applications of velocity functions. *Geophysics 34*(6), 859–881.

Tarantola, A. (1987). *Inverse problem theory.* Elsevier Science B.V.

Wapenaar, C. P. A., G. L. Peels, V. Budejicky, and A. J. Berkhout (1989). Inverse extrapolation of primary seismic waves. *Geophysics 54*(7), 853–863.

Weglein, A. B., W. E. Boyce, and J. E. Anderson (1981). Obtaining three-dimensional velocity information directly from reflection seismic data: An inverse scattering formalism. *Geophysics 46*(8), 1116–1120.

Weglein, A. B., F. A. Gasparotto, P. M. Carvalho, and R. H. Stolt (1997). An inverse-scattering series method for attenuating multiples in seismic reflection data. *Geophysics 62*(6), 1975–1989.

Weglein, A. B., K. H. Matson, D. J. Foster, P. M. Carvalho, D. Corrigan, and S. A. Shaw (2000). Imaging and inversion at depth without a velocity model: Theory, concepts and initial evaluation. In *70th Annual Internat. Mtg., Soc. Expl. Geophys., Expanded Abstracts*, pp. 1016–1019. Soc. Expl. Geophys.

Weglein, A. B., K. H. Matson, D. J. Foster, S. A. Shaw, P. M. Carvalho, and D. Corrigan (2002). Predicting the correct spatial location of reflectors without knowing or determining the precise medium and wave velocity: initial concept, algorithm and analytic and numerical example. *Journal of Seismic Exploration 10*, 367–382.

Weglein, A. B. and B. G. Secrest (1990). Wavelet estimation for a multidimensional acoustic or elastic earth. *Geophysics 55*(7), 902–913.

Zhang, H. and A. B. Weglein (2003). Target identification using the inverse scattering series; inversion of large-contrast, variable velocity and density acoustic media. *Mission-Oriented Seismic Research Program 2*, 196–209.

Ziolkowski, A. (1991). Why don't we measure seismic signatures? *Geophysics 56*(2), 190–201.

Appendix A: Solution for $\alpha_1(z)$

The first term in the inverse series for 1-D constant density acoustic media can be written

$$\psi(z_m;\omega) = \psi_0(z_m;\omega) + \int_{-\infty}^{\infty} G_0(z_m|z';\omega)k_0^2\alpha_1(z')\psi_0(z'|z_m;\omega)dz' \tag{A-1}$$

where

$$G_0(z_m|z';\omega) = \frac{e^{ik_0|z_m-z'|}}{2ik_0} \tag{A-2}$$

$$\psi_0(z'|z_m;\omega) = e^{ik_0(z'-z_m)} \tag{A-3}$$

$$\psi(z_m;\omega) - \psi_0(z_m;\omega) = \psi_s(z_m;\omega), \tag{A-4}$$

z_m is the measurement depth, and $k_0 = \omega/c_0$. The reference medium is chosen to be a homogeneous wholespace with velocity c_0 and the incident wavefield is written as a pseudo plane wave that passes depth z_m at time $t = 0$. Making use of the fact that all scattering points are below the measurement surface ($z' > z_m$)

$$\begin{aligned}\psi_s(z_m;\omega) &= k_0^2 \int_{-\infty}^{\infty} \frac{e^{ik_0(z'-z_m)}}{2ik_0}\alpha_1(z')e^{ik_0(z'-z_m)}dz' \\ &= k_0^2 \frac{e^{-2ik_0z_m}}{2ik_0}\int_{-\infty}^{\infty}\alpha_1(z')e^{2ik_0z'}dz'.\end{aligned} \tag{A-5}$$

So

$$\begin{aligned}\int_{-\infty}^{\infty}\alpha_1(z')e^{2ik_0z'}dz' &= \frac{-2\psi_s(z_m;\omega)}{ik_0}e^{2ik_0z_m} \\ &= -2c_0\frac{\psi_s(z_m;\omega)}{i\omega}e^{i\omega\tau} \text{ where } \tau = 2z_m/c_0\end{aligned} \tag{A-6}$$

Performing an inverse Fourier transform, we get

$$\begin{aligned}\alpha_1(z) &= \frac{-2}{c_0}\int_{-\infty}^{\infty} -2c_0\frac{\psi_s(z_m;\omega)}{i\omega}e^{i\omega(\tau-2z/c_0)}d\omega \\ &= 4\int_{-\infty}^{z}\psi_s(z_m;z')dz'\end{aligned} \tag{A-7}$$

where $z' = (c_0t/2 - z_m)$.

Appendix B: Separation of α_2 terms

The second term in the inverse series can be written

$$\int_{-\infty}^{\infty} G_0(z_g|z';k_0)k_0^2\alpha_2(z')\psi_0(z'|z_s;k_0)dz' =$$
$$-\int_{-\infty}^{\infty} G_0(z_g|z'';k_0)k_0^2\alpha_1(z'')\int_{-\infty}^{\infty} G_0(z''|z';k_0)k_0^2\alpha_1(z')\psi_0(z'|z_s;k_0)dz'dz'' \tag{B-1}$$

where

$$G_0(z_g|z';k_0) = \frac{e^{ik_0|z_g-z'|}}{2ik_0}$$
$$\psi_0(z'|z_s;k_0) = e^{ik_0(z'-z_s)}$$
$$k_0 = \omega/c_0$$

So

$$e^{-2ik_0z_m}\int_{-\infty}^{\infty}\frac{k_0^2}{2ik_0}\alpha_2(z')e^{2ik_0z'}dz' =$$
$$-e^{-2ik_0z_m}\int_{-\infty}^{\infty}\frac{k_0^4}{(2ik_0)^2}\alpha_1(z'')e^{ik_0z''}\int_{-\infty}^{\infty}e^{ik_0|z''-z'|}\alpha_1(z')e^{ik_0z'}dz'dz'' \tag{B-2}$$

As might be expected, the location of the measurment surface (z_m) cancels since this information is carried in α_1. Then cancelling some i's and k_0's yields

$$\frac{2}{ik_0}\int_{-\infty}^{\infty}\alpha_2(z')e^{2ik_0z'}dz' = \int_{-\infty}^{\infty}\alpha_1(z'')e^{ik_0z''}\int_{-\infty}^{\infty}e^{ik_0|z''-z'|}\alpha_1(z')e^{ik_0z'}dz'dz'' \tag{B-3}$$

and considering the absolute value in the exponential reveals a symmetry

$$\begin{aligned}\frac{2}{ik_0}\tilde{\alpha}_2(-2k_0) &= \int_{-\infty}^{\infty}\alpha_1(z'')e^{ik_0z''}\int_{-\infty}^{\infty}H(z''-z')e^{ik_0(z''-z')}\alpha_1(z')e^{ik_0z'}dz'dz'' \\ &+ \int_{-\infty}^{\infty}\alpha_1(z'')e^{ik_0z''}\int_{-\infty}^{\infty}H(z'-z'')e^{ik_0(z'-z'')}\alpha_1(z')e^{ik_0z'}dz'dz'' \\ &= 2\int_{-\infty}^{\infty}\alpha_1(z'')e^{ik_0z''}\int_{-\infty}^{\infty}H(z'-z'')e^{ik_0(z'-z'')}\alpha_1(z')e^{ik_0z'}dz'dz''\end{aligned}$$

$$\tilde{\alpha}_2(-2k_0) = \int_{-\infty}^{\infty}\alpha_1(z'')\int_{-\infty}^{\infty}ik_0H(z'-z'')\alpha_1(z')e^{2ik_0z'}dz'dz'' \tag{B-4}$$

Integrating by parts

$$\begin{aligned} u &= \int_{-\infty}^{\infty} \alpha_1(z'')H(z'-z'')\alpha_1(z')dz'' \\ dv &= ik_0 e^{2ik_0 z'}dz' \\ \frac{du}{dz'} &= \int_{-\infty}^{\infty} \alpha_1(z'')\left(\delta(z'-z'')\alpha_1(z') + H(z'-z'')\frac{d}{dz'}\alpha_1(z')\right)dz'' \\ &= \alpha_1^2(z') + \int_{-\infty}^{\infty}\left(\alpha_1(z'')H(z'-z'')\frac{d}{dz'}\alpha_1(z')\right)dz'' \\ v &= \frac{e^{2ik_0 z'}}{2} \end{aligned}$$

Therefore,

$$\begin{aligned} \tilde{\alpha}_2(-2k_0) = &\left[\int_{-\infty}^{\infty}\alpha_1(z'')H(z'-z'')\alpha_1(z')dz''\frac{e^{2ik_0z'}}{2}\right]_{z'=-\infty}^{\infty} \\ &- \frac{1}{2}\left(\int_{-\infty}^{\infty}\alpha_1^2(z')e^{2ik_0z'}dz'\right) \\ &- \frac{1}{2}\left(\int_{-\infty}^{\infty}\int_{-\infty}^{\infty}\alpha_1(z'')H(z'-z'')dz''\frac{d}{dz'}\left(\alpha_1(z')\right)e^{2ik_0z'}dz'\right) \end{aligned} \tag{B-5}$$

The first term is taken to be zero under the assumption that the scattering potential is confined to some finite region $z_m < z' < \infty$. Then, performing an inverse Fourier transform on both sides yields

$$\alpha_2(z) = -\frac{1}{2}\left(\alpha_1^2(z) + \left[\frac{d}{dz}\alpha_1(z)\right]\int_0^z \alpha_1(z')dz'\right) \tag{B-6}$$

Appendix C: Separation of α_3 terms

The third term in the inverse series can be written

$$\begin{aligned}
&\int_{-\infty}^{\infty} G_0(z_g,z';k_0)k_0^2\alpha_3(z')\psi_0(z'|z_s;k_0)dz' = \\
&\quad -\int_{-\infty}^{\infty} G_0(z_g,z'';k_0)k_0^2\alpha_1(z'')\int_{-\infty}^{\infty} G_0(z'',z';k_0)k_0^2\alpha_2(z')\psi_0(z'|z_s;k_0)dz'dz'' \\
&\quad -\int_{-\infty}^{\infty} G_0(z,z'';k_0)k_0^2\alpha_2(z'')\int_{-\infty}^{\infty} G_0(z'',z';k_0)k_0^2\alpha_1(z')\psi_0(z'|z_s;k_0)dz'dz'' \\
&\quad -\int_{-\infty}^{\infty} G_0(z,z''';k_0)k_0^2\alpha_1(z''')\int_{-\infty}^{\infty} G_0(z''',z'';k_0)k_0^2\alpha_1(z'') \\
&\quad \times\int_{-\infty}^{\infty} G_0(z'',z';k_0)k_0^2\alpha_1(z')\psi_0(z'|z_s;k_0)dz'dz''dz''' \qquad \text{(C-1)}
\end{aligned}$$

which on substitution of G_0 and ψ_0 (Eqs. A-2 and A-3) reduces to

$$\tilde{\alpha}_3(-2k_0) = \tilde{I}_1 + \tilde{I}_2 + \tilde{I}_3 \qquad \text{(C-2)}$$

where

$$\begin{aligned}
\tilde{I}_1(-2k_0) &= \frac{ik_0}{2}\int_{-\infty}^{\infty}\alpha_1(z'')e^{ik_0z''}\int_{-\infty}^{\infty}e^{ik_0|z''-z'|}\alpha_2(z')e^{ik_0z'}dz'dz'' \\
\tilde{I}_2(-2k_0) &= \frac{ik_0}{2}\int_{-\infty}^{\infty}\alpha_2(z'')e^{ik_0z''}\int_{-\infty}^{\infty}e^{ik_0|z''-z'|}\alpha_1(z')e^{ik_0z'}dz'dz'' \\
\tilde{I}_3(-2k_0) &= \frac{k_0^2}{4}\int_{-\infty}^{\infty}\alpha_1(z''')e^{ik_0z'''}\int_{-\infty}^{\infty}e^{ik_0|z'''-z''|}\alpha_1(z'') \\
&\quad\times\int_{-\infty}^{\infty}e^{ik_0|z''-z'|}\alpha_1(z')e^{ik_0z'}dz'dz''dz'''
\end{aligned}$$

The first term can be expanded

$$\tilde{I}_1 = \tilde{I}_{11} + \tilde{I}_{12}$$

where

$$\begin{aligned}
\tilde{I}_{11}(-2k_0) &= \frac{ik_0}{2}\int_{-\infty}^{\infty}\alpha_1(z'')\int_{-\infty}^{\infty}H(z''-z')\alpha_2(z')e^{2ik_0z''}dz'dz'' \\
\tilde{I}_{12}(-2k_0) &= \frac{ik_0}{2}\int_{-\infty}^{\infty}\alpha_1(z'')\int_{-\infty}^{\infty}H(z'-z'')\alpha_2(z')e^{2ik_0z'}dz'dz''
\end{aligned}$$

A symmetry exists between $\tilde{I}_1$ and $\tilde{I}_2$, since

$$\tilde{I}_2 = \tilde{I}_{21} + \tilde{I}_{22}$$

where

$$\tilde{I}_{21}(-2k_0) = \frac{ik_0}{2}\int_{-\infty}^{\infty}\alpha_2(z'')\int_{-\infty}^{\infty}H(z''-z')\alpha_1(z')e^{2ik_0z''}dz'dz''$$
$$\tilde{I}_{22}(-2k_0) = \frac{ik_0}{2}\int_{-\infty}^{\infty}\alpha_2(z'')\int_{-\infty}^{\infty}H(z'-z'')\alpha_1(z')e^{2ik_0z'}dz'dz''$$

we see that

$$\tilde{I}_{21} = \tilde{I}_{12}$$
$$\tilde{I}_{22} = \tilde{I}_{11}$$

so

$$\tilde{I}_2 = \tilde{I}_1. \tag{C-3}$$

Integrating $\tilde{I}_{11}$ by parts provides

$$\begin{aligned}
u =& \alpha_1(z'')\int_{-\infty}^{\infty}H(z''-z')\alpha_2(z')dz' \\
dv =& \frac{ik_0e^{2ik_0z''}}{2}dz'' \\
\frac{du}{dz''} =& \alpha_1(z'')\alpha_2(z'') + \int_{-\infty}^{z''}\alpha_2(z')dz'\left[\frac{d}{dz''}\left(\alpha_1(z'')\right)\right] \\
v =& \frac{e^{2ik_0z''}}{4} \\
\tilde{I}_{11}(-2k_0) =& \left[\frac{1}{4}\alpha_1(z'')\int_{-\infty}^{\infty}H(z''-z')\alpha_2(z')dz'e^{2ik_0z''}\right]_{z''=-\infty}^{\infty} \\
&- \frac{1}{4}\int_{-\infty}^{\infty}\alpha_1(z'')\alpha_2(z'')e^{2ik_0z''}dz'' \\
&- \frac{1}{4}\int_{-\infty}^{\infty}\int_{-\infty}^{z''}\alpha_2(z')dz'\left[\frac{d}{dz''}\left(\alpha_1(z'')\right)\right]e^{2ik_0z''}dz''
\end{aligned} \tag{C-4}$$

Similarly, integrating $\tilde{I}_{12}$ by parts yields

$$\begin{aligned}
u =& \alpha_2(z') \int_{-\infty}^{\infty} H(z'-z'')\alpha_1(z'')dz'' \\
dv =& \frac{ik_0 e^{2ik_0 z'}}{2} dz' \\
\frac{du}{dz'} =& \alpha_2(z')\alpha_1(z') + \int_{-\infty}^{z'} \alpha_1(z'')dz'' \left[\frac{d}{dz'}(\alpha_2(z'))\right] \\
v =& \frac{e^{2ik_0 z'}}{4} \\
\tilde{I}_{12}(-2k_0) =& \left[\frac{1}{4}\alpha_2(z') \int_{-\infty}^{\infty} H(z'-z'')\alpha_1(z'')dz'' e^{2ik_0 z'}\right]_{z'=-\infty}^{\infty} \\
& - \frac{1}{4}\int_{-\infty}^{\infty} \alpha_2(z')\alpha_1(z') e^{2ik_0 z'} dz' \\
& - \frac{1}{4}\int_{-\infty}^{\infty}\int_{-\infty}^{z'} \alpha_1(z'')dz'' \left[\frac{d}{dz'}(\alpha_2(z'))\right] e^{2ik_0 z'} dz'
\end{aligned} \tag{C-5}$$

Since the scattering potential is confined to a finite region, the boundary terms in Eqs. (C-4) and (C-5) are equal to zero. Then by Eq. (C-3),

$$\begin{aligned}
\tilde{I}_1 + \tilde{I}_2 =& 2\tilde{I}_1 = 2\left(\tilde{I}_{11} + \tilde{I}_{12}\right) \\
=& -\frac{1}{2}\int_{-\infty}^{\infty} \alpha_1(z'')\alpha_2(z'') e^{2ik_0 z''} dz'' \\
& -\frac{1}{2}\int_{-\infty}^{\infty}\int_{-\infty}^{z''} \alpha_2(z')dz' \left[\frac{d}{dz''}(\alpha_1(z''))\right] e^{2ik_0 z''} dz'' \\
& -\frac{1}{2}\int_{-\infty}^{\infty} \alpha_2(z')\alpha_1(z') e^{2ik_0 z'} dz' \\
& -\frac{1}{2}\int_{-\infty}^{\infty}\int_{-\infty}^{z'} \alpha_1(z'')dz'' \left[\frac{d}{dz'}(\alpha_2(z'))\right] e^{2ik_0 z'} dz'
\end{aligned}$$

Performing an inverse Fourier transform $I_1(z') = \int_{-\infty}^{\infty} \tilde{I}_1(-2k_0) e^{2ik_0 z'} d(-2k_0)$ we have

$$\begin{aligned}
I_1(z') + I_2(z') =& -\frac{1}{2}\alpha_1(z')\alpha_2(z') - \frac{1}{2}\int_{-\infty}^{z'} \alpha_2(z'')dz'' \left[\frac{d}{dz'}(\alpha_1(z'))\right] \\
& -\frac{1}{2}\alpha_2(z')\alpha_1(z') - \frac{1}{2}\int_{-\infty}^{z'} \alpha_1(z'')dz'' \left[\frac{d}{dz'}(\alpha_2(z'))\right] \\
=& -\alpha_1(z')\alpha_2(z') - \frac{1}{2}\int_{-\infty}^{z'} \alpha_2(z'')dz'' \left[\frac{d}{dz'}(\alpha_1(z'))\right] \\
& -\frac{1}{2}\int_{-\infty}^{z'} \alpha_1(z'')dz'' \left[\frac{d}{dz'}(\alpha_2(z'))\right]
\end{aligned} \tag{C-6}$$

Recalling the expression for $\alpha_2(z')$

$$\alpha_2(z') = -\frac{1}{2}\alpha_1^2(z') - \frac{1}{2}\int_{-\infty}^{z'} \alpha_1(z'')dz'' \left[\frac{d}{dz'}\alpha_1(z')\right] \tag{C-7}$$

then to write Eq. C-6 in terms of only α_1 we need to integrate $\alpha_2(z')$:

$$\begin{aligned}\int_{-\infty}^{z''} \alpha_2(z')dz' =& -\frac{1}{2}\int_{-\infty}^{z''} \alpha_1^2(z')dz' \\ & -\frac{1}{2}\int_{-\infty}^{z''}\int_{-\infty}^{z'} \alpha_1(z''')dz''' \left[\frac{d}{dz'}\alpha_1(z')\right] dz'\end{aligned} \tag{C-8}$$

The second integral in Eq. (C-8) can be rewritten

$$-\frac{1}{2}\int_{-\infty}^{\infty} H(z''-z')\int_{-\infty}^{\infty} H(z'-z''')\alpha_1(z''')dz''' \left[\frac{d}{dz'}\alpha_1(z')\right] dz' \tag{C-9}$$

which can be integrated by parts

$$\begin{aligned}u =& H(z''-z')\int_{-\infty}^{\infty} H(z'-z''')\alpha_1(z''')dz''' \\ dv =& -\frac{1}{2}\frac{d}{dz'}\left(\alpha_1(z')\right)dz' \\ \frac{du}{dz'} =& H(z''-z')\int_{-\infty}^{\infty}\delta(z'-z''')\alpha_1(z''')dz''' \\ & -\delta(z''-z')\int_{-\infty}^{\infty} H(z'-z''')\alpha_1(z''')dz''' \\ =& H(z''-z')\alpha_1(z') - \delta(z''-z')\int_{-\infty}^{z'}\alpha_1(z''')dz''' \\ v =& -\frac{1}{2}\alpha_1(z')\end{aligned}$$

which leads to

$$\begin{aligned}\int_{-\infty}^{\infty} udv =& \left[-\frac{1}{2}\alpha_1(z')H(z''-z')\int_{-\infty}^{z'}\alpha_1(z''')dz'''\right]_{z'=-\infty}^{\infty} \\ & +\frac{1}{2}\int_{-\infty}^{\infty}\alpha_1(z')H(z''-z')\alpha_1(z')dz' \\ & -\frac{1}{2}\int_{-\infty}^{\infty}\delta(z''-z')\alpha_1(z')\int_{-\infty}^{z'}\alpha_1(z''')dz'''dz' \\ =& \frac{1}{2}\int_{-\infty}^{z''}\alpha_1^2(z')dz' - \frac{1}{2}\alpha_1(z'')\int_{-\infty}^{z''}\alpha_1(z''')dz'''.\end{aligned} \tag{C-10}$$

Therefore, the integral of $\alpha_2(z')$ (Eq.C-8) becomes

$$\int_{-\infty}^{z''} \alpha_2(z')dz' = -\frac{1}{2}\alpha_1(z'')\int_{-\infty}^{z''} \alpha_1(z''')dz'''. \tag{C-11}$$

It is interesting to see that the terms that are the integrals of α_1 squared cancel. To simplify Eq. (C-6), we also need to differentiate $\alpha_2(z')$:

$$\begin{aligned}\left[\frac{d}{dz'}\alpha_2(z')\right] =& -\frac{1}{2}\left(2\alpha_1(z')\frac{d}{dz'}\alpha_1(z')\right) \\ & -\frac{1}{2}\left(\int_{-\infty}^{z'}\alpha_1(z'')dz''\left[\frac{d^2}{dz'^2}\alpha_1(z')\right]\right) \\ & -\frac{1}{2}\frac{d}{dz'}\left(\int_{-\infty}^{\infty}H(z'-z'')\alpha_1(z'')dz''\right)\left[\frac{d}{dz'}\alpha_1(z')\right] \\ =& -\frac{3}{2}\alpha_1(z')\left[\frac{d}{dz'}\alpha_1(z')\right] \\ & -\frac{1}{2}\int_{-\infty}^{z'}\alpha_1(z'')dz''\left[\frac{d^2}{dz'^2}\alpha_1(z')\right].\end{aligned} \tag{C-12}$$

Therefore, substituting Eqs. (C-11) and (C-12) into Eq. (C-6), we have

$$\begin{aligned}I_1(z')+I_2(z') =& \frac{1}{2}\alpha_1^3(z')+\frac{1}{2}\alpha_1(z')\int_{-\infty}^{z'}\alpha_1(z'')dz''\left[\frac{d}{dz'}\alpha_1(z')\right] \\ & +\frac{1}{4}\alpha_1(z')\int_{-\infty}^{z'}\alpha_1(z'')dz''\left[\frac{d}{dz'}\alpha_1(z')\right] \\ & +\frac{3}{4}\alpha_1(z')\int_{-\infty}^{z'}\alpha_1(z'')dz''\left[\frac{d}{dz'}\alpha_1(z')\right] \\ & +\frac{1}{4}\left(\int_{-\infty}^{z'}\alpha_1(z'')dz''\right)^2\left[\frac{d^2}{dz'^2}\alpha_1(z')\right]\end{aligned}$$

$$\begin{aligned}I_1(z)+I_2(z) =& \frac{1}{2}\alpha_1^3(z)+\frac{3}{2}\alpha_1(z)\int_{-\infty}^{z}\alpha_1(z')dz'\left[\frac{d}{dz}\alpha_1(z)\right] \\ & +\frac{1}{4}\left(\int_{-\infty}^{z}\alpha_1(z')dz'\right)^2\left[\frac{d^2}{dz^2}\alpha_1(z)\right]\end{aligned} \tag{C-13}$$

Now consider the third term in Eq. (C-2), namely

$$\tilde{I}_3 = \tilde{I}_{31}+\tilde{I}_{32}+\tilde{I}_{33}+\tilde{I}_{34}$$

where

$$\tilde{I}_{31}(-2k_0) = \frac{k_0^2}{4}\int_{-\infty}^{\infty}\alpha_1(z''')e^{2ik_0z'''}\int_{-\infty}^{\infty}H(z'''-z'')\alpha_1(z'') \times\int_{-\infty}^{\infty}H(z''-z')\alpha_1(z')dz'dz''dz''' \tag{C-14}$$

$$\tilde{I}_{32}(-2k_0) = \frac{k_0^2}{4}\int_{-\infty}^{\infty}\alpha_1(z''')\int_{-\infty}^{\infty}H(z''-z''')\alpha_1(z'')e^{2ik_0z''} \times\int_{-\infty}^{\infty}H(z''-z')\alpha_1(z')dz'dz''dz''' \tag{C-15}$$

$$\tilde{I}_{33}(-2k_0) = \frac{k_0^2}{4}\int_{-\infty}^{\infty}\alpha_1(z''')\int_{-\infty}^{\infty}H(z''-z''')\alpha_1(z'') \times\int_{-\infty}^{\infty}H(z'-z'')\alpha_1(z')e^{2ik_0z'}dz'dz''dz''' \tag{C-16}$$

$$\tilde{I}_{34}(-2k_0) = \frac{k_0^2}{4}\int_{-\infty}^{\infty}\alpha_1(z''')e^{2ik_0z'''}\int_{-\infty}^{\infty}H(z'''-z'')\alpha_1(z'')e^{-2ik_0z''} \times\int_{-\infty}^{\infty}H(z'-z'')\alpha_1(z')e^{2ik_0z'}dz'dz''dz''' \tag{C-17}$$

Equation (C-17) is equivalent to that for "W_{333}" (Eq. 5.8 in Matson (1997)), except for the substitution $V_1 = k_0^2\alpha_1$. The Heaviside functions in this equation ensure that $z''' > z''$ and $z' > z''$ so that the first and third scattering points are deeper than the second scattering point; hence the "W" diagram interpretation of the internal multiple attenuation algorithm. We will return to this equation a little later on.

Switching variables reveals that $\tilde{I}_{33} = \tilde{I}_{31}$. Notice that $k_0^2 = \frac{-(2ik_0)^2}{4}$ and performing an inverse Fourier transform over the conjugate variable $-2k_0$ yields

$$\begin{aligned}
I_3 =& 2I_{31} + I_{32} + I_{34} \\
=& -\frac{1}{8}\frac{d^2}{dz'''^2}\left(\alpha_1(z''')\int_{-\infty}^{\infty}\int_{-\infty}^{\infty}H(z'''-z'')\alpha_1(z'')H(z''-z')\alpha_1(z')dz'dz''\right) \\
&-\frac{1}{16}\frac{d^2}{dz'''^2}\left(\alpha_1(z''')\int_{-\infty}^{\infty}\int_{-\infty}^{\infty}H(z'''-z'')\alpha_1(z'')H(z'''-z')\alpha_1(z')dz'dz''\right) \\
&-\frac{1}{16}\frac{d^2}{dz'''^2}\left(\alpha_1(z''')\int_{-\infty}^{\infty}\int_{-\infty}^{\infty}H(z'''-z'')\alpha_1(z'') \right. \\
&\qquad\left.\times H(z'-z'')\alpha_1(z')e^{2ik_0z'}e^{-2ik_0z''}dz'dz''\right)
\end{aligned}$$

$$
\begin{aligned}
2I_{31}(z''') = &-\frac{1}{8}\frac{d}{dz'''}\left(\frac{d}{dz'''}\left(\alpha_1(z''')\right)\int_{-\infty}^{\infty}\right.\\
&\left.\times\int_{-\infty}^{\infty}H(z'''-z'')\alpha_1(z'')H(z''-z')\alpha_1(z')dz'dz''\right)\\
&-\frac{1}{8}\frac{d}{dz'''}\left(\alpha_1(z''')\int_{-\infty}^{\infty}\alpha_1(z''')H(z'''-z')\alpha_1(z')dz'\right)\\
=&-\frac{1}{8}\int_{-\infty}^{z'''}\alpha_1(z'')\int_{-\infty}^{z''}\alpha_1(z')dz'dz''\left[\frac{d^2}{dz'''^2}\alpha_1(z''')\right]\\
&-\frac{1}{8}\alpha_1(z''')\int_{-\infty}^{z'''}\alpha_1(z')dz'\left[\frac{d}{dz'''}\alpha_1(z''')\right]\\
&-\frac{1}{4}\alpha_1(z''')\int_{-\infty}^{z'''}\alpha_1(z')dz'\left[\frac{d}{dz'''}\alpha_1(z''')\right]-\frac{1}{8}\alpha_1^3(z''')\\
=&-\frac{1}{8}\int_{-\infty}^{z'''}\alpha_1(z'')\int_{-\infty}^{z''}\alpha_1(z')dz'dz''\left[\frac{d^2}{dz'''^2}\alpha_1(z''')\right]\\
&-\frac{3}{8}\alpha_1(z''')\int_{-\infty}^{z'''}\alpha_1(z')dz'\left[\frac{d}{dz'''}\alpha_1(z''')\right]-\frac{1}{8}\alpha_1^3(z''')
\end{aligned}
\tag{C-18}
$$

The nested integral in the first expression can be simplified as follows

$$
\begin{aligned}
u =&\int_{-\infty}^{z'}\alpha_1(z'')dz''\\
dv =&\alpha_1(z')\\
du =&\alpha_1(z')dz'\\
v =&\int_{-\infty}^{z'}\alpha_1(z'')dz''\\
\int_{-\infty}^{z}\alpha_1(z')\int_{-\infty}^{z'}\alpha_1(z'')dz''dz' =&\left(\int_{-\infty}^{z'}\alpha_1(z'')dz''\right)^2\\
&-\int_{-\infty}^{z}\alpha_1(z')\int_{-\infty}^{z'}\alpha_1(z'')dz''dz'\\
=&\frac{1}{2}\left(\int_{-\infty}^{z'}\alpha_1(z'')dz''\right)^2
\end{aligned}
\tag{C-19}
$$

So equation (C-18) becomes

$$2I_{31}(z) = -\frac{1}{16}\left(\int_{-\infty}^{z}\alpha_1(z')dz'\right)^2\left[\frac{d^2}{dz^2}\alpha_1(z)\right] - \frac{3}{8}\alpha_1(z)\int_{-\infty}^{z}\alpha_1(z')dz'\left[\frac{d}{dz}\alpha_1(z)\right] - \frac{1}{8}\alpha_1^3(z) \tag{C-20}$$

and

$$\begin{aligned} I_{32}(z''') &= -\frac{1}{16}\frac{d}{dz'''}\left(\frac{d}{dz'''}\left(\alpha_1(z''')\right)\left(\int_{-\infty}^{z'''}\alpha_1(z'')dz''\right)^2\right) \\ &\quad -\frac{1}{8}\frac{d}{dz'''}\left(\alpha_1^2(z''')\int_{-\infty}^{z'''}\alpha_1(z'')dz''\right) \\ &= -\frac{1}{16}\left(\int_{-\infty}^{z'''}\alpha_1(z'')dz''\right)^2\left[\frac{d^2}{dz'''^2}\alpha_1(z''')\right] \\ &\quad -\frac{2}{16}\alpha_1(z''')\int_{-\infty}^{z'''}\alpha_1(z'')dz''\left[\frac{d}{dz'''}\alpha_1(z''')\right] \\ &\quad -\frac{1}{4}\alpha_1(z''')\int_{-\infty}^{z'''}\alpha_1(z')dz'\left[\frac{d}{dz'''}\alpha_1(z''')\right] \\ &\quad -\frac{1}{8}\alpha_1^3(z''') \end{aligned}$$

$$I_{32}(z) = -\frac{1}{16}\left(\int_{-\infty}^{z}\alpha_1(z')dz'\right)^2\left[\frac{d^2}{dz^2}\alpha_1(z)\right] - \frac{6}{16}\alpha_1(z)\int_{-\infty}^{z}\alpha_1(z')dz'\left[\frac{d}{dz}\alpha_1(z)\right] - \frac{1}{8}\alpha_1^3(z) \tag{C-21}$$

Finally, consider $\tilde{I}_{34}$ (Eq. C-17)

$$\begin{aligned} \tilde{I}_{34}(-2k_0) = &-\frac{1}{16}\int_{-\infty}^{\infty}(2ik_0)^2\alpha_1(z''')\int_{-\infty}^{\infty}H(z'''-z'')\alpha_1(z'') \\ &\times\int_{-\infty}^{\infty}H(z'-z'')\alpha_1(z')e^{2ik_0(z'''-z''+z')}dz'dz''dz''' \end{aligned}$$

and substitute $u = (z''' - z'' + z')$ to eliminate z''

$$\tilde{I}_{34}(-2k_0) = -\frac{1}{16}\int_{-\infty}^{\infty}(2ik_0)^2\alpha_1(z''')\int_{\infty}^{-\infty}H(u-z')\alpha_1(z'''+z'-u) \times \int_{-\infty}^{\infty}H(u-z''')\alpha_1(z')e^{2ik_0u}dz'(-du)dz'''$$

Notice that $dz'' = -du$ and the limits of integration of z'' and u are opposite. Switching the direction of the u integral introduces an overall minus sign. Performing an inverse Fourier transform yields

$$\begin{aligned}
I_{34}(u) = &-\frac{1}{16}\frac{\partial^2}{\partial u^2}\left(\int_{-\infty}^{\infty}\right. \\
&\left.\times\int_{-\infty}^{\infty}\alpha_1(z''')H(u-z')\alpha_1(z'''+z'-u)H(u-z''')\alpha_1(z')dz'dz'''\right) \\
= &-\frac{1}{16}\frac{\partial}{\partial u}\left(\int_{-\infty}^{\infty}\int_{-\infty}^{\infty}\alpha_1(z''')\right. \\
&\times\delta(u-z')\alpha_1(z'''+z'-u)H(u-z''')\alpha_1(z')dz'dz''') \\
&-\frac{1}{16}\frac{\partial}{\partial u}\left(\int_{-\infty}^{\infty}\int_{-\infty}^{\infty}\alpha_1(z''')\right. \\
&\times H(u-z')\alpha_1(z'''+z'-u)\delta(u-z''')\alpha_1(z')dz'dz''') \\
&-\frac{1}{16}\frac{\partial}{\partial u}\left(\int_{-\infty}^{\infty}\int_{-\infty}^{\infty}\alpha_1(z''')\right. \\
&\left.\times H(u-z')\frac{\partial}{\partial u}\left(\alpha_1(z'''+z'-u)\right)H(u-z''')\alpha_1(z')dz'dz'''\right) \\
= &-\frac{1}{16}\frac{\partial}{\partial u}\left(\int_{-\infty}^{\infty}\alpha_1^2(z''')H(u-z''')\alpha_1(u)dz'''\right) \\
&-\frac{1}{16}\frac{\partial}{\partial u}\left(\int_{-\infty}^{\infty}\alpha_1^2(z')H(u-z')\alpha_1(u)dz'\right) \\
&-\frac{1}{16}\frac{\partial}{\partial u}\left(\int_{-\infty}^{\infty}\int_{-\infty}^{\infty}\alpha_1(z''')\right. \\
&\left.\times H(u-z')\frac{\partial}{\partial u}\left(\alpha_1(z'''+z'-u)\right)H(u-z''')\alpha_1(z')dz'dz'''\right)
\end{aligned}$$

The first two expressions are equal and, when the differentiation is carried out, the last

expression creates three integrals, two of which are also equal:

$$\begin{aligned}
I_{34}(u) = &-\frac{1}{8}\alpha_1^3(u) - \frac{1}{8}\int_{-\infty}^{u}\alpha_1^2(z''')dz'''\left[\frac{\partial}{\partial u}\alpha_1(u)\right] \\
&-\frac{1}{16}\int_{-\infty}^{\infty}\int_{-\infty}^{\infty}H(u-z''')\alpha_1(z''')\delta(u-z')\alpha_1(z') \\
&\qquad\times\left[\frac{\partial}{\partial u}\alpha_1(z'''+z'-u)\right]dz'dz''' \\
&-\frac{1}{16}\int_{-\infty}^{\infty}\int_{-\infty}^{\infty}H(u-z')\alpha_1(z')\delta(u-z''')\alpha_1(z''') \\
&\qquad\times\left[\frac{\partial}{\partial u}\alpha_1(z'''+z'-u)\right]dz'dz''' \\
&-\frac{1}{16}\int_{-\infty}^{u}\int_{-\infty}^{u}\alpha_1(z''')\alpha_1(z')\left[\frac{\partial^2}{\partial u^2}\alpha_1(z'''+z'-u)\right]dz'dz'''
\end{aligned} \tag{C-22}$$

Then summing the two integrals that are equal in Eq. (C-22) we get

$$\begin{aligned}
2\times\Bigg(&-\frac{1}{16}\int_{-\infty}^{\infty}\int_{-\infty}^{\infty}H(u-z''')\alpha_1(z''')\delta(u-z')\alpha_1(z') \\
&\qquad\times\left[\frac{\partial}{\partial u}\alpha_1(z'''+z'-u)\right]dz'dz'''\Bigg) \\
=&\frac{1}{8}\alpha_1(u)\int_{-\infty}^{\infty}H(u-z''')\alpha_1(z''')\left[\frac{d}{dz'''}\alpha_1(z''')\right]dz''' \\
=&\int_{-\infty}^{\infty}pdq
\end{aligned} \tag{C-23}$$

where

$$\begin{aligned}
p =&\alpha_1(z''')H(u-z''') \\
dq =&\frac{1}{8}\alpha_1(u)\left[\frac{d}{dz'''}\alpha_1(z''')\right] \\
\frac{dp}{dz'''} =&\left[\frac{d}{dz'''}\alpha_1(z''')\right]H(u-z''') - \alpha_1(z''')\delta(u-z''') \\
q =&\frac{1}{8}\alpha_1(u)\alpha_1(z''')
\end{aligned}$$

Notice that the change in sign in Eq. (C-23) reflects the fact that the derivative with respect to u was carried out before the delta function acted on it. Since α_1 was a function of $-u$,

then a minus sign was introduced. Then

$$\begin{aligned}\int_{-\infty}^{\infty} pdq =& 0 - \frac{1}{8}\alpha_1(u)\int_{-\infty}^{\infty} H(u-z''')\alpha_1(z''')\left[\frac{d}{dz'''}\alpha_1(z''')\right]dz''' \\ &+ \frac{1}{8}\alpha_1(u)\int_{-\infty}^{\infty}\alpha_1^2(z''')\delta(u-z''')dz''' \\ =& -\int_{-\infty}^{\infty} p\ dq + \frac{1}{8}\alpha_1^3(u) \\ =& \frac{1}{16}\alpha_1^3(u) \end{aligned} \tag{C-24}$$

Substituting Eq. (C-24) into Eq. (C-22) yields

$$\begin{aligned} I_{34}(u) = &-\frac{1}{16}\alpha_1^3(u) - \frac{1}{8}\int_{-\infty}^{u}\alpha_1^2(z''')dz'''\left[\frac{\partial}{\partial u}\alpha_1(u)\right] \\ &- \frac{1}{16}\int_{-\infty}^{u}\int_{-\infty}^{u}\alpha_1(z''')\alpha_1(z')\left[\frac{\partial^2}{\partial u^2}\alpha_1(z'''+z'-u)\right]dz'dz''' \end{aligned} \tag{C-25}$$

The last term in this equation can be integrated by parts:

$$I_{343}(u) = -\frac{1}{16}\int_{-\infty}^{\infty} H(u-z''')\alpha_1(z''')\int_{-\infty}^{\infty} p\ dq\ dz''' \tag{C-26}$$

where

$$\begin{aligned} p &= H(u-z')\alpha_1(z') \\ dq &= \left[\frac{\partial^2}{\partial u^2}\alpha_1(z'''+z'-u)\right]dz' \\ \frac{dp}{dz'} &= H(u-z')\frac{d}{dz'}\alpha_1(z') - \delta(u-z')\alpha_1(z') \\ q &= -\left[\frac{\partial}{\partial u}\alpha_1(z'''+z'-u)\right] \end{aligned}$$

The boundary values are zero:

$$[p\ q]_{z'=-\infty}^{\infty} = \left[-H(u-z')\alpha_1(z')\frac{\partial}{\partial u}\alpha_1(z'''+z'-u)\right]_{z'=-\infty}^{\infty} = 0 \tag{C-27}$$

so Eq. (C-26) becomes

$$
\begin{aligned}
& I_{343}(u) = 0 \\
& -\frac{1}{16}\int_{-\infty}^{\infty} H(u-z''')\alpha_1(z''')\left[\int_{-\infty}^{u}\frac{d}{dz'}\left(\alpha_1(z')\right)\frac{\partial}{\partial u}\alpha_1(z'''+z'-u)dz'\right]dz''' \\
& +\frac{1}{16}\int_{-\infty}^{\infty} H(u-z''')\alpha_1(z''')\left[\int_{-\infty}^{\infty}\delta(u-z')\alpha_1(z')\frac{\partial}{\partial u}\alpha_1(z'''+z'-u)dz'\right]dz''' \\
& = -\frac{1}{16}\int_{-\infty}^{u}\frac{d}{dz'}\left(\alpha_1(z')\right)\int_{-\infty}^{\infty} H(u-z''')\alpha_1(z''')\frac{\partial}{\partial u}\alpha_1(z'''+z'-u)dz'''dz' \\
& \quad -\frac{1}{16}\alpha_1(u)\int_{-\infty}^{u}\alpha_1(z''')\frac{d}{dz'''}\alpha_1(z''')dz''' \\
& = -\frac{1}{16}\int_{-\infty}^{u}\frac{d}{dz'}\left(\alpha_1(z')\right)\int_{-\infty}^{\infty} H(u-z''')\alpha_1(z''')\frac{\partial}{\partial u}\alpha_1(z'''+z'-u)dz'''dz' \\
& \quad -\frac{1}{32}\alpha_1^3(u)
\end{aligned}
\tag{C-28}
$$

As before, the derivative with respect to u was carried out before the integration with the delta function, which introduced the change in sign. Now performing the z''' integration (Eq. C-28) by parts in the same fashion gives

$$
\int_{-\infty}^{\infty} H(u-z''')\alpha_1(z''')\frac{\partial}{\partial u}\alpha_1(z'''+z'-u)dz''' = \int_{-\infty}^{\infty} p\ dq
$$

where

$$
\begin{aligned}
p &= H(u-z''')\alpha_1(z''') \\
dq &= \frac{\partial}{\partial u}\alpha_1(z'''+z'-u)dz''' \\
\frac{dp}{dz'''} &= H(u-z''')\frac{d}{dz'''}\alpha_1(z''') - \delta(u-z''')\alpha_1(z''') \\
q &= -\alpha_1(z'''+z'-u)
\end{aligned}
\tag{C-29}
$$

So

$$
\begin{aligned}
\int_{-\infty}^{\infty} p\ dq =& 0 + \left[\int_{-\infty}^{u}\frac{d}{dz'''}\left(\alpha_1(z''')\right)\alpha_1(z'''+z'-u)dz'''\right] \\
& -\left[\int_{-\infty}^{\infty}\delta(u-z''')\alpha_1(z''')\alpha_1(z'''+z'-u)dz'''\right] \\
=& \left[\int_{-\infty}^{u}\frac{d}{dz'''})\alpha_1(z''')\right)\alpha_1(z'''+z'-u)dz'''\right] - \alpha_1(u)\alpha_1(z')
\end{aligned}
$$

and inserting this expression into Eq. (C-28) gives

$$\begin{aligned} I_{343} =& -\frac{1}{16}\int_{-\infty}^{u}\frac{d}{dz'}\left(\alpha_1(z')\right)\left[\int_{-\infty}^{u}\frac{d}{dz'''}\alpha_1(z''')\alpha_1(z'''+z'-u)dz'''\right]dz' \\ &+\frac{1}{16}\alpha_1(u)\int_{-\infty}^{u}\alpha_1(z')\frac{d}{dz'}\alpha_1(z')dz'+\frac{1}{32}\alpha_1^3(u) \\ =& -\frac{1}{16}\int_{-\infty}^{u}\int_{-\infty}^{u}\frac{d}{dz'}\left(\alpha_1(z')\right)\frac{d}{dz'''}\left(\alpha_1(z''')\right)\alpha_1(z'''+z'-u)dz'''dz' \\ &-\frac{1}{32}\alpha_1^3(u)+\frac{1}{32}\alpha_1^3(u) \end{aligned} \tag{C-30}$$

which, when substituted into Eq. (C-25), gives the last piece of the $G_0V_1G_0V_1G_0V_1\psi_0$ term

$$\begin{aligned} I_{34}(z) =& -\frac{1}{16}\alpha_1^3(z)-\frac{1}{8}\int_{-\infty}^{z}\alpha_1^2(z')dz'\left[\frac{\partial}{\partial z}\alpha_1(z)\right] \\ &-\frac{1}{16}\int_{-\infty}^{z}\int_{-\infty}^{z}\frac{d}{dz'}\left(\alpha_1(z')\right)\frac{d}{dz''}\left(\alpha_1(z'')\right)\alpha_1(z''+z'-z)dz''dz' \end{aligned} \tag{C-31}$$

Finally, summing Eqs. (C-13), (C-20), (C-21) and (C-31), yields

$$\begin{aligned} \alpha_3(z) =& I_1(z)+I_2(z)+I_3(z)=2I_1+I_{31}+I_{32}+I_{33}+I_{34} \\ =& 2I_1+2I_{31}+I_{32}+I_{34} \\ =& (\text{Eq. C-13})+(\text{Eq. C-20})+(\text{Eq. C-21})+(\text{Eq. C-31}) \\ =& \frac{1}{2}\alpha_1^3(z)+\frac{3}{2}\alpha_1(z)\int_{-\infty}^{z}\alpha_1(z')dz'\left[\frac{d}{dz}\alpha_1(z)\right] \\ &+\frac{1}{4}\left(\int_{-\infty}^{z}\alpha_1(z')dz'\right)^2\left[\frac{d^2}{dz^2}\alpha_1(z)\right] \\ &-\frac{1}{16}\left(\int_{-\infty}^{z}\alpha_1(z')dz'\right)^2\left[\frac{d^2}{dz^2}\alpha_1(z)\right] \\ &-\frac{3}{8}\alpha_1(z)\int_{-\infty}^{z}\alpha_1(z')dz'\left[\frac{d}{dz}\alpha_1(z)\right]-\frac{1}{8}\alpha_1^3(z) \\ &-\frac{1}{16}\left(\int_{-\infty}^{z}\alpha_1(z')dz'\right)^2\left[\frac{d^2}{dz^2}\alpha_1(z)\right] \\ &-\frac{6}{16}\alpha_1(z)\int_{-\infty}^{z}\alpha_1(z')dz'\left[\frac{d}{dz}\alpha_1(z)\right]-\frac{1}{8}\alpha_1^3(z) \\ &-\frac{1}{16}\alpha_1^3(z)-\frac{1}{8}\int_{-\infty}^{z}\alpha_1^2(z')dz'\left[\frac{d}{dz}\alpha_1(z)\right] \\ &-\frac{1}{16}\int_{-\infty}^{z}\int_{-\infty}^{z}\frac{d}{dz'}\left(\alpha_1(z')\right)\frac{d}{dz''}\left(\alpha_1(z'')\right)\alpha_1(z''+z'-z)dz''dz' \end{aligned} \tag{C-32}$$

There are four $\alpha_1^3(z')$ terms, three terms that are $\alpha_1 \int \alpha_1 [\alpha_1']$ and three terms that are $(\int \alpha_1)^2 [\alpha_1'']$. Summing up, Eq. (C-32) reduces to

$$\begin{aligned}\alpha_3(z) =& \frac{3}{16}\alpha_1^3(z) + \frac{3}{4}\alpha_1(z)\int_{-\infty}^{z}\alpha_1(z')dz'\left[\frac{d}{dz}\alpha_1(z)\right] \\ &+ \frac{1}{8}\left(\int_{-\infty}^{z}\alpha_1(z')dz'\right)^2\left[\frac{d^2}{dz^2}\alpha_1(z)\right] \\ &- \frac{1}{8}\int_{-\infty}^{z}\alpha_1^2(z')dz'\left[\frac{d}{dz}\alpha_1(z)\right] \\ &- \frac{1}{16}\int_{-\infty}^{z}\int_{-\infty}^{z}\left[\frac{d}{dz'}\alpha_1(z')\right]\left[\frac{d}{dz''}\alpha_1(z'')\right]\alpha_1(z''+z'-z)dz''dz' \end{aligned} \quad \text{(C-33)}$$

The *leading* order (LO) inverse series imaging term in α_3 is

$$\alpha_3^{IS_{LO}}(z) = \frac{1}{8}\left(\int_{-\infty}^{z}\alpha_1(z')dz'\right)^2\left[\frac{d^2}{dz^2}\alpha_1(z)\right]$$

which produce the expected coefficients for a known analytic data example. $\alpha_3^{IS_{LO}}$ is contributed to by all three componenents of the third term of the inverse series, i.e., $G_0V_2G_0V_1\psi_0$, $G_0V_1G_0V_2\psi_0$ and $G_0V_1G_0V_1G_0V_1\psi_0$.

Target identification using the inverse scattering series; inversion of large-contrast, variable velocity and density acoustic media

Haiyan Zhang and Arthur B. Weglein
University of Houston

Abstract

A new task specific multiparameter estimation subseries of the inverse scattering series is derived and tested for a velocity and density varying 1D earth. Tests are encouraging and indicate that one term beyond linear provides significant improvement beyond standard practice.

1 Introduction

The original inverse series research aimed at separating imaging and inversion tasks on primaries (Weglein et al., 2002) was developed for a 1D acoustic constant density medium and a plane wave at normal incidence. In this work we move a step closer to seismic exploration relevance by extending that earlier work to variations in both velocity and density and allowing for point sources and receivers over a 1-D earth. Tests with analytic data indicate significant added value, beyond linear estimates, in terms of both the proximity to actual value and the increased range of angles over which the improved estimates are useful.

This work is another step towards using the task specific parameter estimation inverse series for identifying large contrast targets with either specular or diffractive wave responses.

2 Inverse scattering and seismic processing objectives

Consider the basic wave equations

$$LG = \delta \tag{1}$$

$$L_0 G_0 = \delta \tag{2}$$

where L and L_0 are respectively the differential operators that describe wave propagation in the actual and reference medium, and G and G_0 are the corresponding Green's functions.

We define the perturbation $V = L_0 - L$ (Weglein et al., 2002). The Lippmann-Schwinger equation

$$G = G_0 + G_0 V G \tag{3}$$

relates G, G_0 and V (see, e.g., Taylor, 1972). Iterating this equation back into itself generates the Born series

$$G = G_0 + G_0 V G_0 + G_0 V G_0 V G_0 + \cdots . \tag{4}$$

Then the scattered field $\psi_s \equiv G - G_0$ can be written as

$$\begin{aligned} \psi_s &= G_0 V G_0 + G_0 V G_0 V G_0 + \cdots \\ &= (\psi_s)_1 + (\psi_s)_2 + \cdots \end{aligned} \tag{5}$$

where $(\psi_s)_n$ is the portion of ψ_s that is n^{th} order in V. The measured values of ψ_s are the data, D, where

$$D = (\psi_s)_{ms} = (\psi_s)_{on\ the\ measurement\ surface}.$$

Expanding V as a series in orders of D (Weglein et al. 1997)

$$V = V_1 + V_2 + \cdots \tag{6}$$

then substituting Eq.(6) into Eq.(5) and evaluating Eq.(5) on the measurement surface yields

$$D = [G_0(V_1 + V_2 + \cdots)G_0]_{ms} + [G_0(V_1 + V_2 + \cdots)G_0(V_1 + V_2 + \cdots)G_0]_{ms} + \cdots . \tag{7}$$

Setting terms of equal order in the data equal, leads to the equations that determine V_1, V_2, $\ldots$ from D and G_0.

$$D = [G_0 V_1 G_0]_{ms} \tag{8}$$

$$0 = [G_0 V_2 G_0]_{ms} + [G_0 V_1 G_0 V_1 G_0]_{ms} \tag{9}$$

$$\vdots$$

3 Derivation of α_1, β_1, α_2 and β_2

To find V is to perform 'inversion', i.e., medium identification. If we associate tasks with inversion: (1) Removal of free-surface multiples (2) Removal of internal multiples (3) Image primaries to correct spatial locations and finally (4) Identify medium properties, then these tasks are directly achievable in terms of data, D, and reference information only.

To illustrate task (4), we will consider a 1-D acoustic two-parameter earth model (e.g. bulk modulus and density or velocity and density). Beginning with the 3-D acoustic wave equations in the actual and reference medium (Weglein et al. 1997, Clayton and Stolt, 1981)

$$(\frac{\omega^2}{K(\mathbf{r})} + \nabla \cdot \frac{1}{\rho(\mathbf{r})}\nabla)G(\mathbf{r},\mathbf{r}';\omega) = \delta(\mathbf{r}-\mathbf{r}') \tag{10}$$

$$(\frac{\omega^2}{K_0(\mathbf{r})} + \nabla \cdot \frac{1}{\rho_0(\mathbf{r})}\nabla)G_0(\mathbf{r},\mathbf{r}';\omega) = \delta(\mathbf{r}-\mathbf{r}') \tag{11}$$

Then the perturbation is

$$V = L_0 - L = \frac{\omega^2\alpha}{K_0} + \nabla \cdot \frac{\beta}{\rho_0}\nabla \tag{12}$$

Where $\alpha = 1 - \frac{K_0}{K}$, $\beta = 1 - \frac{\rho_0}{\rho}$, K is P-bulk modulus, c is P-wave velocity and K, c and density ρ have the relation $K = c^2\rho$.

Now we assume both ρ_0 and c_0 are constants, then Eq.(11) becomes

$$(\frac{\omega^2}{c_0^2} + \nabla^2)G_0(\mathbf{r},\mathbf{r}';\omega) = \rho_0\delta(\mathbf{r}-\mathbf{r}') \tag{13}$$

and for the 1-D case, the perturbation V has the following form

$$V(z,\nabla) = \frac{\omega^2\alpha(z)}{K_0} + \frac{1}{\rho_0}\beta(z)\frac{\partial^2}{\partial x^2} + \frac{1}{\rho_0}\frac{\partial}{\partial z}\beta(z)\frac{\partial}{\partial z}. \tag{14}$$

Similarly, we expand $V(z,\nabla)$, $\alpha(z)$ and $\beta(z)$ respectively as

$$V(z,\nabla) = V_1(z,\nabla) + V_2(z,\nabla) + \cdots, \tag{15}$$

$$\alpha(z) = \alpha_1(z) + \alpha_2(z) + \cdots, \tag{16}$$

$$\beta(z) = \beta_1(z) + \beta_2(z) + \cdots. \tag{17}$$

Then we have

$$V_1(z,\nabla) = \frac{\omega^2\alpha_1(z)}{K_0} + \frac{1}{\rho_0}\beta_1(z)\frac{\partial^2}{\partial x^2} + \frac{1}{\rho_0}\frac{\partial}{\partial z}\beta_1(z)\frac{\partial}{\partial z} \tag{18}$$

$$V_2(z,\nabla) = \frac{\omega^2\alpha_2(z)}{K_0} + \frac{1}{\rho_0}\beta_2(z)\frac{\partial^2}{\partial x^2} + \frac{1}{\rho_0}\frac{\partial}{\partial z}\beta_2(z)\frac{\partial}{\partial z} \tag{19}$$

$$\vdots$$

Substitute Eq.(18) into Eq.(8) and we can get the linear solution for $\alpha_1(z)$ and $\beta_1(z)$ as a function of data D

$$\widetilde{D}(q_g,\theta,z_g,z_s) = -\frac{\rho_0}{4}e^{-iq_g(z_s+z_g)}[\frac{1}{\cos^2\theta}\widetilde{\alpha_1}(-2q_g) + (1-\tan^2\theta)\widetilde{\beta}_1(-2q_g)] \tag{20}$$

where the subscripts s and g denote source and receiver respectively, and q_g, θ and $k = \omega/c_0$ are shown in Fig.1, and they have the following relations (Matson, 1997)

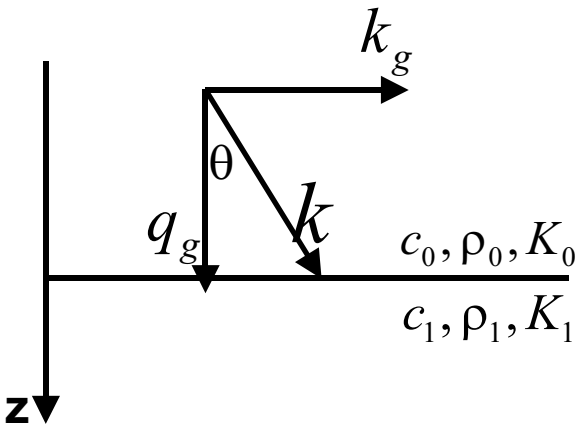

Figure 1: The relation between θ, k and q_g.

$$q_g = q_s = k\cos\theta$$

$$k_g = k_s = k\sin\theta$$

Similarly, substitute Eq.(19) into Eq.(9), and we can get the solution for $\alpha_2(z)$ and $\beta_2(z)$ as

a function of $\alpha_1(z)$ and $\beta_1(z)$

$$\begin{aligned}
\frac{1}{\cos^2\theta}\alpha_2(z) + (1-\tan^2\theta)\beta_2(z) &= -\frac{1}{2\cos^4\theta}\alpha_1^2(z) \\
&+ \frac{1}{\cos^4\theta}\alpha_1(z)\beta_1(z) \\
&- (\frac{3}{2} + \tan^2\theta + \frac{1}{2}\tan^4\theta)\beta_1^2(z) \\
&- \frac{1}{2\cos^4\theta}\alpha_1^{'}(z)\int_0^z dz^{'}\alpha_1(z^{'}) \\
&+ \frac{1}{2\cos^4\theta}\alpha_1^{'}(z)\int_0^z dz^{'}\beta_1(z^{'}) \\
&+ \frac{1}{2}(\tan^4\theta - 1)\beta_1^{'}(z)\int_0^z dz^{'}\alpha_1(z^{'}) \\
&- \frac{1}{2}(\tan^4\theta - 1)\beta_1^{'}(z)\int_0^z dz^{'}\beta_1(z^{'}) \qquad (21)
\end{aligned}$$

For a single-interface example, we can see that only the first three terms on the right hand side contribute to amplitude, the other four terms are the "image moving" terms. As shown in Eq.(20) and Eq.(21), for two different angles of θ, we can determine α_1, β_1 and then α_2, β_2.

4 Numerical test

Consider a one-interface example (shown as Fig.2), the interface surface is at $z = a$, and suppose $z_s = z_g = 0$.

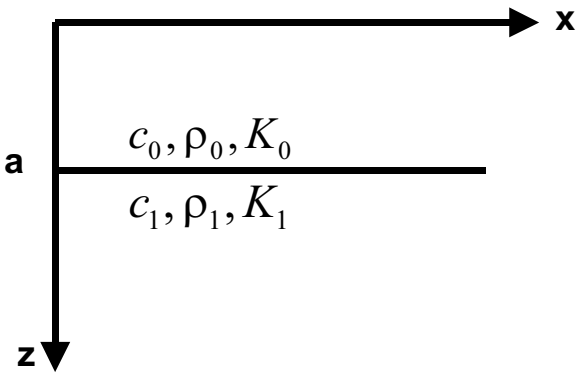

Figure 2: One interface example.

In this case, the reflection coefficient has the following form (Keys, 1989)

$$R(\theta) = \frac{(\rho_1/\rho_0)(c_1/c_0)\sqrt{1-\sin^2\theta} - \sqrt{1-(c_1^2/c_0^2)\sin^2\theta}}{(\rho_1/\rho_0)(c_1/c_0)\sqrt{1-\sin^2\theta} + \sqrt{1-(c_1^2/c_0^2)\sin^2\theta}}. \tag{22}$$

Using perfect data (Clayton and Stolt, 1981)

$$\widetilde{D}(q_g,\theta) = \rho_0 R(\theta)\frac{e^{2iq_g a}}{2iq_g}, \tag{23}$$

and substituting Eq.(23) into Eq.(20), we get

$$\frac{1}{\cos^2\theta}\alpha_1(z) + (1-\tan^2\theta)\beta_1(z) = 4R(\theta)H(z-a). \tag{24}$$

Then, choosing two different angles to solve for α_1 and β_1

$$\beta_1(\theta_1,\theta_2) = 4\frac{R(\theta_1)\cos^2\theta_1 - R(\theta_2)\cos^2\theta_2}{\cos 2\theta_1 - \cos 2\theta_2} \tag{25}$$

$$\alpha_1(\theta_1,\theta_2) = \beta_1(\theta_1,\theta_2) + 4\frac{R(\theta_1) - R(\theta_2)}{\tan^2\theta_1 - \tan^2\theta_2}. \tag{26}$$

Similarly, we can get α_2 and β_2

$$\begin{aligned}\frac{1}{\cos^2\theta}\alpha_2(z) + (1-\tan^2\theta)\beta_2(z) = &-\frac{1}{2\cos^4\theta}\alpha_1^2(z) + \frac{1}{\cos^4\theta}\alpha_1(z)\beta_1(z) \\ &-(\frac{3}{2} + \tan^2\theta + \frac{1}{2}\tan^4\theta)\beta_1^2(z)\end{aligned} \tag{27}$$

$$\begin{aligned}\beta_2(\theta_1,\theta_2) = \{&[-\frac{1}{2}\alpha_1^2(\theta_1,\theta_2) + \alpha_1(\theta_1,\theta_2)\beta_1(\theta_1,\theta_2)][\frac{1}{\cos^2\theta_1} - \frac{1}{\cos^2\theta_2}] - \frac{1}{2}\beta_1^2(\theta_1,\theta_2) \\ &[\cos^2\theta_1 - \cos^2\theta_2 + \frac{\sin^4\theta_1}{\cos^2\theta_1} - \frac{\sin^4\theta_2}{\cos^2\theta_2}]\}/\{\cos 2\theta_1 - \cos 2\theta_2\}\end{aligned} \tag{28}$$

$$\begin{aligned}\alpha_2(\theta_1,\theta_2) = \beta_2(\theta_1,\theta_2) + \{&[-\frac{1}{2}\alpha_1^2(\theta_1,\theta_2) + \alpha_1(\theta_1,\theta_2)\beta_1(\theta_1,\theta_2)][\frac{1}{\cos^4\theta_1} - \frac{1}{\cos^4\theta_2}] \\ &-\beta_1^2(\theta_1,\theta_2)[\tan^2\theta_1 - \tan^2\theta_2 + \frac{1}{2}\tan^4\theta_1 - \frac{1}{2}\tan^4\theta_2]\}/\{\tan^2\theta_1 - \tan^2\theta_2\}\end{aligned} \tag{29}$$

Now, for a specific model, $\rho_0 = 1.0g/cm^3$, $\rho_1 = 1.1g/cm^3$, $c_0 = 1500m/s$, $c_1 = 1700m/s$, let's see how the nonlinear terms contribute to the changes in the P-wave bulk modulus, density, impedance and velocity.

In the figures, we give the results corresponding to different pairs of θ_1 and θ_2. From Fig.3, we can see that when we add α_2 to α_1, the result is much closer to the exact value of α. Furthermore, the result is better behaved over a larger range of precritical angles; the values of $\alpha_1 + \alpha_2$ change slowly.

Similarly, from Fig.4, we can also see the results of $\beta_1 + \beta_2$ are much better than those of β_1. And also the results of $\frac{\Delta I}{I}$ (see Fig.5) and $\frac{\Delta c}{c}$ (see Fig.6). Especially, we noticed that values of $(\frac{\Delta c}{c})_1$ are always greater than zero, that is, the sign of $(\Delta c)_1$ is positive, which is same as that of the exact value Δc. We will state about it in the next section.

5 Special parameters for linear inversion

In general, linear inversion will produce errors in earth property prediction since the relationship between data and earth property changes is nonlinear.

Manifestation:

When $\Delta(property) = 0$, linear prediction of $\Delta(property) \neq 0$

$\Rightarrow$ When $\Delta(property) > 0$, linear prediction of $\Delta(property)$ *can be* < 0.

There is a special parameter for linear inversion of acoustic media, that never suffers the latter problem.

From Eq.(22) we can see when $c_0 = c_1$, the reflection coefficient is independent of θ, then from the linear Eq.(26), we have

$$\left(\frac{\Delta c}{c}\right)_1 = \frac{1}{2}(\alpha_1 - \beta_1) = 0 \ when \ \Delta c = 0$$

i.e., when $\Delta c = 0$, $(\Delta c)_1 = 0$. This generalizes to when $\Delta c > 0$, then $(\Delta c)_1 > 0$, or when $\Delta c < 0$, then $(\Delta c)_1 < 0$, as well. Which can be shown as below:

The reflection coefficient is

$$R(\theta) = \frac{(\rho_1/\rho_0)(c_1/c_0)\sqrt{1-\sin^2\theta} - \sqrt{1-(c_1^2/c_0^2)\sin^2\theta}}{(\rho_1/\rho_0)(c_1/c_0)\sqrt{1-\sin^2\theta} + \sqrt{1-(c_1^2/c_0^2)\sin^2\theta}}.$$

Let

$$A(\theta) = (\rho_1/\rho_0)(c_1/c_0)\sqrt{1-\sin^2\theta},$$

$$B(\theta) = \sqrt{1 - (c_1^2/c_0^2)\sin^2\theta}.$$

Then

$$R(\theta_1) - R(\theta_2) = 2\frac{A(\theta_1)B(\theta_2) - B(\theta_1)A(\theta_2)}{[A(\theta_1) + B(\theta_1)]\,[A(\theta_2) + B(\theta_2)]}$$

where the denominator is greater than zero. The numerator is

$$2\,[A(\theta_1)B(\theta_2) - B(\theta_1)A(\theta_2)] = 2(\rho_1/\rho_0)(c_1/c_0)\left[\sqrt{1-\sin^2\theta_1}\sqrt{1-(c_1^2/c_0^2)\sin^2\theta_2} - \sqrt{1-\sin^2\theta_2}\sqrt{1-(c_1^2/c_0^2)\sin^2\theta_1}\right].$$

Then we let

$$C = \sqrt{1-\sin^2\theta_1}\sqrt{1-(c_1^2/c_0^2)\sin^2\theta_2} > 0$$

$$D = \sqrt{1-\sin^2\theta_2}\sqrt{1-(c_1^2/c_0^2)\sin^2\theta_1} > 0$$

Then

$$C^2 - D^2 = \left(\frac{c_1^2}{c_0^2} - 1\right)(sin^2\theta_1 - sin^2\theta_2)$$

Then, as $c_1 > c_0$ and $\theta_1 > \theta_2$, we have

$$\left(\frac{c_1^2}{c_0^2} - 1\right)(sin^2\theta_1 - sin^2\theta_2) > 0$$

Then

$$R(\theta_1) - R(\theta_2) > 0$$

and as $c_1 < c_0$ and $\theta_1 > \theta_2$, we have

$$\left(\frac{c_1^2}{c_0^2} - 1\right)(sin^2\theta_1 - sin^2\theta_2) < 0$$

Then

$$R(\theta_1) - R(\theta_2) < 0$$

For the single interface example, we have

$$\alpha_1(\theta_1,\theta_2) - \beta_1(\theta_1,\theta_2) = 4\frac{R(\theta_1) - R(\theta_2)}{\tan^2\theta_1 - \tan^2\theta_2}$$

So as $c_1 > c_0$, $\alpha_1(\theta_1, \theta_2) - \beta_1(\theta_1, \theta_2) > 0$, then $(\Delta c)_1 > 0$; similarly, as $c_1 < c_0$, $\alpha_1(\theta_1, \theta_2) - \beta_1(\theta_1, \theta_2) < 0$, then $(\Delta c)_1 < 0$.

We are currently generalizing these equations to an elastic Earth model. The strategy is to combine information from special linear parameters with added value from inversion beyond linear. We also note that when the velocity doesn't change across an interface, the Born inverse doesn't change and looking at the integrand of "image moving" terms (see Eq.(21)) $\alpha_1 - \beta_1$, the image doesn't move.

The imaging and inversion subseries automatically accommodate an adequate velocity model. They determine the degree of adequacy of the velocity model from all the data, and act accordingly.

6 Conclusion

Including terms beyond linear in earth property identification subseries provides added value. We are encouraged by these results. The next step is to study the elastic case using three parameters (see, e.g., Boyse, 1986 and Boyse and Keller, 1986).

Acknowledgements

We thank Bogdan Nita and Simon Shaw for valuable discussions, and we are grateful that R. Keys, R. Stolt, T.H. Tan and Jingfeng Zhang are working with us on this project.

References

Boyse, W. E., Wave propagation and inversion in slightly inhomogeneous media, p.40. (1986)

Boyse, W.E. and Keller J.B., Inverse elastic scattering in three dimensions, 1986: J. Acoust. Soc. Am., **79**, 215–218.

Clayton, R.W., R.H. Stolt, A Born-WKBJ inversion method for acoustic reflection data for attenuating multiples in seismic reflection data, Geophysics **46**, 11, 1559-1567 (1981).

Keys, R.G., Polarity reversals in reflections from layered media, 1989: Geophysics, **54**, 7, 900–905.

Matson, K. H., An inverse scattering series method for attenuating elastic multiples from multicomponent land and ocean bottom seismic data, Ph.D thesis, University of British Columbia, p. 18. (1997)

Taylor, J. R., Scattering theory: the quantum theory of nonrelativistic collisions, 1972: John Wiley & Sons, Inc., p. 133.

Weglein, A.B., F.A. Araújo Gasparotto, P.M. Carvalho and R.H. Stolt, An inverse-scattering series method for attenuating multiples in seismic reflection data, Geophysics **62**, 6, 1975-1989 (1997).

Weglein, A.B., D.J. Foster, K.H. Matson, S.A. Show, P.M. Carvalho and D. Corrigan, Predicting the correct spatial location of reflectors without knowing or determining the precise medium and wave velocity: initial concept, algorithm and analytic and numerical example, Journal of Seismic Exploration 10, 367-382 (2002).

α (Bulk modulus)

exact value of α=0.292 critical angle=61.9⁰

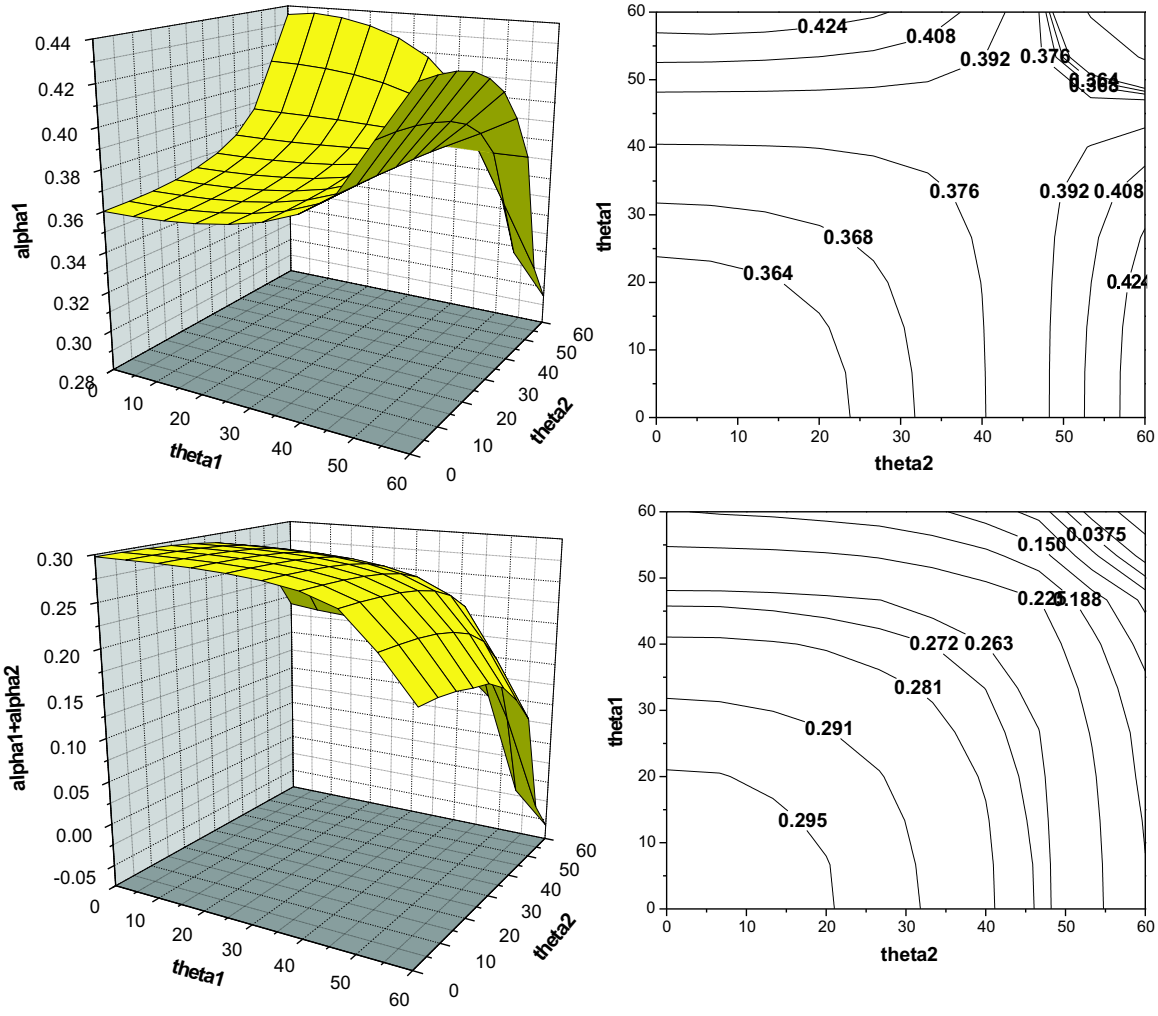

Figure 3: α_1 (top) and $\alpha_1 + \alpha_2$ (bottom).

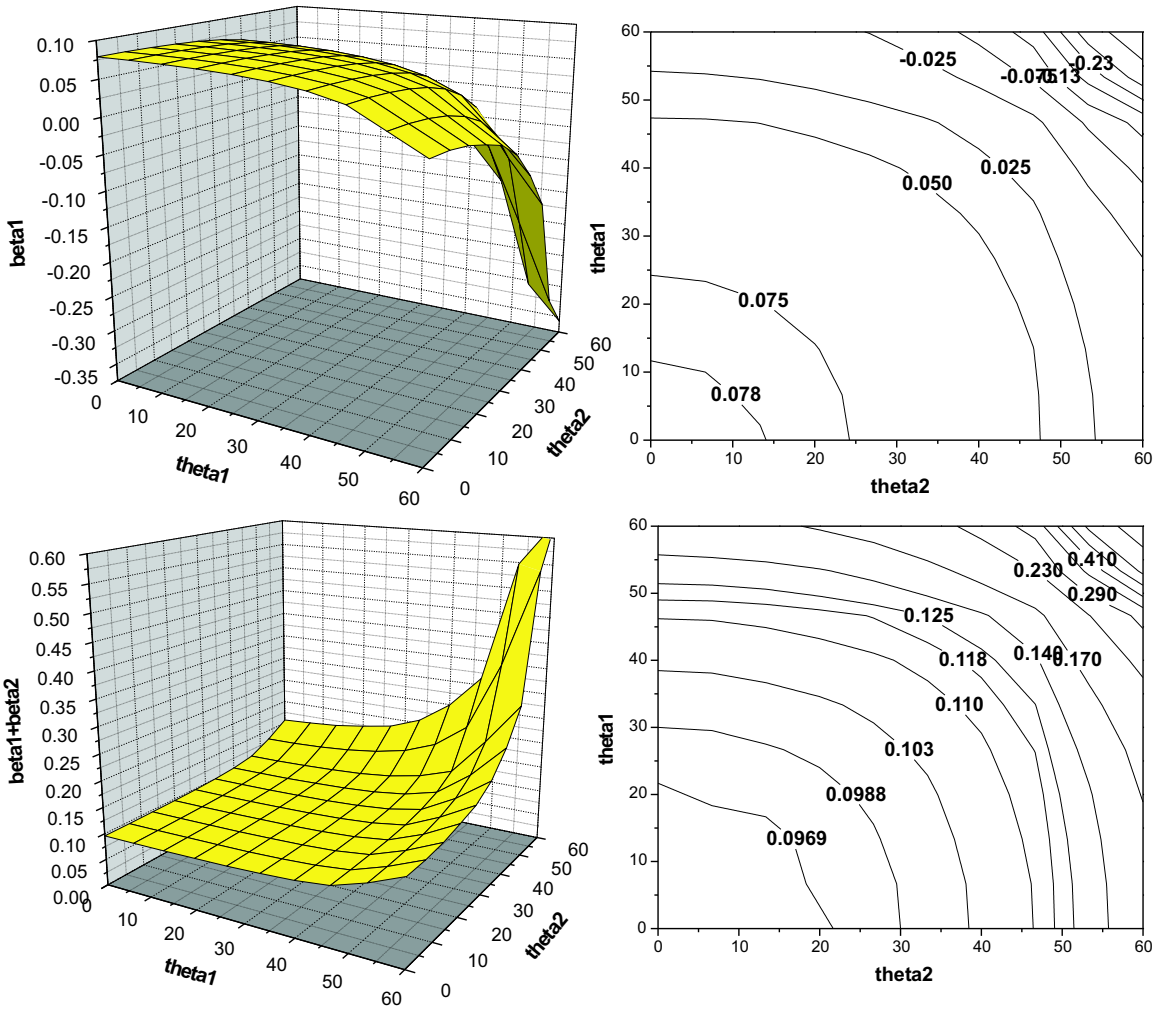

Figure 4: β_1 (top) and $\beta_1 + \beta_2$ (bottom).

$\frac{\Delta I}{I}$ (P-wave impedance)

exact value of $\frac{\Delta I}{I} = 0.198$ **critical angle=61.9^0**

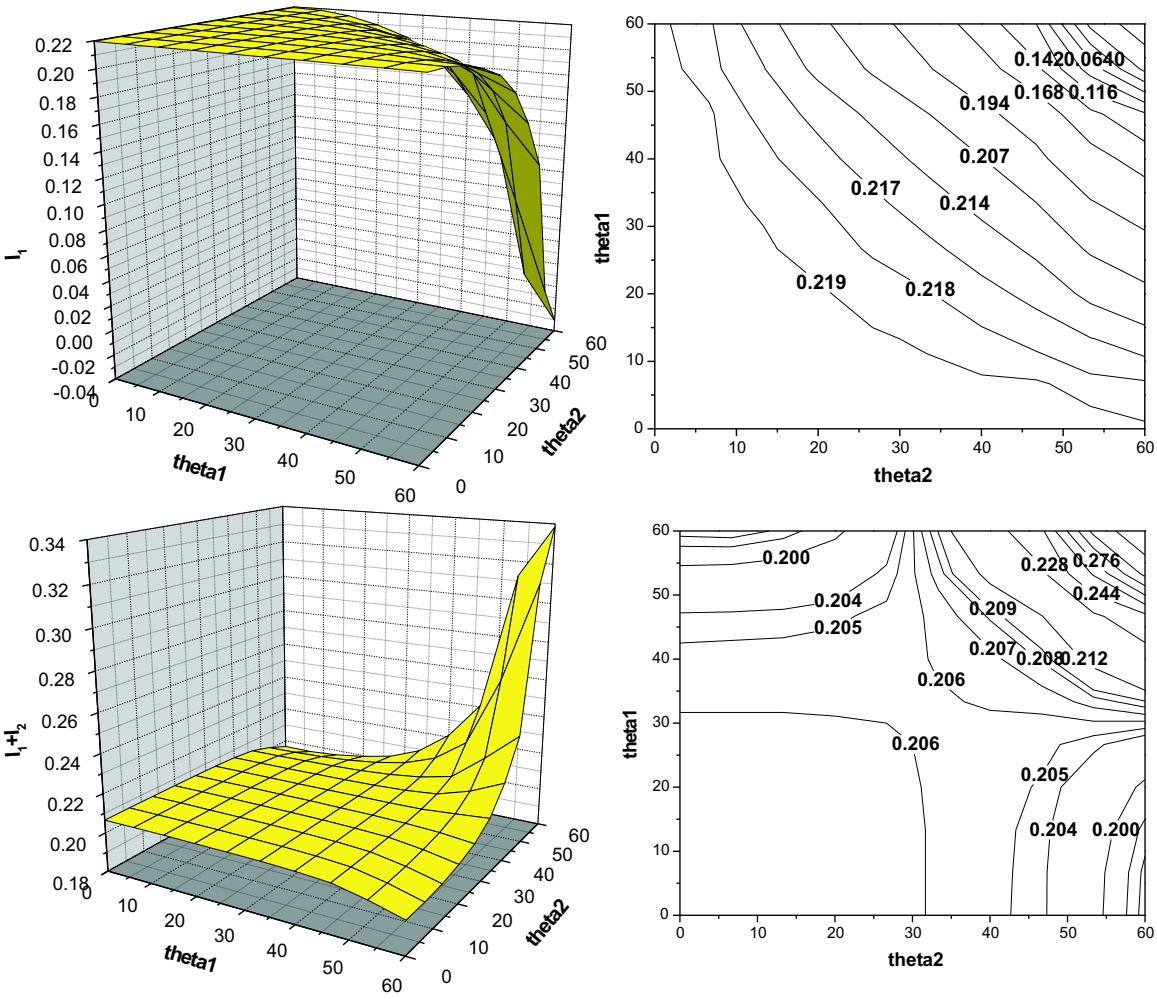

Figure 5: Linear approximation to change in impedance $\left(\frac{\Delta I}{I}\right)_1 = \frac{1}{2}(\alpha_1 + \beta_1)$ (top). Sum of linear and first non-linear terms $\left(\frac{\Delta I}{I}\right)_1 + \left(\frac{\Delta I}{I}\right)_2 = \left(\frac{\Delta I}{I}\right)_1 + \frac{1}{2}\left[\frac{1}{4}(\alpha_1 - \beta_1)^2 + (\alpha_2 + \beta_2)\right]$ (bottom).

$\frac{\Delta c}{c}$ **(P-wave velocity)**

exact value of $\frac{\Delta c}{c} = 0.118$ **critical angle=61.9^0**

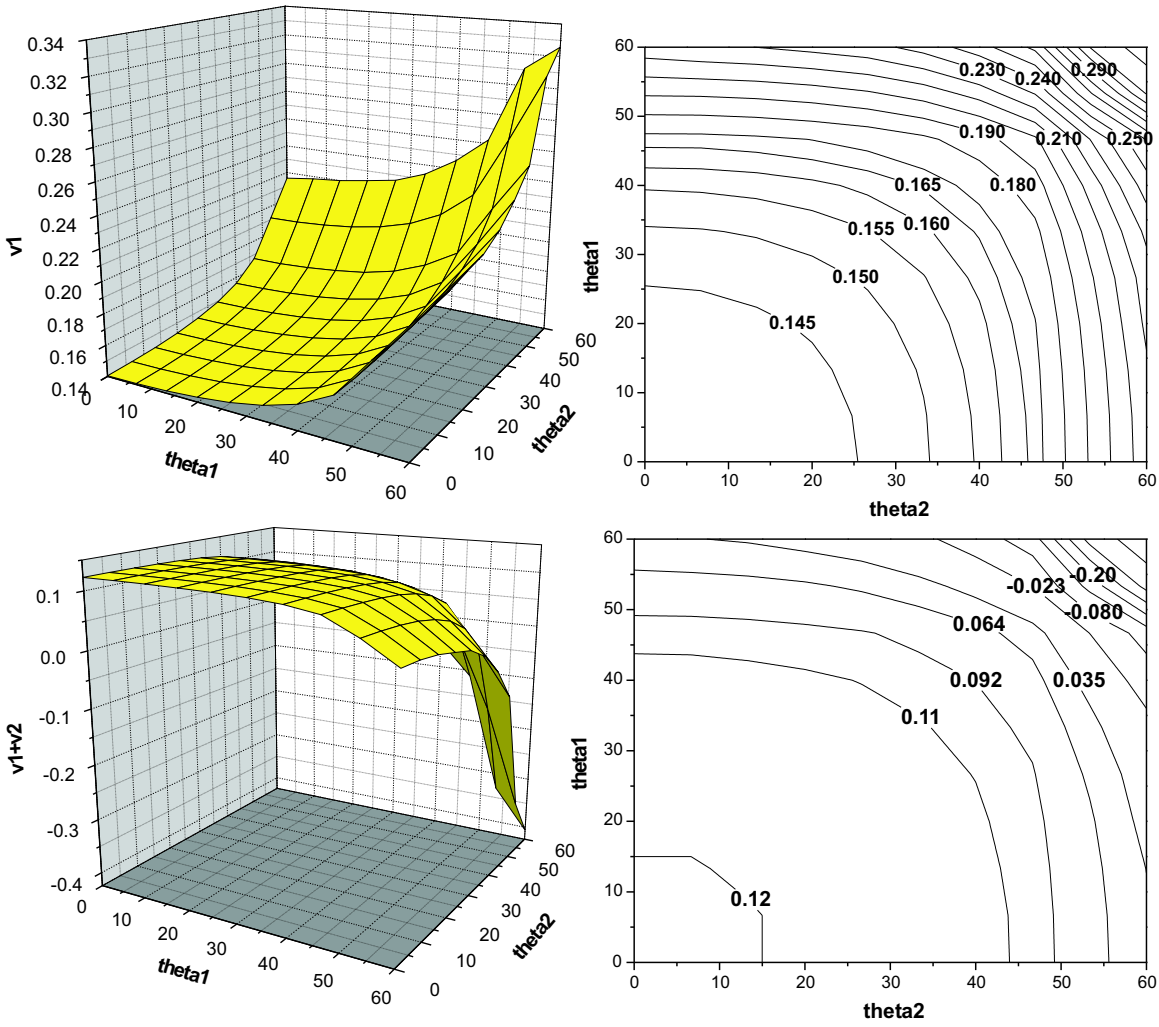

Figure 6: Linear approximation to change in velocity $\left(\frac{\Delta c}{c}\right)_1 = \frac{1}{2}(\alpha_1 - \beta_1)$ (top). Sum of linear and first non-linear terms $\left(\frac{\Delta c}{c}\right)_1 + \left(\frac{\Delta c}{c}\right)_2 = \left(\frac{\Delta c}{c}\right)_1 + \frac{1}{2}\left[\frac{1}{4}(\alpha_1 + \beta_1)^2 - \beta_1^2 + (\alpha_2 - \beta_2)\right]$ (bottom).

Initial analysis of the inverse scattering series for variable background

Fang Liu, Haiyan Zhang, Arthur Weglein
University of Houston

Abstract

We present a derivation of the first two terms of the inverse scattering series that accommodate a smoothly varying background velocity. A WKBJ Green's function is assumed for reference propagation. Shaw et al. (2003) separate the second term in the series, using a constant reference medium, into contributions appropriate for the tasks of imaging and parameter estimation. We provide the generalization of that task separation for a variable background, $c_0(z)$.

1 Introduction

The current imaging and inversion sub-series derived from the inverse scattering series assume a constant background model (e.g. Shaw et al. 2003., H. Zhang and Weglein 2003). These sub-series demonstrate robust convergence when both the magnitude and duration of the difference between actual and reference are large. However, the next important practical issue concerns the rate of convergence. Early analysis and testing indicate that the rate of convergence will improve when the difference between actual and reference media is reduced.

Advances in multiple removal technology (See e.g. Weglein 1999) allow improved estimates of the subsurface velocity model. These two facts encourage the development of imaging and inversion sub-series that can accommodate a variable velocity model.

This paper represents the first effort in that direction. It provides the first two terms in the inverse series for a one parameter (variable velocity, constant density) acoustic medium. The reference medium $c_0(z)$ is assumed to be smooth, thereby allowing a WKBJ waveform to be appropriate. The separation of the second term in the $c_0(z)$ background inverse series into reflector imaging at depth is the near-term objective.

While the mathematical derivation of the second term is laborious and non-trivial the result is remarkably compact and can easily be shown to reduce to the earlier constant background case.

2 Motivation for using a closer approximation to the actual medium

With the discovery of the leading order imaging sub-series, which has the nice property of converging for any contrast, and the inversion sub-series, which is the only candidate

for a direct inversion for multi-dimensional, corrugated, high-contrast Earth, a huge amount of additional computation is demanded. Only one term in the imaging or inversion sub-series may take CPU cycles equivalent to that of traditional migration. A typical 3D time migration may need several months to be executed on a super computer like SP2 or a PC cluster. That's why we need to accelerate the series summation by incorporating the roughly inadequate estimated velocity to form an adequate image.

How can we accelerate the series computation? One factor is the choice of the reference medium. The rate of convergence is much better if the reference medium is closer to the actual medium.

Constant background inversion assumes no a priori information is available. This nice property also has its negative side: the rate of convergence is relatively slow. After free-surface and internal multiples are removed, a more accurate velocity trend is available. We can incorporate this a priori information into the inverse scattering series to speed up the series calculation.

The use of $c_0(z)$ is motivated by the fact that, on a global scale, the structure of the Earth is dominated by the overwhelming influence of gravity. The structure of the earth can be much better approximated by a vertically varying but horizontally uniform model than a uniform velocity field filling the whole space. Our $c_0(z)$ reference model offers a much closer approximation to the actual earth.

3 Equations need to be solved:

Following Weglein et al. (1997), we will calculate the perturbation terms V_1, V_2, … using the inverse series:

$$\begin{aligned} D &= G_0 V_1 G_0 \\ 0 &= G_0 V_2 G_0 + G_0 V_1 G_0 V_1 G_0 \\ 0 &= G_0 V_3 G_0 + G_0 V_1 G_0 V_2 G_0 + G_0 V_2 G_0 V_1 G_0 + G_0 V_1 G_0 V_1 G_0 V_1 G_0 \\ &\bullet\bullet\bullet \end{aligned} \tag{1}$$

where D is the data obtained on the measurement surface, and all the expressions above are supposed to be evaluated on the measurement surface. G_0 is the Green's function of the reference medium, which cannot be easily obtained if the reference velocity is not constant or piecewise constant. In the next section, we explain the complexity of obtaining an analytical Green's function for an arbitrary medium.

4 WKBJ Green's function:

Let's consider the simplest case, when both the earth and the experiment are 1D. Then the Green's function satisfies the following inhomogeneous second-order differential equation (expressed in the frequency domain).

$$\frac{\partial^2 G(z,z_s,\omega)}{\partial z^2}+\left(\frac{\omega}{c(z)}\right)^2 G(z,z_s,\omega)=\delta(z-z_s) \tag{2}$$

where z_s is the coordinate of the source. In order to solve the equation above, we have to consider its corresponding homogeneous equation:

$$\frac{\partial^2 G(z,z_s,\omega)}{\partial z^2}+\left(\frac{\omega}{c(z)}\right)^2 G(z,z_s,\omega)=0 \tag{3}$$

It can be written in a more general form:

$$\frac{d^2 P(z)}{dz^2}+f(z)P(z)=0 \tag{4}$$

The seemingly very simple equation is of great importance in both mathematics and physics because any linear homogeneous second-order equation may be put in this form. Finding a precise solution to the problem of Green's function for variable background is mathematically equivalent to solving the problem above analytically. Since this problem had already been proved analytically unsolvable for arbitrary f(z), our precise Green's function is in general impossible to find.

In quantum mechanics, WKBJ methods had been developed by Wentzel, Kramers, Brillouin, Jeffreys to approximate the equation above. The WKBJ solutions to the homogeneous equation (4) (Methews and Walker, equation 1-90, page 28) are:

$$P(z)=\frac{1}{\sqrt[4]{f(z)}}\left\{c_1\exp\left(i\int^z\sqrt{f(x)}dx\right)+c_2\exp\left(-i\int^z\sqrt{f(x)}dx\right)\right\} \tag{5}$$

where c_1 and c_2 are arbitrary constants. Interested readers may refer to Yedlin's paper for constructing WKBJ Green's function in two dimensions.

Note that there are 2 linearly independent solutions to the homogeneous equation (3):

$$P(z,z_s,\omega)=\begin{cases} a_1\sqrt{\dfrac{c(z)}{\omega}}\exp\left(i\omega\displaystyle\int_{z_s}^{z}\frac{du}{c(u)}\right) \\ a_2\sqrt{\dfrac{c(z)}{\omega}}\exp\left(-i\omega\displaystyle\int_{z_s}^{z}\frac{du}{c(u)}\right)\end{cases} \tag{6}$$

where a_1 and a_2 are arbitrary constants. We are now in the position to construct the Green's function satisfying equation (2). It will consist of 2 parts, one for $z<z_s$, and one for $z>z_s$. The final result should be continuous at $z=z_s$, but the first derivative with respect to z will have a jump of magnitude 1, so the second derivative will have a δ-function behavior at $z=z_s$.

$$G(z,z_s,\omega)=\begin{cases} a_1\sqrt{\dfrac{c(z)}{\omega}}\exp\left(i\omega\displaystyle\int_{z_s}^{z}\frac{du}{c(u)}\right) & z>z_s \\ a_2\sqrt{\dfrac{c(z)}{\omega}}\exp\left(-i\omega\displaystyle\int_{z_s}^{z}\frac{du}{c(u)}\right) & z<z_s \end{cases} \tag{7}$$

Continuity at $z=z_s$ means that $a_1=a_2=a$. Now lets look at the left and right first derivative when $z=z_s$.

$$\begin{cases} \lim\limits_{z\to z_s^+}\dfrac{\partial G(z,z_s)}{\partial z}=\left.\dfrac{\partial G_1(z,z_s)}{\partial z}\right|_{z=z_s}=a\left\{i\sqrt{\dfrac{\omega}{c(z_s)}}+\dfrac{c'(z_s)}{2\sqrt{\omega c(z_s)}}\right\} \\ \lim\limits_{z\to z_s^-}\dfrac{\partial G(z,z_s)}{\partial z}=\left.\dfrac{\partial G_2(z,z_s)}{\partial z}\right|_{z=z_s}=a\left\{\dfrac{-i\omega}{\sqrt{c(z_s)}}+\dfrac{c'(z_s)}{2\sqrt{\omega c(z_s)}}\right\} \end{cases}$$

$$1=\lim_{z\to z_s^+}\frac{\partial G(z,z_s)}{\partial z}-\lim_{z\to z_s^-}\frac{\partial G(z,z_s)}{\partial z}=i2a\sqrt{\frac{\omega}{c(z_s)}}$$

$$\Rightarrow \qquad a=\frac{1}{2i}\sqrt{\frac{c(z_s)}{\omega}}$$

So we have our causal WKBJ Green's function:

$$G(z,z_s,\omega)=\frac{\sqrt{c(z)c(z_s)}}{2i\omega}\exp\left(i\omega\left|\int_{z_s}^{z}\frac{du}{c(u)}\right|\right) \tag{8}$$

5 Solving the problems with WKBJ Green's function:

5.1 Solving for $\alpha_1(z)$

The first problem stated in equation (1) is:

$$D(z_g,z_s,\omega)=\int_{-\infty}^{\infty}dz'\,G_0(z_g,z',\omega)V_1(z')G_0(z',z_s,\omega) \tag{9}$$

Without losing any generality, we assume both the source and the receiver located at 0 depth, that is: $z_g=z_s=0$. As in the case of constant background, let's define:

$$\alpha_1(z) = \left(\frac{\omega}{c(z)}\right)^{-2} V_1(z). \tag{10}$$

We can also define a function similar to travel time in the reference medium, but having a negative value when traveling upwards.

$$\tau(z_1, z_2) = \int_{z_1}^{z_2} \frac{du}{c(u)} \tag{11}$$

After applying a Fourier transform we change equation (9) into:

$$\int_{-\infty}^{\infty} d\omega D(0,0,\omega) e^{-i\omega 2\tau(0,z)} = \int_{-\infty}^{\infty} d\omega \left\{ \int_{-\infty}^{\infty} dz' G_0(0,z',\omega) V_1(z') G_0(z',0,\omega) \right\} e^{-i\omega 2\tau(0,z)} \tag{12}$$

Solving the equation above (see Appendix A), we obtain:

$$-\frac{c(0)\pi}{4} \alpha_1(z) = \int_{-\infty}^{\infty} d\omega D(0,0,\omega) e^{-i\omega 2\tau(0,z)} \tag{13}$$

We can also use other incident wave-fields, the one commonly used in 1D constant background scattering series can be obtained by multiplying G_0 with 2ik. It's better than G_0 itself in presenting data in the time domain because its time-domain representation is a spike, but that of G_0 is a Heaviside function. A more realistic wavelet in seismic exploration would be G_0 multiplied by 2ik. So the data in the frequency domain will also be multiplied by 2ik =2iω/c(0), let's denote this data after changing wavelet by $D_w(z_g, z_s, \omega)$. We have:

$$D_W(0,0,\omega) = D(0,0,\omega)\frac{2i\omega}{c(0)}$$

$$D(0,0,\omega) = \frac{D_W(0,0,\omega)}{i2\omega / c(0)}$$

$$\alpha_1(z) = -\frac{4}{c(0)\pi} \int_{-\infty}^{\infty} d\omega \frac{D_W(0,0,\omega)}{i2\omega / c(0)} e^{-i\omega 2\tau(0,z)} \xrightarrow{t=2\tau(0,z)} -\frac{4}{\pi} \int_{-\infty}^{\infty} d\omega \frac{D_W(0,0,\omega)}{i2\omega} e^{-i\omega t}$$

$$\frac{d\alpha_1(z)}{dt} = \frac{2}{\pi} \int_{-\infty}^{\infty} d\omega D_W(0,0,\omega) e^{-i\omega t} = \frac{2}{\pi} \int_{-\infty}^{\infty} d\omega D_W(0,0,\omega) e^{-i\omega t}$$

$$\frac{d\alpha_1(z)}{dt} = \frac{2}{\pi} \int_{-\infty}^{\infty} d\omega D_W(0,0,\omega) e^{-i\omega t} = 4\widetilde{D}_W(0,0,t)$$

$$\alpha_1(z) = 4 \int_{-\infty}^{2\tau(0,z)} \widetilde{D}_W(0,0,t) dt \tag{14}$$

where $\widetilde{D}_W(0,0,t)$ is the seismic trace in the time domain. Just as in the case of constant background, α_1 is a trace integral in the time domain. The α_1 formula in constant background can be expressed as:

$$\alpha_1(z) = \frac{8}{c_0} \int_{-\infty}^{2z/c_0} \tilde{D}(0,0,t)dt$$

It positions the events in the time domain uniformly into space according to the reference velocity c_0. Compared with the corresponding α_1 formula, equation (14) has the flexibility to position the events non-uniformly in time domain according to a variable velocity trend, an additional power looks like migration.

5.2 Solving for $\alpha_2(z)$

The second problem stated in equation (1) is:

$$G_0 V_2 G_0 = -G_0 V_1 G_0 V_1 G_0$$

Applying the same Fourier transform as before, we have:

$$\int_{-\infty}^{\infty} G_0 V_2 G_0 e^{-i\omega 2\tau(0,z)} d\omega = \int_{-\infty}^{\infty} -G_0 V_1 G_0 V_1 G_0 e^{-i\omega 2\tau(0,z)} d\omega \tag{15}$$

Solving for the equation above (see Appendix B), we have:

$$-\frac{c(0)\pi}{4}\alpha_2(z) = \frac{c(0)\pi}{8}\left\{\alpha_1^2(z) + c(z)\alpha'_1(z)\int_{-\infty}^{z} dz' \frac{\alpha_1(z')}{c(z')}\right\}$$

So we can express $\alpha_2(z)$ (in terms of $\alpha_1(z)$) as:

$$\alpha_2(z) = -\frac{1}{2}\left\{\alpha_1^2(z) + c(z)\alpha'_1(z)\left\{\int_{-\infty}^{z} dz' \frac{\alpha_1(z')}{c(z')}\right\}\right\} \tag{16}$$

In a special case of constant background, $c'(z) \equiv 0$, we have:

$$\alpha_2(z) = -\frac{1}{2}\left\{\alpha_1^2(z) + \alpha'_1(z)\left\{\int_{-\infty}^{z} dz' \alpha_1(z')\right\}\right\} \tag{17}$$

Equation (17) agrees with the $\alpha_2(z)$ term in the constant background inversion. If $c'(z) \neq 0$, there will be additional terms in equation (16). We will study these terms further and identify their use in imaging and inversion.

6 Future work

Future work will include: (1) Calculating terms beyond $\alpha_2(z)$. (2) Identifying the specific sub-series that perform different inversion tasks. (3) Numerically testing the convergence properties of these sub-series. (4) Working out the corresponding terms in multi-dimensions, which are currently approximately solved only for the first (linear) term.

7 Conclusion

Two terms in the inversion scattering series with variable background have been calculated with a WKBJ Green's function in 1D. The inverse equations can be precisely solved using Fourier transform. The first term introduces more flexibility to position the events in the time domain non-uniformly by a varying velocity trend. More work, including numerical tests, is needed to study newly discovered terms.

8 Acknowledgement

We would like to thank Dr. Bogdan Nita for pointing out a simplification in the derivation of these equations. We are grateful to the sponsors for the MOSRP for supporting this research.

References

Clayton, R. W., and Stolt R. H., (1981) A Born WKBJ inversion method for acoustic reflection data: Geophysics, **46**, 1559-1567

Cohen J. K., Hagin F. G., (1985) Velocity inversion using a stratified reference: Geophysics, **50**, 1689-1700

Foster D. J., Carrion P. M., (1984) Short Note, Born inversion with a variable background velocity Geophysics, **49**, 1794-1797

Mathews J., Walker R. L., (1970) Mathematical Method of Physics: New York W.A. Benjamin, 27-37

Shaw, S.A, Weglein, A.B., Foster, D.J., Matson, K.H., and Keys, R.G., (2003) Isolation of a leading order depth imaging series and analysis of its convergence properties, Mission-Oriented Seismic Research Program Report **2** P. 157-195.

Stolt R. H., (1980) A WKBJ inversion for the acoustic wave equation in a layered media: SEP Reports ,**25**,167-174

Stolt R. H., Weglein A. B., (1985) Migration and inversion of seismic data: Geophysics, **50**, 2458-2472

Weglein A. B. (1982) Nearfield inverse scattering formalism for the three-dimensional wave equation: The inclusion of a-priori velocity information: J. Acoust. Sco. Am., **71**, 5 1179-1182

Weglein A. B., Gasparotto F. A., Carvalho P. M., Stolt R. H. (1997) An inverse-scattering series for attenuating multiples in seismic reflection data: Geophysics, **62**, 1957-1989

Weglein A. B. (1999) Multiple attenuation: an overview of recent advances and the road ahead: The Leading Edge, **18**, 40-44

Weglein A. B., Foster D. J., Matson, K. H., Shaw S. A., Carvalho P. M., Corrigan D., (2002) Predicting the Correct Spatial Location of Reflectors without Knowing or Determining the Precise Medium and Wave Velocity: Initial Concept, Algorithm and Numerical Example: Journal of Seismic Exploration, **10**, 367-382

Yedlin, M., (1980) Uniform Asymptotic Expansion of the Green's Function for the Two-dimensional Acoustic Equation: SEP Reports ,**25**, 159-165

Zhang, H. and Weglein, A.B., (2003) Target identification using the inverse scattering series; inversion of large-contrast, variable velocity and density acoustic media, Mission-Oriented Seismic Research Program Report **2**, p.196-209

Appendix A --- deriving $\alpha_1(z)$

Using the WKBJ Green's function (7), we have:

$$\int_{-\infty}^{\infty} dz' G_0(0,z',\omega) V_1(z') G_0(z',0,\omega)$$

$$= \int_{-\infty}^{\infty} dz' \frac{1}{2i} \sqrt{\frac{c(0)}{\omega}\frac{c(z')}{\omega}} \exp\left(i\omega \left| \int_{z'}^{0} \frac{dz''}{c(z'')} \right| \right) \left(\frac{\omega}{c(z')} \right)^2 \alpha_1(z') \frac{1}{2i} \sqrt{\frac{c(0)}{\omega}\frac{c(z')}{\omega}} \exp\left(i\omega \left| \int_{z'}^{0} \frac{dz''}{c(z'')} \right| \right)$$

We assume that no perturbation occurs for $z<0$, that is: $z < 0 \Rightarrow \alpha_1(z) = 0$, we can simplify the expression above further:

$$= -\frac{1}{4} \int_{-\infty}^{\infty} dz' \exp\left(i2\omega \int_{0}^{z'} \frac{dz''}{c(z'')} \right) \frac{c(0)\alpha_1(z')}{c(z')} = -\frac{c(0)}{4} \int_{-\infty}^{\infty} dz' \exp\left(i2\omega\tau(0,z')\right) \frac{\alpha_1(z')}{c(z')}$$

So the right-hand-side of (10a) is:

$$\int_{-\infty}^{\infty} d\omega \left\{ \int_{-\infty}^{\infty} dz' G_0(0,z',\omega) V_1(z') G_0(z',0,\omega) \right\} e^{-i\omega 2\tau(0,z)}$$

$$= \int_{-\infty}^{\infty} d\omega \left\{ -\frac{c(0)}{4} \int_{-\infty}^{\infty} dz' e^{i2\omega\tau(0,z')} \frac{\alpha_1(z')}{c(z')} \right\} e^{-i\omega 2\tau(0,z)}$$

By switching the order of integration, we have:

$$= -\frac{c(0)}{4} \int_{-\infty}^{\infty} dz' \frac{\alpha_1(z')}{c(z')} \int_{-\infty}^{\infty} d\omega e^{i\omega\{2\tau(0,z')-2\tau(0,z)\}}$$

$$= -\frac{c(0)}{4}(2\pi)\int_{-\infty}^{\infty} dz' \frac{\alpha_1(z')}{c(z')}\delta(2\tau(0,z')-2\tau(0,z))$$

$$= -\frac{c(0)\pi}{2}\int_{-\infty}^{\infty} dz' \frac{\alpha_1(z')}{c(z')}\delta(2\tau(0,z)-2\tau(0,z'))$$

Let's apply the formula for integration with δ-function (A-1) in Appendix 3 (here we take $\psi(z)=\frac{\alpha_1(z)}{c(z)}$). We have:

$$-\frac{c(0)\pi}{2}\int_{-\infty}^{\infty} dz' \frac{\alpha_1(z')}{c(z')}\delta(2\tau(0,z)-2\tau(0,z'))$$

$$= -\frac{c(0)\pi}{2}\frac{\alpha_1(z)}{c(z)}\frac{c(z)}{2} = -\frac{c(0)\pi}{4}\alpha_1(z)$$

Appendix B --- deriving $\alpha_2(z)$

The left-hand-side of (13) can be similarly calculated as in Appendix A. The only difference is changing 1 to 2, all other derivations are the same. Here we give the final result:

$$-\frac{c(0)\pi}{4}\alpha_2(z).$$

But the right-hand-side is more tedious, the derivation procedure is:

$$G_0V_1G_0V_1G_0$$

$$= \int_{-\infty}^{\infty} dz' G_0(z_g,z',\omega)\left(\frac{\omega}{c(z')}\right)^2\alpha_1(z')\int_{-\infty}^{\infty} dz'' G_0(z',z'',\omega)\left(\frac{\omega}{c(z'')}\right)^2\alpha_1(z'')G_0(z'',z_s,\omega)$$

$$= \int_{-\infty}^{\infty} dz' \frac{1}{2i}\sqrt{\frac{c(0)c(z')}{\omega^2}}e^{i\omega|\tau(0,z')|}\left(\frac{\omega}{c(z')}\right)^2\alpha_1(z')\int_{-\infty}^{\infty} dz'' \frac{1}{2i}\sqrt{\frac{c(z')c(z'')}{\omega^2}}e^{i\omega|\tau(z',z'')|}\left(\frac{\omega}{c(z'')}\right)^2\alpha_1(z'')\frac{1}{2i}\sqrt{\frac{c(0)c(z'')}{\omega^2}}e^{i\omega|\tau(z'',0)|}$$

$$= -\frac{c(0)}{8i}\omega\int_{-\infty}^{\infty} dz' e^{i\omega|\tau(0,z')|}\frac{\alpha_1(z')}{c(z')}\int_{-\infty}^{\infty} dz'' e^{i\omega|\tau(z',z'')|}\frac{\alpha_1(z'')}{c(z'')}e^{i\omega|\tau(0,z'')|}$$

We assume that no perturbation occurs for $z<0$, that is: $z<0 \Rightarrow \alpha_1(z)=0$, we can simplify the expression above further:

$$= -\frac{c(0)}{8i}\omega\int_{-\infty}^{\infty} dz' e^{i\omega\tau(0,z')}\frac{\alpha_1(z')}{c(z')}\int_{-\infty}^{\infty} dz'' e^{i\omega|\tau(z',z'')|}\frac{\alpha_1(z'')}{c(z'')}e^{i\omega\tau(0,z'')}$$

By defining: $\psi_1(z) = \frac{\alpha_1(z)}{c(z)}$, we have:

$$= -\frac{c(0)}{8i}\omega \int_{-\infty}^{\infty} dz' e^{i\omega\tau(0,z')}\psi_1(z')\int_{-\infty}^{\infty} dz''\left\{H(z''-z')e^{i\omega\tau(z',z'')} + H(z'-z'')e^{i\omega\tau(z'',z')}\right\}\psi_1(z'')e^{i\omega\tau(0,z'')}$$

$$= \frac{c(0)}{8}(i\omega)\int_{-\infty}^{\infty} dz' e^{i\omega\tau(0,z')}\psi_1(z')\int_{-\infty}^{\infty} dz''\left\{H(z''-z')e^{i\omega\tau(z',z'')} + H(z'-z'')e^{i\omega\tau(z'',z')}\right\}\psi_1(z'')e^{i\omega\tau(0,z'')}$$

Now we can calculate the Fourier transform of the right-hand-side:

$$\int_{-\infty}^{\infty}(-G_0V_1G_0V_1G_0)e^{-i2\omega\tau(0,z)}d\omega = \frac{c(0)}{8}\{I_1 + I_2\}$$

where I_1 is calculated as:

$$I_1 = -\int_{-\infty}^{\infty}\left\{i\omega\int_{-\infty}^{\infty} dz'\psi_1(z')\int_{-\infty}^{\infty} dz''\{H(z''-z')\}\psi_1(z'')e^{i\omega 2\tau(0,z'')}\right\}e^{-i2\omega\tau(0,z)}d\omega$$

$$= \int_{-\infty}^{\infty} dz'\psi_1(z')\int_{-\infty}^{\infty} dz'' H(z''-z')\psi_1(z'')\int_{-\infty}^{\infty} d\omega(-i\omega)e^{-i\omega\{2\tau(0,z)-2\tau(0,z'')\}}$$

$$= (2\pi)\int_{-\infty}^{\infty} dz'\psi_1(z')\int_{-\infty}^{\infty} dz'' H(z''-z')\psi_1(z'')\delta'(2\tau(0,z) - 2\tau(0,z''))$$

Let's apply the formula for integration with δ-function (A-2) in Appendix C (here we take $\psi(z'') = \psi_1(z'')H(z''-z') = \frac{\alpha_1(z'')}{c(z'')}H(z'-z'')$). The expression above can be simplified further as:

$$= \frac{c^2(z)\pi}{2}\int_{-\infty}^{\infty} dz'\psi_1(z')\{\delta(z-z')\psi_1(z) + H(z-z')\psi'_1(z)\}$$
$$+ \frac{c(z)c'(z)\pi}{2}\int_{-\infty}^{\infty} dz'\psi_1(z')H(z-z')\psi_1(z)$$

$$= \frac{c^2(z)\pi}{2}\left\{\psi_1^2(z) + \psi'_1(z)\int_{-\infty}^{z} dz'\psi_1(z')\right\} + \frac{c(z)c'(z)\pi}{2}\psi_1(z)\int_{-\infty}^{z} dz'\psi_1(z')$$

$$= \frac{\pi}{2}\left\{c^2(z)\psi_1^2(z) + \right\} + \frac{\pi}{2}c(z)[c(z)\psi'_1(z) + c'(z)\psi_1(z)]\int_{-\infty}^{z} dz'\psi_1(z')$$

$$= \frac{\pi}{2}\left\{c^2(z)\psi_1^2(z)\right\} + \frac{\pi}{2}c(z)[c(z)\psi_1(z)]'\int_{-\infty}^{z} dz'\psi_1(z')$$

$$= \frac{\pi}{2}\left\{\alpha_1^2(z)\right\} + \frac{\pi}{2}c(z)[\alpha_1(z)]'\int_{-\infty}^{z} dz'\psi_1(z')$$

$$= \frac{\pi}{2}\left\{\alpha_1^2(z)\right\} + \frac{\pi}{2} c(z)\alpha'_1(z)\int_{-\infty}^{z} dz' \frac{\alpha'_1(z')}{c(z')}$$
$$= \frac{\pi}{2}\left\{\alpha_1^2(z) + c(z)\alpha'_1(z)\int_{-\infty}^{z} dz' \frac{\alpha'_1(z')}{c(z')}\right\}$$

Similarly, I_2 can be calculated as:

$$I_2 = -\int_{-\infty}^{\infty}\left\{ i\omega \int_{-\infty}^{\infty} dz'\psi_1(z')\int_{-\infty}^{\infty} dz''\left\{H(z'-z'')\right\}\psi_1(z'')e^{i\omega 2\tau(0,z')}\right\} e^{-i2\omega\tau(0,z)} d\omega$$
$$= \int_{-\infty}^{\infty} dz'\psi_1(z')\int_{-\infty}^{\infty} dz'' H(z'-z'')\psi_1(z'')\int_{-\infty}^{\infty} d\omega(-i\omega)e^{-i\omega\{2\tau(0,z)-2\tau(0,z')\}}$$
$$= (2\pi)\int_{-\infty}^{\infty} dz'\psi_1(z')\int_{-\infty}^{\infty} dz'' H(z'-z'')\psi_1(z'')\delta'(2\tau(0,z)-2\tau(0,z'))$$
$$= \int_{-\infty}^{\infty} dz''\psi_1(z'')\int_{-\infty}^{\infty} dz'\psi_1(z')H(z'-z'')\delta'(2\tau(0,z)-2\tau(0,z'))$$

Let's apply the formula for integration with δ-function (A-2) in Appendix C (here we take $\psi(z') = \psi_1(z')H(z'-z'') = \frac{\alpha_1(z')}{c(z')}H(z''-z')$). We have:

$$= \frac{c^2(z)\pi}{2}\int_{-\infty}^{\infty} dz''\psi_1(z'')\left\{\delta(z-z'')\psi_1(z) + H(z-z'')\psi'_1(z)\right\}$$
$$+ \frac{c(z)c'(z)\pi}{2}\psi_1(z)\int_{-\infty}^{\infty} dz''\psi_1(z'')H(z-z'')$$
$$= \frac{c^2(z)\pi}{2}\left\{\psi_1^2(z) + \psi'_1(z)\int_{-\infty}^{z} dz''\psi_1(z'')\right\} + \frac{c(z)c'(z)\pi}{2}\psi'_1(z)\int_{-\infty}^{z} dz''\psi_1(z'')$$
$$= \frac{\pi}{2}\left\{c^2(z)\psi_1^2(z)\right\} + \frac{c(z)\pi}{2}\left\{\left(c(z)\psi'_1(z) + c'(z)\psi_1(z)\right)\int_{-\infty}^{z} dz''\psi_1(z'')\right\}$$

$$= \frac{\pi}{2}\left\{c^2(z)\psi_1^2(z)\right\} + \frac{c(z)\pi}{2}\left\{\left(c(z)\psi_1(z)\right)'\int_{-\infty}^{z} dz''\psi_1(z'')\right\}$$
$$= \frac{\pi}{2}\left\{c^2(z)\psi_1^2(z)\right\} + \frac{c(z)\pi}{2}\left\{\alpha'_1(z)\int_{-\infty}^{z} dz'\frac{\alpha_1(z')}{c(z')}\right\}$$
$$= \frac{\pi}{2}\left\{\alpha_1^2(z) + \alpha'_1(z)c(z)\int_{-\infty}^{z} dz'\frac{\alpha_1(z')}{c(z')}\right\}$$

In summary, we have:

$$\int_{-\infty}^{\infty}\left(-G_0V_1G_0V_1G_0\right)e^{-i2\omega\tau(0,z)}d\omega=\frac{c(0)}{8}\{I_1+I_2\}$$
$$=\frac{c(0)\pi}{8}\left\{\alpha_1^2(z)+\alpha'_1(z)c(z)\int_{-\infty}^{z}dz'\frac{\alpha_1(z')}{c(z')}\right\}$$

Appendix C --- Integral with δ-function and its first derivative

In this paper, the function inside δ-function and it's first derivative will always be the 2-way travel time between 0 and z:

$$f(z)=2\int_0^z\frac{dz'}{c(z')}=2\tau(0,z)$$

where z is depth, c(u) is a function of reference velocity. Let's consider it's relation with it's inverse (denoted here by g):

$u=f(z)$ and $z=g(u)=f^{-1}(u)$

If $u_0=f(z_0)$. We have: $g'(u_0)=\frac{1}{f'(z_0)}$

Now it's time to calculate the following integral:

$$\int_{-\infty}^{\infty}dz\{\psi(z)\delta(f(z_0)-f(z))\}$$

where ψ(z) is an arbitrary function.

After changing integration variable: $u=f(z)$ and $u_0=f(z_0)$

We have $dz=g'(u)du$,

$$\int_{-\infty}^{\infty}dz\{\psi(z)\delta(f(z_0)-f(z))\}=\int_{-\infty}^{\infty}du\{\psi(g(u))\delta(u_0-u)\}g'(u)$$
$$=\int_{-\infty}^{\infty}du\{\psi(g(u))g'(u)\delta(u_0-u)\}$$
$$=\psi(g(u_0))g'(u_0)=\psi\left(f^{-1}(u_0)\right)g'(u_0)$$
$$=\psi(z_0)g'(u_0)=\psi(z_0)\frac{1}{f'(z_0)}=\frac{\psi(z_0)}{f'(z_0)}=\frac{\psi(z_0)c(z_0)}{2}\qquad\text{(A-1)}$$

Now it's time to calculate the integral with the first derivative of δ-function:

$$\int_{-\infty}^{\infty} dx\{\psi(z)\delta'(f(z_0)-f(z))\}$$

where ψ(z) is an arbitrary function.

After changing integration variable: $u = f(z)$ and $u_0 = f(z_0)$

We have $dz = g'(u)du$,

$$\int_{-\infty}^{\infty} dx\{\psi(z)\delta'(f(z_0)-f(z))\} = \int_{-\infty}^{\infty} du\{\psi(g(u))g'(u)\delta'(u_0-u)\}$$

Denote: $\varphi(u) = \psi(g(u))g'(u)$

We have:

$$\int_{-\infty}^{\infty} du\{\psi(g(u))g'(u)\delta'(u_0-u)\} = \int_{-\infty}^{\infty} du\{\varphi(u)\delta'(u_0-u)\}$$

$$= -\int_{-\infty}^{\infty} \varphi(u)d\delta'(u_0-u) = [-\varphi(u)\delta(u_0-u)]_{x=-\infty}^{x=\infty} + \int_{-\infty}^{\infty} \delta(u_0-u)d\varphi(u)$$

$$= \int_{-\infty}^{\infty} \delta(u_0-u)\varphi'(u)du = \varphi'(u_0)$$

$$= \frac{d}{du}\{\psi(g(u))g'(u)\}\Big|_{u=u_0}$$

$$= \psi'(g(u))[g'(u)]^2 + \psi(g(u))g''(u)\Big|_{u=u_0}$$

$$= \psi'(g(u_0))[g'(u_0)]^2 + \psi(g(u_0))g''(u_0)$$

$$= \psi'(f^{-1}(u_0))[g'(u_0)]^2 + \psi(f^{-1}(u_0))g''(u_0)$$

$$= \frac{\psi'(x_0)}{[f'(x_0)]^2} + \psi(x_0)g''(u_0)$$

In the expression above, $g''(u_0)$ can be calculated by:

$$g''(u) = \frac{d}{du}\{g'(u)\}$$

Because: $g = f^{-1}$, we have:

$$g''(u) = \frac{d}{du}\left\{\frac{1}{f'(z)}\right\} = \frac{d}{dz}\left\{\frac{1}{f'(z)}\right\}/\frac{du}{dz} = \frac{d}{dz}\left\{\frac{1}{f'(z)}\right\}\frac{1}{f'(z)} = \frac{-f''(z)}{[f'(z)]^3}$$

So we have:

$$\int_{-\infty}^{\infty} du\{\psi(g(u))g'(u)\delta'(u_0-u)\} = \frac{\psi'(x_0)}{[f'(x_0)]^2} + \psi(x_0)g''(u_0)$$

$$= \frac{\psi'(z_0)}{[f'(z_0)]^2} - \psi(z_0)\frac{f''(z_0)}{[f'(z_0)]^3} = \frac{\psi'(z_0)c^2(z_0)}{4} + \frac{\psi(z_0)c^3(z_0)}{8}\frac{2c'(z_0)}{c^2(z_0)}$$

$$= \frac{c(z_0)}{4}\{\psi'(z_0)c(z_0) + \psi(z_0)c'(z_0)\} \qquad \text{(A-2)}$$